

**BRANCHING RATIOS OF THE CHARGED KAON  
DECAYS AND RADIATIVE CORRECTIONS FOR  
THE  $K \rightarrow \pi E \nu$  DECAY MODE**

by

**A. Baratt**

Submitted to the Graduate Faculty of  
the School of Arts and Sciences, Department of Physics and  
Astronomy in partial fulfillment  
of the requirements for the degree of  
B.Sc. In Physics, Hebrew University of Jerusalem, 1993  
M.Sc. In Physics, University of Pittsburgh, 2001

University of Pittsburgh

2004

UNIVERSITY OF PITTSBURGH  
SCHOOL OF ARTS AND SCIENCES, DEPARTMENT OF PHYSICS AND  
ASTRONOMY

This dissertation was presented

by

A. Baratt

It was defended on

February 24th 2004

and approved by

Prof. Julia A. Thompson

Prof. Steven P. Levitan

Prof. Vladimir P. Savinov

Prof. Eric S. Swanson

Prof. Raymond S. Willey

Dissertation Director: Prof. Julia A. Thompson

# BRANCHING RATIOS OF THE CHARGED KAON DECAYS AND RADIATIVE CORRECTIONS FOR THE $K \rightarrow \pi E \nu$ DECAY MODE

A. Baratt, PhD

University of Pittsburgh, 2004

The CMD-2 experiment at the VEPP-2M accelerator at the Budker Institute of Nuclear Physics has collected  $\approx 1$  million charged kaon decays, from which we extract a clean sample of  $\approx 74,000 K^+$  decays, with  $\approx 50,000 K^+ \rightarrow \mu^+ \nu$ , 18,000  $K^+ \rightarrow \pi^+ \pi^0$ , 4000 ( $K^+ \rightarrow \pi^0 \mu^+ \nu + K^+ \rightarrow \pi^0 e^+ \nu$ ), and 2000 ( $K^+ \rightarrow \pi^+ \pi^+ \pi^- + K^+ \rightarrow \pi^+ \pi^0 \pi^0$ ) events. Based on these samples we present measurement of  $R_{2body} \equiv Br(K^+ \rightarrow \pi^+ \pi^0) / Br(K^+ \rightarrow \mu^+ \nu) = 0.3292 \pm 0.0048 \text{ stat} \pm 0.011 \text{ sys}$ ,  $R_{semilep} \equiv (Br(K^+ \rightarrow \pi^0 \mu^+ \nu) + Br(K^+ \rightarrow \pi^0 e^+ \nu)) / Br(K^+ \rightarrow \pi^+ \pi^0) = 0.477 \pm 0.016 \text{ stat} \pm 0.10 \text{ sys}$ , and  $R_{3pion} \equiv (Br(K^+ \rightarrow \pi^+ \pi^+ \pi^-) + Br(K^+ \rightarrow \pi^+ \pi^0 \pi^0)) / Br(K^+ \rightarrow \pi^+ \pi^0) = 0.315 \pm 0.014 \text{ stat} \pm 0.054 \text{ sys}$ . The ratio of the two semileptonic decays is extracted from the  $K^-$  decays only and yields  $R_{e\mu} \equiv Br(K \rightarrow \pi^0 e \nu) / Br(K \rightarrow \pi^0 \mu \nu) = 1.97 \pm 0.09 \text{ stat} \pm 0.81 \text{ sys}$ . The strength of these measurements is the presence of all the major decay modes and systematics different from some other experiments.

In this dissertation I also consider the radiative corrections for the  $K_{e3}$  decay. This decay is of particular importance since it provides the best way to extract the value of the  $V_{us}$  element of the CKM matrix. In turn, precise knowledge of  $V_{us}$  is needed to resolve a long standing problem with a unitarity test of the CKM matrix.

## TABLE OF CONTENTS

|                                        |    |
|----------------------------------------|----|
| <b>1.0 INTRODUCTION</b>                | 1  |
| 1.1 Background: Leptons and Quarks     | 1  |
| 1.2 Intermediate Interaction Particles | 2  |
| 1.3 Quark Mixing                       | 3  |
| 1.4 CKM Matrix Unitarity               | 4  |
| 1.5 $V_{us}$ and $K_{e3}$ Decay        | 5  |
| 1.6 $\Phi$ Factory                     | 6  |
| 1.7 Modes of the Charged Kaon Decays   | 7  |
| 1.8 Radiative Corrections              | 7  |
| <b>2.0 VEPP-2M COLLIDER COMPLEX</b>    | 9  |
| 2.1 Beam Energy Determination          | 11 |
| 2.2 Beam Luminosity Determination      | 13 |
| <b>3.0 CMD-2 DETECTOR</b>              | 14 |
| 3.1 Tracking System                    | 17 |
| 3.2 CsI Barrel Calorimeter             | 20 |
| 3.3 BGO end-cap calorimeter            | 20 |
| 3.4 Muon Range System                  | 21 |
| 3.5 Triggering System                  | 21 |
| <b>4.0 DATA TAKING</b>                 | 26 |
| 4.1 Data Collection                    | 26 |
| 4.2 Offline Processing                 | 27 |
| 4.3 Event Reconstruction Algorithms    | 27 |

|            |                                                                      |            |
|------------|----------------------------------------------------------------------|------------|
| 4.3.1      | Track Reconstruction . . . . .                                       | 27         |
| 4.3.2      | Reconstruction of Energy Clusters in the Calorimeters . . . . .      | 28         |
| 4.3.3      | Global Reconstruction . . . . .                                      | 28         |
| 4.4        | Selection Criteria and Backgrounds . . . . .                         | 29         |
| 4.4.1      | Event Selection . . . . .                                            | 30         |
| 4.4.2      | Presence of $\pi^0$ Requirement . . . . .                            | 49         |
| 4.4.3      | Background Estimates . . . . .                                       | 55         |
| 4.4.3.1    | Beam–Gas Background . . . . .                                        | 57         |
| 4.4.3.2    | Cosmic Rays Overlaps . . . . .                                       | 59         |
| <b>5.0</b> | <b>SIMULATION . . . . .</b>                                          | <b>60</b>  |
| 5.1        | CMD–2 Simulation Software . . . . .                                  | 60         |
| 5.2        | Fine Tuning of the Charged Kaon Decays Simulation . . . . .          | 65         |
| 5.3        | Charge Asymmetry in the Drift Chamber . . . . .                      | 70         |
| <b>6.0</b> | <b>SEPARATION PARAMETERS . . . . .</b>                               | <b>73</b>  |
| 6.1        | Missing Mass . . . . .                                               | 73         |
| 6.2        | DPE . . . . .                                                        | 77         |
| 6.2.1      | Electron DPE . . . . .                                               | 91         |
| 6.2.2      | Muon DPE . . . . .                                                   | 95         |
| 6.2.3      | Pion DPE . . . . .                                                   | 101        |
| 6.2.4      | Comparison of Experimental and Simulated DPE distributions . . . . . | 107        |
| <b>7.0</b> | <b>ANALYSIS . . . . .</b>                                            | <b>110</b> |
| 7.1        | Ratios to be Measured . . . . .                                      | 110        |
| 7.2        | MM2 analysis . . . . .                                               | 110        |
| 7.2.1      | Expected MM2 Distributions From Simulation . . . . .                 | 111        |
| 7.2.2      | $K \rightarrow \mu\nu$ Distribution: MM2 From Data . . . . .         | 113        |
| 7.2.3      | Analysis Variations . . . . .                                        | 117        |
| 7.3        | DPE analysis . . . . .                                               | 118        |
| <b>8.0</b> | <b>RESULTS . . . . .</b>                                             | <b>122</b> |
| 8.1        | Summary of the Results . . . . .                                     | 125        |
| 8.2        | Systematic Errors . . . . .                                          | 136        |

|            |                                                                                                                                               |            |
|------------|-----------------------------------------------------------------------------------------------------------------------------------------------|------------|
| 8.2.1      | MM2 Fits: Consistency Among Energies . . . . .                                                                                                | 136        |
| 8.2.2      | MM2 Fits: Analysis Variations, $Br(K \rightarrow \pi\pi^0)/Br(K \rightarrow \mu\nu)$ . . . . .                                                | 137        |
| 8.2.3      | MM2 Fits: Analysis Variations,<br>( $Br(K \rightarrow \pi^0\mu\nu) + Br(K \rightarrow \pi^0e\nu)$ )/ $Br(K \rightarrow \pi\pi^0)$ . . . . .   | 138        |
| 8.2.4      | MM2 Fits: Analysis Variations,<br>( $Br(K \rightarrow \pi\pi\pi) + Br(K \rightarrow \pi\pi^0\pi^0)$ )/ $Br(K \rightarrow \pi\pi^0)$ . . . . . | 138        |
| 8.2.5      | Semileptonic Region Excess . . . . .                                                                                                          | 139        |
| 8.2.6      | Systematic Error for the MM2 measurements: $K^+$ . . . . .                                                                                    | 140        |
| 8.2.7      | Systematic Error for the MM2 measurements: $K^-$ . . . . .                                                                                    | 142        |
| 8.2.8      | Systematic Error of the Ratio Obtained from the DPE . . . . .                                                                                 | 144        |
| 8.2.9      | Final Results . . . . .                                                                                                                       | 144        |
| 8.2.10     | Conclusions . . . . .                                                                                                                         | 145        |
| <b>9.0</b> | <b>RADIATIVE CORRECTIONS TO THE <math>K_{E3}^\pm</math> DECAY</b> . . . . .                                                                   | <b>147</b> |
| 9.1        | Introduction and Motivation . . . . .                                                                                                         | 147        |
| 9.2        | Matrix Elements and Kinematics . . . . .                                                                                                      | 150        |
| 9.3        | Virtual and Soft Real Photon Emission . . . . .                                                                                               | 154        |
| 9.4        | Hard Photon Emission. Structure Functions Approach . . . . .                                                                                  | 156        |
| 9.5        | Corrections to the Dalitz Plot and the Electron and Pion Spectra . . . . .                                                                    | 161        |
| 9.6        | Spectral distribution of radiative $K_{e3}$ . . . . .                                                                                         | 166        |
| 9.7        | Discussion of the Results . . . . .                                                                                                           | 167        |
| 9.8        | Appendix A . . . . .                                                                                                                          | 169        |
| 9.9        | Appendix B . . . . .                                                                                                                          | 171        |
| 9.10       | Appendix C . . . . .                                                                                                                          | 174        |
| 9.11       | Appendix D . . . . .                                                                                                                          | 175        |
| 9.12       | Appendix E . . . . .                                                                                                                          | 176        |
| 9.13       | Appendix F . . . . .                                                                                                                          | 180        |
| 9.14       | Appendix G. Lists of the Runs . . . . .                                                                                                       | 183        |
|            | <b>BIBLIOGRAPHY</b> . . . . .                                                                                                                 | <b>207</b> |

## LIST OF TABLES

|    |                                                                                                                                                              |     |
|----|--------------------------------------------------------------------------------------------------------------------------------------------------------------|-----|
| 1  | The now known generations of leptons and quarks. . . . .                                                                                                     | 2   |
| 2  | Main parameters of CMD-2 detector. . . . .                                                                                                                   | 15  |
| 3  | Statistics of the collected data. . . . .                                                                                                                    | 26  |
| 4  | Registration efficiencies for the six simulated modes at 509.5 MeV . . . . .                                                                                 | 47  |
| 5  | Effect of data selection cuts on the data statistics. . . . .                                                                                                | 48  |
| 6  | Effects of the $R_{vertex}$ cut, $\pi^0$ requirement, and cuts that reduce the number of the 'noise' photons. . . . .                                        | 51  |
| 7  | General control input cards. . . . .                                                                                                                         | 63  |
| 8  | Physical processes control input cards. . . . .                                                                                                              | 64  |
| 9  | Percentages of the events that survive the no photons requirement. . . . .                                                                                   | 113 |
| 10 | Numbers of events in regions A and B. . . . .                                                                                                                | 120 |
| 11 | Numbers of events in the regions A and B. . . . .                                                                                                            | 121 |
| 12 | Results of the $\frac{Br(K^+ \rightarrow \pi^+ \pi^0)}{Br(K^+ \rightarrow \mu^+ \nu)}$ measurements. . . . .                                                 | 126 |
| 13 | Results of the $\frac{Br(K^- \rightarrow \pi^- \pi^0)}{Br(K^- \rightarrow \mu^- \nu)}$ measurements. . . . .                                                 | 127 |
| 14 | Results of the $\frac{Br(K^+ \rightarrow \pi^0 \mu^+ \nu) + Br(K^+ \rightarrow \pi^0 e^+ \nu)}{Br(K^+ \rightarrow \pi^+ \pi^0)}$ measurements. . . . .       | 128 |
| 15 | Results of the $\frac{Br(K^- \rightarrow \pi^0 \mu^- \nu) + Br(K^- \rightarrow \pi^0 e^- \nu)}{Br(K^- \rightarrow \pi^- \pi^0)}$ measurements. . . . .       | 129 |
| 16 | Results of the $\frac{Br(K^+ \rightarrow \pi^+ \pi^+ \pi^-) + Br(K^+ \rightarrow \pi^+ \pi^0 \pi^0)}{Br(K^+ \rightarrow \pi^+ \pi^0)}$ measurements. . . . . | 130 |
| 17 | Results of the $\frac{Br(K^- \rightarrow \pi^- \pi^- \pi^+) + Br(K^- \rightarrow \pi^- \pi^0 \pi^0)}{Br(K^- \rightarrow \pi^- \pi^0)}$ measurements. . . . . | 131 |
| 18 | Averages over the energies for $K^+$ measurements . . . . .                                                                                                  | 132 |
| 19 | Averages over the energies for $K^-$ measurements . . . . .                                                                                                  | 133 |
| 20 | Results of the $\frac{Br(K^- \rightarrow \pi^0 e^- \nu)}{Br(K^- \rightarrow \pi^0 \mu^- \nu)}$ measurements in each energy point. . . . .                    | 134 |

|    |                                                                                                                                                |     |
|----|------------------------------------------------------------------------------------------------------------------------------------------------|-----|
| 21 | Results of the $\frac{Br(K^- \rightarrow \pi^0 e^- \nu)}{Br(K^- \rightarrow \pi^0 \mu^- \nu)}$ measurements, averages over the energies. . . . | 135 |
| 22 | Consistency of the results obtained at different energies represented by the $\chi^2/d.f.$ . . . . .                                           | 136 |
| 23 | $\chi^2/d.f.$ of the MM2 fits. . . . .                                                                                                         | 136 |
| 24 | Errors due to the excess in the semileptonic region. . . . .                                                                                   | 139 |
| 25 | Systematic errors for $K^+$ measurements . . . . .                                                                                             | 141 |
| 26 | Systematic errors for $K^-$ measurements . . . . .                                                                                             | 143 |
| 27 | Overall summary of the results. . . . .                                                                                                        | 144 |
| 28 | List of the runs at 509.0 MeV. . . . .                                                                                                         | 183 |
| 29 | List of the runs at 509.5 MeV. . . . .                                                                                                         | 189 |
| 30 | List of the runs at 510.0 MeV. . . . .                                                                                                         | 195 |
| 31 | List of the runs at 510.5 MeV. . . . .                                                                                                         | 201 |
| 32 | List of the runs at 492.0 MeV, used for background investigation. . . . .                                                                      | 205 |
| 33 | List of the runs at 502.0 MeV, used for background investigation. . . . .                                                                      | 206 |

## LIST OF FIGURES

|    |                                                                                                        |    |
|----|--------------------------------------------------------------------------------------------------------|----|
| 1  | The VEPP-2M Accelerator Complex . . . . .                                                              | 11 |
| 2  | Cryogenic Magnetic Detector CMD-2. . . . .                                                             | 14 |
| 3  | Positioning of the wires in the drift chamber and in the Z-chamber . . . . .                           | 17 |
| 4  | Drift chamber performance . . . . .                                                                    | 19 |
| 5  | Selection of $e^-e^+ \rightarrow e^-e^+$ events for the calibration. . . . .                           | 24 |
| 6  | CMD-2 First Level Trigger . . . . .                                                                    | 25 |
| 7  | $\phi$ -meson excitation curve. . . . .                                                                | 29 |
| 8  | Radial distance from the center of the beam pipe to the vertex . . . . .                               | 30 |
| 9  | Radial distance from the center of the beam pipe, for background candidates<br>at 502 Mev. . . . .     | 32 |
| 10 | Kaon's candidate impact parameter in $R - \phi$ plane. . . . .                                         | 32 |
| 11 | Number of tracks in the $R - Z$ plane that make up the vertex. . . . .                                 | 33 |
| 12 | Quality of vertex in the $R - Z$ plane. . . . .                                                        | 34 |
| 13 | Angle between the tracks in the $R-\phi$ plane. . . . .                                                | 35 |
| 14 | Space angle between the tracks. . . . .                                                                | 36 |
| 15 | Polar angle distribution for kaon candidate track. . . . .                                             | 37 |
| 16 | Polar angle distribution for kaon decay product track. . . . .                                         | 37 |
| 17 | Most distant wire being hit by the kaon candidate track, 509.5 MeV data. . .                           | 38 |
| 18 | Momentum of the kaon candidate track, 510.0 MeV data. . . . .                                          | 38 |
| 19 | Distribution of the momentum of the decay product candidate, 509.5 MeV data.                           | 39 |
| 20 | Distribution of the radius of the vertex in $R - \phi$ plane taken from the 509.5<br>MeV data. . . . . | 39 |

|    |                                                                                                                                   |    |
|----|-----------------------------------------------------------------------------------------------------------------------------------|----|
| 21 | Distribution of the $Z$ -coordinate of the vertex taken from the 509.5 MeV data.                                                  | 40 |
| 22 | Tagging kaon decaying at the $Z$ -chamber wall . . . . .                                                                          | 41 |
| 23 | Radial distance from the center of the beam pipe to the intersection point of<br>the two tracks which make up the vertex. . . . . | 42 |
| 24 | Kaon's $dE/dx$ distribution from 510.0 MeV data. . . . .                                                                          | 42 |
| 25 | Decay product's $dE/dx$ distribution from 509.5 MeV data. . . . .                                                                 | 43 |
| 26 | Quality of decay product track in the $R - \phi$ plane from the simulation . . . .                                                | 44 |
| 27 | Quality of decay product track in the $R - Z$ plane from the simulation . . . .                                                   | 45 |
| 28 | Profile histograms of $sr_1$ and $sz_1$ . . . . .                                                                                 | 46 |
| 29 | Mass distributions of reconstructed $\pi^0$ . . . . .                                                                             | 50 |
| 30 | Photon's momentum vs its $\theta$ angle from 510.0 MeV data sample. . . . .                                                       | 52 |
| 31 | Photon's momentum vs its $\theta$ angle from 510.0 MeV $K^+ \rightarrow \pi^+\pi^0$ simulation. .                                 | 53 |
| 32 | Photon's momentum vs its $\theta$ angle from 510.0 MeV $K^+ \rightarrow \pi^0 e^+ \nu$ simulation.                                | 54 |
| 33 | Radius of the vertex in $R - \phi$ plane for the sample of $K_L K_S$ events. . . . .                                              | 56 |
| 34 | Distribution of the $Z$ coordinate of the vertex. . . . .                                                                         | 58 |
| 35 | $\Delta\theta$ for the data and the older version of MC. . . . .                                                                  | 65 |
| 36 | $\Delta\theta$ for the data and the new version of MC. . . . .                                                                    | 67 |
| 37 | Average momentum of $\pi^+$ and $\pi^-$ for the data sample of $K_S K_L$ . . . . .                                                | 68 |
| 38 | Invariant mass of $\pi^+$ and $\pi^-$ for the data sample of $K_S K_L$ . . . . .                                                  | 69 |
| 39 | Number of the wire hits for a data sample. . . . .                                                                                | 70 |
| 40 | Number of the wire hits for simulated positive particles. . . . .                                                                 | 71 |
| 41 | Number of the wire hits for simulated negative particles. . . . .                                                                 | 72 |
| 42 | MM2 distribution for 510.0 MeV sample . . . . .                                                                                   | 73 |
| 43 | MM2 for all 6 decay modes simulated at 509.5 MeV. . . . .                                                                         | 75 |
| 44 | Decay product momentum for all 6 decay modes simulated at 509.5 MeV. . .                                                          | 76 |
| 45 | DPE for all simulated modes, $K^+$ decays. . . . .                                                                                | 79 |
| 46 | DPE for all simulated modes, $K^-$ decays. . . . .                                                                                | 80 |
| 47 | DPE versus momentum for all simulated modes, $K^+$ decays. . . . .                                                                | 81 |
| 48 | DPE versus momentum for all simulated modes, $K^-$ decays. . . . .                                                                | 82 |
| 49 | $E_{clus}$ versus momentum for all simulated modes, $K^+$ decays. . . . .                                                         | 83 |

|    |                                                                                                        |     |
|----|--------------------------------------------------------------------------------------------------------|-----|
| 50 | $E_{clus}$ versus momentum for all simulated modes, $K^-$ decays. . . . .                              | 84  |
| 51 | DPE distribution for the data sample of 509.5 MeV, $K^+$ decays. . . . .                               | 85  |
| 52 | DPE distribution for the data sample of 509.5 MeV, $K^-$ decays. . . . .                               | 86  |
| 53 | DPE versus momentum for the data sample of 509.5 MeV, $K^+$ decays. . . . .                            | 87  |
| 54 | DPE versus momentum for the data sample of 509.5 MeV, $K^-$ decays. . . . .                            | 88  |
| 55 | $E_{clus}$ versus momentum for the data sample of 509.5 MeV, $K^+$ decays. . . . .                     | 89  |
| 56 | $E_{clus}$ versus momentum for the data sample of 509.5 MeV, $K^-$ decays. . . . .                     | 90  |
| 57 | DPE for data sample and for simulation with and without radiative corrections. . . . .                 | 91  |
| 58 | $E_{clus}$ for data sample and for simulation with and without radiative corrections. . . . .          | 92  |
| 59 | Momentum for data sample and for simulation with and without radiative corrections. . . . .            | 93  |
| 60 | $E_{clus}/P$ for data sample and for simulation with and without radiative corrections. . . . .        | 94  |
| 61 | DPE for muons selected from 509.5 MeV data, $K^+$ decays. . . . .                                      | 95  |
| 62 | DPE for muons selected from 509.5 MeV data, $K^-$ decays. . . . .                                      | 96  |
| 63 | DPE versus momentum for muons selected from 509.5 MeV data, $K^+$ decays. . . . .                      | 97  |
| 64 | DPE versus momentum for muons selected from 509.5 MeV data, $K^-$ decays. . . . .                      | 98  |
| 65 | $E_{clus}$ versus momentum for muons selected from 509.5 MeV data, $K^+$ decays. . . . .               | 99  |
| 66 | $E_{clus}$ versus momentum for muons selected from 509.5 MeV data, $K^-$ decays. . . . .               | 100 |
| 67 | DPE for pions selected from 509.5 MeV data, $K^+$ decays. . . . .                                      | 101 |
| 68 | DPE for pions selected from 509.5 MeV data, $K^-$ decays. . . . .                                      | 102 |
| 69 | DPE versus momentum for pions selected from 509.5 MeV data, $K^+$ decays. . . . .                      | 103 |
| 70 | DPE versus momentum for pions selected from 509.5 MeV data, $K^-$ decays. . . . .                      | 104 |
| 71 | $E_{clus}$ versus momentum for pions selected from 509.5 MeV data, $K^+$ decays. . . . .               | 105 |
| 72 | $E_{clus}$ versus momentum for pions selected from 509.5 MeV data, $K^-$ decays. . . . .               | 106 |
| 73 | DPE distribution for the 510.0 MeV data sample and MC. . . . .                                         | 108 |
| 74 | DPE distributions for the events in the semileptonic MM2 region. . . . .                               | 109 |
| 75 | Experimental MM2 distribution overlaid with the sum of simulated MM2 distributions. . . . .            | 112 |
| 76 | Sample of $K^+ \rightarrow \mu^+\nu$ events overlaid with contaminations from the other modes. . . . . | 115 |

|    |                                                                                                                  |     |
|----|------------------------------------------------------------------------------------------------------------------|-----|
| 77 | MM2 distributions with no photon requirement applied. . . . .                                                    | 116 |
| 78 | MM2 distribution of the expected sum of simulated modes overlaid with the experimental MM2 distribution. . . . . | 123 |
| 79 | MM2 distribution of the fitted sum of simulated modes overlaid with the experimental MM2 distribution. . . . .   | 124 |
| 80 | Virtual photons. . . . .                                                                                         | 149 |
| 81 | Real photons. . . . .                                                                                            | 150 |
| 82 | Kinematically allowed regions . . . . .                                                                          | 153 |
| 83 | Corrections to the Dalitz plot in percents of unperturbed Dalitz density. . . . .                                | 163 |
| 84 | Pion spectrum in Born approximation . . . . .                                                                    | 164 |
| 85 | Electron spectrum in Born approximation . . . . .                                                                | 164 |
| 86 | Correction to the pion spectrum . . . . .                                                                        | 165 |
| 87 | Correction to the electron spectrum . . . . .                                                                    | 165 |

## 1.0 INTRODUCTION

### 1.1 BACKGROUND: LEPTONS AND QUARKS

All known elementary particle physics phenomena are well described by the Standard Model of elementary particles and their fundamental interactions. The Standard Model provides an elegant theoretical framework and is successful in describing and predicting the experimental results obtained to date [2]. In addition to a theory of strong interactions due to the color charges of quarks and gluons, the Standard Model includes a combined theory of weak and electromagnetic interactions called the electroweak theory. The electroweak theory introduces  $W$  and  $Z$  bosons as the carrier particles of weak processes, and photons as mediators to electromagnetic interactions. There are two types of elementary particles: the basic building blocks of the matter themselves known as matter particles and the intermediate interaction particles. The first ones are fermions with spin  $s = 1/2$  and are classified into leptons and quarks. The known leptons are  $e^-$ ,  $\mu^-$ , and  $\tau^-$ ; and their corresponding neutrinos  $\nu_e$ ,  $\nu_\mu$ , and  $\nu_\tau$ . The known quarks are of six different flavors:  $u$ ,  $d$ ,  $s$ ,  $c$ ,  $b$ , and  $t$  and have fractional charge  $Q = 2/3, -1/3, -1/3, 2/3, -1/3, \text{ and } 2/3$  respectively. Leptons are conveniently grouped in pairs. This grouping into pairs also occurs for the quarks. According to the the Standard Model, the number of lepton pairs and quark pairs should be the same. A lepton pair and a quark pair are said to form a generation. The most elementary constituents of matter form three generations which are summarized in table 1.

The quarks have an additional quantum number, the color, which for them can be of three types, generically denoted as  $q_i$ ,  $i = 1, 2, 3$ . We know that color is not seen in nature and therefore the elementary quarks must be confined into the experimentally observed matter particles, the hadrons. These colorless composite particles are classified into baryons and

Table 1: The now known generations of leptons and quarks.

|         | generation 1                               | generation 2                                   | generation 3                                     |
|---------|--------------------------------------------|------------------------------------------------|--------------------------------------------------|
| leptons | $\begin{pmatrix} e \\ \nu_e \end{pmatrix}$ | $\begin{pmatrix} \mu \\ \nu_\mu \end{pmatrix}$ | $\begin{pmatrix} \tau \\ \nu_\tau \end{pmatrix}$ |
| quarks  | $\begin{pmatrix} u \\ d \end{pmatrix}$     | $\begin{pmatrix} c \\ s \end{pmatrix}$         | $\begin{pmatrix} t \\ b \end{pmatrix}$           |

mesons. The baryons are fermions and consist of three quarks; the mesons are bosons and consist of one quark and one antiquark.

## 1.2 INTERMEDIATE INTERACTION PARTICLES

The second kind of elementary particles are the intermediate interaction particles. Within the Standard Model the strong and electroweak interactions are mediated by a boson with spin  $s = 1$ . The photon mediates the electromagnetic interactions; the eight gluons mediate the strong interactions among quarks; and the three weak bosons,  $W^\pm$ ,  $Z$  are the corresponding intermediate bosons of the weak interactions.

As for the theoretical aspects, the Standard Model is a quantum theory that is based on the gauge symmetry  $SU(3)_C \times SU(2)_L \times U(1)_Y$ . This gauge group includes the symmetry group of the strong interactions,  $SU(3)_C$ , and the symmetry group of the electromagnetic interactions,  $SU(2)_L \times U(1)_Y$ . The group symmetry of the electromagnetic interactions,  $U(1)_{em}$ , appears in the Standard Model as a subgroup of  $SU(2)_L \times U(1)_Y$  and it is in this sense that the weak and electromagnetic interactions are said to be unified.

The scalar sector of the Standard Model is not experimentally confirmed yet. The fact

that the weak gauge bosons are massive particles,  $M_W^\pm, M_Z \neq 0$ , indicates that  $SU(3)_C \times SU(2)_L \times U(1)_Y$  is not a symmetry of the vacuum. In contrast, the photon being massless reflects that  $U(1)_{em}$  is a good symmetry of the vacuum. Therefore, the spontaneous symmetry breaking in the Standard Model is

$$SU(3)_C \times SU(2)_L \times U(1)_Y \rightarrow SU(3)_C \times U(1)_{em} \quad (1.1)$$

This pattern is implemented in the Standard Model by means of the so-called Higgs Mechanism which provides the proper masses to the  $W^\pm$  and  $Z$  gauge bosons and to the fermions, and leaves as a consequence the prediction of a new particle: the Higgs boson. It must be a scalar and electrically neutral; it has not been seen in experiments so far.

### 1.3 QUARK MIXING

Before the  $c$  (charm) quark was discovered in 1974, the observed suppression of the strangeness changing decays led to Cabibbo theory, in which the  $d$  quark was assumed to be in reality a mix of the mass eigenstates of the  $d$  and  $s$  quarks:

$$d' = d \cos \theta_C + s \sin \theta_C \quad (1.2)$$

where  $\theta_C$  is the so-called Cabibbo angle ( $\theta_C = 13^\circ$ ). Cabibbo theory was successful in predicting many decay rates but failed to predict the value of the  $K^0 \rightarrow \mu^+ \mu^-$  decay rate: the predicted value turned out to be much higher than that experimentally observed. A solution to this discrepancy was proposed Glashow, Iliopoulos, and Maini in 1970 and was named the GIM mechanism. It predicted the existence of the fourth quark, namely the  $c$  quark that forms a weak isospin doublet with the  $s$  quark. The mass eigenstates were related to the electroweak eigenstates by the orthogonal transformation called Cabibbo matrix:

$$\begin{pmatrix} d' \\ s' \end{pmatrix} = \begin{pmatrix} \cos \theta_C & \sin \theta_C \\ -\sin \theta_C & \cos \theta_C \end{pmatrix} \begin{pmatrix} d \\ s \end{pmatrix} \quad (1.3)$$

The introduction of the  $c$  quark allowed for the additional amplitudes in the  $K^0 \rightarrow \mu^+ \mu^-$  decay that removed the discrepancy between the predicted and observed decay rates. The

important lesson was that we have to distinguish between the electroweak and mass eigenstates of the quarks.

When all known fermions (quarks and leptons) are considered, their weak interaction eigenstates describe the gauge invariant theory. The fermionic mass matrices can be diagonalized in the mass eigenstate basis which relates to the weak eigenstates basis by unitary transformation. As a result, the weak eigenstates of quarks are presented as a mixture of their mass eigenstates. The mixing can be limited to either  $u$  type or  $d$  type quarks but customarily it is chosen to have  $d$ ,  $s$ , and  $b$  quarks mixed, while  $u$ ,  $c$ , and  $t$  remain unmixed.

$$\begin{pmatrix} d' \\ s' \\ b' \end{pmatrix} = \begin{pmatrix} V_{ud} & V_{us} & V_{ub} \\ V_{cd} & V_{cs} & V_{cb} \\ V_{td} & V_{ts} & V_{tb} \end{pmatrix} \begin{pmatrix} d \\ s \\ b \end{pmatrix} \quad (1.4)$$

The unitary matrix in equation 1.4 was introduced by Cabibbo, Kobayashi, and Maskawa and is known as the Cabibbo–Kobayashi–Maskawa (CKM) matrix. The parameters of the CKM matrix are to be determined experimentally.

#### 1.4 CKM MATRIX UNITARITY

Since by definition the CKM matrix is a transformation from one eigenstate basis to another, it should be unitary. Deviations from the unitarity of the CKM matrix may indicate physics beyond the Standard Model; in particular it may indicate existence of the fourth generation of quarks and leptons.

The current values of the elements of the first row of the CKM matrix are: [1]

$$|V_{ud}| = 0.9734 \pm 0.0008, \quad |V_{us}| = 0.2196 \pm 0.0026, \quad |V_{ub}| = 0.0036 \pm 0.0007 \quad (1.5)$$

and

$$|V_{ud}|^2 + |V_{us}|^2 + |V_{ub}|^2 = 0.9957 \pm 0.0019 . \quad (1.6)$$

This contradicts the unitarity of the CKM matrix by 2.3 standard deviations. The value of the  $V_{us}$  element is derived from the  $K \rightarrow \pi^0 e \nu$  decay, usually referred to as  $K_{e3}$  decay. The uncertainty brought to the above expression by  $V_{us}$  is about the same as the uncertainty from  $V_{ud}$ . Therefore reducing the error in the  $V_{us}$  matrix element would reduce substantially the error in the whole unitarity equation.

## 1.5 $V_{US}$ AND $K_{E3}$ DECAY

The value of the  $V_{us}$  element can be determined either from  $K_{e3}$  decay or from the hyperon decays. In terms of theoretical input, extracting  $V_{us}$  from  $K_{e3}$  decay is easier: while both vector and axial currents contribute in hyperon decays, only the vector current is present in  $K_{e3}$  decay. The matrix element for  $K_{e3}$  decay has the general structure

$$M = \frac{G_F}{\sqrt{2}} V_{us}^* F_\nu(t) \bar{u}(p_\nu) \gamma_\nu (1 + \gamma_5) v(p_e) \quad (1.7)$$

where

$$F_\nu(t) = \frac{1}{\sqrt{2}} [(p + p')_\nu f_+(t) + (p - p') f_-(t)]. \quad (1.8)$$

Here  $f_+$  and  $f_-$  are the form factors that depend on the square of the four momentum transfer to the leptons:

$$t = (p - p')^2 = (p_e + p_\nu)^2. \quad (1.9)$$

Using the Dirac equation one can see that the second term in eq 1.8 becomes proportional to the electron mass and therefore is always neglected, so that  $f_-$  becomes irrelevant. As for  $f_+(t)$ , in the  $K_{e3}$  analysis it is customary to assume its linear dependence on the momentum transfer:

$$f_+(t) = f_+(0) \left( 1 + \lambda_+ \frac{t}{m_\pi^2} \right). \quad (1.10)$$

As a result

$$d\Gamma(K \rightarrow \pi e \nu) \propto |V_{us}|^2 \times |f_+(0)|^2 \times \left( 1 + \lambda_+ \left( \frac{t}{m_\pi^2} \right) \right)^2 dt \quad (1.11)$$

and there is no correlation between the three different contributions. The relative uncertainty of  $|V_{us}|$  extracted from the  $K_{e3}$  decay is

$$\sigma_{V_{us}} = |V_{us}| \left[ \pm 0.5 \frac{\sigma_{\Gamma}}{\Gamma} \pm 0.047 \frac{\sigma_{\lambda_+}}{\lambda_+} \pm \frac{\sigma_{f_+(0)}}{f_+(0)} \right] \quad (1.12)$$

Uncertainty of the decay rate contains uncertainty due to the radiative corrections that will be discussed below;  $\lambda_+$  is obtained from experiment and according to PDG [1]  $\lambda_+ = 0.0276 \pm 0.0021$ ;  $f_+(0)$  is calculated within the framework of the chiral perturbation theory and now is known to the order  $p^6$  [3]. The PDG fit to all charged kaon decay data gives  $Br(K_{e3}) = (4.87 \pm 0.06)\%$ .

## 1.6 $\Phi$ FACTORY

The data for this dissertation was collected by the CMD-2 experiment at the VEPP-2M  $e^+e^-$  collider at the Budker Institute of Nuclear Physics in Novosibirsk. This accelerator, at the center of mass energies of about 1020 MeV, produces  $\phi$ -mesons with cross section at the peak of about  $4.2 \mu\text{b}$ , with very little background. Since  $\phi$  decays into  $K^+K^-$  in about 49.2% of the cases, VEPP-2M served as copious supply of  $K^+K^-$  pairs. With our total luminosity of approximately  $5.5 \text{ pb}^{-1}$ , we have collected in our samples at the beam energies of 509.0, 509.5, 510.0, and 510.5 about  $2.0 \times 10^7$   $\phi$ -mesons, which corresponds to approximately 10 million  $K^+K^-$  pairs, of which about 680,000 have either  $K^+$  or  $K^-$  decaying in the fiducial volume. Further cuts to assure a clean, well-measured sample of events reduce this further to 150,000. For our analysis we used only  $K^+$  data for some measurements and  $K^-$  data for the other; so the final sample size is about 75,000 (table 5) yielding substantial samples of each of the major kaon decays. This sample size makes our measurements competitive with the previous ones; as of 2002 the biggest sample used for charged kaon decay measurements was 45,000 [1]. Measurements of charged kaon branching ratios have large potential for serious systematic errors, and an experiment, like ours, able to study all (or most) of the decay modes should be able to make substantial cross checks and better understand these systematic errors, thus making an important contribution to the study of these decays.

## 1.7 MODES OF THE CHARGED KAON DECAYS

Charged kaons have 6 major decay modes with the following branching ratios stated in the Particle Data Group [1]:

|                                     |                       |
|-------------------------------------|-----------------------|
| $K^+ \rightarrow \mu^+ \nu$         | $(63.43 \pm 0.17)\%$  |
| $K^+ \rightarrow \pi^0 e^+ \nu$     | $(4.87 \pm 0.06)\%$   |
| $K^+ \rightarrow \pi^0 \mu^+ \nu$   | $(3.27 \pm 0.06)\%$   |
| $K^+ \rightarrow \pi^+ \pi^0$       | $(21.13 \pm 0.14)\%$  |
| $K^+ \rightarrow \pi^+ \pi^0 \pi^0$ | $(1.73 \pm 0.04)\%$   |
| $K^+ \rightarrow \pi^+ \pi^+ \pi^-$ | $(5.576 \pm 0.031)\%$ |

As discussed above, the  $K^+ \rightarrow \pi^0 e^+ \nu$  mode is of particular importance. Though in this experiment we did not manage to measure  $K^+ \rightarrow \pi^0 e^+ \nu$  directly, the ratios of the branchings that we measured (listed in the Abstract) will help to reduce the uncertainty of the  $K^+ \rightarrow \pi^0 e^+ \nu$  branching ratio. Experimental techniques used in the analysis and described here may be of interest for the future experiments. In particular they may be of interest for the KLOE group, working at DAΦNE, a similar  $e^+e^-$  accelerator in Frascati.

## 1.8 RADIATIVE CORRECTIONS

Reliable radiative corrections, potentially of the order of a few percent, are necessary to extract the  $V_{us}$  matrix element from the  $K_{e3}$  decay width with high precision. The existing calculations of the radiative corrections to the  $K_{e3}$  decay were performed independently by E.S.Ginsberg [5] and T.Becherrawy [6] in the late 60's. Their results for corrections to the decay rate, Dalitz plot, pion and electron spectra disagree, in some places quite sharply; for example Ginsberg's correction to the decay rate is  $-0.45\%$  while that of Becherrawy is  $-2\%$  (corresponding to corrections to the total width  $\Gamma_{K_{e3}}$  of  $0.45\%$  and  $2\%$  respectively). In addition, calculations by E.S.Ginsberg are ultraviolet cutoff sensitive. Recently the radiative corrections to the  $K_{e3}$  decay were calculated in the framework of Chiral Perturbation Theory (ChPT) [3]; however the authors did not present the Dalitz plot corrections and correction to

the full width in their paper. In this dissertation another calculation is presented. Some of the techniques used in this calculation are different from the ones used in previous calculations.

## 2.0 VEPP-2M COLLIDER COMPLEX

The electron–positron collider VEPP–2M [7] is an  $e^+e^-$  machine operating in the energy range 2E from 0.4 to 1.4 GeV, covering the energies of the  $\rho$ ,  $\omega$ , and  $\phi$  resonances.

The collider complex VEPP-2M consists of

- an injector with 3 MeV linear accelerator ILU
- 200 MeV electron synchrotron B-3M
- 900 MeV booster synchrotron BEP for accumulation of electrons and positrons
- 700 MeV collider VEPP-2M

The VEPP-2M Accelerator Complex consists of four components and is shown in Fig. 1: a linear accelerator, a synchrotron, Booster ring (BEP), and the 9 meter diameter colliding beam storage ring VEPP-2M. The linear accelerator begins with a thermal gun consisting of a lanthanum oxide cathode heated by a filament to dissociate electrons from atoms. The free electrons are first accelerated by a +30 kV grid pulsed every 30 ns to match the resonant frequency of the accelerator cavity, and then accelerated across a potential difference of 2.5 MV which results in 10 Amperes of electron current upon exit and transfer to the synchrotron.

In the synchrotron, the coupling of betatron (spatial) and synchrotron (energy) oscillations during acceleration reduces the phase space of the stored orbits and upon exit there remains 1.2 Amperes of electron current at 250 MeV. At this point the electron bunch is 80 cm long and 1 cm<sup>2</sup> in cross section. After this, the electron bunches are sent to fill the former VEPP-2 ring which has been rebuilt [8] into the BEP Booster Ring by the addition of a new magnet lattice and evacuated chamber capable of higher vacuum pressures. In BEP, the electron bunch length is 30 cm because of different magnet optics, and the bunch is accelerated up to the required beam energy before it is passed to the curved transfer line

into VEPP-2M as can be seen in Fig. 1: The VEPP-2M beam optics provide a 'ribbon' bunch which is 2 – 3 cm in length and of  $200\mu\text{m} \times 50\mu\text{m}$  horizontal–vertical dimensions.

After an electron current is stored in VEPP-2M, the electron bunches from the synchrotron are used to create positrons. Upon traversing a  $50\mu\text{m}$  beryllium vacuum chamber membrane the electrons pass through a lithium lens 20 cm long by 5 cm diameter which is subjected to a pulse of 100 kA for  $100\mu\text{s}$ . This serves to provide an intense magnetic field inside the lithium which focuses the electron beam down to horizontal and vertical dimensions of  $100\mu\text{m}$  on a tungsten target 3 mm in length by 2 mm diameter. The positively charged particles produced in the target are passed through another lithium lens for defocusing and the remaining beam transfer line selects positrons for accumulation in BEP. The efficiency of positron production is  $10^{-4}$  which results in  $120\mu\text{A}$  beam current. (During the electron cycle, the beam current efficiency is  $10^{-1}$  through the same lithium lens system (with less focusing field) while the positron production target has been moved 2 mm off the beam focus point.) The BEP positron bunch is then accelerated to the required beam energy and injected into VEPP-2M by the straight transfer line which can be seen in Fig. 1.

There are four straight sections of VEPP-2M: two accelerator structures and two physics detectors. The accelerator structures are a Wiggler-magnet [9] and a Radiofrequency (RF)-cavity. The Wiggler-magnet increases the phase space of the particles in orbit which in turn increases the achievable beam luminosity (and which renders VEPP-2M a bright source of synchrotron radiation). The peak luminosity achieved at the  $\phi$ -meson energy of  $2E_{beam} = 1020$  MeV with the Wiggler turned on was  $5 \cdot 10^{30}\text{cm}^{-2}\text{sec}^{-1}$  with electron and positron currents of 40 mA each [10].

On the other side of the ring, at each turn the RF cavity maintains the stored particles' constant energy by a radio frequency of 16.667 MHz which gives a bunch crossing cycle time of 60 ns, and with a twelfth harmonic of 200 MHz to guide the opposite particle bunches simultaneously onto the only two collision points in VEPP-2M. The two detectors (CMD-2 and SND) serve complementary goals: the Cryogenic Magnetic Detector (CMD-2) with a 1.5 Tesla superconducting magnet, 60 cm diameter cylindrical drift chamber, barrel and end cap calorimeter geometry is well suited for charged particle detection while the non-magnetic Spherical Neutral Detector (SND) with 25 cm diameter drift chamber and spherical

calorimeter geometry is well suited for photon detection and neutral decay modes. This data was taken in the CMD-2 detector which will be described in more detail below.

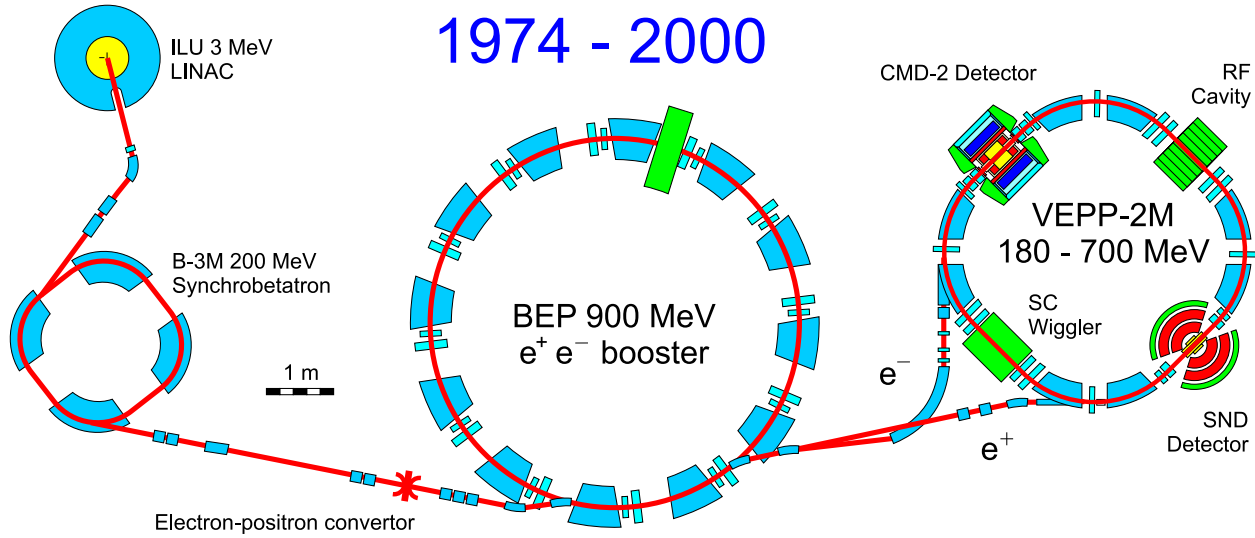


Figure 1: The VEPP-2M Accelerator Complex consists of a Linac, a 200 MeV synchrotron B3M, a booster BEP, and the colliding beam storage ring VEPP-2M. Positrons enter VEPP-2M by the straight transfer line from BEP, electrons through the curved line.

## 2.1 BEAM ENERGY DETERMINATION

The electron beam energy is determined in several different ways.

- The magnetic field in VEPP-2M determines the momentum and energy of the stored particles. The coil current in the dipole magnets is measured directly; the magnetic field is measured by nuclear magnetic resonance (NMR) in an identical dipole magnet connected in series with those of VEPP-2M but situated in the level beneath it.
- Another set of methods uses the CMD-2 apparatus itself to measure  $e^+e^-$  annihilation final states to determine the beam energy. One method uses either  $K^+K^-$  or  $K_LK_S$  in the final state and is valid only above kaon pair production threshold. Near threshold, most of the initial state energy goes to the kaon masses and the kaons have low momentum.

Low momentum particles are well measured in the drift chamber since lower momentum particles bend more and the DC resolution improves with increasing curvature. Using the precisely known masses of the charged kaons, the momentum measurement is converted to energy by the relativistic formula  $E = \sqrt{p^2 + m^2}$ . This method has a systematic error of 184 keV, mostly arising from uncertainty in cross sections of interactions of kaons with nuclei of the materials of the detector [11].

In the neutral kaon case, the  $K_L$  typically does not decay until it is outside the drift chamber, while the  $K_S$  decays quickly to two pions easily seen in the DC. Analyzing the  $K_S$  decay in its rest frame, and performing a Lorentz boost to the laboratory frame, the angle between the two pions exhibits a minimum which depends on the 'Lorentz boost'  $E_K/m_K$ , where  $E_K = E_{beam}$ . Hence measurement of the minimum of the two pion space angle can be used to determine the energy of the beam.

- By far the most precise beam energy determination method is the resonant beam depolarization technique developed at BINP [12]. With a general accuracy of  $\Delta E/E < 10^{-4}$ , for  $E_{beam} = 500$  MeV this corresponds to beam energy uncertainty of 15 keV. This technique exploits the fact that the electron spin precession frequency,  $\omega_s$ , is energy dependent and that an applied high frequency longitudinal (beam-axis) magnetic field is resonant at  $\omega_d$  with  $\omega_s$ . Measurement of  $\omega_s$  determines the circulation frequency of the particles in the colliding beams which in turn measures their momentum (see App. E).

In practice, after colliding beam data taking with CMD-2 is finished at a given energy point, VEPP-2M is filled with electrons at high energy where synchrotron radiation induces polarization most efficiently. The polarized beam is then lowered in energy (adiabatically, which means no polarization is lost) back down to the previous experimental energy. The subsequent scan through the resonance induces depolarization which determines the resonant frequency and hence energy. It is noted that the error on the resonant depolarization measurement of the average energy is far smaller than the actual spread in energy of particles in the colliding beams, which is of order 180 - 300 keV, depending on operation of the Wiggler magnet.

## 2.2 BEAM LUMINOSITY DETERMINATION

As for the beam energy, there are complementary methods for determination of the online beam luminosity, based on QED calculations of fundamental processes and the measured number of events of a given type. The main processes are scattering of electrons and positrons with and without the emission of Bremsstrahlung photons.

In general, Bhabha scattering consists of t-channel (scattering) contributions and s-channel (annihilation) contributions. The s and t-channel contributions interfere. However, in the forward region (along the colliding beam axis) the t-channel contributions dominate and the interference is negligible.

The cross sections for these processes have been calculated to fourth order in QED [13]. These cross sections are used with the number of events, detection efficiencies and corrections to determine the luminosity by the following relations:

$$L = \frac{N_\gamma}{\sigma_0^\gamma(1 + \delta_\gamma)\epsilon_\gamma} = \frac{N_{\gamma\gamma}}{\sigma_0^{\gamma\gamma}(1 + \delta_{\gamma\gamma})\epsilon_{\gamma\gamma}} = \frac{N_{ee}}{\sigma_0^{ee}(1 + \delta_{ee})\epsilon_{ee}} \quad (2.1)$$

where  $\gamma$ , and  $\gamma\gamma$  stand for single and double bremsstrahlung,  $ee$  stands for Bhabha events,  $N_i$  is the number of detected events,  $\epsilon_i$  its overall efficiency,  $\epsilon_0^i$  the lowest order QED cross section and  $\delta_i$  is the overall correction for the i-th process. The Bhabha events are detected by CMD-2 in the barrel region (transverse to the beam axis) both during data taking ('online') and during later analysis ('offline'). The single and double Bremsstrahlung are detected online in the forward small-angle (t-channel dominated) region by luminosity monitors external to CMD-2.

### 3.0 CMD-2 DETECTOR

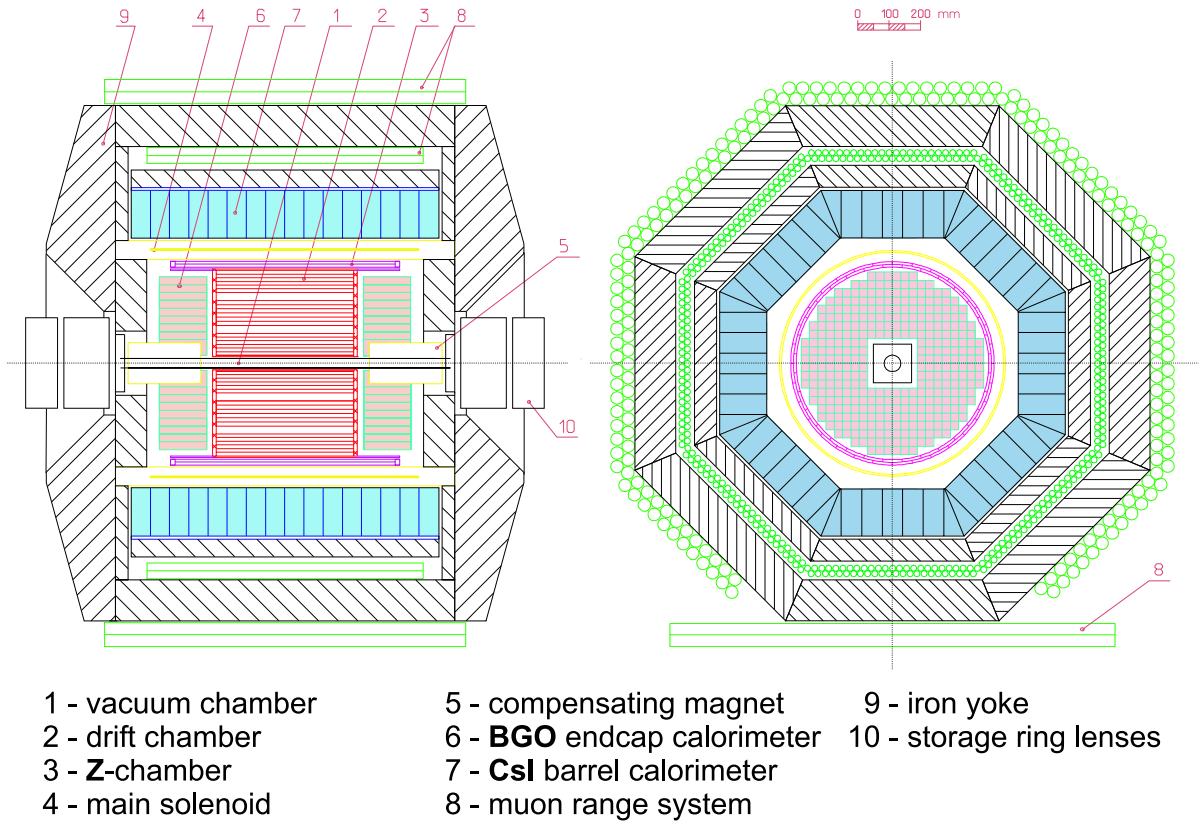


Figure 2: Cryogenic Magnetic Detector CMD-2.

The general-purpose Cryogenic Magnetic Detector CMD-2 (Fig. 2) [14] collected data at VEPP-2M from 1992 to 2000 studying the center-of-mass energy range from 0.36 to 1.4 GeV. The overall integrated  $e^+e^-$  luminosity collected is about  $25 \text{ pb}^{-1}$ . It allows to study, with high precision, many channels of  $e^+e^-$  annihilation to hadrons and rare decays of the light

vector mesons [15]. Fig. 2 shows CMD-2 in  $R - \phi$  and  $R - Z$  projections and the main parameters of the CMD-2 detector are listed in table 2.

Table 2: Main parameters of CMD-2 detector.

| System                     | CMD-2                                                                                                                                                                                                             |
|----------------------------|-------------------------------------------------------------------------------------------------------------------------------------------------------------------------------------------------------------------|
| Drift chamber              | 512 sensitive wires<br>$\sigma_{R-\phi} = 250 \mu\text{m}$ , $\sigma_Z = 5 \text{ mm}$ ,<br>$\sigma_\theta = 15 \cdot 10^{-3}$ , $\sigma_\phi = 7 \cdot 10^{-3}$ ,<br>$\sigma_{dE/dx} = 0.2 \cdot E$              |
| Z-chamber                  | Double layers proportional chamber with cathode strips<br>anode wires are combined to $2 \times 32$ sectors, number of cathode strips - 512<br>$\sigma_Z = 250 \div 1000 \mu\text{m}$ , $\sigma_t = 5 \text{ ns}$ |
| Barrel Calorimeter         | 892 CsI crystals in 8 octants<br>readout PMT<br>thickness $8.1 X_0$<br>$\sigma_E/E = 8\%$ , $\sigma_{\theta,\phi} = 0.03 \div 0.02 \text{ rad}$<br>at $E_\gamma = 100 \div 700 \text{ MeV}$                       |
| continued on the next page |                                                                                                                                                                                                                   |

| System                      | CMD-2                                                                                                                                                                                               |
|-----------------------------|-----------------------------------------------------------------------------------------------------------------------------------------------------------------------------------------------------|
| Endcap<br>Calorimeter       | 680 BGO crystals in 2 endcaps<br>readout vacuum phototriodes<br>thickness $13.4 X_0$<br>$\sigma_E/E = 8 \div 4\%$ , $\sigma_{\theta,\phi} = 0.03 \div 0.02$ rad<br>at $E_\gamma = 100 \div 700$ MeV |
| Range system                | Streamer tubes, 2 double layers, $\sigma_Z=5$ cm                                                                                                                                                    |
| Superconductive<br>solenoid | Magnetic field 1 T, thickness $0.38 X_0$                                                                                                                                                            |

### 3.1 TRACKING SYSTEM

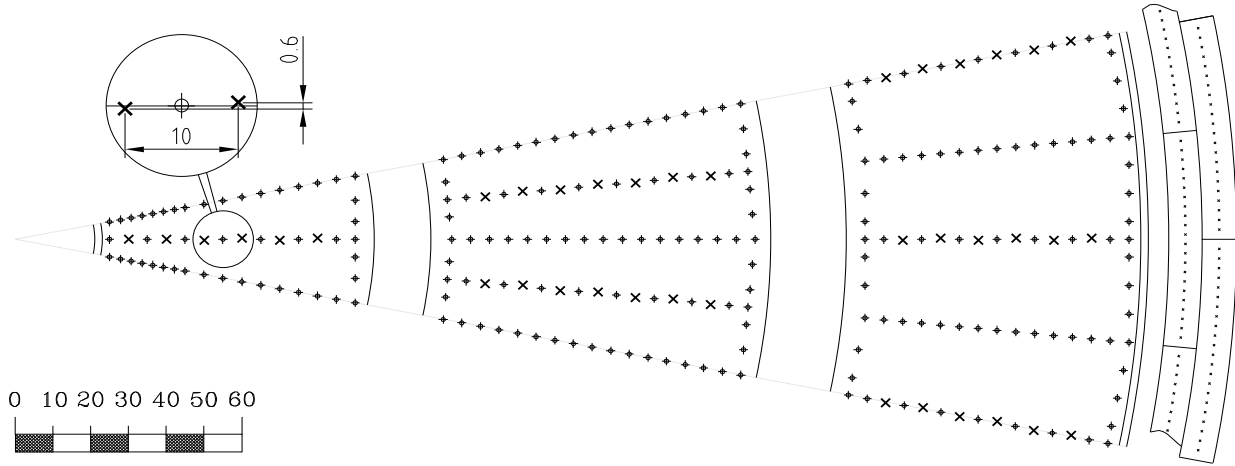


Figure 3: Positioning of the wires in the drift chamber and in the Z-chamber

The tracking system of the detector consists of a cylindrical drift chamber [16] (DC) with 80 jet-type drift cells arranged in three superlayers with wires parallel to the beam. A double layer multiwire proportional chamber (called the Z-chamber, or ZC) with wires oriented along the beam axis and with cathode and anode readout is placed outside the DC. The wire positions in both chambers are shown in Fig. 3.

The outer radius of the DC is 30 cm, and the length of the sensitive volume is 42 cm. The Z-chamber wires are 80 cm long and cover bigger solid angle than the DC. Both chambers are mounted inside a thin ( $0.38 X_0$ ) superconducting solenoid which creates an azimuthally symmetric magnetic field of 1.0 T. The uniformity of the field is better than 1.5% over the DC volume. The chamber is ventilated with a gas mixture of  $80\%Ar + 20\%iC_4H_{10}$ .

From the wire radius, the drift time, and charge division, all three coordinates of the charged particle track in the DC are determined, with about  $230 - 250 \mu m$  resolution in the plane transverse to the beam ( $R - \phi$  plane) and  $0.4 - 0.5$  cm in the Z-longitudinal direction. The momentum resolution is  $2 - 3\%$  for 200 MeV pions from  $K_S \rightarrow \pi^+\pi^-$  decays and about  $4 - 5\%$  for 500 MeV electrons from  $e^+e^-$  elastic scattering (Bhabha) events.

Fig. 4a shows the distribution of the average momentum for collinear events in the

region of the  $\phi$ -meson resonance. The peaks come from Bhabha scattering events, from the  $e^+e^- \rightarrow K^+K^-$  decays and from  $e^+e^- \rightarrow K_S K_L$  with consequent  $K_S \rightarrow \pi^+\pi^-$  decay in which the average momentum of two pions has a narrow distribution around 220 MeV. Histograms in Figs. 4b,d demonstrate the resolution of the acollinearity angle for collinear  $e^+e^-$  events. Fig. 4c shows the  $dE/dx$  response vs momentum of the ionizing particles. Slow kaons that come from the  $\phi$ -meson decays are easily identified and separated from electrons and light mesons. Plot 4c is based on the older  $dE/dx$  calibration. The analysis described in this dissertation uses the newer  $dE/dx$  calibration. The resolution averaged over all track angles was found to be 0.05 cm. The Z-chamber adds another 2.4% radiation lengths to the thickness of the matter in front of CsI calorimeter, but this energy loss is acceptable both because of the Z-chamber importance in particle reconstruction and because its anode information is used in the event trigger.

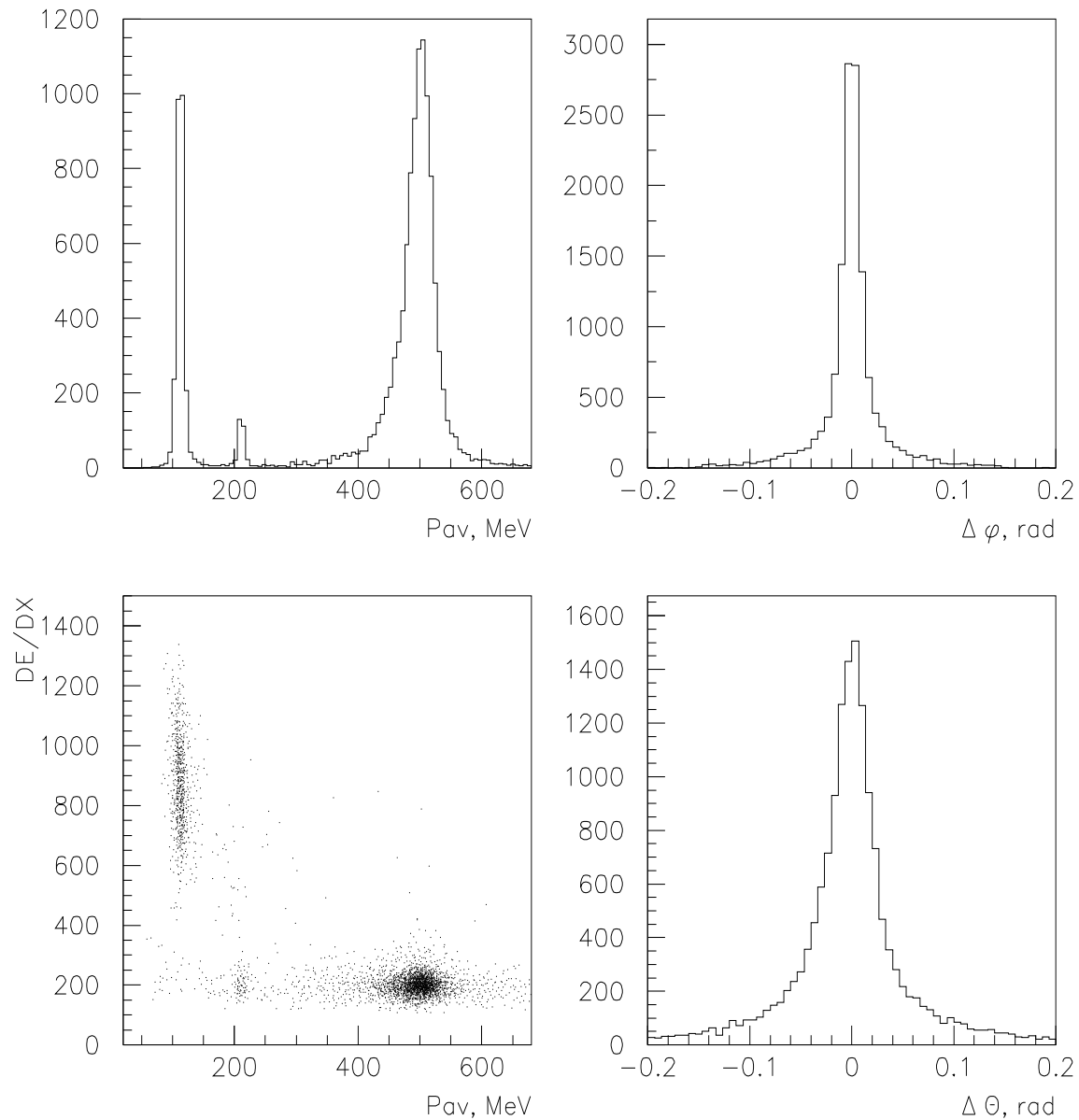


Figure 4: Drift chamber performance: a (upper left)–average momentum for collinear events near the  $\phi$ -meson resonance; b,d (upper right and lower right)–resolution of the acollinearity angle for collinear  $e^+e^-$  events, transverse to (b) and along (d) the beam direction; c (lower left)– $dE/dx$  response vs momentum of the ionizing particles. In the analysis described in this dissertation, a newer calibration was used, which shifts the average kaon  $dE/dx$  to  $\approx 6000$  KeV cm<sup>2</sup>/g.

### 3.2 CSI BARREL CALORIMETER

The CsI barrel calorimeter [17] consists of 892 crystals and is  $8.1 X_0$  deep. The crystals are built into 8 separate octants with 7 linear modules in each. Each module contains 16 crystals. Five of these modules are constructed of the parallelepiped blocks with a  $6 \times 6 \times 15\text{cm}^3$  size while the two edge modules consist of crystals with a special pyramid-like shape to assure close contact of the octants while keeping approximately the same scintillator thickness in these regions. A total solid angle of  $0.7 \times 4\pi$  steradians is subtended. The readout is performed by BINP FEU-60 photomultipliers.

For the photons the calorimeter has an angular resolution of  $0.02 - 0.03$  radians and an energy resolution of  $8 - 10\%$  (FWHM/2.36) in the energy range  $100 - 500$  MeV. Elastic Bhabha events (with known initial energy) were used for the calibration and for the luminosity determination as discussed above. Figure 5 shows the 2-dimensional distribution of the energy depositions for two tracks from collinear events with the beam energy of 420 MeV. One can see concentrations of events corresponding to  $e^-e^+ \rightarrow e^-e^+$  events and to  $e^-e^+ \rightarrow \mu^-\mu^+$  events, with horizontal and vertical bands due to cosmic events.

### 3.3 BGO END-CAP CALORIMETER

The end-cap calorimeter [18] placed inside the solenoid consists of 680 BGO crystals. The thickness of the calorimeter for normally incident particles is  $13.4X_0$ . The crystals are assembled in linear modules which in turn assembled in blocks of 6, 8, and 10 modules. The size of each crystal is  $2.5 \times 2.5 \times 2.5\text{cm}^3$  and there are 340 crystals in each cap.

As in the case of the barrel CsI calorimeter, the calibration is made using collinear Bhabha and cosmic events. The energy resolution is  $\sigma_E/E = 4.6\%/\sqrt{E(\text{GeV})}$  and the angular resolution is  $\sigma_{\phi,\theta} = 2.0\%/\sqrt{E(\text{GeV})}$  in the range 100 to 700 MeV. Since the angular distribution of Bhabha events peaks along the Z axis the inner crystals closest to the beam are used in online luminosity monitoring. Together the barrel and end-cap calorimeters cover a solid angle of  $0.92 \times 4\pi$  steradians.

### 3.4 MUON RANGE SYSTEM

The muon range system [19] consists of two double layers of streamer tubes operating in a self-quenching streamer mode and is aimed at separation of pions and muons.

The inner part of the system is placed inside the iron yoke just after the CsI calorimeter and covers 55% of the solid angle. It consists of 8 modules with 48 streamer tubes in each. For a pion the probability to hit the system and imitate a muon is 35% for a single track and 10% for collinear tracks. The outer part is placed outside the yoke and covers 48% of the solid angle. The five upper modules have 32 tubes each while the three lower ones have 24 tubes each. The muon and pion separation in the outer system is characterized by probabilities of 10% and 1% for a single and collinear tracks respectively.

The spatial resolution, determined from cosmic rays, is 50-70 mm along a wire and the detection efficiency of the double layer is more than 97%.

### 3.5 TRIGGERING SYSTEM

The detector has four independent triggers – three neutrals and one charged. Fig. 6 shows the scheme of the triggering system. The charged trigger was used for this data.

The charged particle trigger [20] is started by a coincidence of hits in overlapping inner and outer ZC sectors with the beam crossing time. The required time resolution of less than 60 ns is determined by the VEPP-2M bunch crossing frequency. For the fast gas mixture of  $CF_4 + 10\%iC_4H_{10}$ , averaged over four hits, a time jitter of around 5 ns is seen. After a successful ZC coincidence, there follows a comparison of the active DC and ZC anode wires with pre-defined track masks, corresponding to different momenta and angles. The coincidence pulse is delayed by the 450 ns maximum drift time in the DC before it starts the CAMAC-resident Tracking Processor (TP) unit which searches through the track masks. The TP requires 320 ns for its decision; if it finds a match, the TP generates a common stop signal for the digitizing KLUKVA modules. If no such stop signal is sent  $1.2\mu s$  after beam crossing, the KLUKVA modules are cleared for the next event. The 20 beam crossings which are lost in this dead time should be considered negligible because the expected event rates,

from  $\mu\text{b}$ -order resonant cross sections and luminosities approaching  $50 \mu\text{b}^{-1}\text{s}^{-1}$ , are of order Hz while the bunch crossing frequency is 16.667 MHz.

Different DC and ZC mask patterns may be loaded into the programmable RAM of the TP. The single mask pattern which has been used for CMD2 data taking consists of 5 symmetrically spaced crescents (two of each polarity and a high momentum arc in the middle). To provide more flexibility in associating different DC sub-units to different crescents, the DC sub-unit is defined by half-cell fragments. Accordingly, the DC KLUKVA Primary Trigger modules provide logical OR signals for the wires in each fragment. In the first layer, the fragments have 3 wires each, while the second layer fragments have 4 and 3 wires each. The wires of the third cell layer of the DC are not used in the trigger to increase the solid angle of the track search.

For the purposes of storing the masks in TP resident memory, the ZC sectors are taken in groups of four, loosely defining sixteen regions of 20 crescents each, 5 for each ZC sector base point. Each crescent, in turn, consists of 12 fragments, two or three from each of the four fragment layers (in the first two DC cell layers), which are stored on a single 4k x 1 RAM chip. So 40 chips accommodate two groups of 4 ZC sectors each on opposite ends of the ZC in the same 40 ns, while 8 such cycles in rotation can accommodate the entire 64 sectors of the ZC in 320 ns. The regions are loosely defined in that neighboring crescents use some of the same neighboring fragments, as is also the case with neighboring regions. This redundancy improves the efficiency of the TP.

In a given colliding beam event then, each active set of ZC sector and DC fragments corresponds to an address in RAM where either a 0 or 1 has been previously set in the trackfinder mask. After the 320 ns TP cycle time, the presence of at least one positive bit is sufficient to generate a 'Track Found' logic pulse. This pulse is used both to generate the common stop signal for digitization and by the mixed trigger.

In the context of the mixed KLUKVA trigger, the ZC and TP status define the flags Z and T respectively. The presence or absence of a ZC sector hit or a track in the TP is indicated by the Z or T flags set high or low, respectively. Three conditions can be handled differently by the mixed KLUKVA trigger:

1.  $Z = 0$  T ignored (No ZC activity implies no start of the TP)

2.  $Z = 1$   $T = 1$  (ZC hit with TP Track Found)
3.  $Z = 1$   $T = 0$  (ZC hit with no TP Track Found).

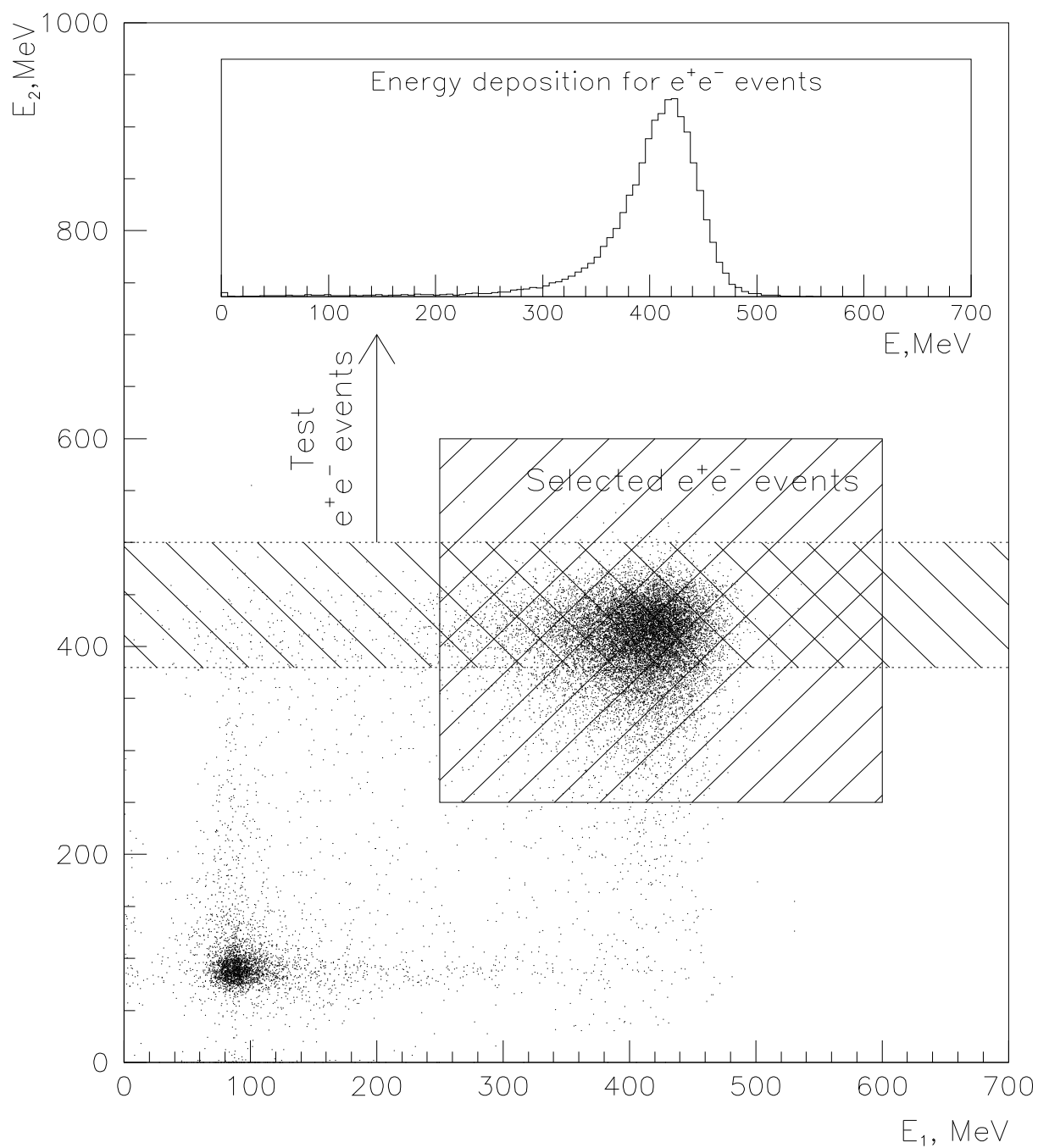


Figure 5: Selection of  $e^-e^+ \rightarrow e^-e^+$  events for the calibration. The  $X$  and  $Y$  axes show energy depositions for two tracks from collinear events, at somewhat more than 800 MeV center of mass energy.

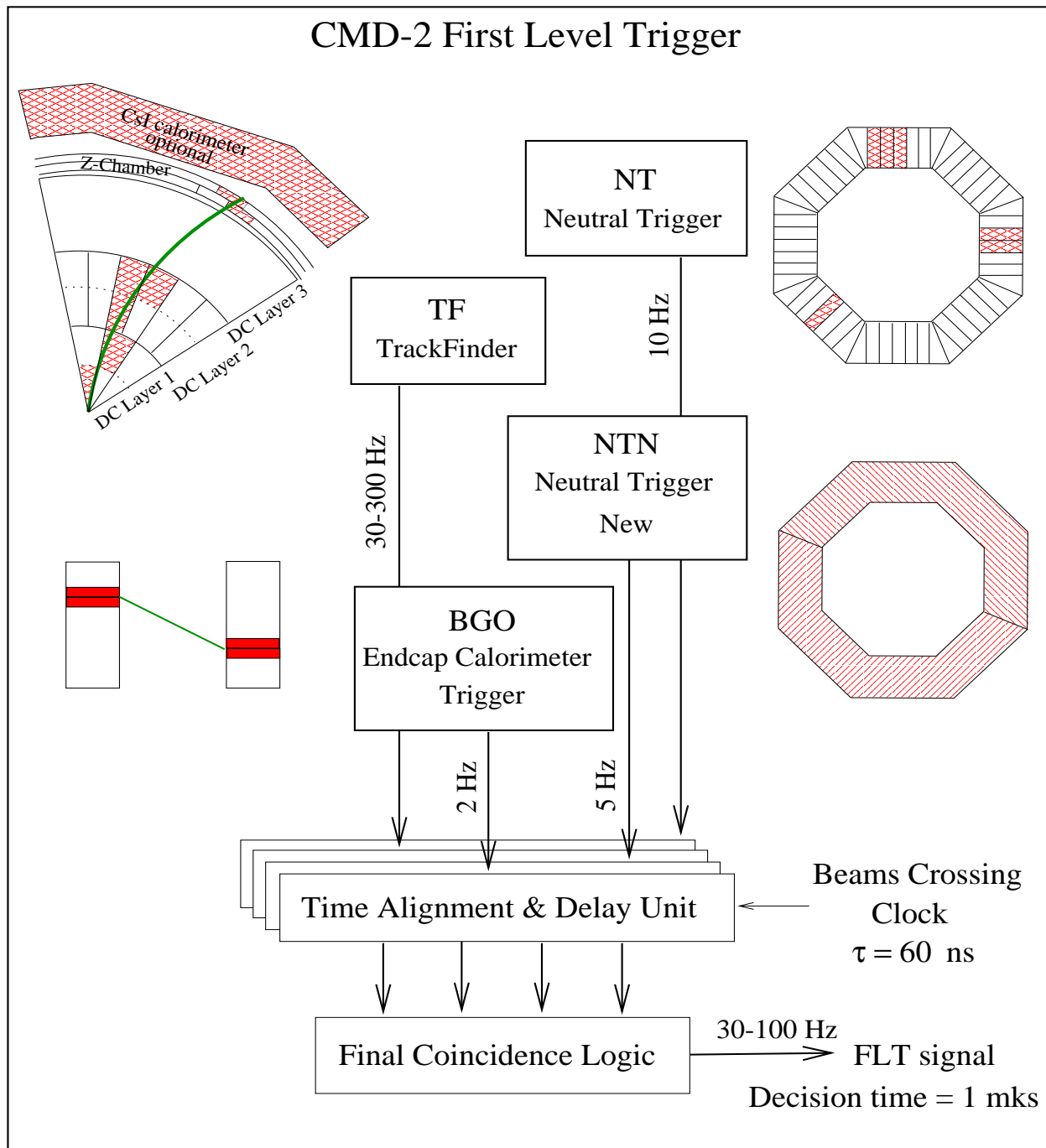


Figure 6: CMD-2 First Level Trigger

## 4.0 DATA TAKING

### 4.1 DATA COLLECTION

The energy range of  $\phi$ -meson was scanned twice: in 1996 and 1998. In 1998 a total of 21 million  $\phi$  events were recorded. We do not use 1996 data because of its low statistics and high systematics.

Table 3 shows numbers of events and total luminosities collected at the energy points used in the analysis. The energies 509.0, 509.5, 510.0, and 510.5 MeV are the  $\phi$ -meson energies at which the  $K^+K^-$  pairs are produced, the energies 492.0 and 502.0 were used for the background checks. Detailed tables with information about each particular run are given in Appendix G.

Table 3: Statistics of the collected data at the beam energy points used in the analysis.

| beam energy, MeV | number of events | total luminosity, $nb^{-1}$ |
|------------------|------------------|-----------------------------|
| 509.0            | 44419244         | 1618.918                    |
| 509.5            | 42143475         | 1545.491                    |
| 510.0            | 39721147         | 1477.744                    |
| 510.5            | 25045421         | 946.823                     |
| 492.0            | 5847585          | 279.161                     |
| 502.0            | 4459995          | 206.609                     |

## 4.2 OFFLINE PROCESSING

The latest version of the offline reconstruction was used in this analysis. When applied to clean  $e^+e^-$  events when the drift chamber was new (about year 1992), the reconstruction efficiency of a single track is approximately 99%. As the chamber aged or for more complicated event topologies the efficiency may be as low as 94%.

## 4.3 EVENT RECONSTRUCTION ALGORITHMS

### 4.3.1 Track Reconstruction

Specifics of the methods and algorithms of track finding and reconstruction changed in the course of the analysis as the understanding of the specifics of the drift chamber improved. Here I present the general overview of the algorithms.

The track finding algorithm uses information from wire hits: their numbers, measured times and amplitudes of the signals to determine the coordinates of the sources of primary ionization. The reconstruction algorithm is similar to that used in the trigger. First, groups are found at the cell level and then these groups are checked for continuity to make a track. The points in the  $R - \phi$  plane are gathered in groups corresponding to the tracks of charged particles. First the fragments of tracks that are contained in one cell are reconstructed. Then, if a certain group of the fragments can be fit by a circle, the fragments are merged into a single track. Taking into account energy loss, from the radius of the fitting circle and the coordinates of its center the program calculates the transverse momentum  $P_{\perp}$ , the charge of the particle, its azimuth angle  $\phi$ , the minimum distance from the circle to the production point in the  $R - \phi$  plane ( $R_{min}$ ) and the deviation of the points from the circle— $\sigma_r$ . If two or more tracks are found, the program looks for vertices. Then points belonging to same track are fit in the  $R - Z$  plane by a spiral. From this fit the polar angle  $\theta$ , the  $Z$ -coordinate nearest to the beam point ( $Z_{min}$ ), and the deviation of the points from the fitting curve ( $\sigma_z$ ) are calculated. For the fit in the  $R - Z$  plane the information from the  $Z$ -chamber is taken into account. Points from two tracks that make up a vertex are fit simultaneously along with

the requirement that the intersection point in the  $R - \phi$  plane has the same  $Z$ -coordinate in both tracks. Information from each reconstructed track is placed in the ZEBRA banks.

### 4.3.2 Reconstruction of Energy Clusters in the Calorimeters

Amplitude and timing information are recorded for all crystals with signal amplitude above a pre-set threshold. With this information, the reconstruction program performs the following:

- Addresses, channel numbers, and amplitudes read from the electronics are used to determine the numbers of the crystals and the energy deposition. For each such crystal, the crystal number used in the reconstruction is calculated from the electronic address and the energy deposition is then recalculated, making use of the calibration coefficients for that crystal.
- Cluster search: a cluster is defined as a group of neighboring crystals in which the deposition exceeds  $E_{min} = 1$  MeV and at least one crystal has deposition greater than 8 MeV. Connected crystals are crystals that touch each other by surface, edge, or angle.
- Calculation of the energy depositions and coordinates of the clusters: energy deposition of a cluster is the sum of the energy depositions in the individual crystals that make up the cluster. The angle of a cluster is the angle of a straight line connecting the vertex and center of mass of the cluster.
- Calculation of the most probable energy and angles of the particle which produced the cluster. It is assumed that the particle is a photon or electron; a correction is provided to account for the larger energy deposition for electrons.

### 4.3.3 Global Reconstruction

When reconstruction of tracks and clusters is finished, the next step is creation of the global reconstruction banks that contain information from all parts of the detector. Each track is projected into the calorimeter region. If the projection falls within the matching angle of a cluster, the track and the cluster are joined, and the energy deposition of the cluster is considered as the energy deposition of the particle that left the track. Clusters that do not match any track are called free clusters and considered as energy depositions by photons.

#### 4.4 SELECTION CRITERIA AND BACKGROUNDS

The decays of  $\phi(1020)$ -meson provide convenient source of the  $K^+K^-$  pairs. The main decay modes of  $\phi(1020)$  are  $K^+K^- - (49.2 \pm 0.7)\%$ ,  $K_LK_S - (33.8 \pm 0.6)\%$ ,  $\rho\pi + \pi^+\pi^-\pi^0 - (15.5 \pm 0.6)\%$ , and  $\eta\gamma - (1.297 \pm 0.033)\%$ . Fig. 7 shows cross section of  $e^+e^- \rightarrow \phi \rightarrow K_S K_L$ . Its peak value is about  $1.4 \mu\text{b}$  which can also be estimated by multiplying the total cross section of  $4.2 \mu\text{b}$  by  $Br(\phi \rightarrow K_S K_L)$ .

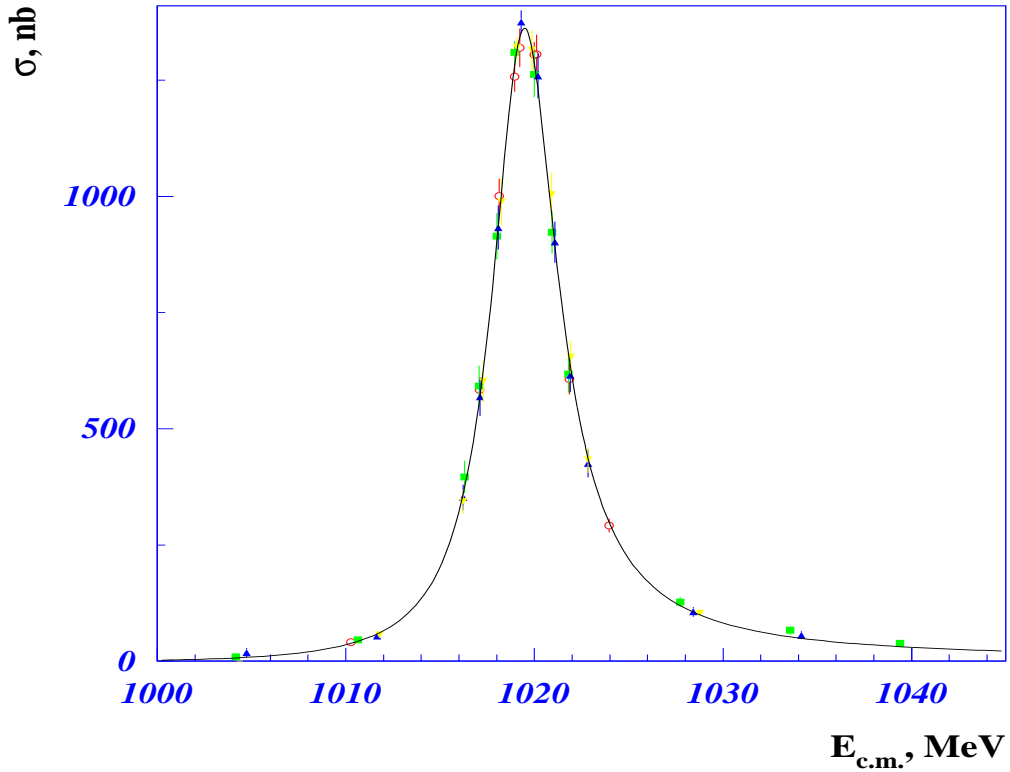


Figure 7:  $\phi$ -meson excitation curve. The plot is taken from [22]. The cross section shown on this plot is that of  $e^+e^- \rightarrow \phi \rightarrow K_S K_L$ . The shown cross section at the peak is the total cross section  $4.2 \mu\text{b}$  times  $Br(\phi \rightarrow K_S K_L)$ , or about  $1.4 \mu\text{b}$ .

This section describes how to separate  $K^+K^-$  pairs from the other decay  $\phi(1020)$  modes and from non-resonance background.

#### 4.4.1 Event Selection

For the purposes of this analysis, events were chosen with one recognized charged particle vertex (with one apparently incoming kaon decaying with only one (apparent) charged particle detected in the final state). Photons were recorded but not required. Both charges of kaons were considered in our analysis, but treated separately as required by the differences in hadronic interactions at these low energies.

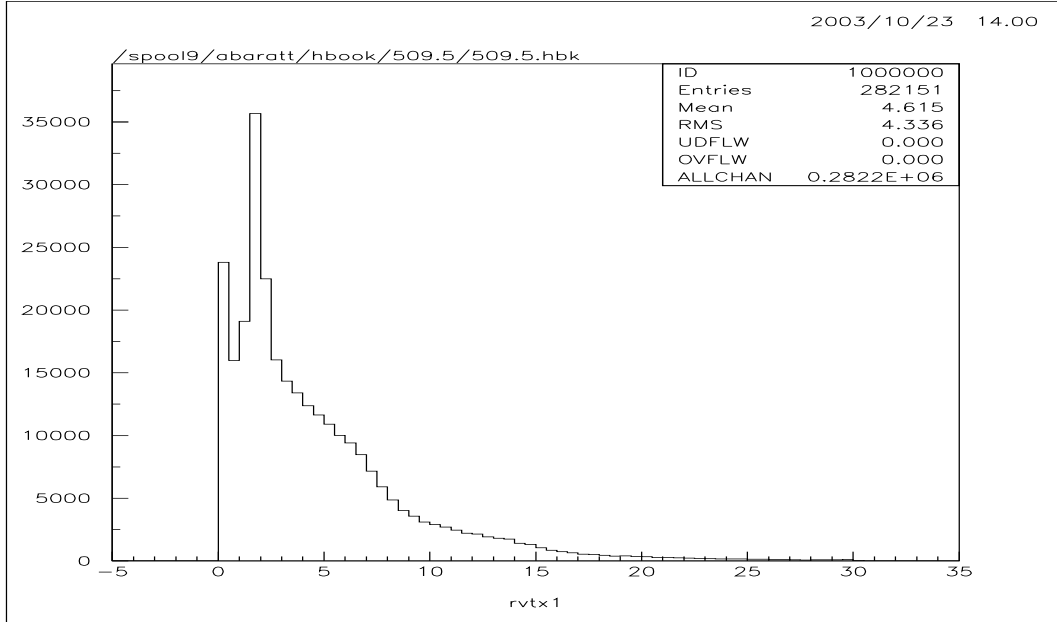


Figure 8: Radial distance from the center of the beam pipe to the vertex ( $R_{vertex_{xy}}$ ) for events that passed the first selection criteria. The beam pipe outer radius is at  $\approx 1.7$  cm.

While the " $\phi$  factory" concept is beautiful in principle, in practice there are contaminations to the kaon decays from interactions of particles with the beam pipe: beam  $e^\pm$ ; produced pions, muons or kaons; or decay products. Figure 8 shows the radial distance from the beam pipe for all events, with minimal selection (after PASS1, discussed below). The excess of events near the position of the beam pipe is evident.

A background which proved to be important for positive kaons is beam scraping by electrons (negative charge) in the beam, interacting with a nucleus. The freed proton mimics a kaon, and the electron mimics a decay particle. This background was studied by looking

at the data taken below the  $\phi$ -resonance, at the beam energies of 492 and 502 MeV. Its radial distribution at 502 MeV is shown in Figure 9. In order to avoid such backgrounds, and others associated with interactions in the beam pipe, in the final analysis we used only events with  $R_{vertex_{xy}}$  between 3 cm and 8 cm.

The analysis was done in stages. The following preliminary (PASS1) cuts were imposed:

1. number of tracks in the  $R - \phi$  plane that make up the vertex equals 2;
2. number of wire hits made by each track is greater than 5;
3. total charge at the vertex is 0 (corresponding to one incident charged track decaying with only one charged track (of the same sign) present in the final state);
4. space angle between the tracks is less than 2.9 rad to remove the background coming from  $K_L K_S$  events;
5.  $Z$ -coordinate of the vertex is between  $-20$  and  $+20$  cm;
6. polar angle  $\theta$  between  $0.45$  and  $\pi - 0.45$  rad (to allow reasonable measurement of the particle angles and momenta);
7. kaon candidate track extrapolation in the  $R - \phi$  plane is within 0.3 cm of the beam intersection point, and the decay candidate track between 0.3 cm and 15 cm. We also call this parameter 'impact parameter in the  $R - \phi$  plane', Fig. 10 shows its distribution;
8. the kaon candidate should have measured momentum between  $-55$  MeV and  $+25$  MeV of the measured central value kaon momentum.

After PASS1 and an additional requirement that the transverse distance of the decay vertex from the beam pipe be between 3 cm and 8 cm, about 300,000 tagged kaon decays were selected (half  $K^+$  and half  $K^-$ ).

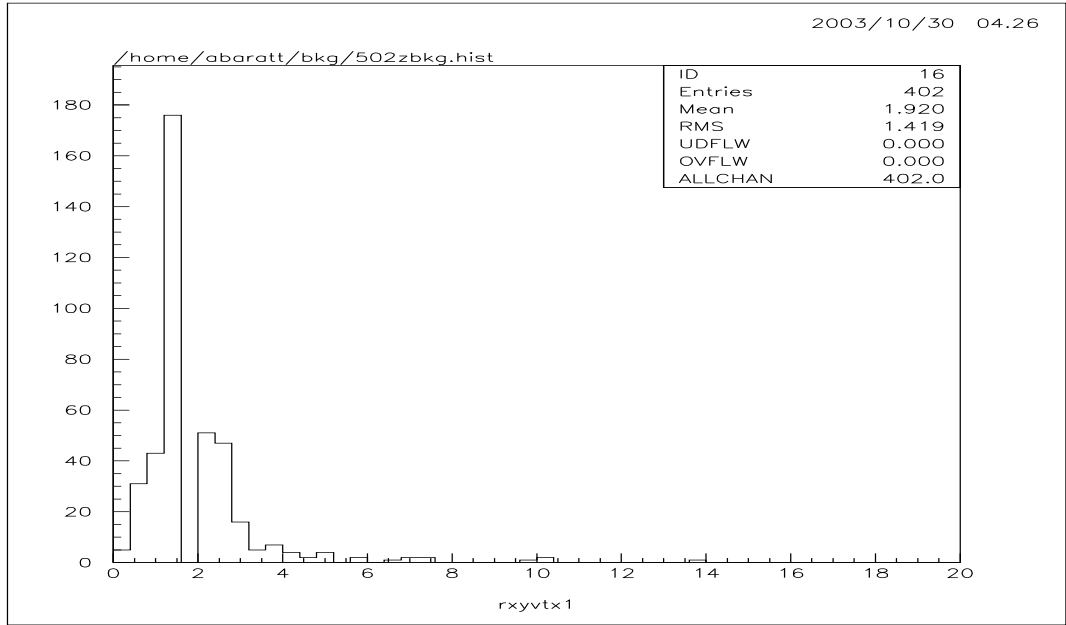


Figure 9: Radial distance from the center of the beam pipe, for background candidates at 502 MeV. The beam pipe outer radius is at  $\approx 1.7$  cm.

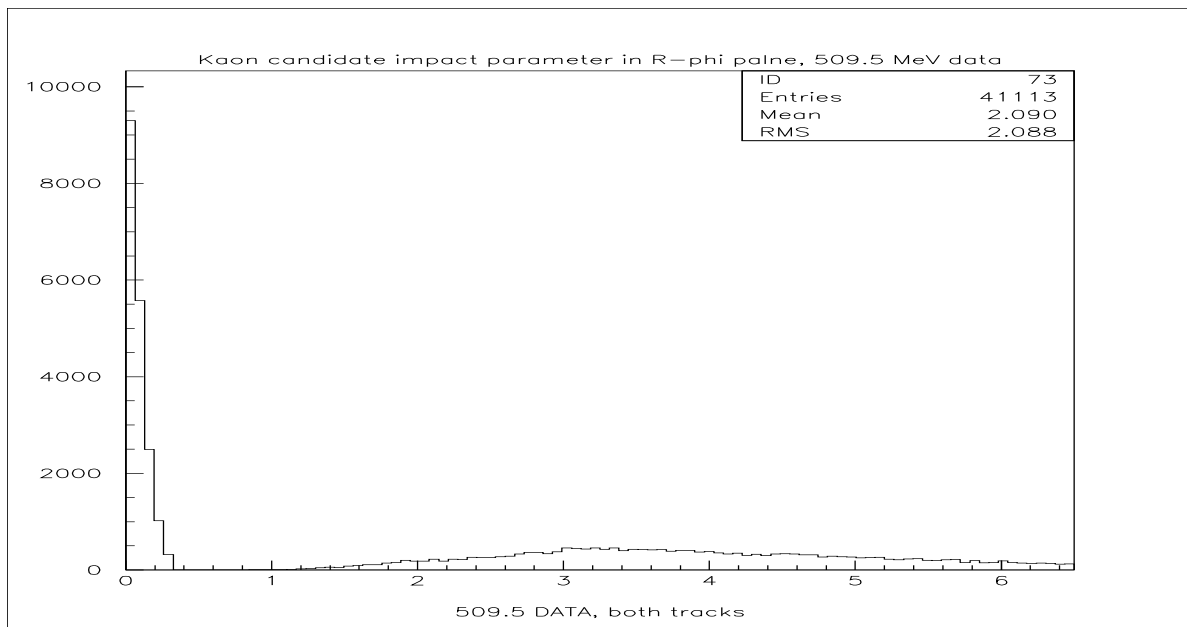


Figure 10: Kaon's candidate impact parameter in  $R - \phi$  plane.

PASS2 tightened these cuts, requiring:

1. there is only one vertex in the event;
2. number of tracks in the  $R-Z$  plane that make up the vertex equals 2 (Fig. 11). Together with requirement 1 from PASS1 it makes sure there are only two tracks in the vertex;

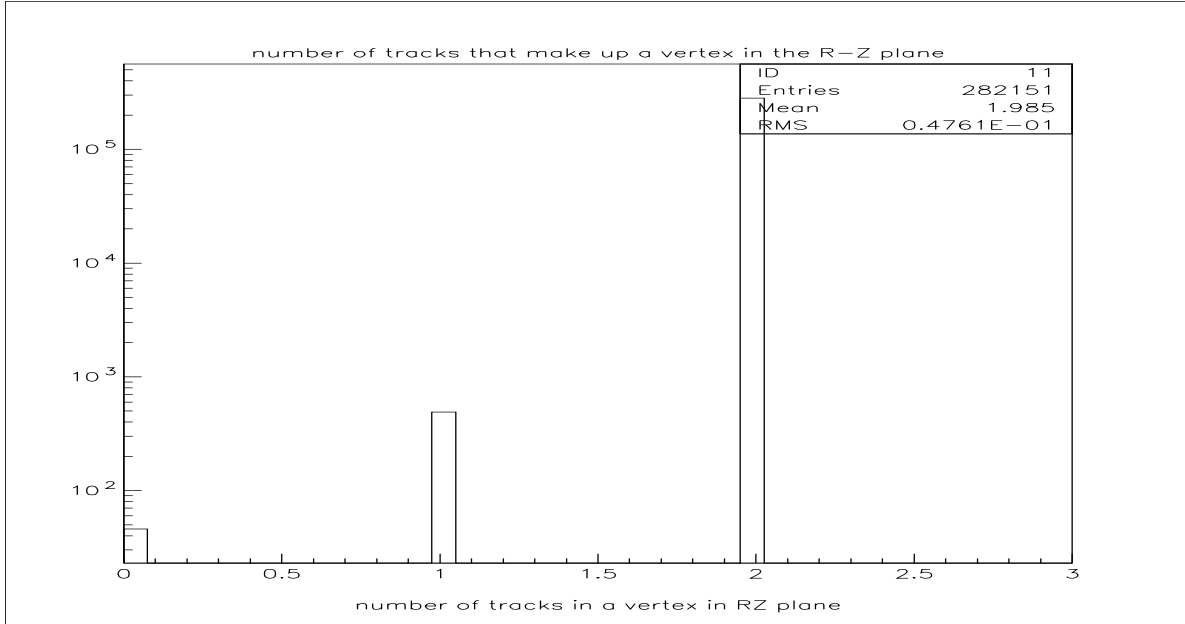


Figure 11: Number of tracks in the  $R-Z$  plane that make up the vertex.

3. the vertex to be of good quality ( $0 < \chi_{z1} < 0.1$ , shown in figure 12, and  $\chi_{r1} < 10$ );
4. the angle between the two tracks in the  $R-\phi$  plane to be between 0.4 and 2.8 radians, and the space angle to be less than 2.6 radians. The plots of the two angles are shown in Figs. 13 and 14;
5. the polar angle  $0.90 < \theta < \pi - 0.90$  for both tracks (to give good angular and momentum resolution in the drift chamber and energy deposit in the CsI calorimeter), figures 15 and 16;
6. the kaon candidate track to be long (the number of the most distant wire being hit by this track is greater than 15, figure 17) and to have momentum within 15 MeV of the central value for the given run's beam energy (to avoid various physical backgrounds, figure 18);

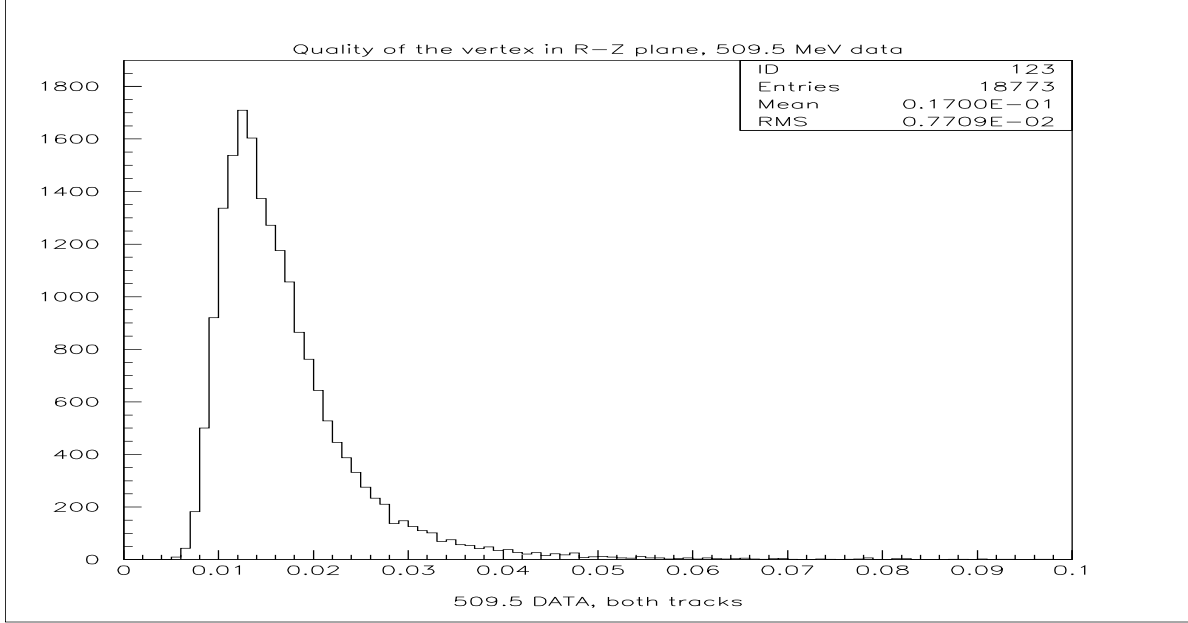


Figure 12: Quality of vertex in the  $R - Z$  plane.

7. the momentum of the decay product candidate to be greater than 75 MeV, the distribution is shown in Fig. 19;
8. the radius of the vertex in the  $R - \phi$  plane to be between 3 cm and 8 cm. Distribution of the radius is shown in Fig. 20;
9. the  $Z$ -coordinate of the vertex to be between  $-7$  and  $+7$  cm. Distribution of the  $Z$ -coordinate is shown in Fig. 21;
10. the radius of the intersection point of two tracks in  $R - \phi$  plane to be either smaller than 28 cm or greater than 32 cm (the inner radius of the DC wall is 30 cm). Some of the events whose radius of the intersection point of two tracks is between 28 cm and 32 cm have one of the kaons decayed at the wall and its decay product mimics the decay product of the kaon that decayed at the vertex. Two examples of such events are in Fig. 22. Fig. 23 shows distribution of the radius of intersection of two tracks, which has a peak around 30 cm which corresponds to the inner radius of the  $Z$ -chamber;
11.  $dE/dx$  of the kaon track to be greater than 5500 KeV cm<sup>2</sup>/g. This cut removes events in which a decay product track was mistakenly interpreted as kaon track. Since  $dE/dx$

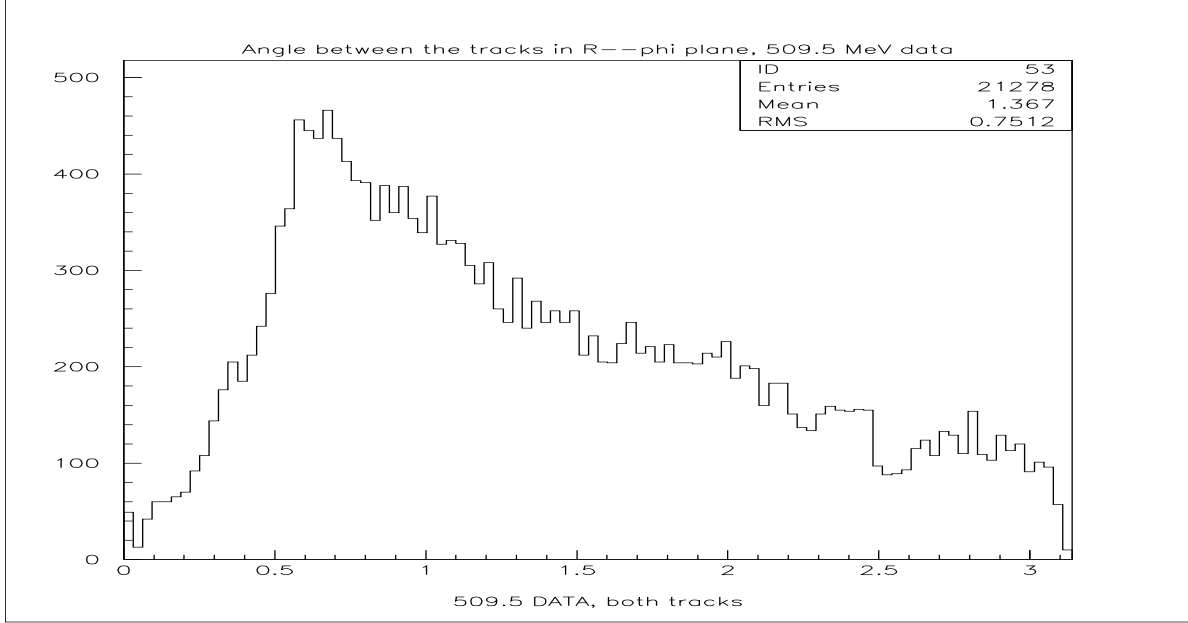


Figure 13: Angle between the tracks in the  $R-\phi$  plane.

is not simulated correctly by our simulation program, I apply this cut to the data only in one version of the analysis and use it in a likelihood manner on both the data and the simulation in another version. Kaon's  $dE/dx$  distribution taken from 510.0 MeV data is shown in Fig. 24, decay product's  $dE/dx$  distribution taken from 509.5 MeV data is shown in Fig. 25

12. cut on qualities of the kaon track in the  $R-\phi$  and the  $R-Z$  planes:  $\sigma_R < 0.045$  and  $\sigma_Z < 0.4$ . These two quantities are not simulated correctly and are used in the same way as the kaon  $dE/dx$  is used (as described above).

Fig 28 shows profile histograms of  $\sigma_R$  and  $\sigma_Z < 0.4$  versus momentum of the decay product. These plots show that there is no correlation between the quality of the kaon track and momentum of the decay product, therefore cuts on  $\sigma_R$  and  $\sigma_Z < 0.4$  do not discriminate against different decay modes and this justifies the application of these cuts to the data only.

In the final analysis additional selection criteria were imposed on both kaon and decay candidate tracks to remove particles with unlikely ionization loss in the drift chamber and

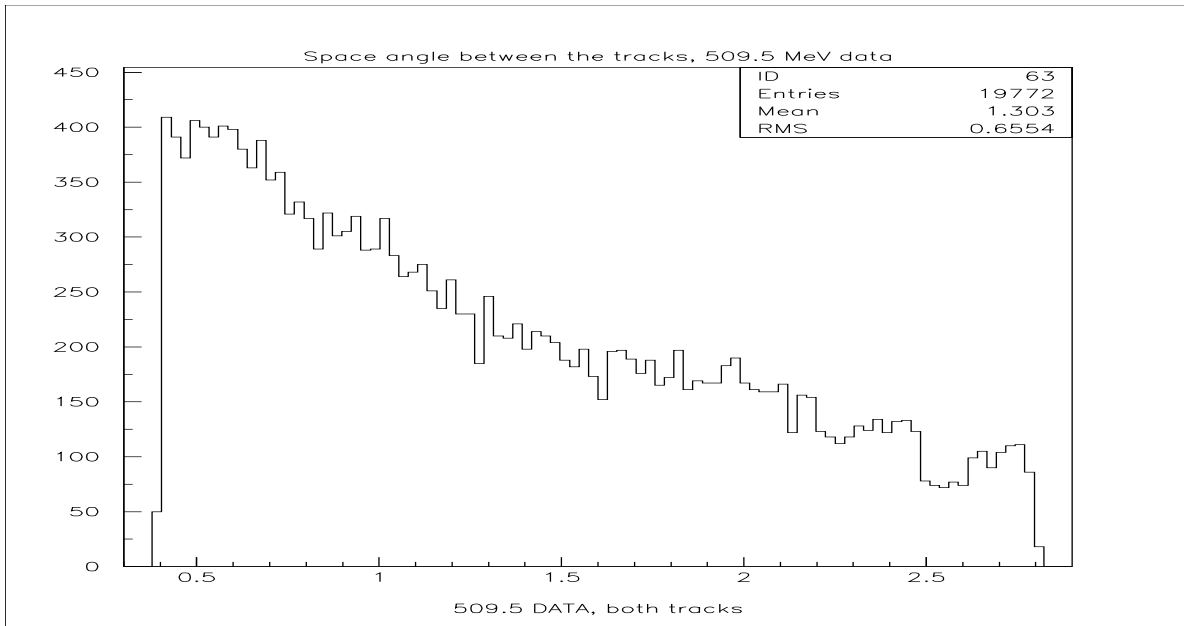


Figure 14: Space angle between the tracks.

to require that the tracks be well measured in both the  $r$  and  $Z$  planes of the drift chamber. Variations in the treatment of these characteristics are discussed under systematic error estimation.

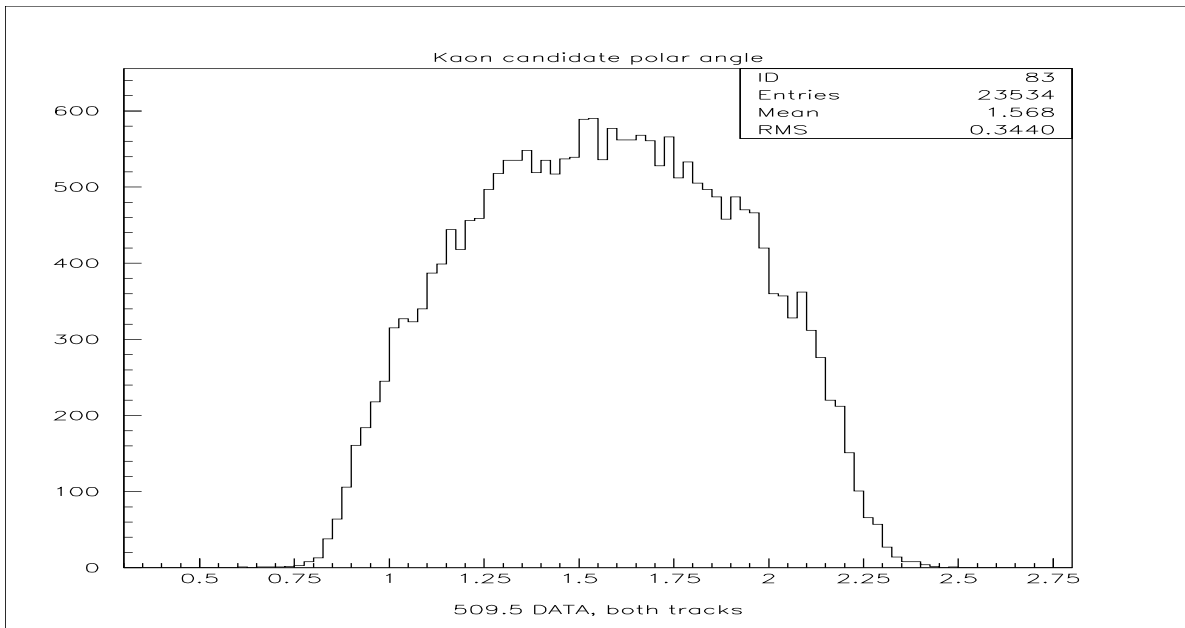


Figure 15: Polar angle distribution for kaon candidate track.

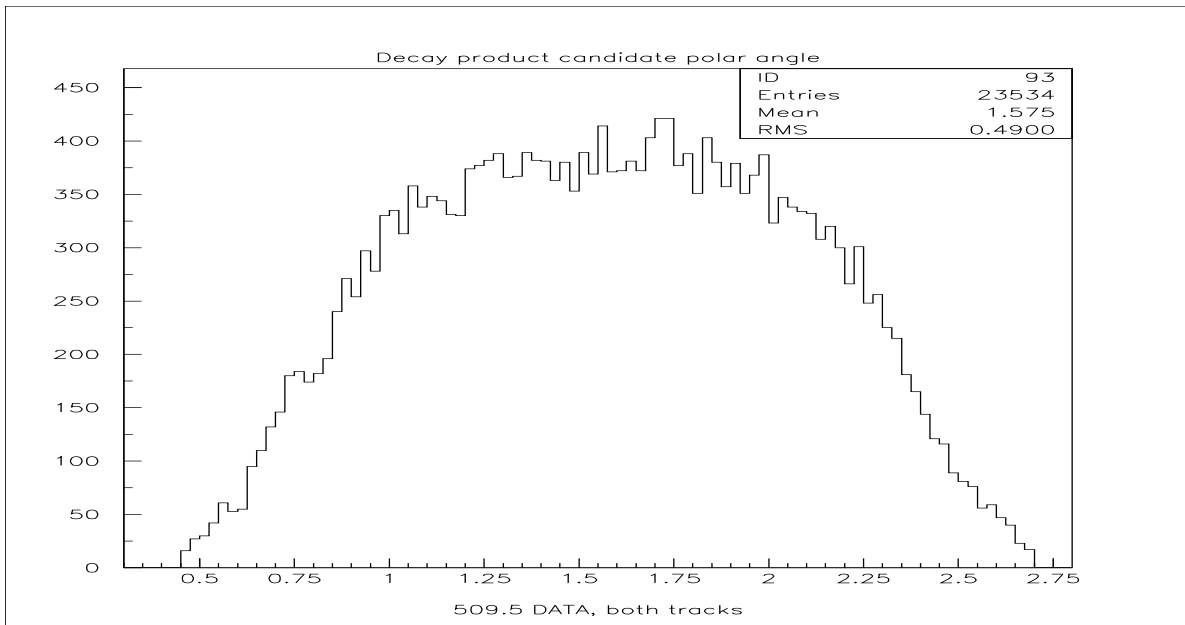


Figure 16: Polar angle distribution for kaon decay product track.

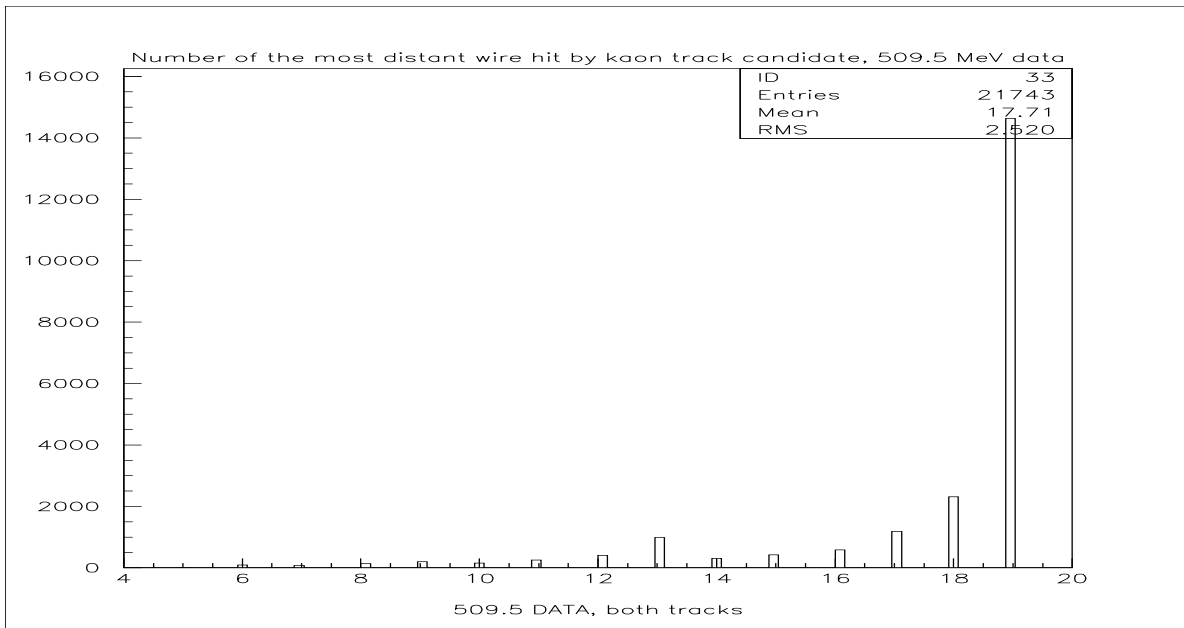


Figure 17: Most distant wire being hit by the kaon candidate track, 509.5 MeV data.

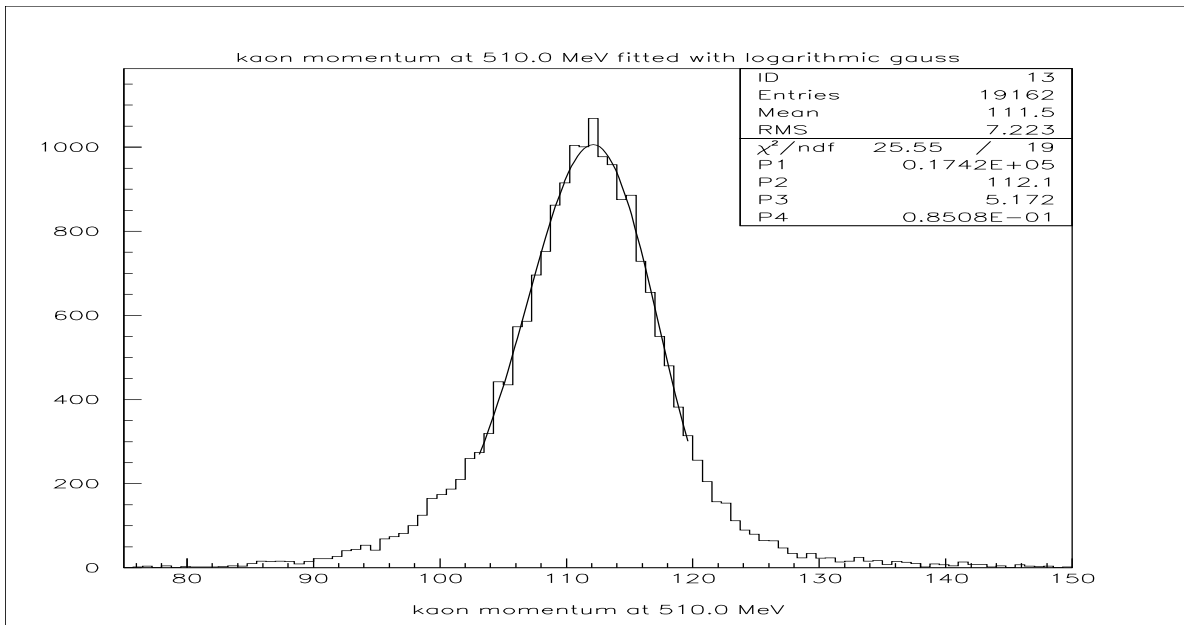


Figure 18: Momentum of the kaon candidate track, 510.0 MeV data.

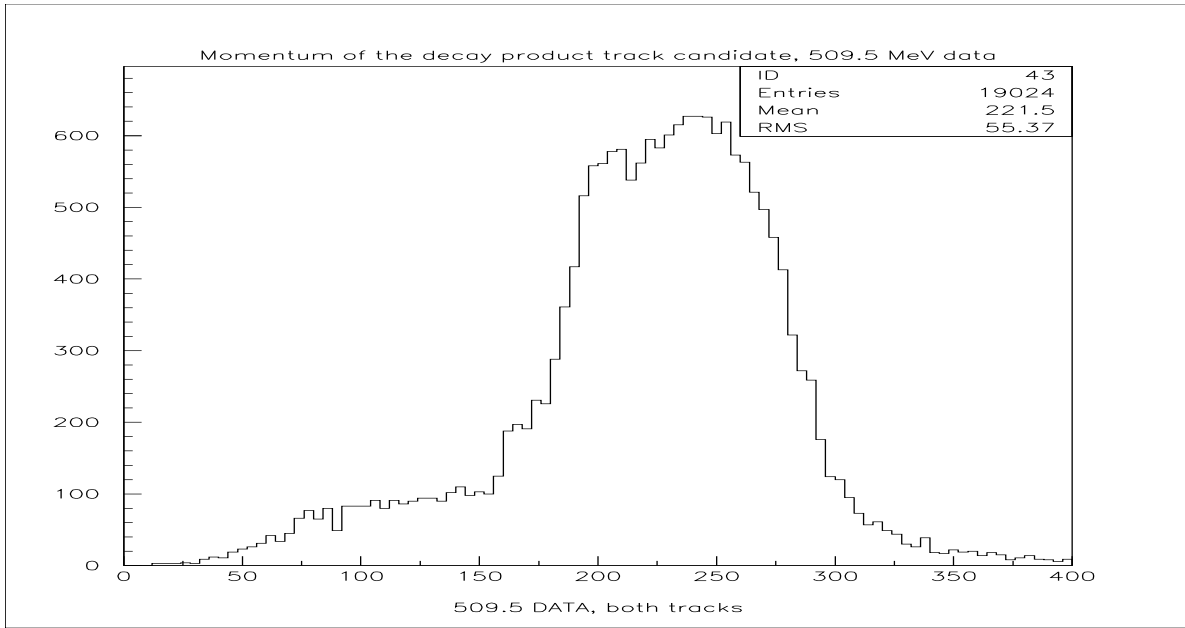


Figure 19: Distribution of the momentum of the decay product candidate, 509.5 MeV data.

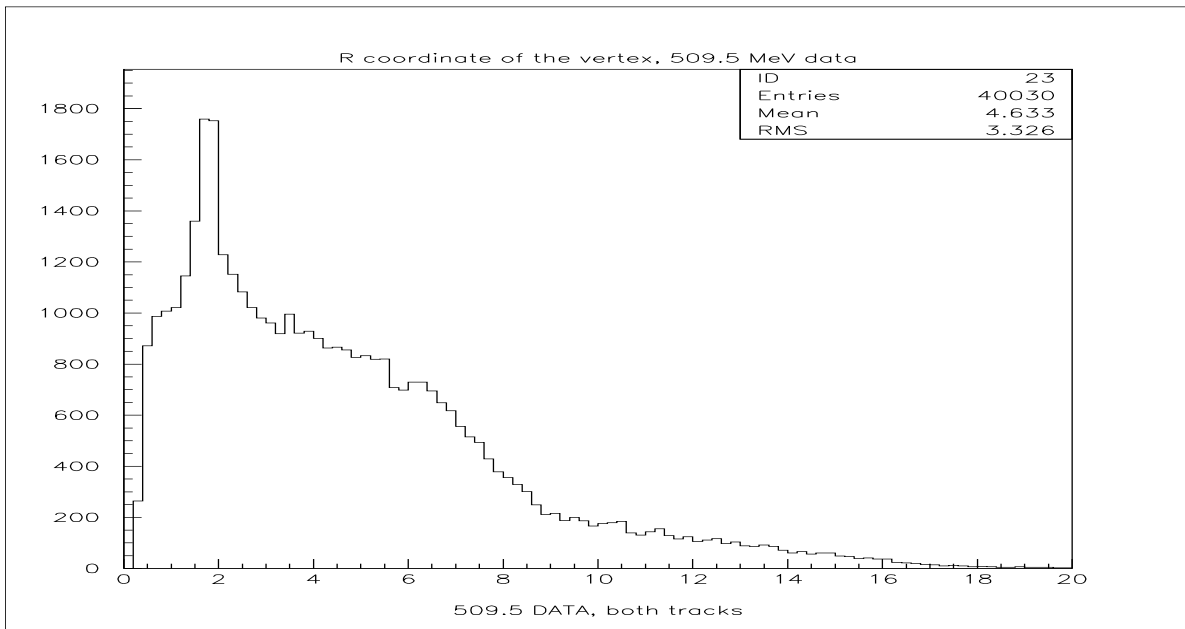


Figure 20: Distribution of the radius of the vertex in  $R - \phi$  plane taken from the 509.5 MeV data.

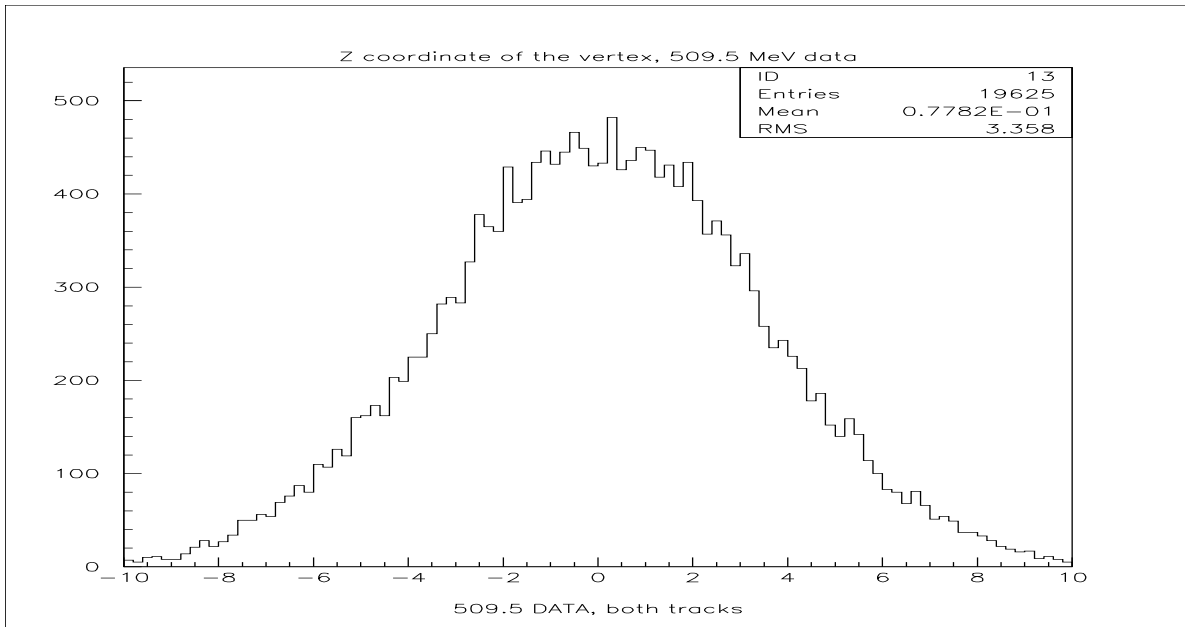


Figure 21: Distribution of the  $Z$ -coordinate of the vertex taken from the 509.5 MeV data.

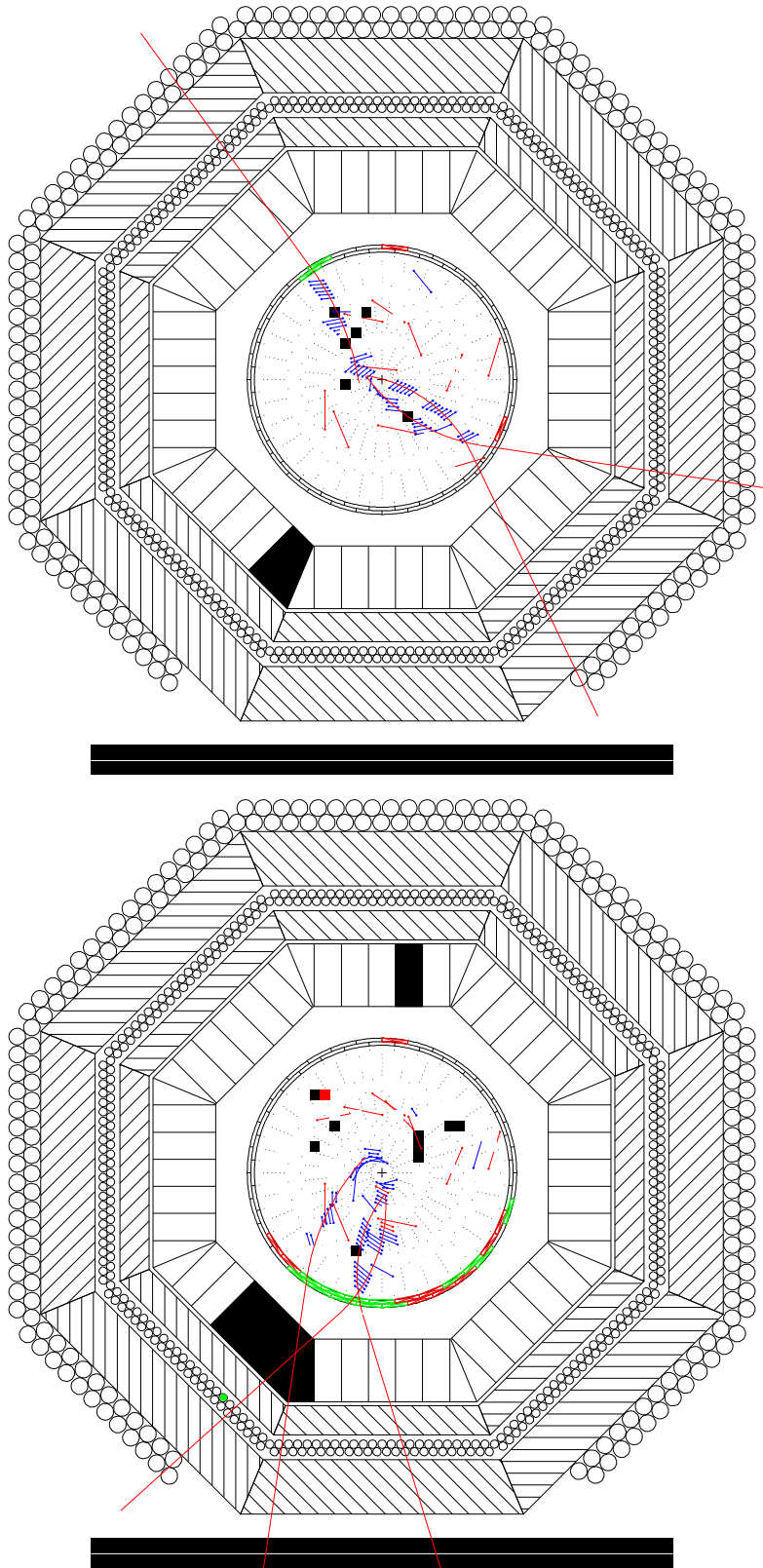


Figure 22: Tagging kaon decaying at the Z-chamber wall

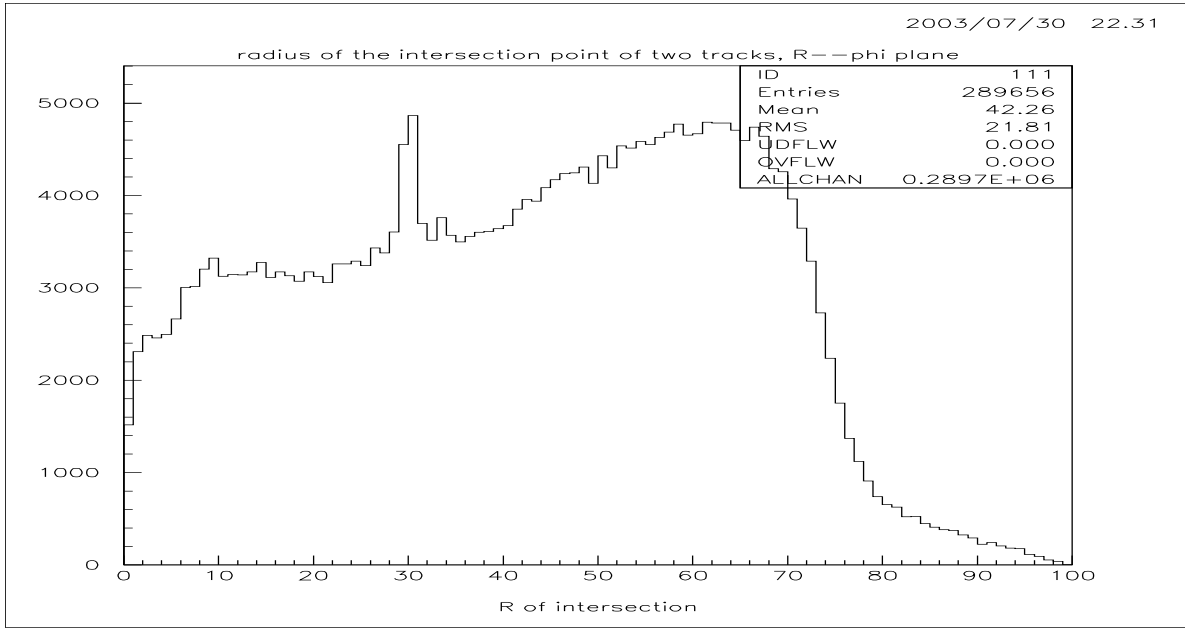


Figure 23: Radial distance from the center of the beam pipe to the intersection point of the two tracks which make up the vertex.

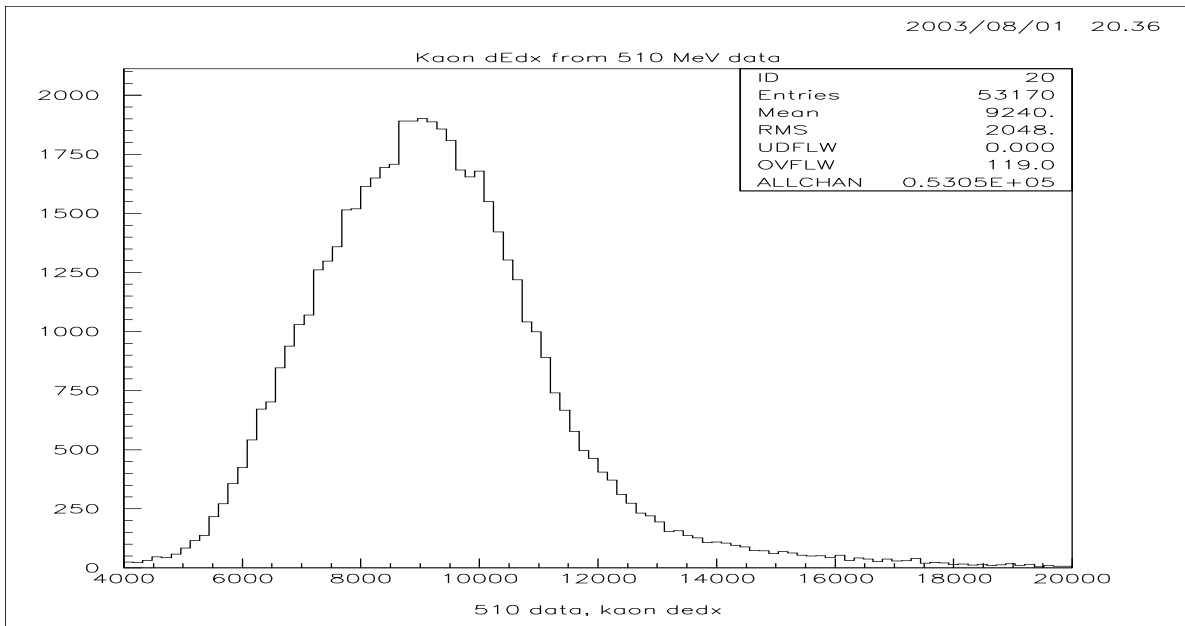


Figure 24: Kaon's  $dE/dx$  distribution from 510.0 MeV data.

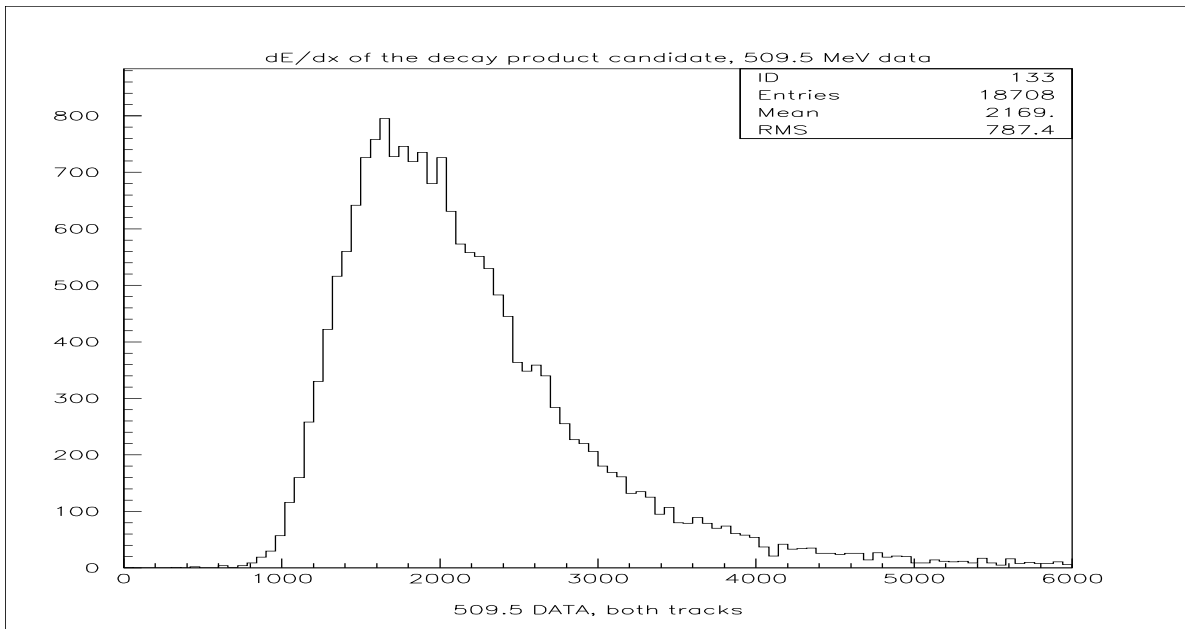


Figure 25: Decay product's  $dE/dx$  distribution from 509.5 MeV data.

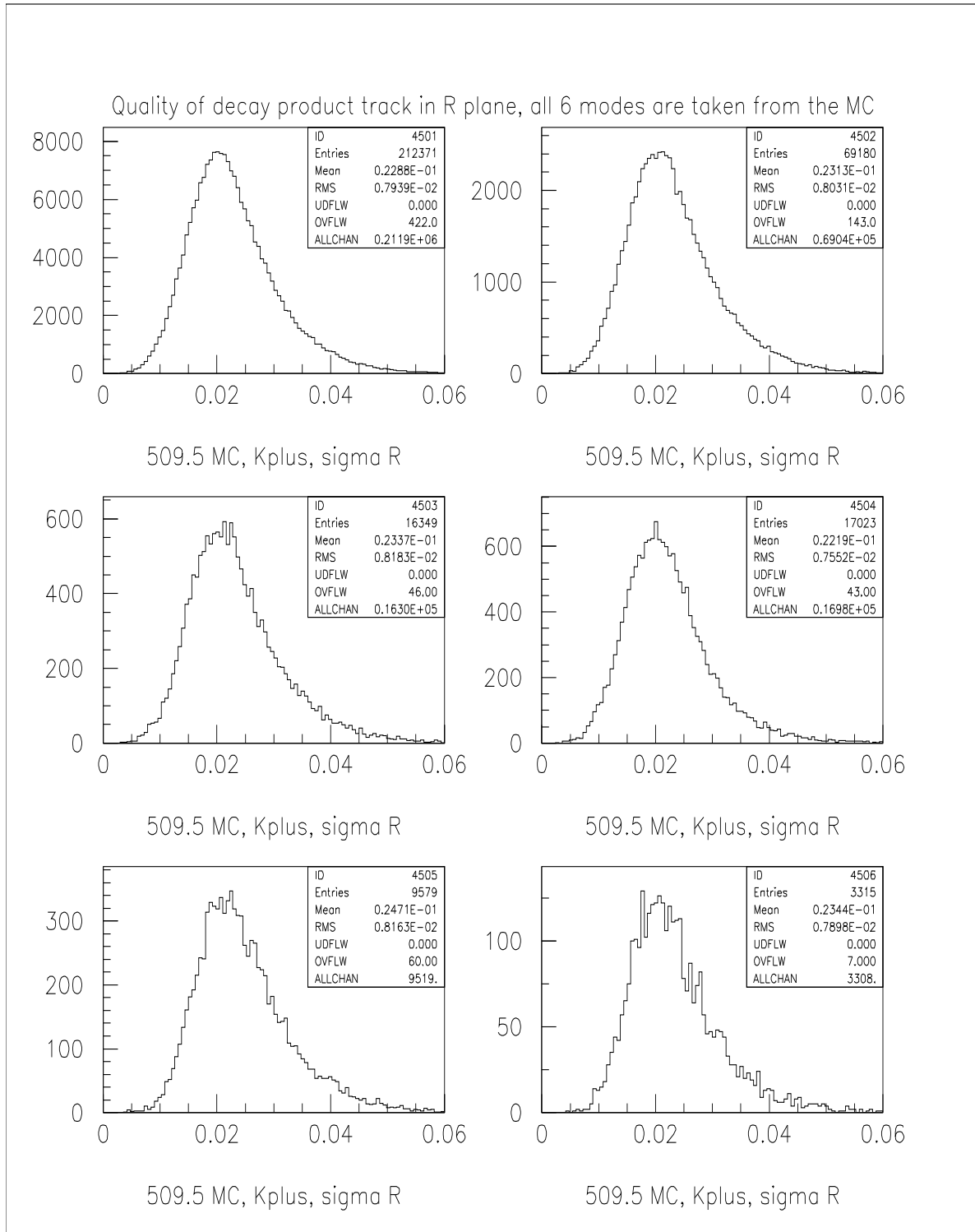


Figure 26: Quality of decay product track in the  $R - \phi$  plane. All 6 decay modes simulated at 509.5 MeV, upper left is  $K^+ \rightarrow \mu\nu$ , upper right is  $K^+ \rightarrow \pi^+\pi^0$ , middle left is  $K^+ \rightarrow \pi^0\mu\nu$ , middle right is  $K^+ \rightarrow \pi^0e\nu$ , lower left is  $K^+ \rightarrow \pi^+\pi^+\pi^-$ , lower right is  $K^+ \rightarrow \pi^+\pi^0\pi^0$ .

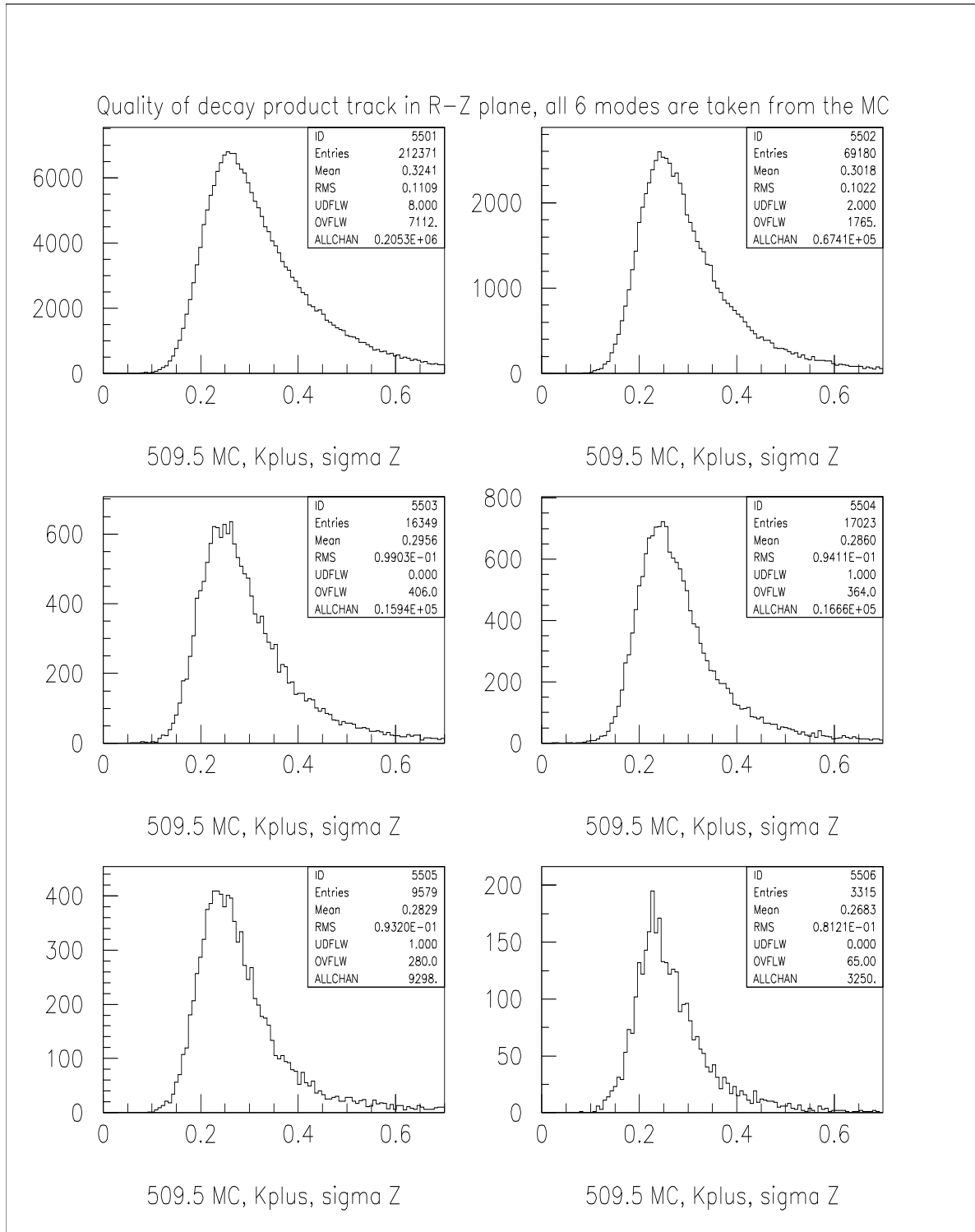


Figure 27: Quality of decay product track in the  $R - Z$  plane. All 6 decay modes simulated at 509.5 MeV, upper left is  $K^+ \rightarrow \mu\nu$ , upper right is  $K^+ \rightarrow \pi^+\pi^0$ , middle left is  $K^+ \rightarrow \pi^0\mu\nu$ , middle right is  $K^+ \rightarrow \pi^0e\nu$ , lower left is  $K^+ \rightarrow \pi^+\pi^+\pi^-$ , lower right is  $K^+ \rightarrow \pi^+\pi^0\pi^0$ .

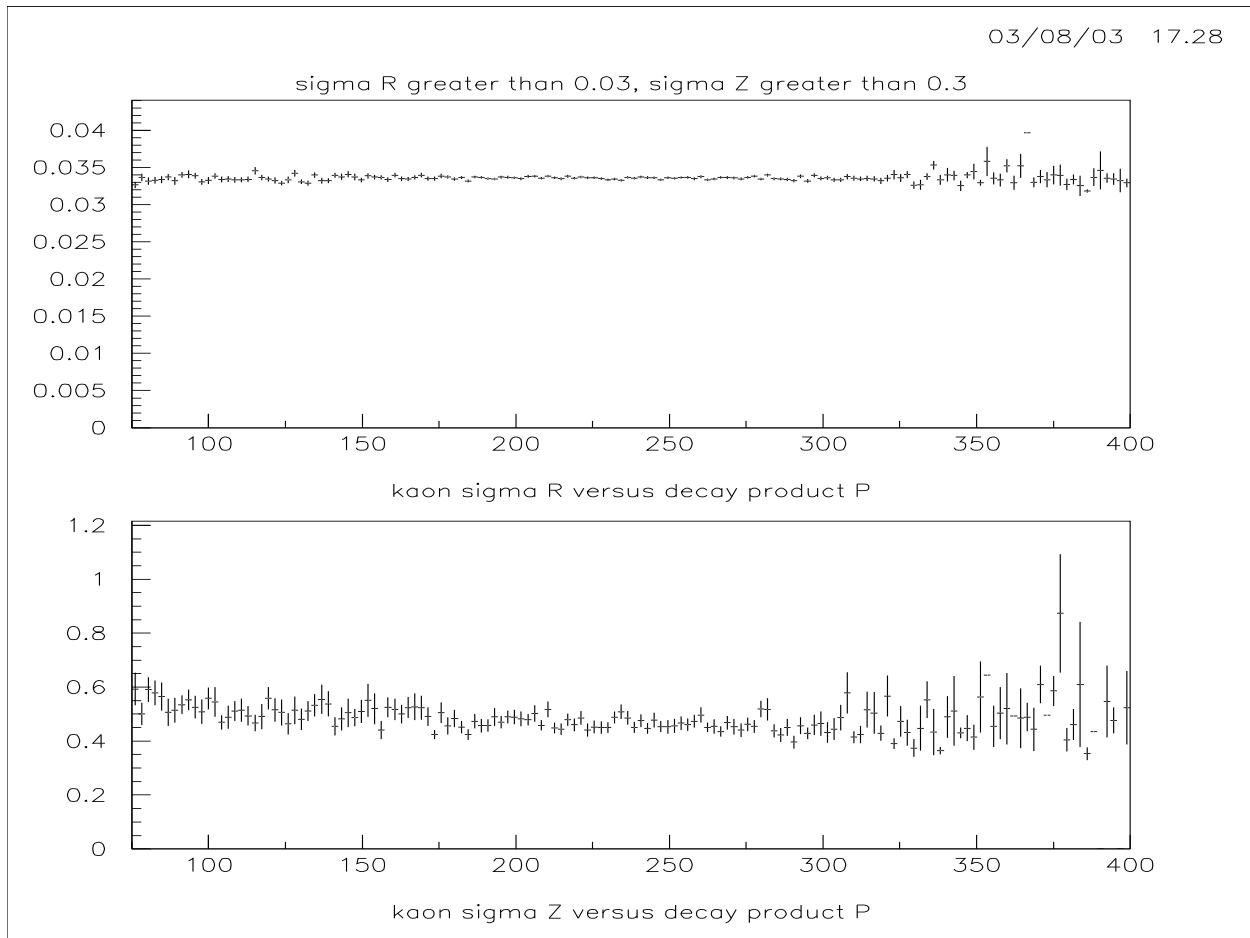


Figure 28: Profile histograms of  $sr_1$  (kaon's track quality in the  $R - \phi$  plane) and  $sz_1$  (kaon's track quality in the  $R - Z$  plane) versus momentum of the decay product. Only tracks with poor quality were used for these histograms:  $sr_1 > 0.03$  for the upper plot and  $sz_1 > 0.3$  for the lower plot.

Table 4 shows the registration efficiencies of the six simulated decay modes when all of the listed selection criteria are applied. The samples of 509.5 MeV with  $K^+$  decaying were used.

Table 4: Registration efficiencies for the six simulated modes at 509.5 MeV,  $K^+$  decaying. All of the listed selection criteria are applied.

| mode                                | registration efficiency |
|-------------------------------------|-------------------------|
| $K^+ \rightarrow \mu^+ \nu$         | 0.00998                 |
| $K^+ \rightarrow \pi^+ \pi^0$       | 0.00974                 |
| $K^+ \rightarrow \mu^+ \pi^0 \nu$   | 0.00771                 |
| $K^+ \rightarrow e^+ \pi^0 \nu$     | 0.00791                 |
| $K^+ \rightarrow \pi^+ \pi^+ \pi^-$ | 0.00439                 |
| $K^+ \rightarrow \pi^+ \pi^0 \pi^0$ | 0.00453                 |

Table 5 shows the effect of selection criteria on our data statistics.

Table 5: Effect of data selection cuts on the data statistics. The numbers in this table are scaled from a sample of events of beam energy 509.5 MeV (this energy provides about a third of the total event sample. Results from other beam energies on the  $\phi$  resonance are similar). The removal of events with small radial distance from the beam removes  $K_S$  decays to two pions and also interactions in the beam pipe. Other cuts are intended to require well-measured events.

| Selection Criterion                                                                  | Remaining Sample Size |
|--------------------------------------------------------------------------------------|-----------------------|
| Produced $K^\pm = \mathcal{L} \times \sigma_\phi \times Br(\phi \rightarrow K^+K^-)$ | $\approx 10$ million  |
| Decay vertex 3-8 cm from beam pipe                                                   | $\approx 680,000$     |
| PASS1 cuts                                                                           | $\approx 300,000$     |
| PASS2 cuts                                                                           | $\approx 150,000$     |
| $K^+$ decays in this analysis                                                        | 75,000                |

#### 4.4.2 Presence of $\pi^0$ Requirement

Requiring presence of  $\pi^0$  reduces background.  $\pi^0$  is reconstructed by checking all possible combinations of pairs of photons available in given event. The pair that has invariant mass closest to  $m_{\pi^0}$  is taken as the one that was produced by decay of  $\pi^0$ . However, the sample of events with reconstructed  $\pi^0$  is contaminated by events in which a wrong pair of photons was picked: it happens when one or two photons in the pair come from processes different from  $\pi^0$  decay. Reducing the number of noise photons reduces the number of misreconstructed pions. In this analysis we discriminated against noise photons by additional requirement that the photons have momentum above 40 MeV and polar angle between 0.85 and 2.3 radians. The distributions of reconstructed masses without and with the additional requirement are shown in figure 29.

In table 6 effect of the  $\pi^0$  requirement on the background is compared with some other background reducing cuts. The beam energies 492.0 and 502.0 MeV are far off the  $\phi$ -meson resonance and no creation of  $K^+ K^-$  pair is possible; therefore, the events from these energies that pass through our cuts are pure background. In table 6 the following cuts are considered:

1. standard set of cuts discussed before (including  $1.7 < R_{vertex} < 2.2$ );
2. standard set of cuts with  $3 < R_{vertex}$  with the kaon track cuts: cuts on kaon's  $dE/dx$  and kaon's qualities of track;
3. standard cuts with the presence of  $\pi^0$  requirement;
4. standard cuts with the presence of  $\pi^0$  requirement where  $\pi^0$  is constructed from two photons that pass tougher selection cuts:  $\theta$  angle of each photon is between 0.85 and 2.3 radians and momentum of each photon is greater than 40 MeV. Figures 30–32 illustrate how these selection criteria reduce number of the noise photons.

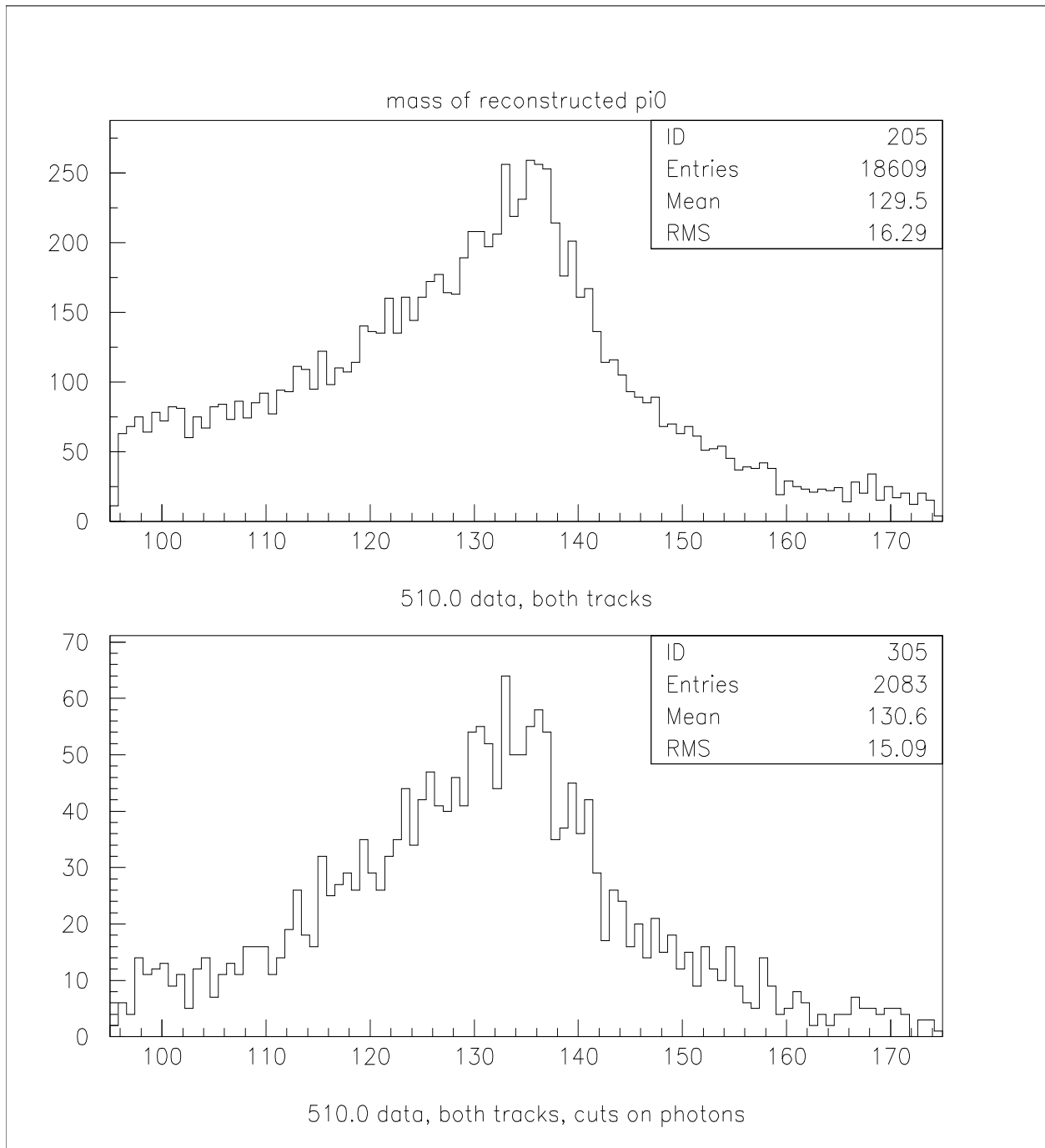


Figure 29: Mass distributions of reconstructed  $\pi^0$ . The lower plot obtained with additional requirement that the photons have momentum above 40 MeV and polar angle between 0.85 and 2.3 radians. Only one  $\pi^0$  combination is plotted per event.

Table 6: Effects of the  $R_{vertex}$  cut,  $\pi^0$  requirement, and cuts that reduce the number of the 'noise' photons.

|                                                               | 492.0 MeV |       | 502.0 MeV |       | 510.0 MeV |       |
|---------------------------------------------------------------|-----------|-------|-----------|-------|-----------|-------|
| luminosity                                                    | 279.2     |       | 206.6     |       | 1477.7    |       |
|                                                               | $K^+$     | $K^-$ | $K^+$     | $K^-$ | $K^+$     | $K^-$ |
| standard cuts                                                 | 2         | 223   | 6         | 396   |           |       |
| standard cuts, $3 < R_{vertex}$ ,<br>kaon track cuts          | 0         | 16    | 0         | 19    | < 7       | 110   |
| standard cuts, $\pi^0$ requirement                            | 0         | 37    | 0         | 56    |           |       |
| standard cuts, $\pi^0$ requirement,<br>$\gamma$ 's not in bkg | 0         | 2     | 0         | 6     | < 7       | 30    |
| conditions 2 and 4 combined                                   | 0         | 0     | 0         | 1     | < 7       | 3     |

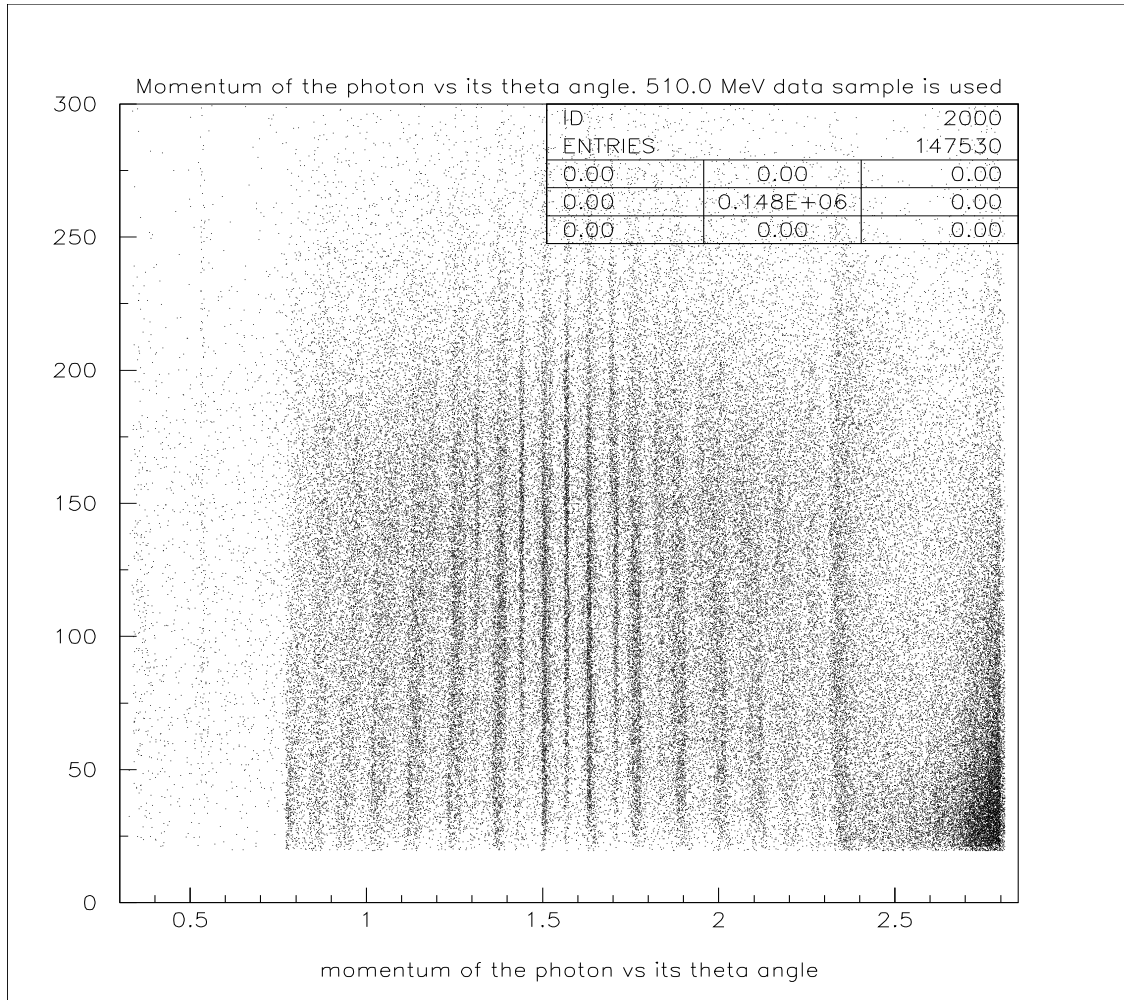


Figure 30: Photon's momentum vs its  $\theta$  angle from 510.0 MeV data sample. The vertical striations on the plot are caused by the calorimeter granularity.

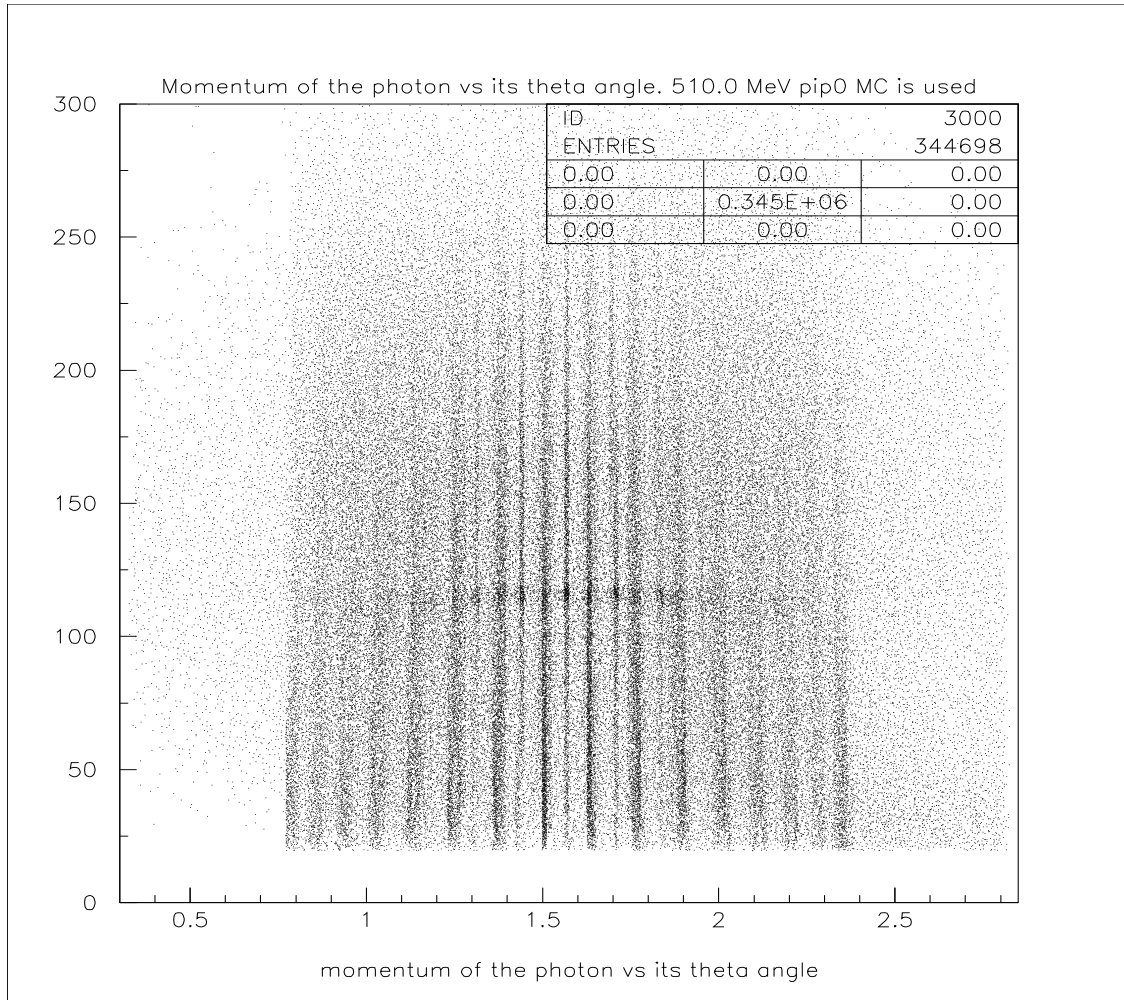


Figure 31: Photon's momentum vs its  $\theta$  angle from 510.0 MeV  $K^+ \rightarrow \pi^+\pi^0$  simulation. The vertical striations on the plot are caused by the calorimeter granularity.

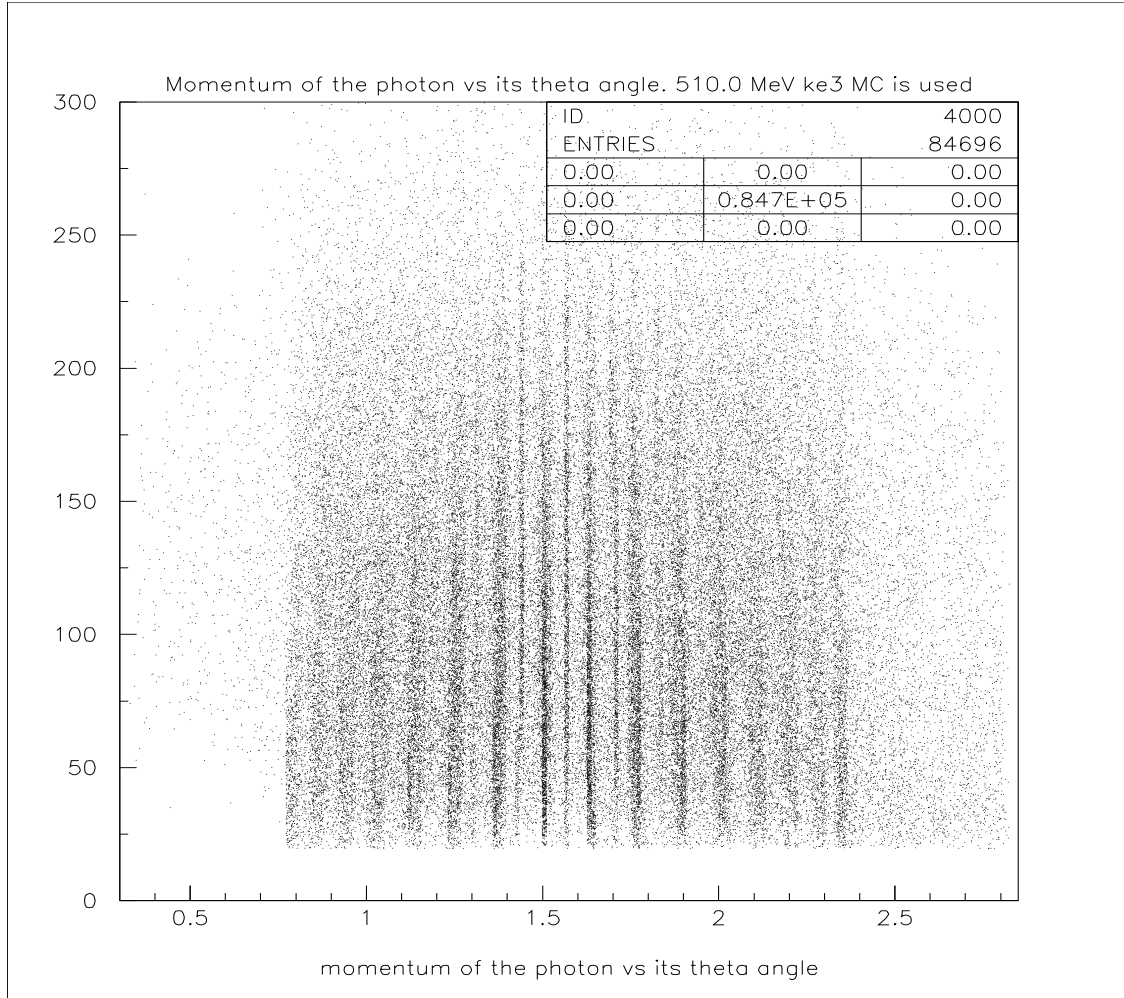


Figure 32: Photon's momentum vs its  $\theta$  angle from 510.0 MeV  $K^+ \rightarrow \pi^0 e^+ \nu$  simulation. The vertical striations on the plot are caused by the calorimeter granularity.

### 4.4.3 Background Estimates

The most serious background comes from interactions or scattering in the beam pipe or beam gas. As discussed above, this background was substantially removed for  $K^+$  decays by the requirement of  $R_{vertex_{xy}}$  between 3 and 8 cm.

Two other candidates for the background are  $\phi \rightarrow K_L K_S$  with subsequent  $K_S \rightarrow \pi^+ \pi^-$  and  $\phi \rightarrow \pi^+ \pi^- \pi^0$ . For the estimate of the background from  $\phi \rightarrow K_L K_S$  we used a simulated sample of  $6.3 \times 10^6$  events. The main discrimination against the  $K_L K_S$  background comes from the  $3 < R_{vertex_{xy}} < 8$  cut. The  $R_{vertex_{xy}}$  distribution for the sample of  $K_L K_S$  events at 509.0 MeV is shown in figure 33. The reconstruction efficiency for such events is found to be  $0.146 \times 10^{-4}$  while the average reconstruction efficiency of charged kaon decay is 0.013. Therefore we estimate that in a given sample of  $\phi$ -meson decays

$$\frac{N_{K_L K_S}}{N_{K^+ K^-}} = 7.7 \times 10^{-4} \quad (4.1)$$

On the missing mass plot about half of the  $K_L K_S$  background is located in the predominantly  $K \rightarrow \pi \pi^0$  region while another half is in the predominantly semileptonic region. Since semileptonic decays make up about 8% of charged kaons decays, the  $K_L K_S$  background makes up about 0.5% of the semileptonic signal. This estimate was done with an  $R_{vertex_{xy}}$  requirement of greater than 2 cm, and will be further reduced with our final selection criteria.

The background from  $\phi \rightarrow \pi^+ \pi^- \pi^0$  is also estimated from MC simulation and it is found that this background does not make more than 0.1% of the entire  $K^+ K^-$  sample. The main discriminator against this sort of background is the requirement that one of the tracks has impact parameter in the  $R - \phi$  plane less than 0.3 cm while that of the other track is greater than 0.3 cm. The impact parameter of the charged pion tracks is similar to that of the charged kaon events. The missing mass distribution of the  $\phi \rightarrow \pi^+ \pi^- \pi^0$  events is uniform. As for the  $K_L K_S$  backgrounds, this estimate was done with  $R_{vertex_{xy}}$  greater than 2 cm, and will be further reduced with our final selection criteria.

The absence of background was checked by comparing the Z distribution for data and simulated events. Remaining events beyond  $|Z_{vertex}|$  of 10 cm were negligible, and showed no particular tendency to clump in any particular kinematic region. Comparable fractions of

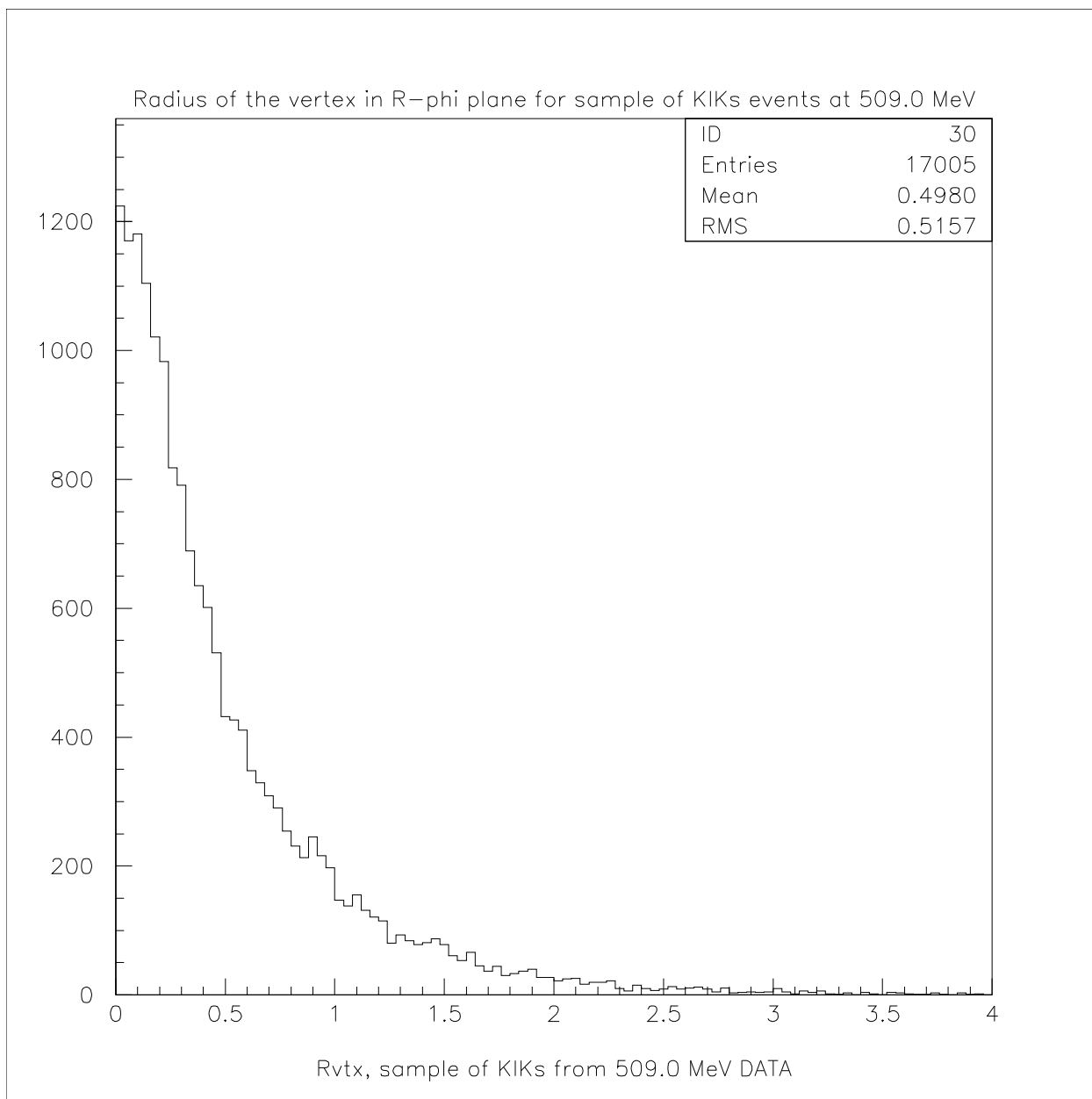


Figure 33: Radius of the vertex in  $R-\phi$  plane for the sample of  $K_L K_S$  events at 509.0 MeV.

events in the data and simulation showed  $|Z_{vertex}|$  beyond 10 cm from the nominal interaction point. Figure 34 shows the  $Z_{vertex}$  distribution for  $K^+K^-$  data at 509.6 MeV.

**4.4.3.1 Beam–Gas Background** A more or less precise estimate of how many  $e^- + N \rightarrow e^- + p^+ + N'$  events can mimic  $K^\pm$  events would be a very difficult task. Here I give some rough estimate to show that the number of the observed background events is consistent with what one might expect from the residual gas background.

The expected number of the protons can be written as

$$N_p = \frac{I}{e} t \sigma N_{nuc} l \epsilon \quad (4.2)$$

where  $I$  is an average beam current,  $e$  – electron charge,  $t$  – total acquisition time,  $l = 40\text{cm}$  – fiducial length,  $\sigma$  – cross section for knocking off a proton,  $N_{nuc}$  – effective density of the protons,  $\epsilon = 0.03$  – detection efficiency estimated from the charged kaon decay simulation. For the samples with beam energies of 492 and 502 MeV the average beam currents are 43.2 mA and 45.7 mA, correspondingly. Total acquisition time is  $1.05 \cdot 10^8$  sec. and  $8.03 \cdot 10^7$  sec., correspondingly. I assume that each electron–nucleus interaction knocks off a proton.

To estimate  $N_{nuc}$  I use  $P = nkT$  with  $T = 300\text{K}$  and  $P = 3 \pm 2\text{nTorr}$ . The latter is taken from direct measurement. This leads to  $N_{nuc} = 9.7 \cdot 10^{13}/m^3$ . The expected composition of the residual gas is [23]  $H_2 - 30\%$ ,  $CH_4 - 10\%$ ,  $CO - 20\%$ , and  $CO_2 - 40\%$ . Thus, on the average each nucleus contains 13.2 protons. To estimate  $\sigma$ , I use the Mott formula to calculate the electron–proton cross section (though Mott formula implies spinless target its use is adequate for targeted precision) and multiply it by 13.2.

$$\frac{d\sigma}{d\Omega} = \frac{\alpha^2}{4|\vec{p}|^2 \beta^2 \sin^4(\theta/2)} \left( 1 - \beta^2 \sin^2 \frac{\theta}{2} \right) \quad (4.3)$$

Since I am trying to estimate the background at the beam energy of 510 MeV we used the cut  $73 < P_{tagging} < 153$  MeV/c. Using simple scattering kinematics we found that these momentum limits translate into  $1.34 < \theta < 1.46$ . Integrating eq (4.3) over  $0 < \phi < 2\pi$  and  $1.34 < \theta < 1.46$  we obtain  $\sigma = 0.05\mu$  barn for 492 MeV and 502 MeV electrons. Then from eq (4.2) we get 2178 events for 492 MeV and 1762 events for 502 MeV. The numbers that we observe are 225 for 492 MeV and 402 for 502 MeV. Here I list some potential sources of the systematic error of this estimation:

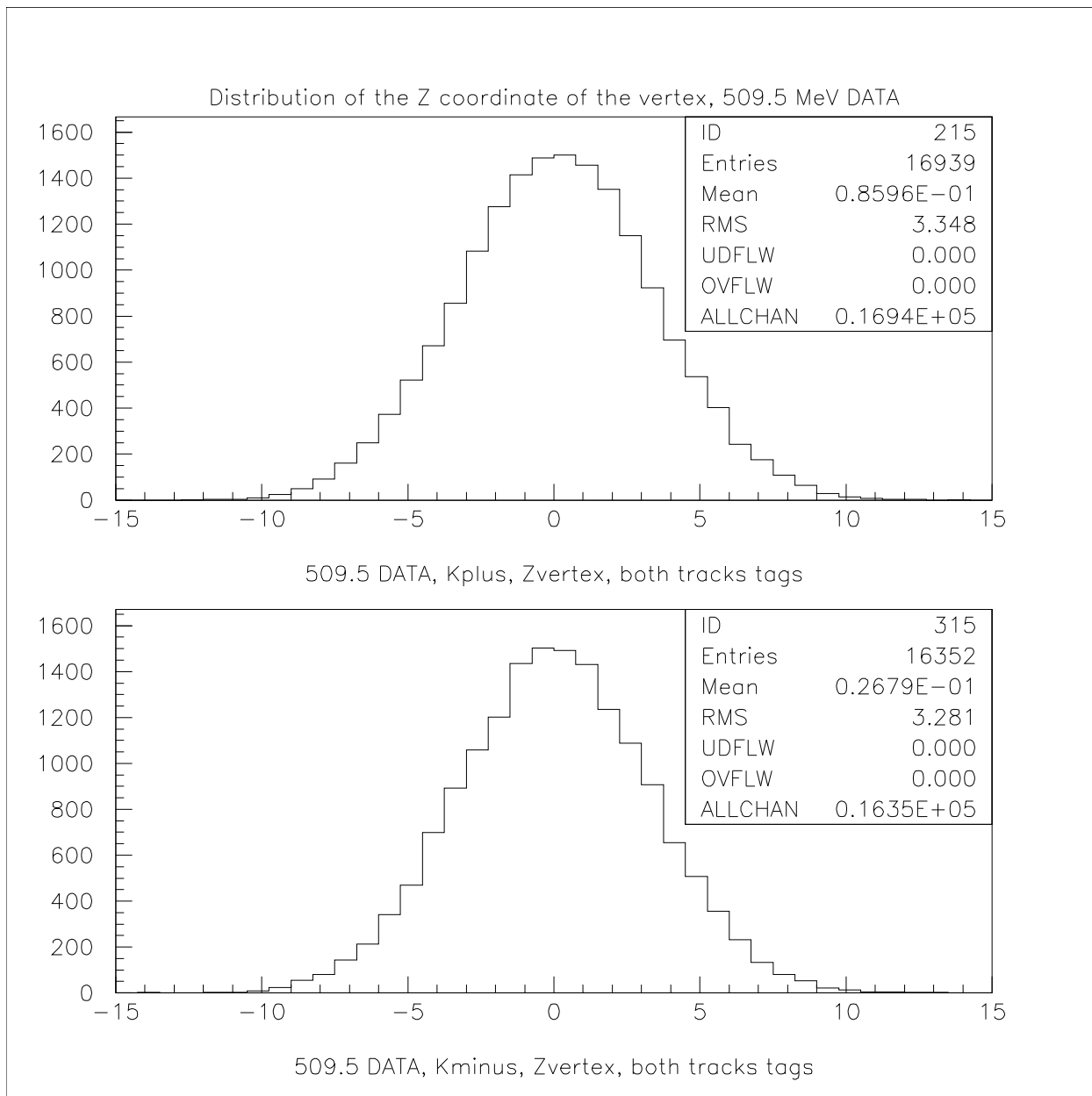


Figure 34: Distribution of the  $Z$  coordinate of the vertex.  $K^+K^-$  data at 509.5 MeV data is used. The upper plot corresponds to the decays of  $K^+$ , the lower to the decays of  $K^-$ .

- I don't account for the energy losses that are needed to 'extract' proton from a nucleus.
- I don't account for proton's losses in the pipe and in the drift chamber.
- Actual registration efficiency for  $e^- + N \rightarrow e^- + p^+ + N'$  event might be quite different from registration efficiency of charged kaon decay.

**4.4.3.2 Cosmic Rays Overlaps** Here I estimate the probability that cosmic event overlaps with useful kaon decay event. The area of the detector is approximately  $1m^2 = 10000cm^2$ , the arrival rate of the cosmic rays is about  $10^{-2}/cm^2/sec$ , and the sensitive time of detector per event is  $1\mu s$ . Then the probability of the overlap is

$$10^{-2}/cm^2/sec \times 10000cm^2 \times 10^{-6}sec = 10^{-4} \quad (4.4)$$

This is a rough estimate but it is probably enough to rule out these overlaps as a source of considerable background.

## 5.0 SIMULATION

### 5.1 CMD-2 SIMULATION SOFTWARE

The full simulation program for the CMD-2 detector is based on GEANT [24] package developed at CERN. GEANT consists of a collection of programs on whose basis simulation programs for a specific detector can be developed. One can use GEANT in the interactive mode which is very convenient in the debugging stage. One has to have a main program from which the following subroutines are called:

- GZEBRA—initializes the ZEBRA package which controls dynamic memory allocation.
- GINIT—initializes the GEANT variables.
- GFFGO—reads and interprets the input cards.
- GZINIT—initializes the memory allocation for ZEBRA.
- GPART—creates particles' data structures.
- GMATE—fills the materials tables.
- UGEOM—describes geometry of specific detector.
- GPHYSI—prepares cross sections and energy-loss tables for all materials used in the detector.
- GRUN—creates a loop over the simulated events.
- UGLAST—finishes the program execution, writes output files.

The subroutine GRUN which controls a cycle over events works as follows. In the beginning of each event it generates primary particles that are created in  $e^+e^-$  collision and their characteristics are stored in a buffer. Then it propagates the particles within the detector. As a particle propagates, all sorts of processes that can happen with this particle are simulated,

and either the kinematic parameters of this particle change correspondingly, or the particle disappears in the interaction, creating other particles, for example in the process of decay. These secondary particles can also be written into the buffer for subsequent propagation in the detector. Propagation of a particle ends when its energy becomes lower than the threshold energy for particles of this type. When all particles in the buffer are processed, the cycle moves on to the next event. The user can control the simulation at different stages using the subroutines that are called by GRUN and setting parameters within GEANT common blocks.

The detector is described as a set of volumes of different geometry. Each volume contains some 'medium' with the properties being the input parameters of the detector simulation. Another GEANT property of a volume is the profile of magnetic field.

In the simulation of the particles' interactions with the detector materials, the following processes were taken into account:

- creation of  $e^+e^-$  pair by photons
- creation of  $\delta$ -electrons
- annihilation of positrons in flight
- bremsstrahlung radiation by electrons, positrons, and muons
- interactions between hadrons and nuclei
- decays of particles in flight
- ionization losses by charged particles
- multiple scattering
- Compton effect on free electrons
- scattering of charged particles by atom-bound electrons
- photoeffect on electronic shells of the atoms
- muon scattering on nuclei
- nuclei fission induced by a photon
- Rayleigh scattering

Hadronic interactions can be simulated at the user's choice by two programs: GHEISHA [25] or FLUKA [26].

Control over the physical processes (switching on and off certain interactions, choice of method of the ionization losses simulation etc), as well as threshold energies for propagation of electrons, photons, and hadrons is established using the standard GEANT input cards. The general control cards and physical processes control cards are listed in tables 7 and 8 correspondingly.

Although the mechanism for including these additional photons existed in the simulation, it was not used, because it was judged to be insufficiently tested and robust.

Table 7: General control input cards.

| KEY    | VAR                           | description                                             | default   |
|--------|-------------------------------|---------------------------------------------------------|-----------|
| RNDM   | NRNDM(1)                      | initial random number                                   | 0         |
|        | NRNDM(2)                      | seeds (2 words)                                         | 0         |
| RUNG   | IDRUN                         | user run number                                         | 1         |
|        | IDEVT                         | first user event number                                 | 0         |
| TRIG   | NEVENT                        | total number of events to process                       | $10^7$    |
| KINE   | IKINE                         | generator flag                                          | 0         |
|        | PKINE                         | 10 user words                                           | $10^{11}$ |
| CUTS   |                               | Kinetic energy cuts in GeV:                             |           |
|        | CUTGAM                        | cut for for gammas                                      | 0.001     |
|        | CUTELE                        | cut for electrons                                       | 0.001     |
|        | CUTNEU                        | cut for neutral hadrons                                 | 0.01      |
|        | CUTHAD                        | cut for charged hadrons                                 | 0.01      |
|        | CUTMUO                        | cut for muons                                           | 0.01      |
|        | BCUTE                         | cut for electron bremsstrahlung                         | 0.001     |
|        | BCUTM                         | cut for muon and hadron<br>bremsstrahlung               | 0.001     |
|        | DCUTE                         | cut for $\delta$ -rays by $e^-$                         | $10^4$    |
|        | DCUTM                         | cut for $\delta$ -rays by $\mu$                         | $10^4$    |
|        | PPCUTM                        | total energy cut for direct<br>pair production by muons | 0.01      |
| TOFMAX | time of flight cut in seconds | $10^{10}$                                               |           |

Table 8: Physical processes control input cards.

| KEY  | VAR   | description                                                                                            | default |
|------|-------|--------------------------------------------------------------------------------------------------------|---------|
| ANNI | IANNI | annihilation                                                                                           | 1       |
| BREM | IBREM | bremsstrahlung                                                                                         | 1       |
| COMP | ICOMP | Compton scattering                                                                                     | 1       |
| DCAY | IDCAY | decay                                                                                                  | 1       |
| DRAY | IDRAY | $\delta$ -ray                                                                                          | 0       |
| HADR | IHADR | hadronic process                                                                                       | 1       |
| LOSS | ILOSS | energy loss                                                                                            | 2       |
| MULS | IMULS | multiple scattering                                                                                    | 1       |
| MUNU | IMUNU | muon nuclear interaction                                                                               | 1       |
| PAIR | IPAIR | pair production                                                                                        | 1       |
| PFIS | IPFIS | photofission                                                                                           | 0       |
| PHOT | IPHOT | photo electric effect                                                                                  | 1       |
| RAYL | IRAYL | Rayleigh scattering                                                                                    | 0       |
| FLUK | IFLUK | flag of GHEISHA/FLUKA choice<br>0–GHEISHA<br>1–FLUKA<br>2–FLUKA with cross sections<br>measured by SND | 0       |

## 5.2 FINE TUNING OF THE CHARGED KAON DECAYS SIMULATION

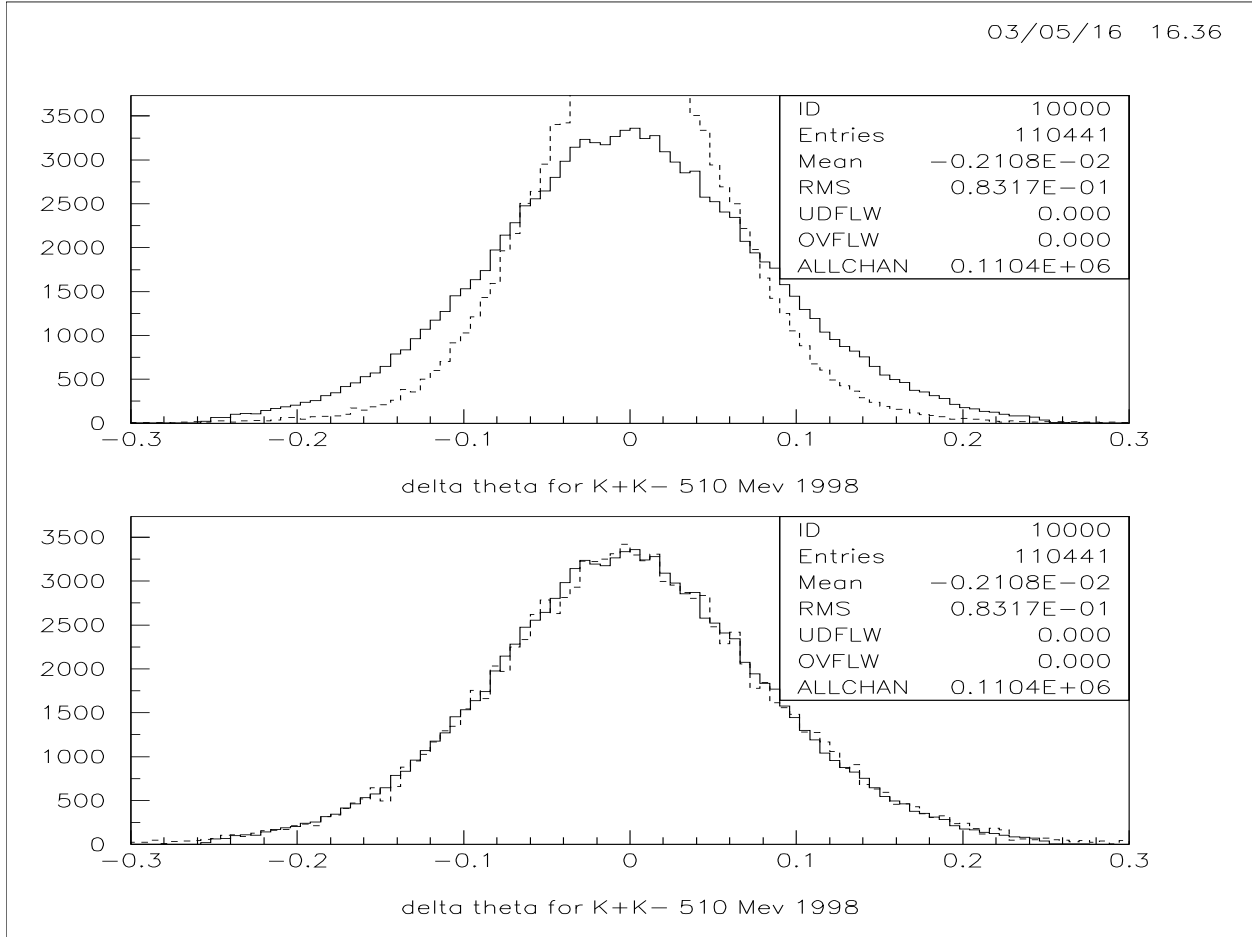


Figure 35: Upper plot is  $\Delta\theta$  for the data and the older version of simulation, lower plot is  $\Delta\theta$  for the data and the new version of simulation. In both plots the data is represented by a solid line, MC simulation — by the dashed line.

The tuning was performed in two steps:

1. Take the  $\phi \rightarrow K^+K^-$  events, they have two long kaon tracks and well defined  $\Delta\theta$  between them. Since  $\theta$  is the angle between a track and the  $Z$  axis,  $\Delta\theta$  depends mostly on the resolution in the  $R-Z$  plane. Compare this data with  $\phi \rightarrow K^+K^-$  simulation; the resolution in the  $R-Z$  plane can be tuned by bringing  $\Delta\theta$  in simulation in correspondence with the one from the data

2. Take the  $K_S \rightarrow \pi^+\pi^-$  events and look at the distribution of invariant mass of  $\pi^+$  and  $\pi^-$  and of the average momentum of the two pions. Both of them have only one peak and more or less symmetric tails. The widths of the peaks are determined by both  $R - Z$  and  $R - \phi$  resolutions, but since by now  $R - Z$  is tuned and fixed, we can tune the  $R - \phi$  resolution

Figs. 35 and 36 illustrate the first step of the tuning — tuning of the resolution in the  $R - Z$  plane; Figs. 37 and 38 illustrate the second step — tuning of the resolution in the  $R - \phi$  plane.

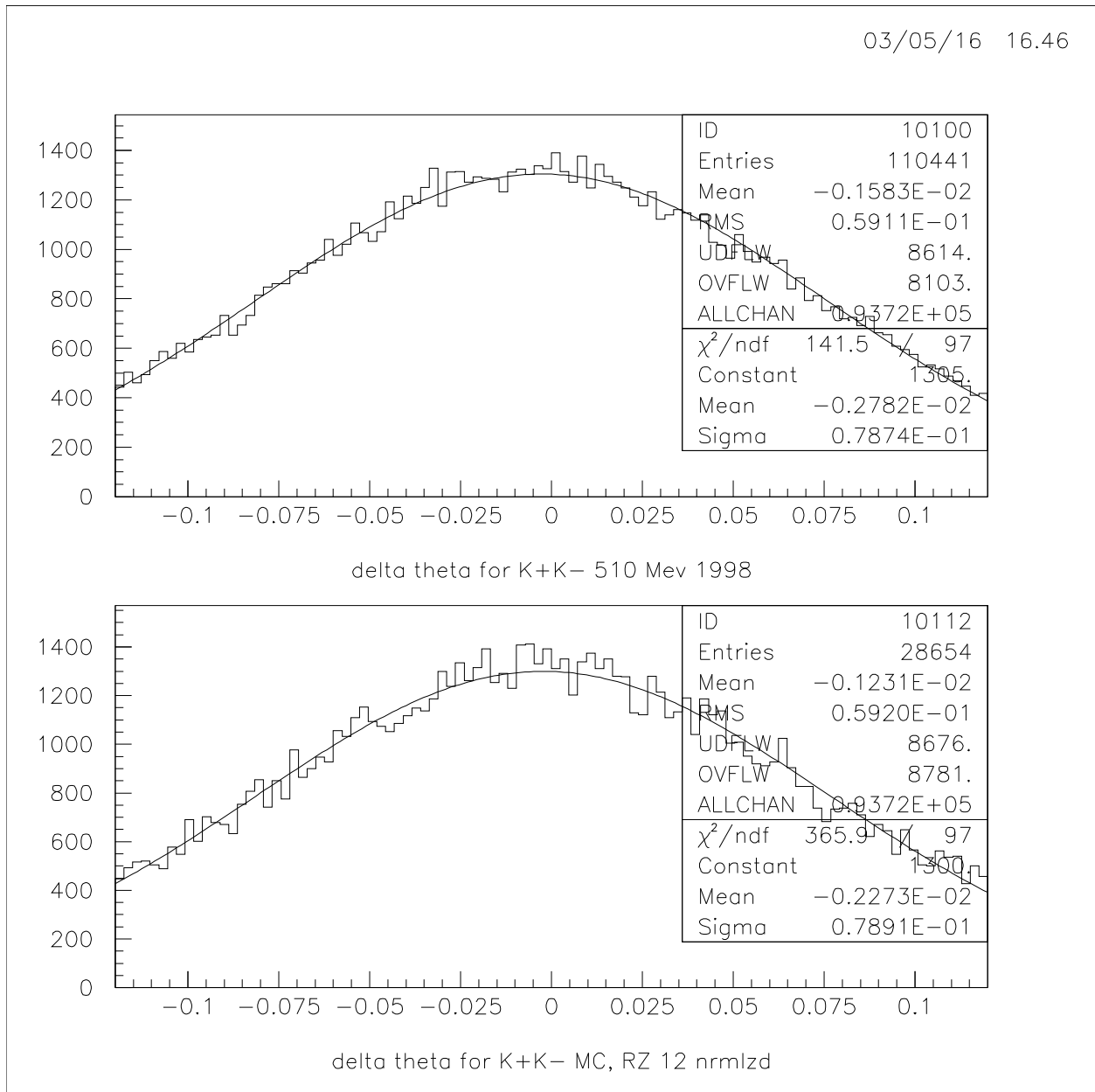


Figure 36: Upper plot is  $\Delta\theta$  for the data, lower plot is  $\Delta\theta$  for the new version of MC. Both are fitted with a gauss. Both the histogram RMS and the Gaussian widths are in good agreement, their differences are within statistical errors.

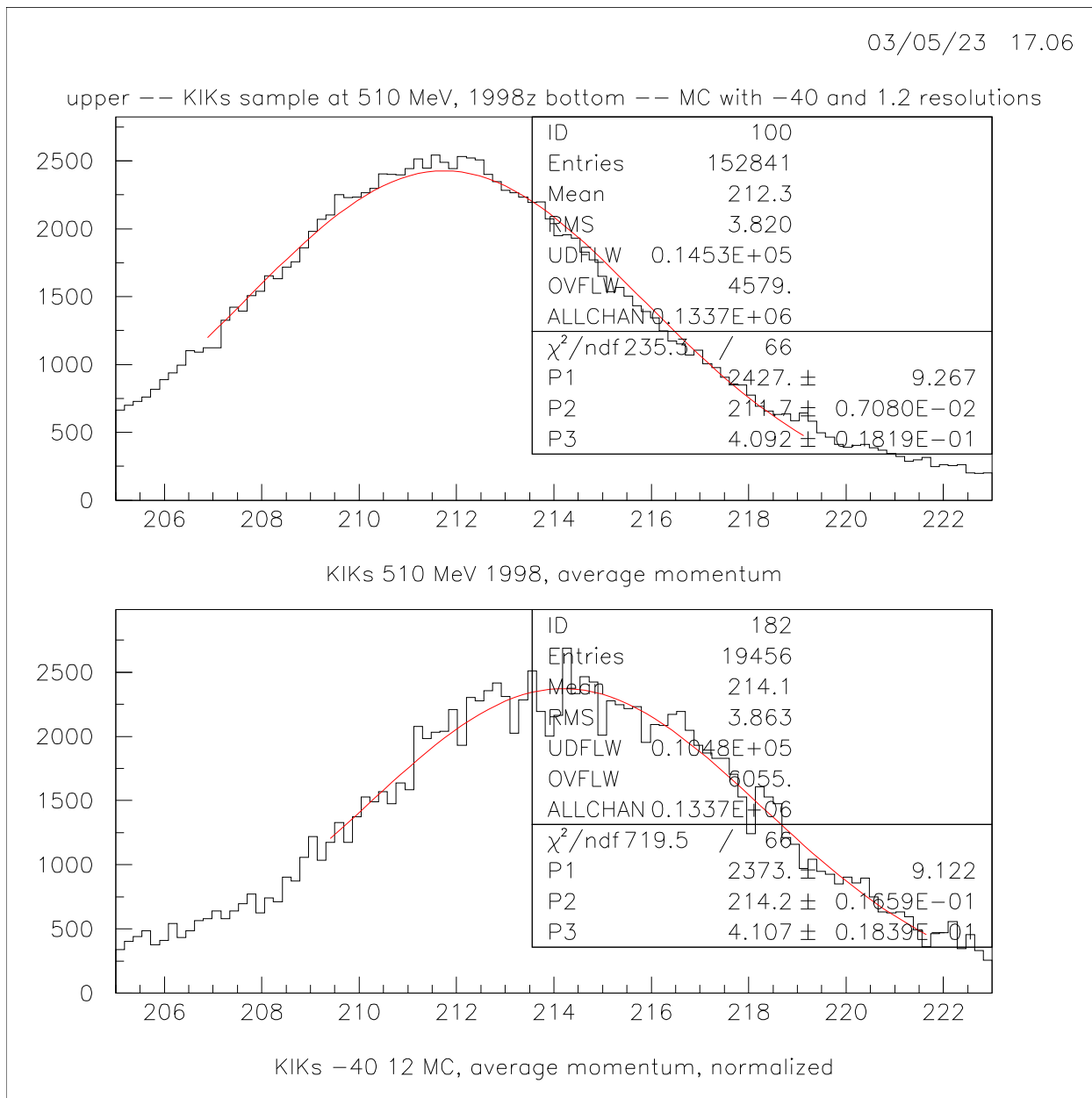


Figure 37: Average momentum of  $\pi^+$  and  $\pi^-$  for the data sample of  $K_S K_L$  — upper plot and new version of MC — lower plot, both fitted with a Gaussian distribution.

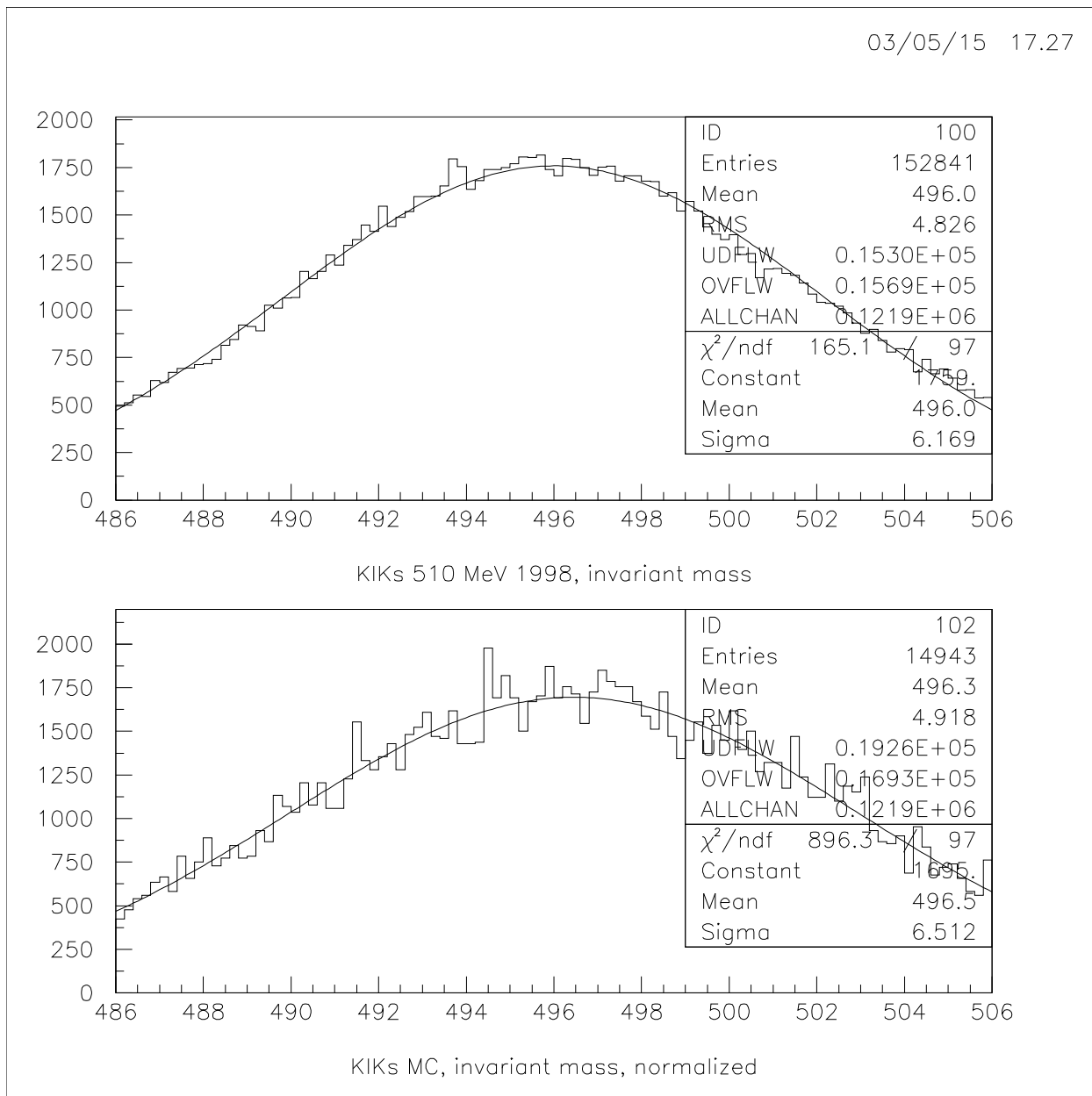


Figure 38: Invariant mass of  $\pi^+$  and  $\pi^-$  for the data sample of  $K_S K_L$  — upper plot and new version of MC — lower plot, both fitted with a gauss.

### 5.3 CHARGE ASYMMETRY IN THE DRIFT CHAMBER

Because of the difference in the rates of strong interaction, positive and negative particles leave slightly different signals in the drift chamber of CMD-2. One of the examples is the number of the wire hits. Figure 39 shows the distributions for the positive and negative products of the kaon decay. The same trend is reflected in the simulation, though not to

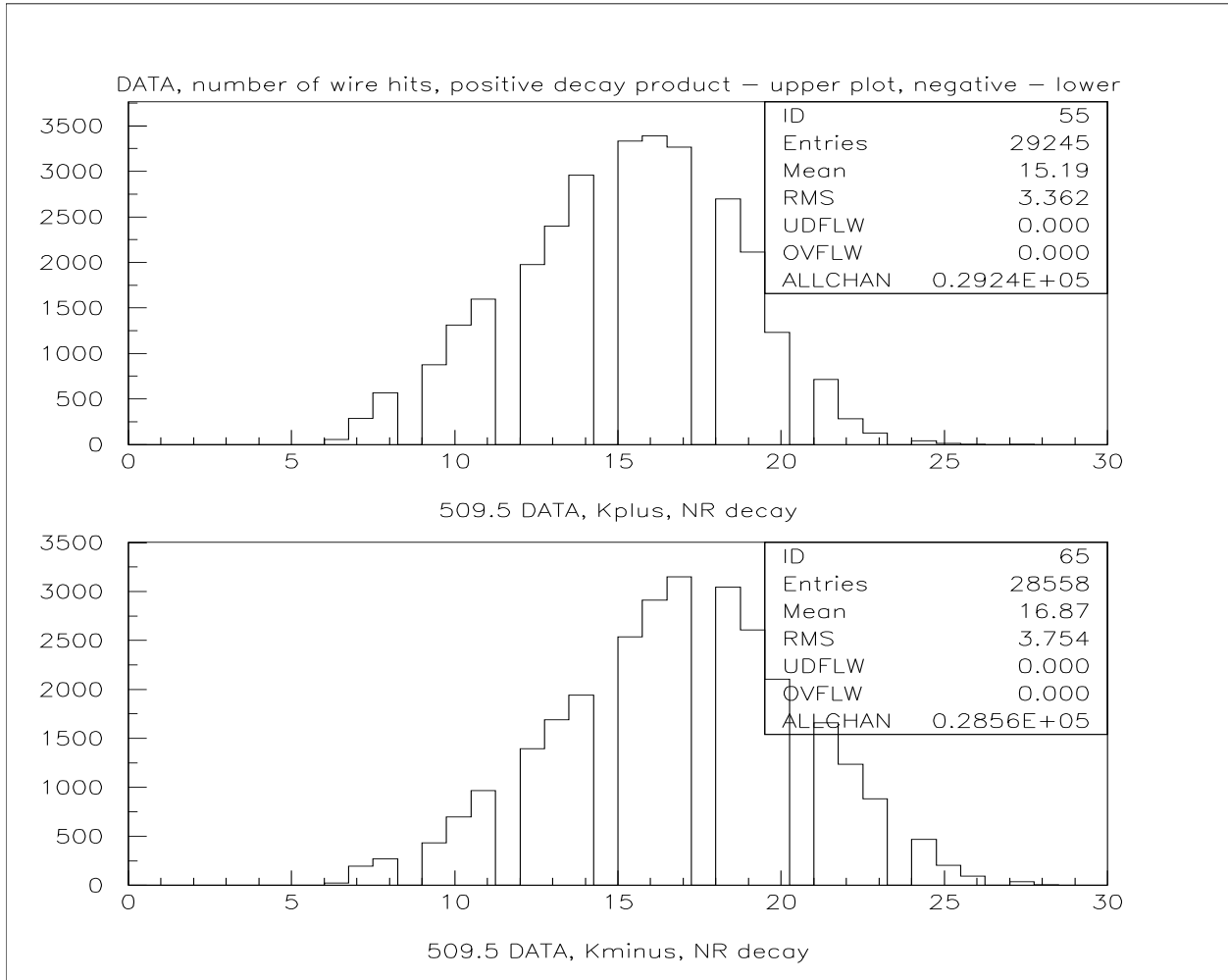


Figure 39: Number of the wire hits for a data sample of 509.5 MeV. The distributions are different for positively and negatively charged particles.

the same degree. Figures 40 and 41 show the number of wire hits distributions for all 6 simulated decay modes for positive and negative particles correspondingly.

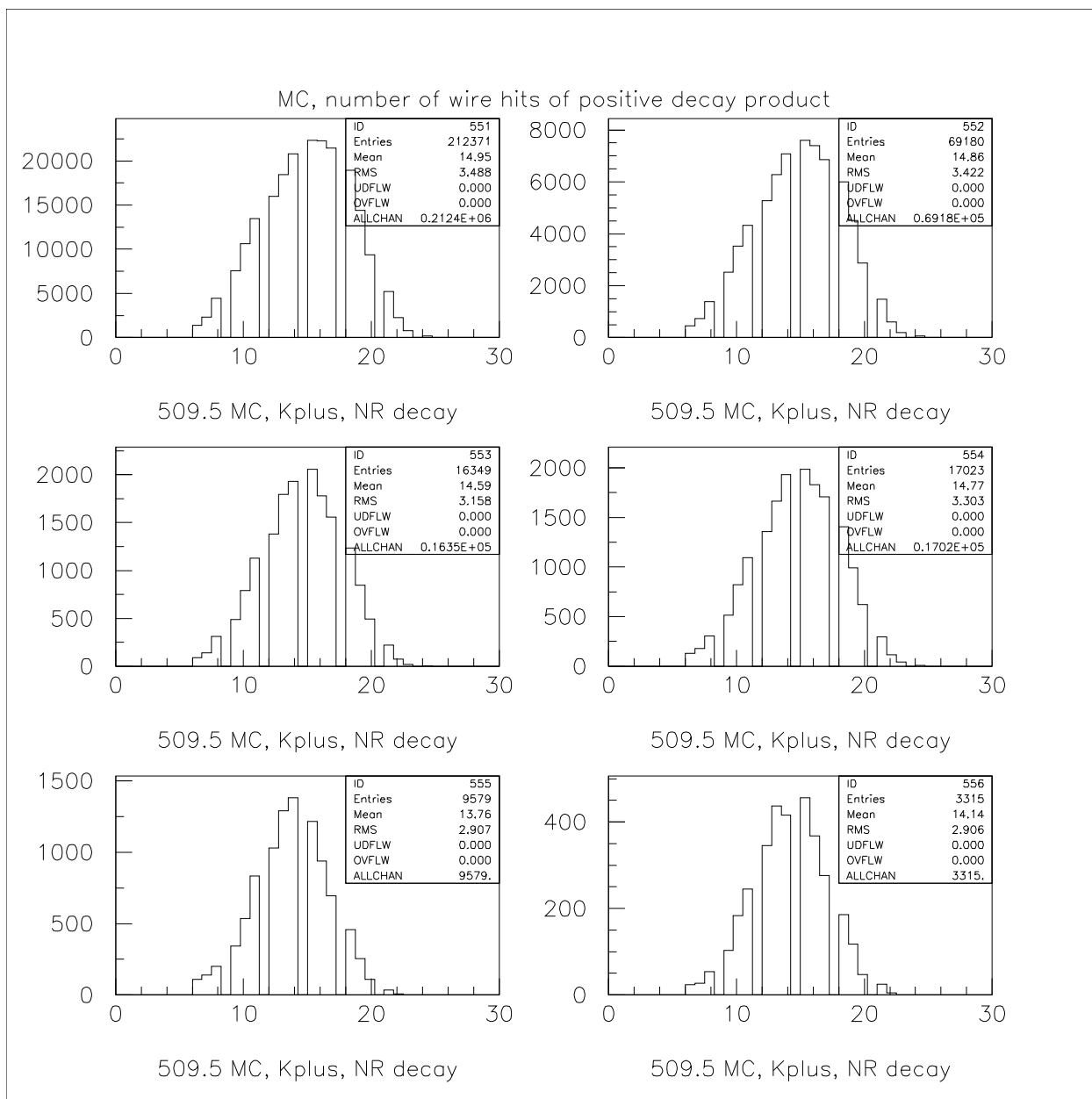


Figure 40: Number of the wire hits for 6 decay modes of  $K^+$ .

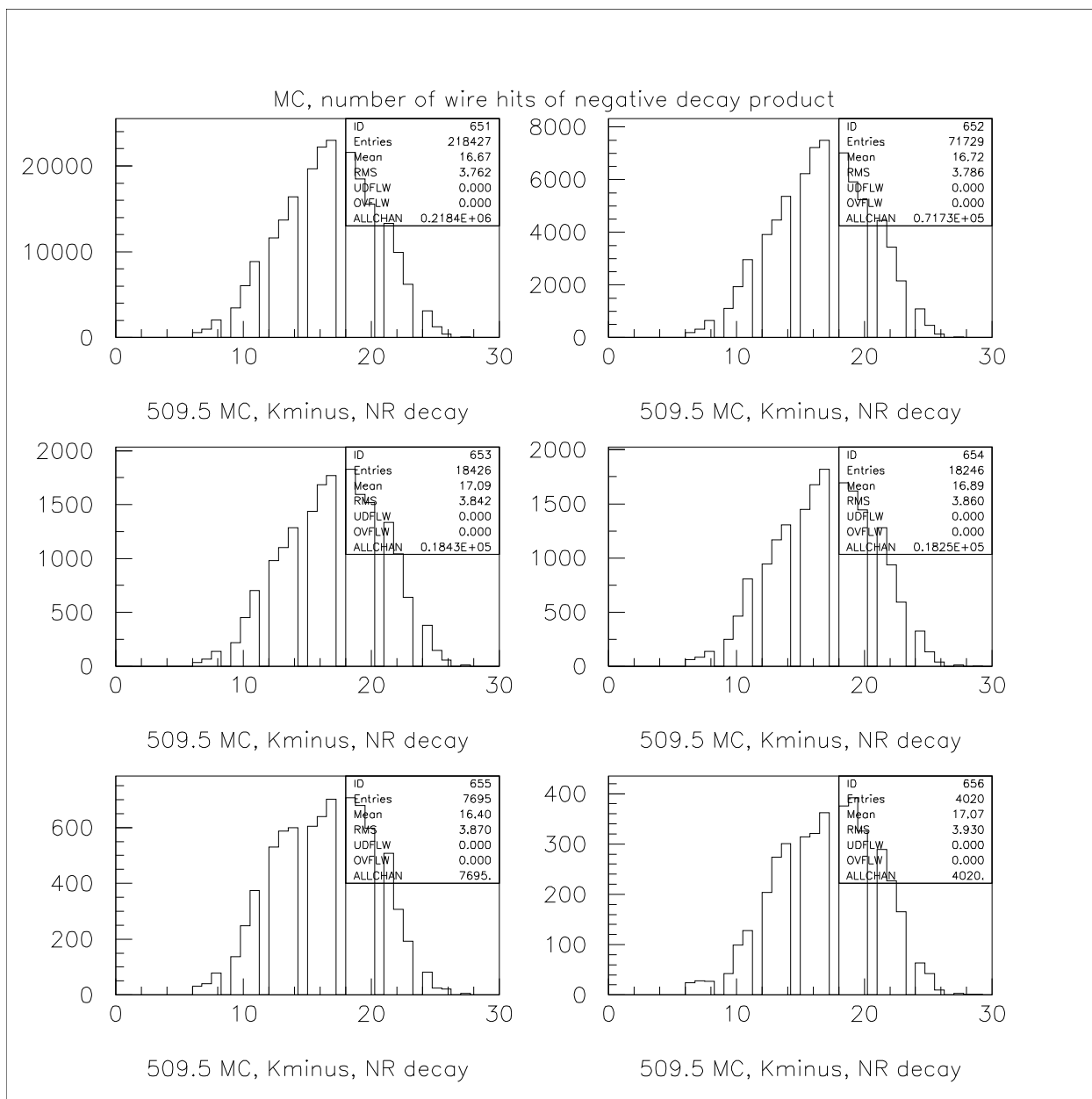


Figure 41: Number of the wire hits for 6 decay modes of  $K^-$ .

## 6.0 SEPARATION PARAMETERS

### 6.1 MISSING MASS

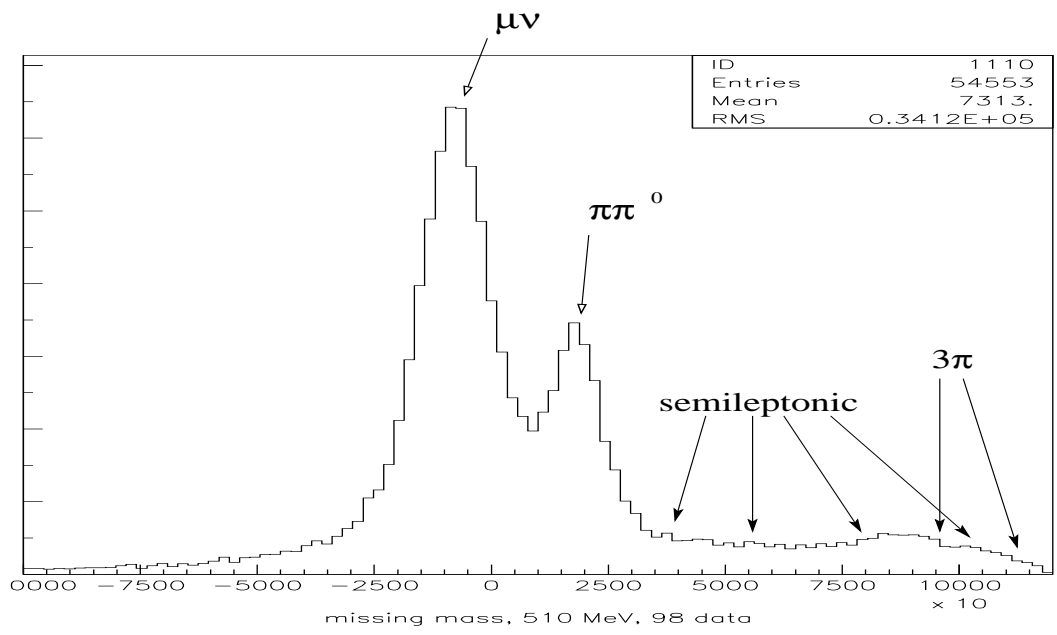


Figure 42: MM2 distribution for 510.0 MeV sample

Kinematics of the initial kaon and decay particle have different characteristics for the

different main decay modes. We have studied different formulations of the kinematic information (including kinematic fits to different hypotheses), but for this analysis we use a quantity "MM2", defined as the missing mass squared between the kaon and the outgoing decay particle, interpreted as a pion:

$$MM2 = (E_{kaon} - E_{decay})^2 - (\vec{P}_{kaon} - \vec{P}_{decay})^2 \quad (6.1)$$

$E_{kaon}$  and  $\vec{P}_{kaon}$  are energy and momentum of the tagging kaon,  $E_{decay}$  and  $\vec{P}_{decay}$  are energy and momentum of the charged decay daughter.  $E_{kaon}$  is equal to  $E_{beam}$ .  $P_{kaon}$  is given by

$$P_{kaon} = \sqrt{E_{beam}^2 - M_K^2} \quad (6.2)$$

and  $E_{decay}$  is given by

$$E_{decay} = \sqrt{P_{decay}^2 + m_\pi^2} \quad (6.3)$$

where  $m_\pi$  is the mass of charged pion.

The MM2 distribution of the data is shown in figure 42. The two peaks correspond to the  $K \rightarrow \mu\nu$  and  $K \rightarrow \pi\pi^0$  decays, while the semileptonic and 3-pion decays are located at the right side of the distribution. The MM2 distributions obtained from the MC simulation are shown in figure 44. The MM2 distributions of  $K_{\mu 3}$  and  $K_{e3}$  overlap almost entirely, and are therefore taken together and effectively treated as one semileptonic mode. The same applies to the  $K \rightarrow \pi^+\pi^+\pi^-$  and  $K \rightarrow \pi^0\pi^0\pi^+$  which are treated together as one 3-pion mode.

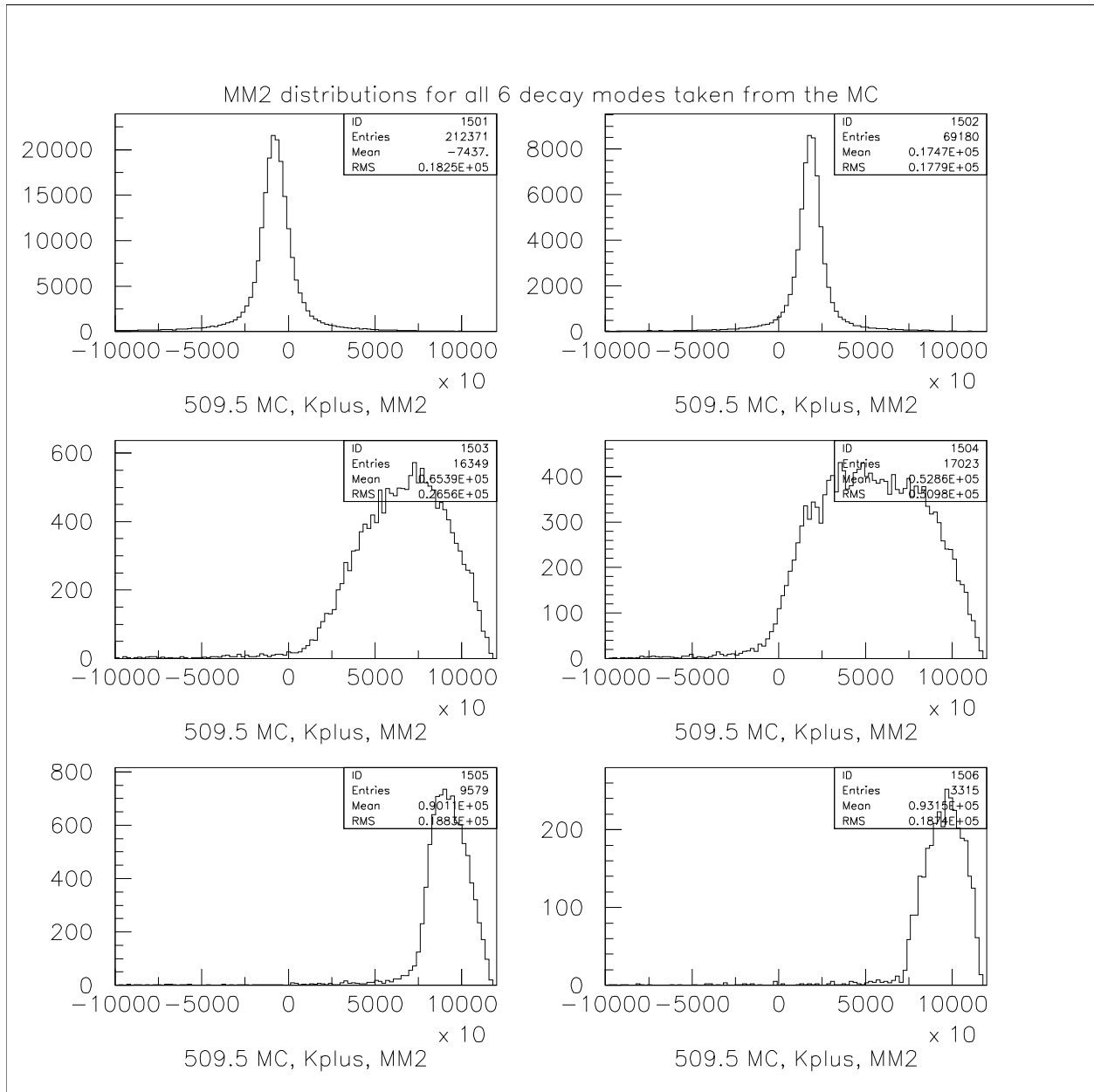


Figure 43: MM2 for all 6 decay modes simulated at 509.5 MeV, upper left is  $K^+ \rightarrow \mu\nu$ , upper right is  $K^+ \rightarrow \pi^+\pi^0$ , middle left is  $K^+ \rightarrow \pi^0\mu\nu$ , middle right is  $K^+ \rightarrow \pi^0e\nu$ , lower left is  $K^+ \rightarrow \pi^+\pi^+\pi^-$ , lower right is  $K^+ \rightarrow \pi^+\pi^0\pi^0$ .

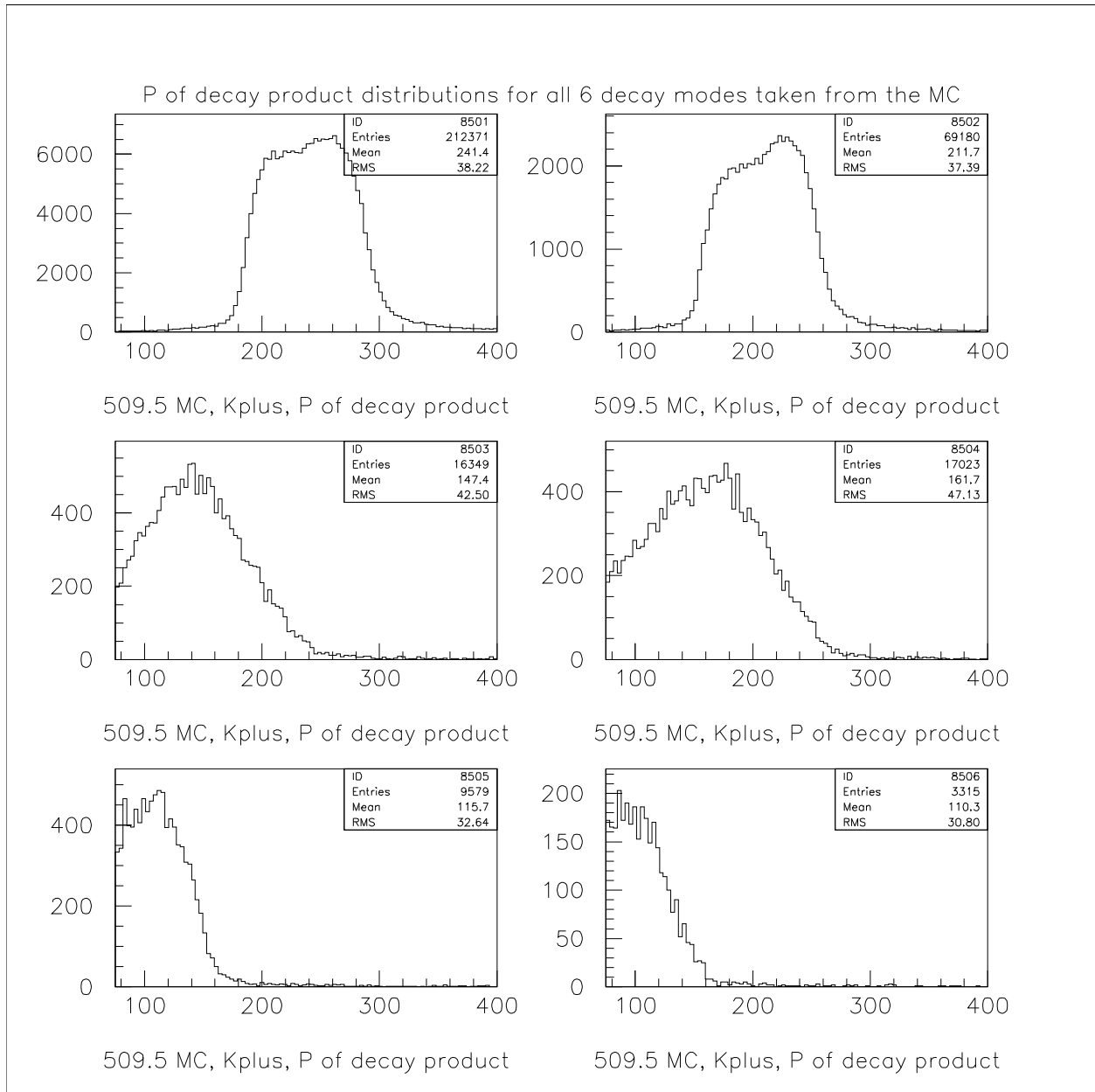


Figure 44: Decay product momentum for all 6 decay modes simulated at 509.5 MeV, upper left is  $K^+ \rightarrow \mu\nu$ , upper right is  $K^+ \rightarrow \pi^+\pi^0$ , middle left is  $K^+ \rightarrow \pi^0\mu\nu$ , middle right is  $K^+ \rightarrow \pi^0e\nu$ , lower left is  $K^+ \rightarrow \pi^+\pi^+\pi^-$ , lower right is  $K^+ \rightarrow \pi^+\pi^0\pi^0$ .

## 6.2 DPE

The parameter called DPE is assigned to a particle and is defined as

$$DPE = P_{dc} - E_{clus} \quad (6.4)$$

where  $P_{dc}$  is the momentum of the particle measured in the drift chamber and  $E_{clus}$  is the energy deposition of the particle in the calorimeter. Obviously, only tracks that have a cluster in the calorimeter may be considered. In fact, when working with DPE, I always request  $E_{clus} > 20$  MeV to discriminate against tracks attached to a noise cluster.

The CsI calorimeter is described in detail in section 3.2. It is 8.1 radiation lengths deep which corresponds to 0.4 nuclear interaction lengths.

The mechanisms by which different particles leave energy depositions in the calorimeter are different. At low energies electrons and positrons lose energy primarily by ionization, although there are contributions from other processes, among them Moller scattering, Bhabha scattering, annihilation [1]. While ionization loss rates rise logarithmically with energy, bremsstrahlung losses rise nearly linearly and dominate above a few tens of MeV in most materials. In this analysis only particles with momentum above 75 MeV were considered; therefore, the depositions of electrons and positrons in the CsI calorimeter are dominated by bremsstrahlung losses, and there are no significant differences between the depositions made by  $e^+$  and  $e^-$ . Due to the relatively large depth of the calorimeter ( $8.1X_0$ ), electrons and positrons deposit all or almost all of their kinetic energy in the calorimeter. Due to their small mass the kinetic energy equals approximately the total energy; therefore, the DPE distribution for electrons and positrons is expected to have mean close to zero. In reality, however, mean DPE for electrons and positrons is slightly more than zero due to loss of energy in the magnet coils.

At sufficiently high energies, radiative processes become more important than ionization for all charged particles. For muons and pions in CsI this critical energy occurs at several GeV. Therefore at the energies dealt with in this analysis, to zero order, muons leave energy by ionization, and both  $\mu^+$  and  $\mu^-$  behave similarly in the ionization process. Also, both can decay  $\mu \rightarrow e\nu_\mu\nu_e$  with lifetime  $\tau = 2.2 \mu\text{sec}$ . The  $\mu^+$  mostly follows this scheme, so

that its energy loss pattern is somewhere between a simply ionizing particle with roughly constant energy losses with momentum, and an electron, with energy losses proportional to the energy of muon.

The behavior of  $\mu^-$  is more complicated. In the CsI calorimeter it is captured by an atom with probability above 80%. It excites the atom into higher excitation states. The atom then cascades down with energy carried away by the photons. Finally, in the K-shell of the atom,  $\mu^-$  can be captured by the nucleus:  $\mu^- + p \rightarrow n + \nu_\mu$ . In this case the muon rest mass energy will be transferred mostly to the neutrino (since the nucleus is much heavier than the muon). Therefore, the  $\mu^-$  energy loss spectrum is sharper, consisting mostly of just kinetic energy of the muon.

Pions behave mostly as  $\mu^+$  but in addition have about 40% chance of interacting strongly in the calorimeter thereby complicating the picture. They may produce  $\pi^0$  through the charge conversion with consequent  $\pi^0 \rightarrow \gamma\gamma$  decay and with electromagnetic cascade produced by the photons. Or they may decay into muons with all the attendant behavior discussed above for muons.

Figures 45–49 show the relevant distributions obtained from the MC simulation for both charges: the DPE distributions, DPE versus momentum distributions, and  $E_{clus}$  versus momentum distributions.

Figures 51–56 show the DPE, DPE versus momentum, and  $E_{clus}$  versus momentum distributions for  $K^+$  and  $K^-$  decaying samples from the 509.5 MeV data.

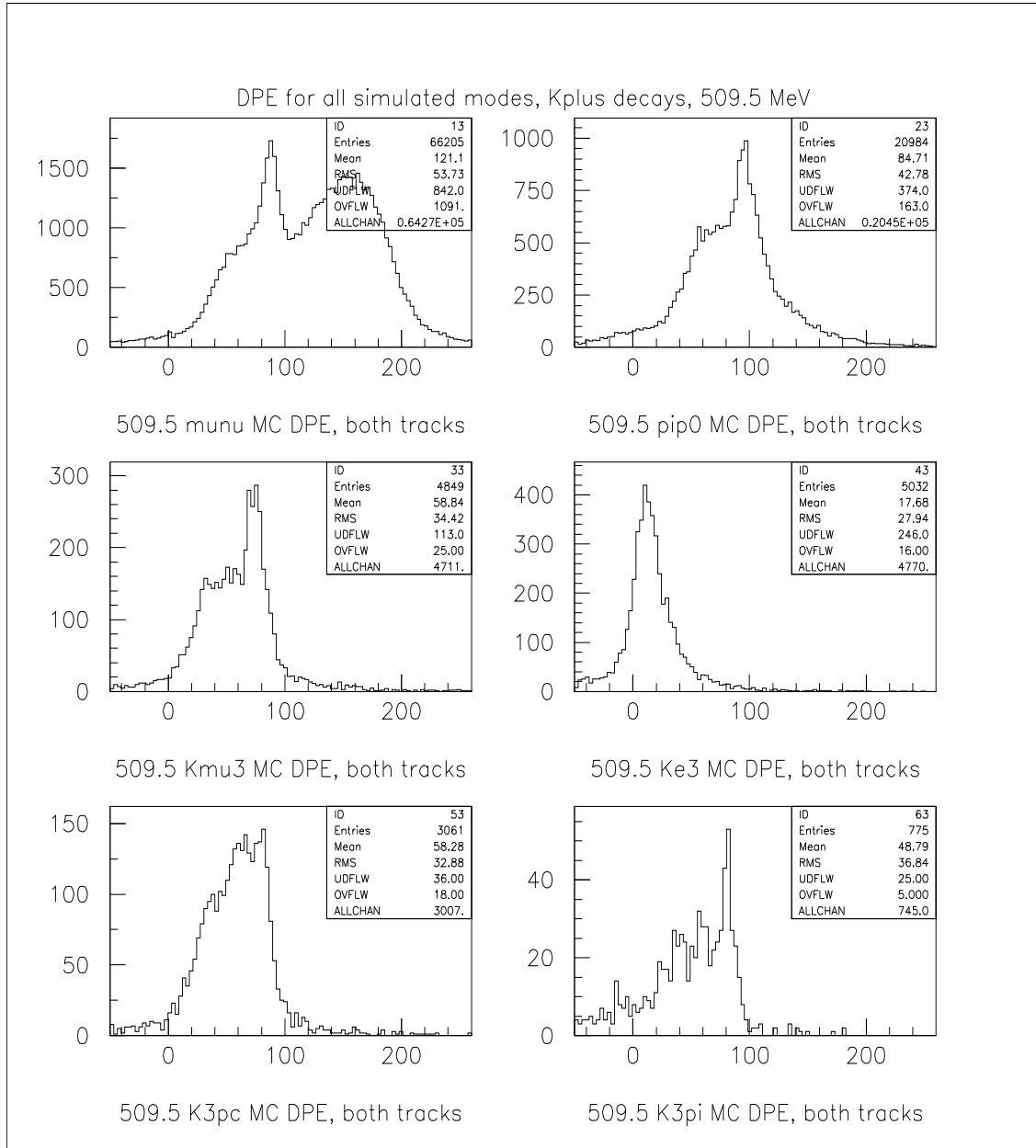


Figure 45: DPE for all simulated modes,  $K^+$  decays, beam energy is 509.5 MeV, upper left is  $K^+ \rightarrow \mu^+ \nu$ , upper right is  $K^+ \rightarrow \pi^+ \pi^0$ , middle left is  $K^+ \rightarrow \pi^0 \mu^+ \nu$ , middle right is  $K^+ \rightarrow \pi^0 e^+ \nu$ , lower left is  $K^+ \rightarrow \pi^+ \pi^+ \pi^-$ , lower right is  $K^+ \rightarrow \pi^+ \pi^0 \pi^0$ .

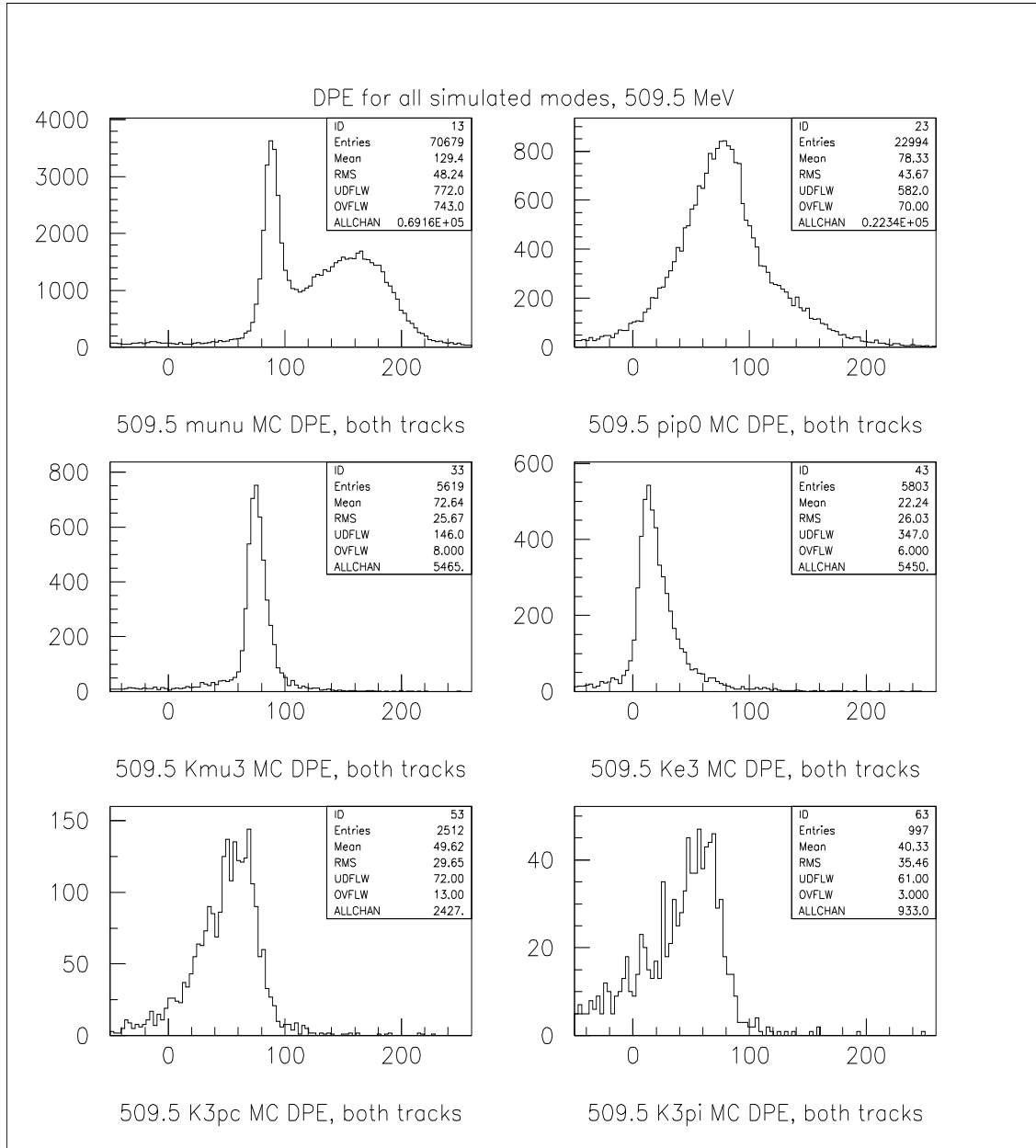


Figure 46: DPE for all simulated modes,  $K^-$  decays, beam energy is 509.5 MeV, upper left is  $K^- \rightarrow \mu^- \nu$ , upper right is  $K^- \rightarrow \pi^- \pi^0$ , middle left is  $K^- \rightarrow \pi^0 \mu^- \nu$ , middle right is  $K^- \rightarrow \pi^0 e^- \nu$ , lower left is  $K^- \rightarrow \pi^- \pi^- \pi^+$ , lower right is  $K^- \rightarrow \pi^- \pi^0 \pi^0$ .

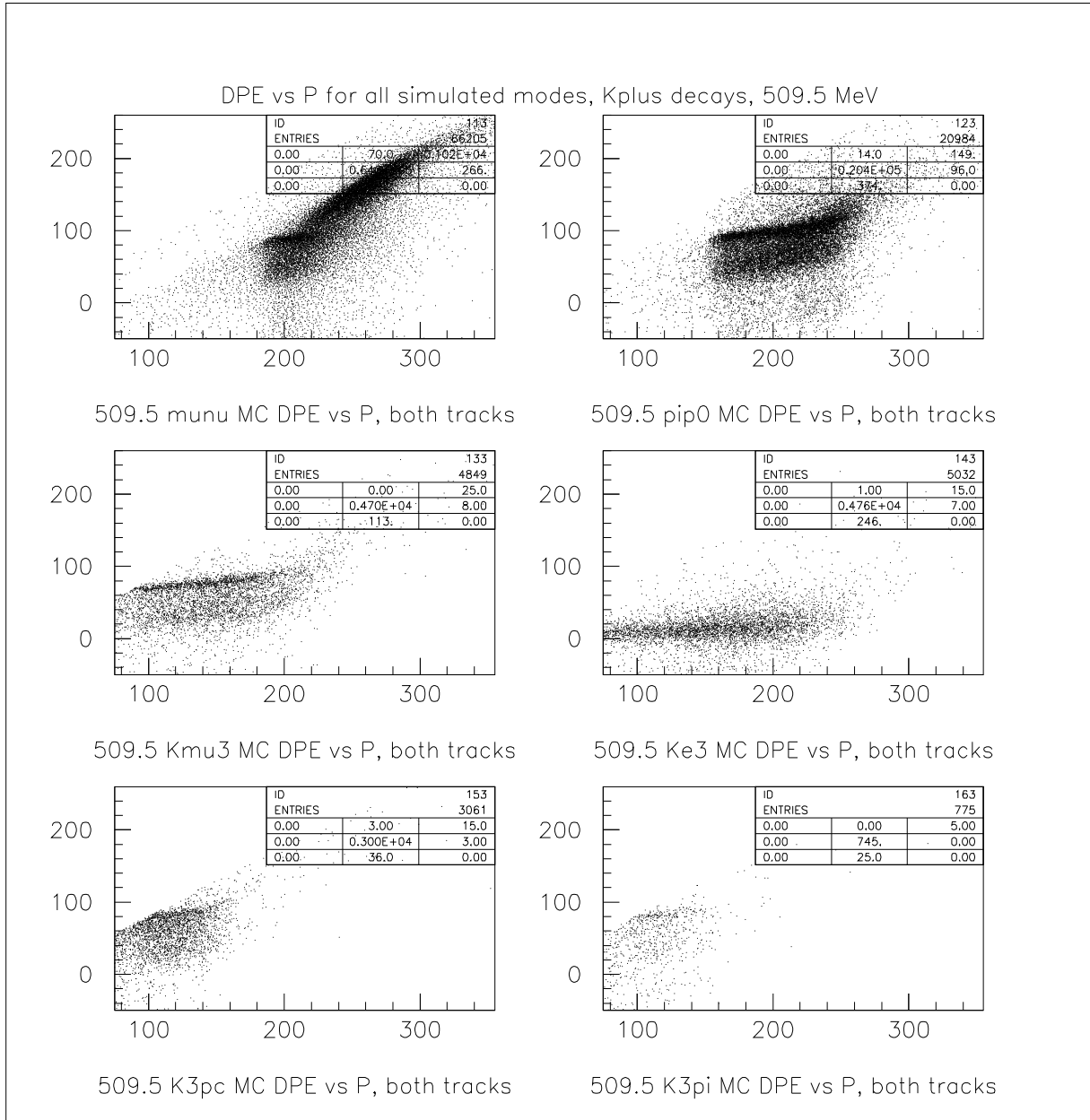


Figure 47: DPE versus momentum for all simulated modes,  $K^+$  decays, beam energy is 509.5 MeV, upper left is  $K^+ \rightarrow \mu^+\nu$ , upper right is  $K^+ \rightarrow \pi^+\pi^0$ , middle left is  $K^+ \rightarrow \pi^0\mu^+\nu$ , middle right is  $K^+ \rightarrow \pi^0e^+\nu$ , lower left is  $K^+ \rightarrow \pi^+\pi^+\pi^-$ , lower right is  $K^+ \rightarrow \pi^+\pi^0\pi^0$ .

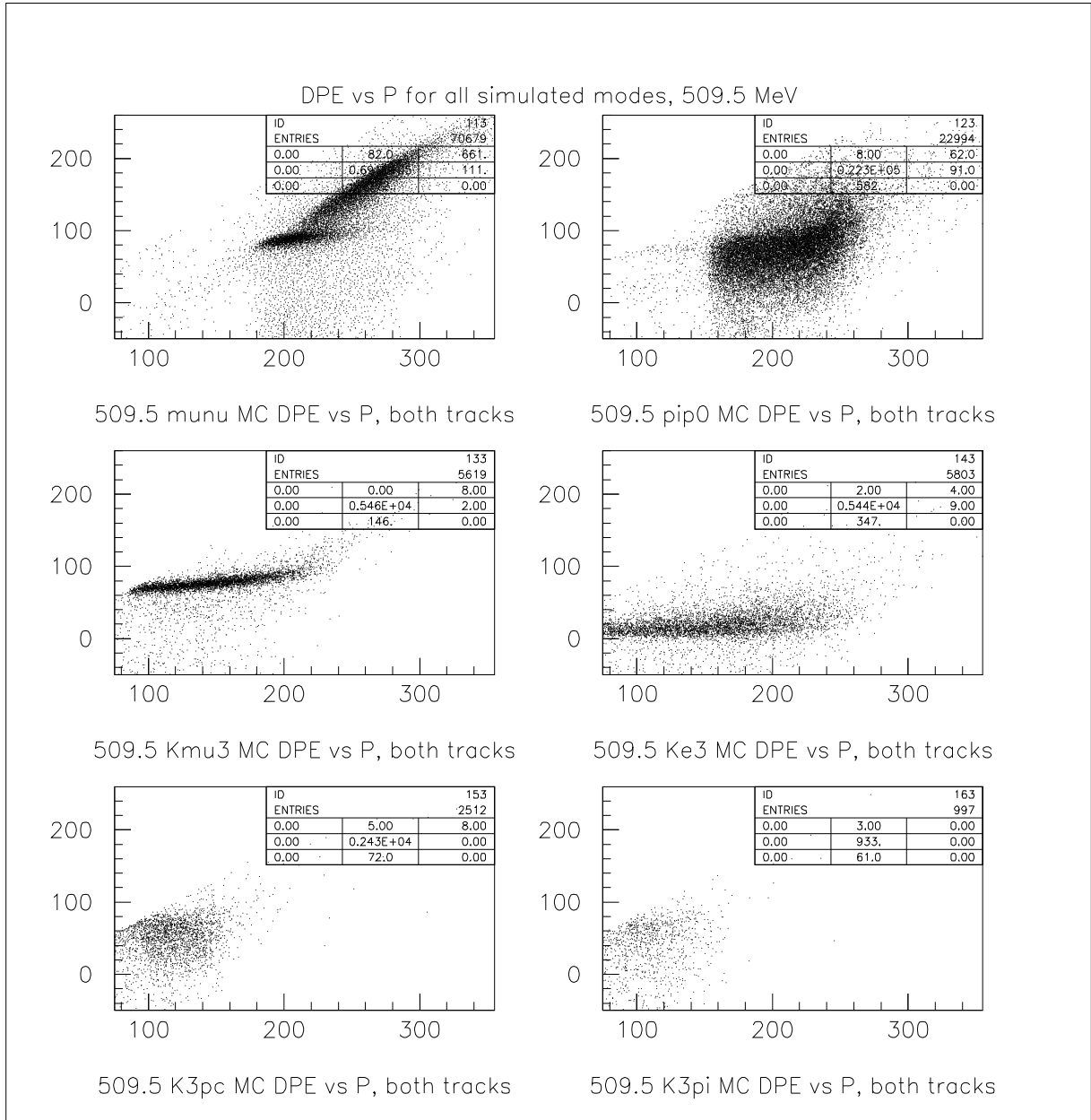


Figure 48: DPE versus momentum for all simulated modes,  $K^-$  decays, beam energy is 509.5 MeV, upper left is  $K^- \rightarrow \mu^- \nu$ , upper right is  $K^- \rightarrow \pi^- \pi^0$ , middle left is  $K^- \rightarrow \pi^0 \mu^- \nu$ , middle right is  $K^- \rightarrow \pi^0 e^- \nu$ , lower left is  $K^- \rightarrow \pi^- \pi^- \pi^+$ , lower right is  $K^- \rightarrow \pi^- \pi^0 \pi^0$ .

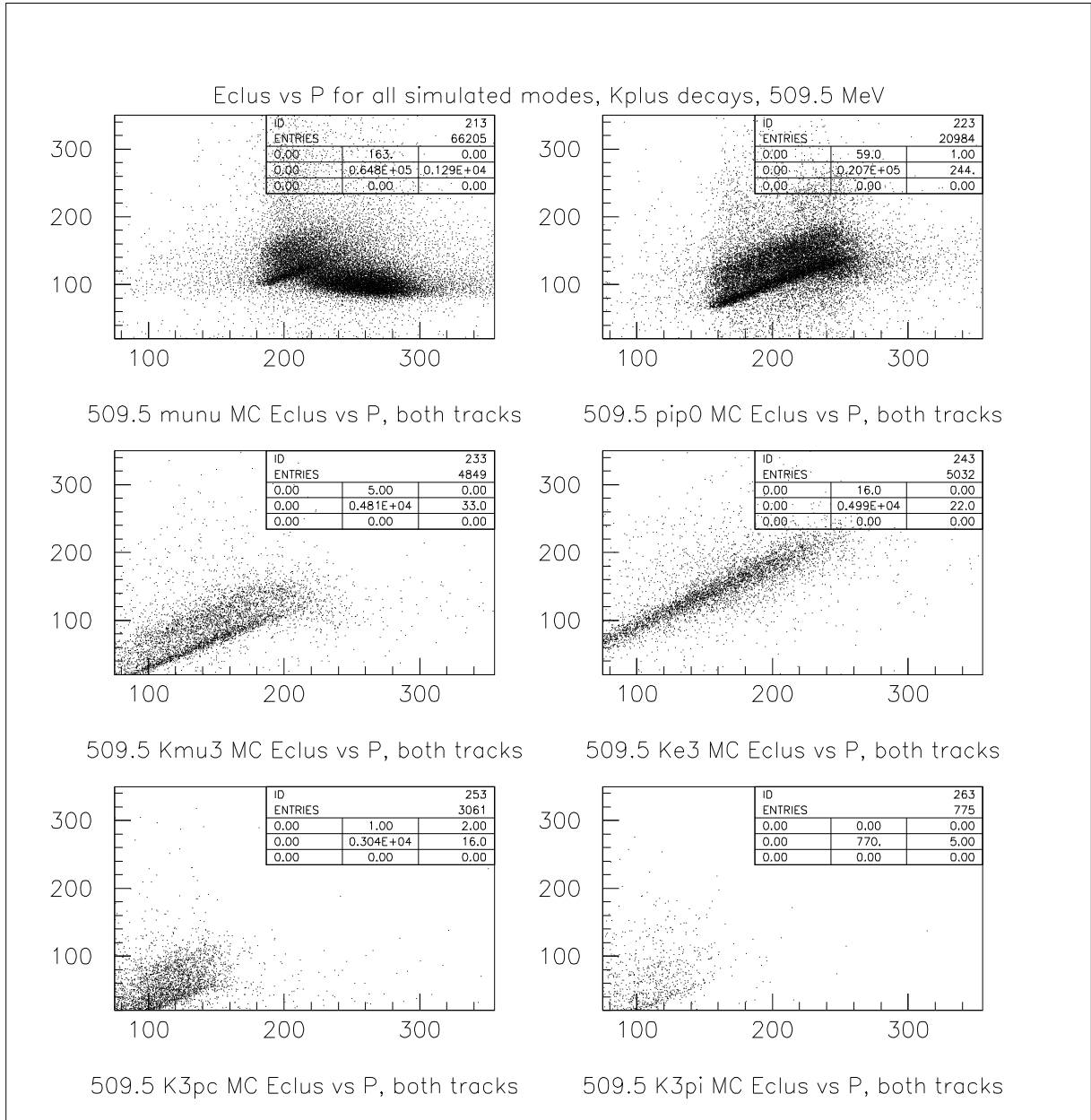


Figure 49:  $E_{clus}$  versus momentum for all simulated modes,  $K^+$  decays, beam energy is 509.5 MeV, upper left is  $K^+ \rightarrow \mu^+\nu$ , upper right is  $K^+ \rightarrow \pi^+\pi^0$ , middle left is  $K^+ \rightarrow \pi^0\mu^+\nu$ , middle right is  $K^+ \rightarrow \pi^0e^+\nu$ , lower left is  $K^+ \rightarrow \pi^+\pi^+\pi^-$ , lower right is  $K^+ \rightarrow \pi^+\pi^0\pi^0$ .

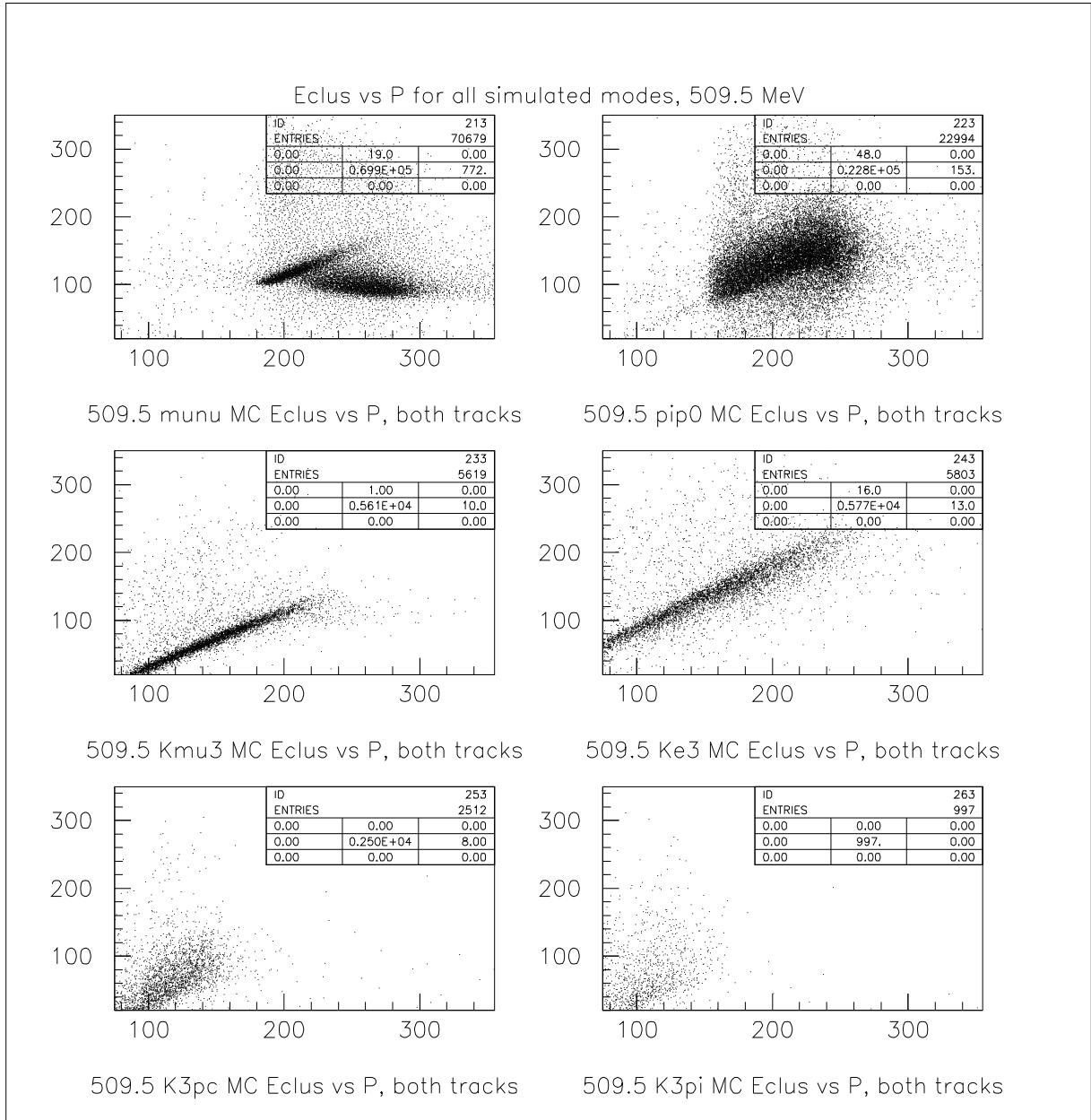


Figure 50:  $E_{clus}$  versus momentum for all simulated modes,  $K^-$  decays, beam energy is 509.5 MeV, upper left is  $K^- \rightarrow \mu^- \nu$ , upper right is  $K^- \rightarrow \pi^- \pi^0$ , middle left is  $K^- \rightarrow \pi^0 \mu^- \nu$ , middle right is  $K^- \rightarrow \pi^0 e^- \nu$ , lower left is  $K^- \rightarrow \pi^- \pi^- \pi^+$ , lower right is  $K^- \rightarrow \pi^- \pi^0 \pi^0$ .

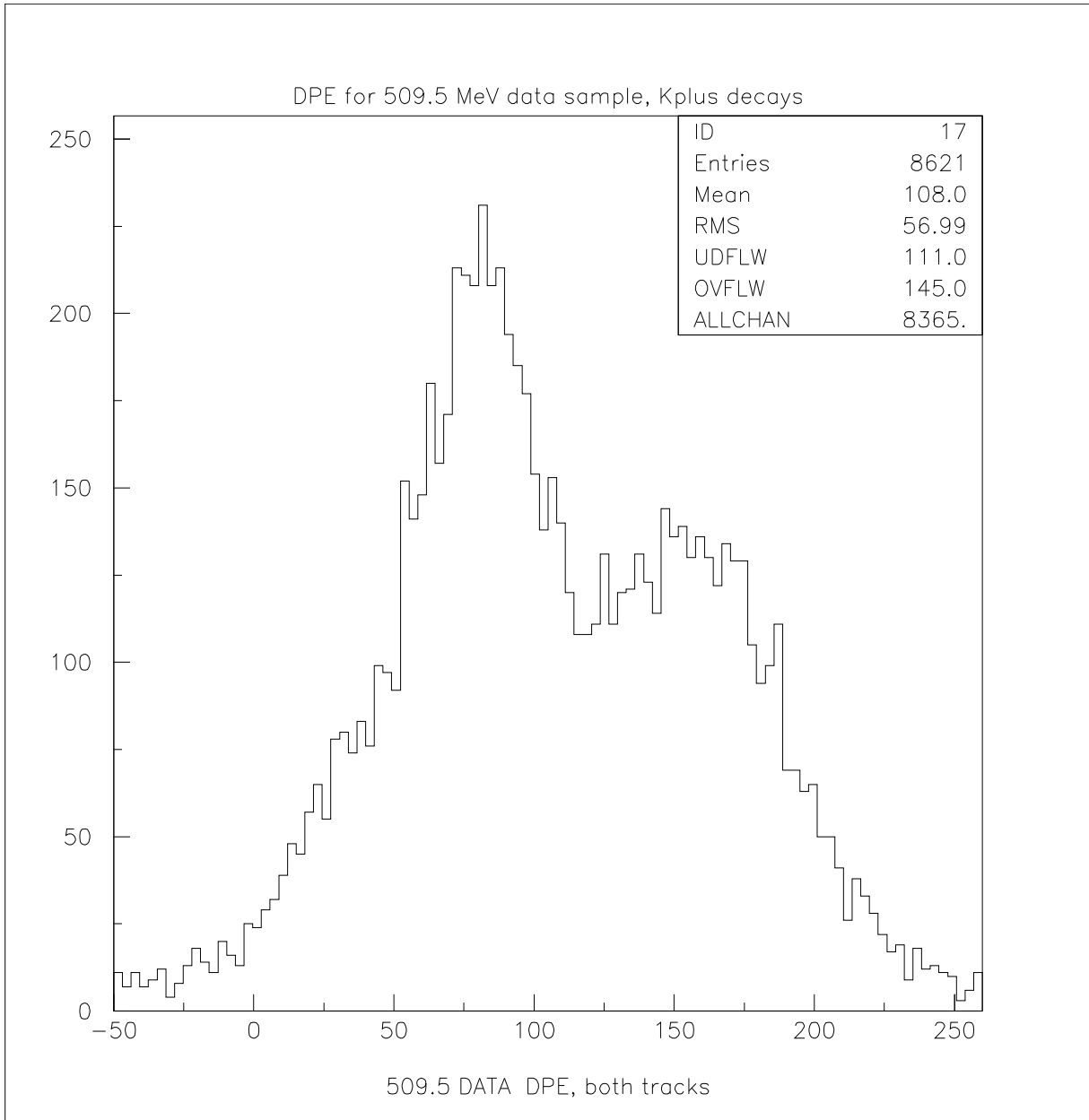


Figure 51: DPE distribution for the data sample of 509.5 MeV,  $K^+$  decays.

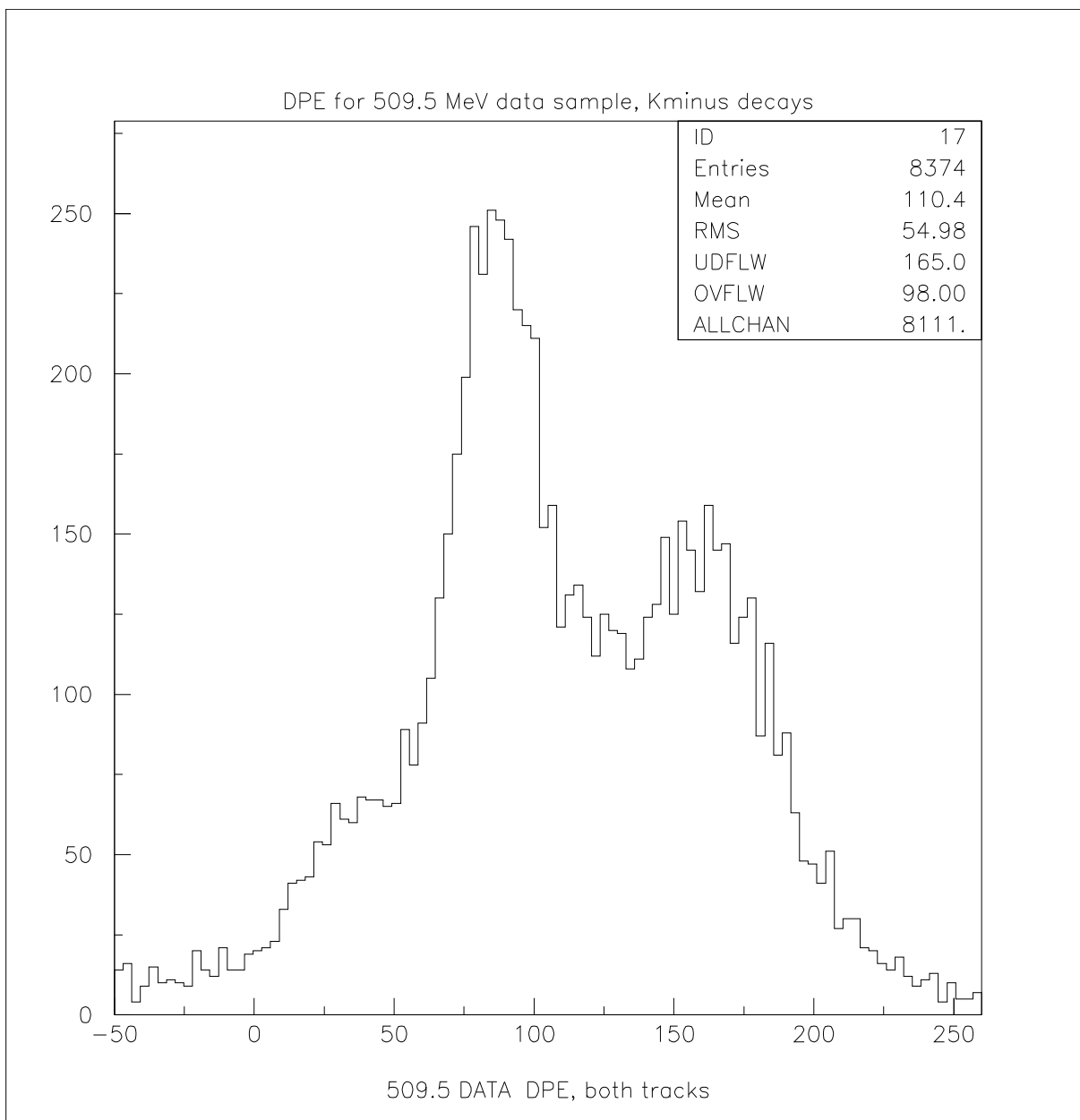


Figure 52: DPE distribution for the data sample of 509.5 MeV,  $K^-$  decays.

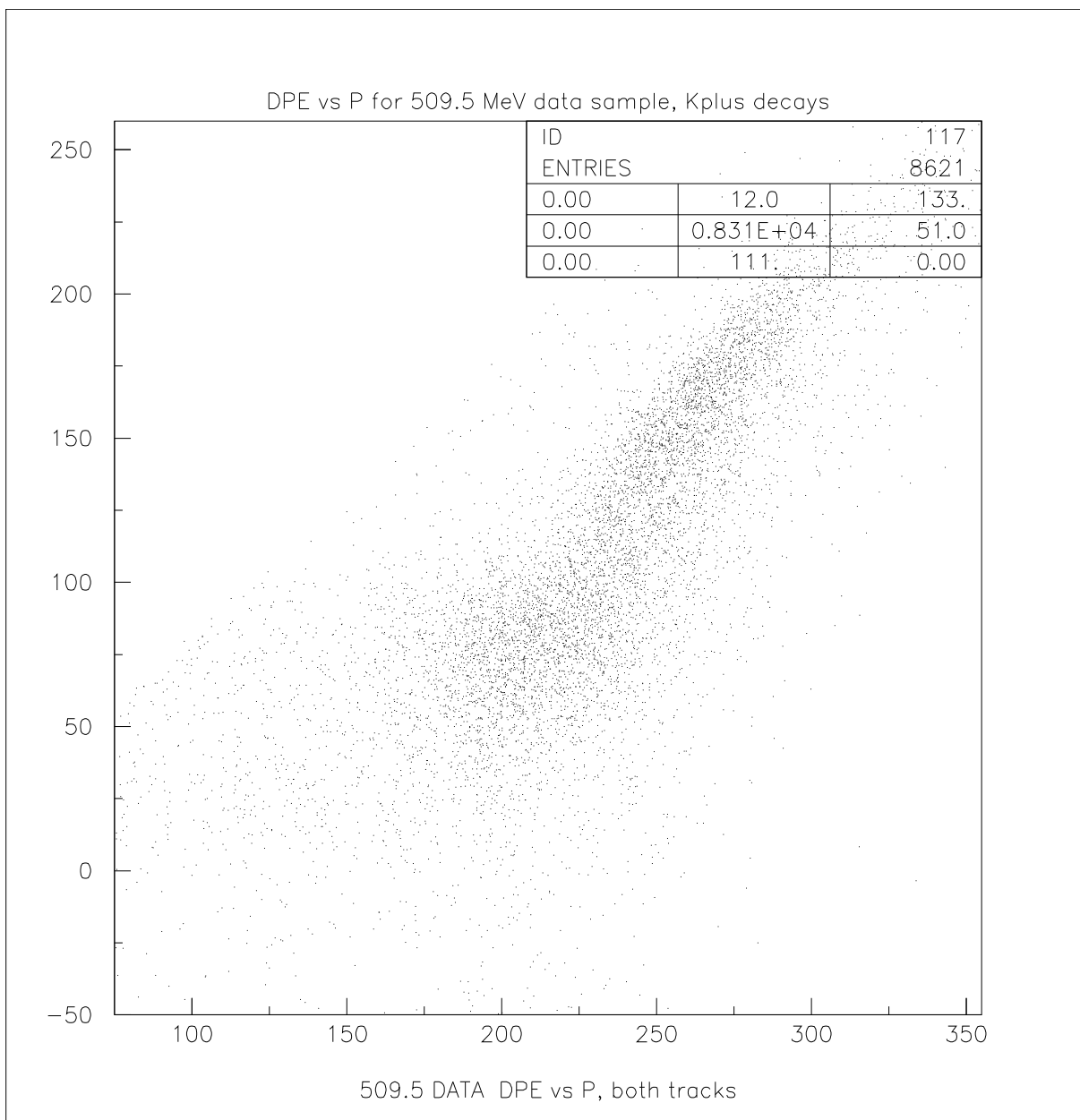


Figure 53: DPE versus momentum for the data sample of 509.5 MeV,  $K^+$  decays.

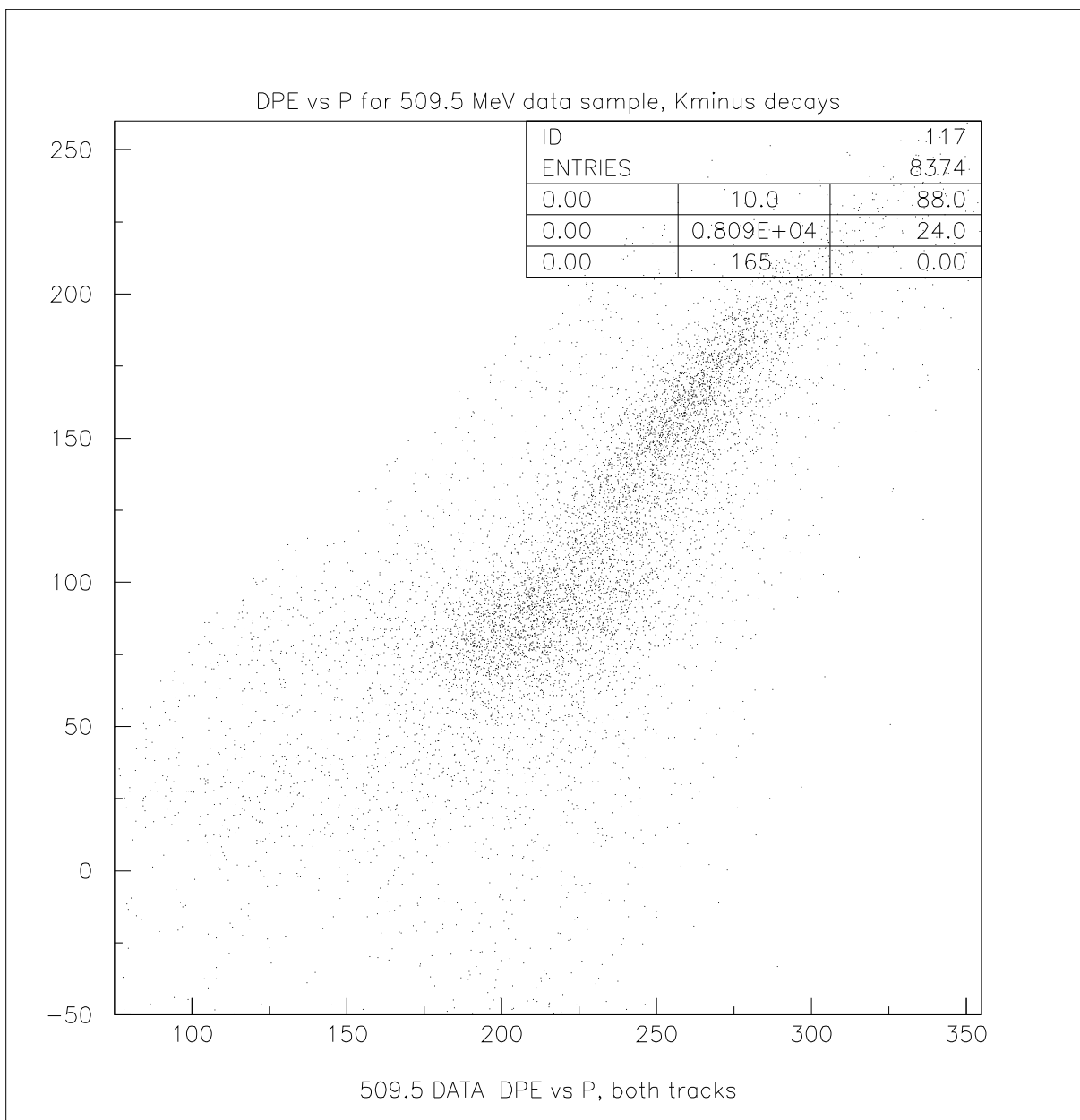


Figure 54: DPE versus momentum for the data sample of 509.5 MeV,  $K^-$  decays.

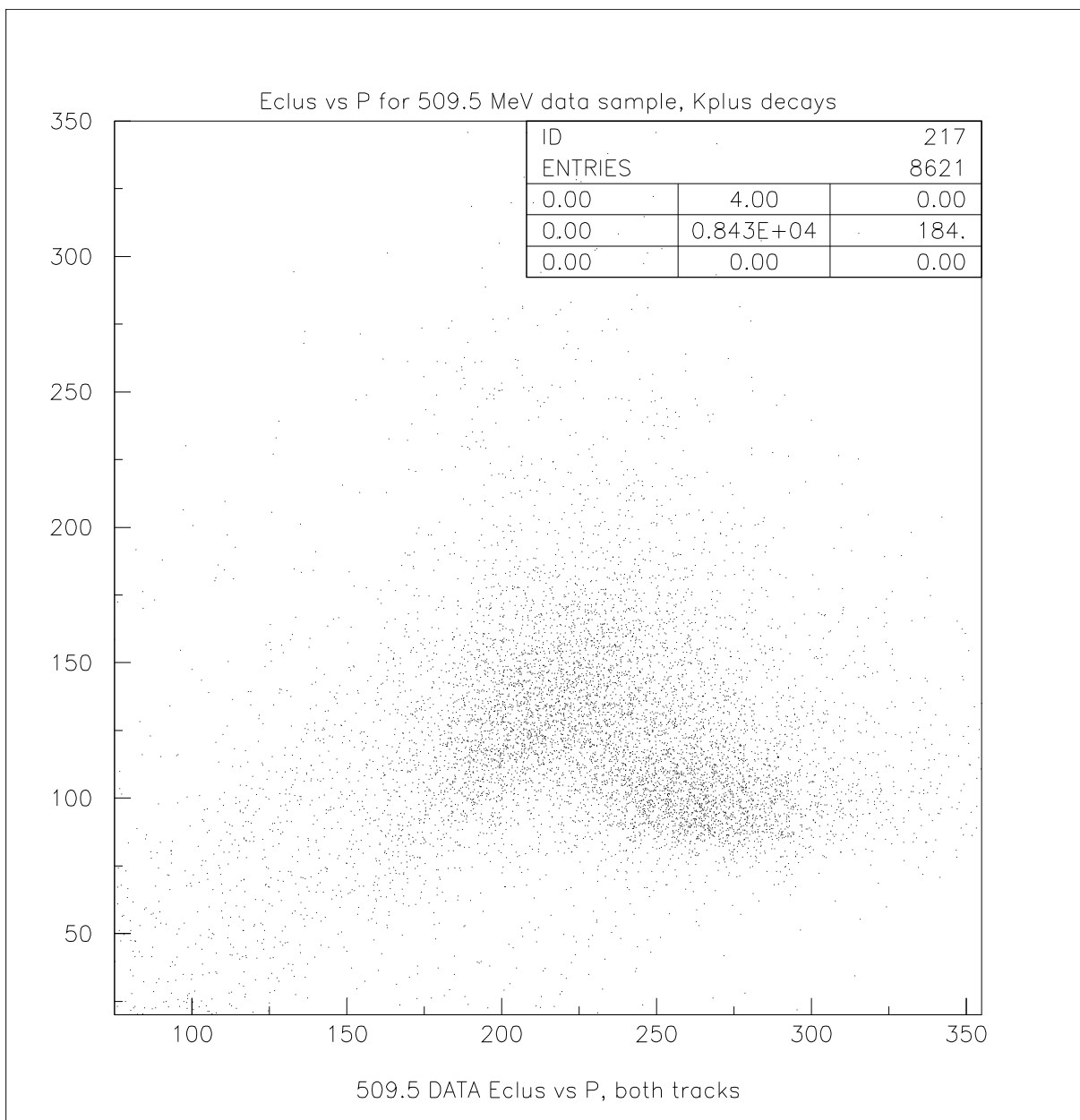


Figure 55:  $E_{clus}$  versus momentum for the data sample of 509.5 MeV,  $K^+$  decays.

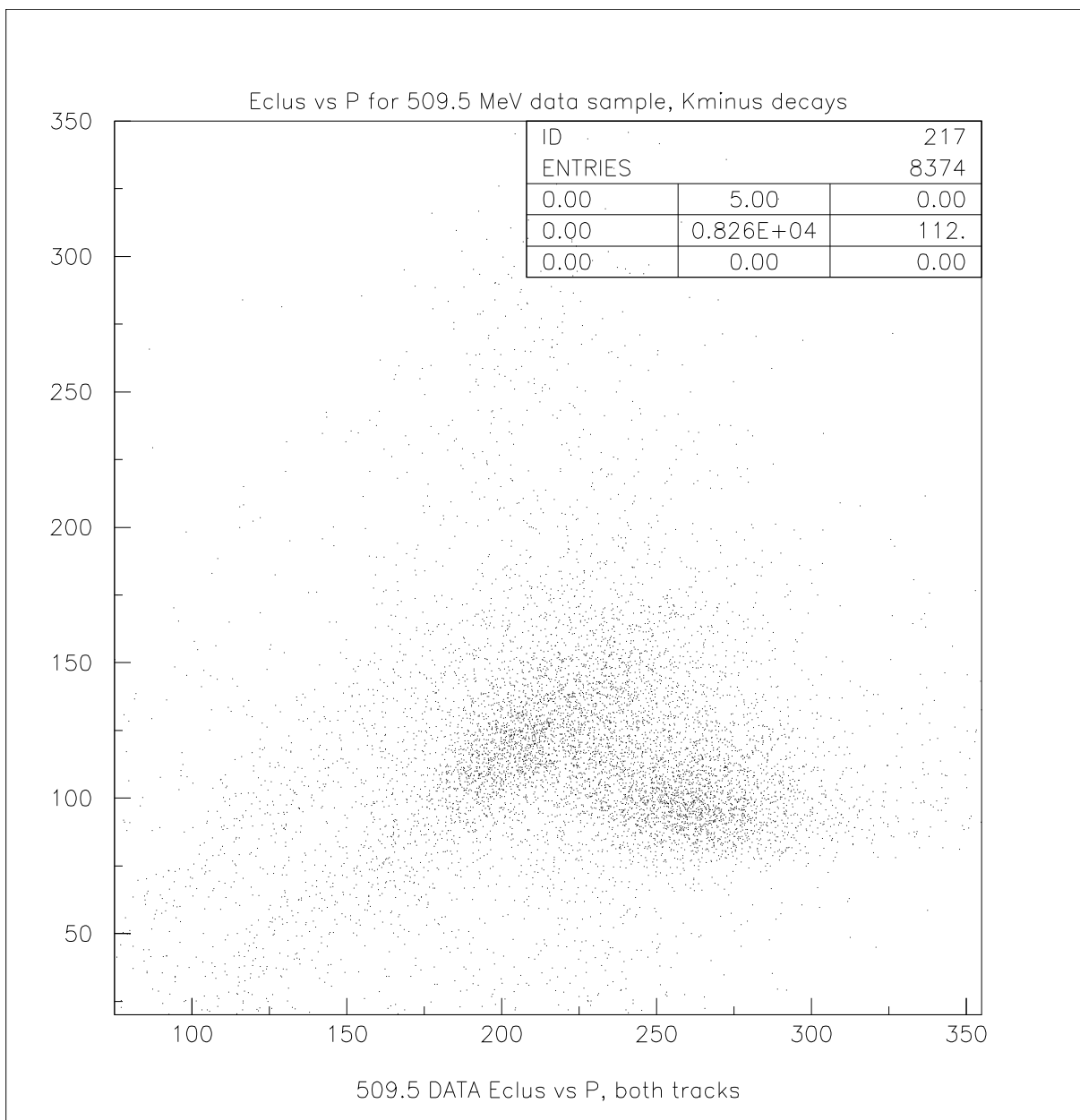


Figure 56:  $E_{clus}$  versus momentum for the data sample of 509.5 MeV,  $K^-$  decays.

## 6.2.1 Electron DPE

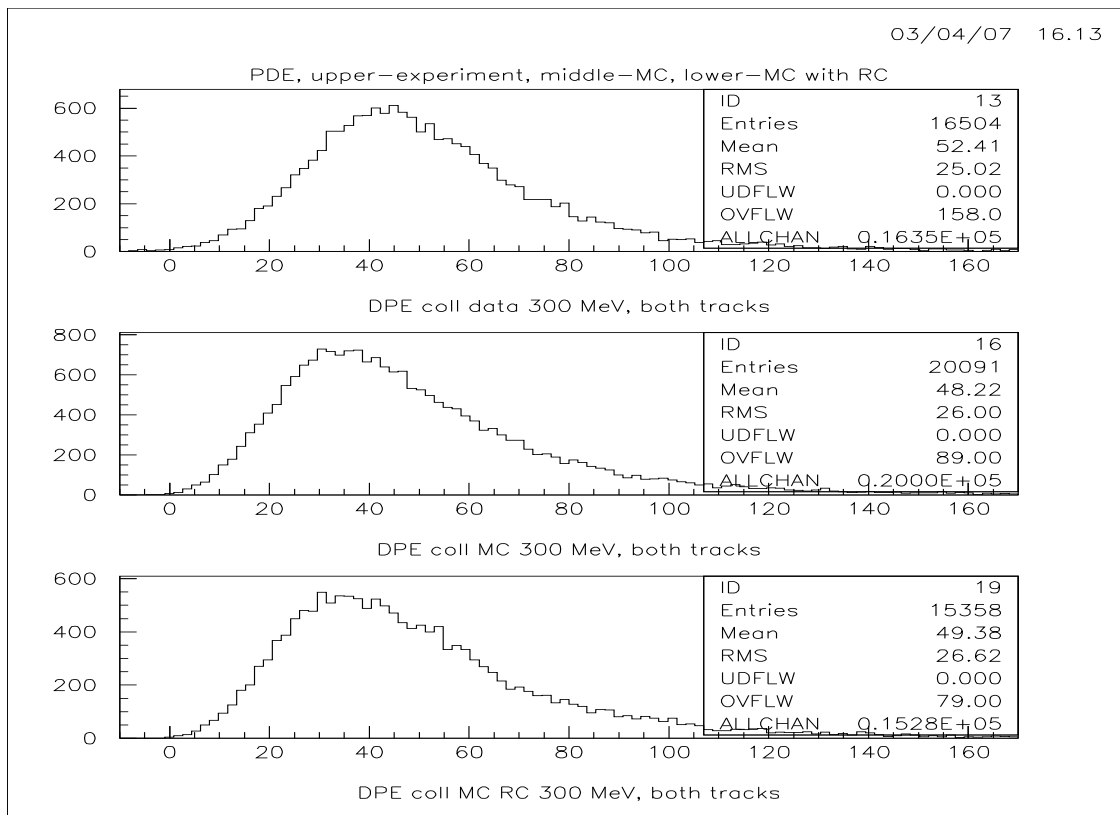


Figure 57: DPE distributions, upper plot – the data, middle – simulation without radiative corrections, lower – simulation with radiative corrections.

While comparing the DPE and  $E_{clus}$  distributions in the collinear events taken from 1998 runs and corresponding simulation we found discrepancies: while the shapes of the distributions are very similar, the distributions from the data are shifted to the left relative to the distributions from the simulation. For example, in 300 MeV data distribution means of both DPE and  $E_{clus}$  are by about 4 MeV smaller than the ones from the simulation. We decided to check if inclusions of radiative corrections in the simulation would improve the situation. The radiative corrections generator used in the simulation takes into account photons emitted by the pair  $e^+e^-$  in the initial state but does not take into account photons emitted in the final state. The results are shown in Figs. 57–60. Though the radiative corrections move the distributions in to better agreement with the data, they do not solve the

existing discrepancies completely. Since the calibration of the CsI calorimeter was made on the basis of simulation; the most probable explanation of these discrepancies is the numerous changes that were made in the simulation software during the course of the analysis.

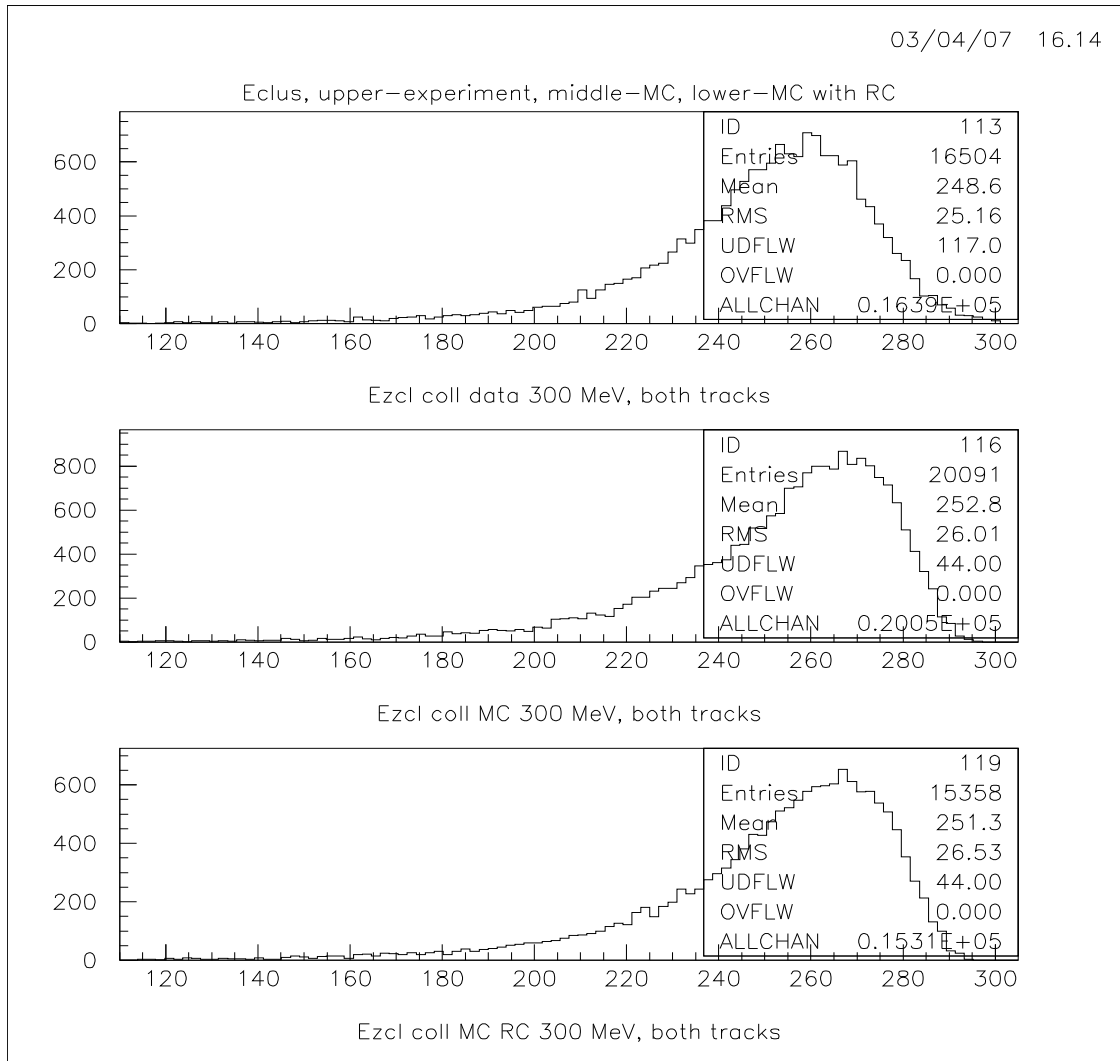


Figure 58:  $E_{clus}$ , upper plot – the data, middle–simulation without radiative corrections, lower–simulation with radiative corrections

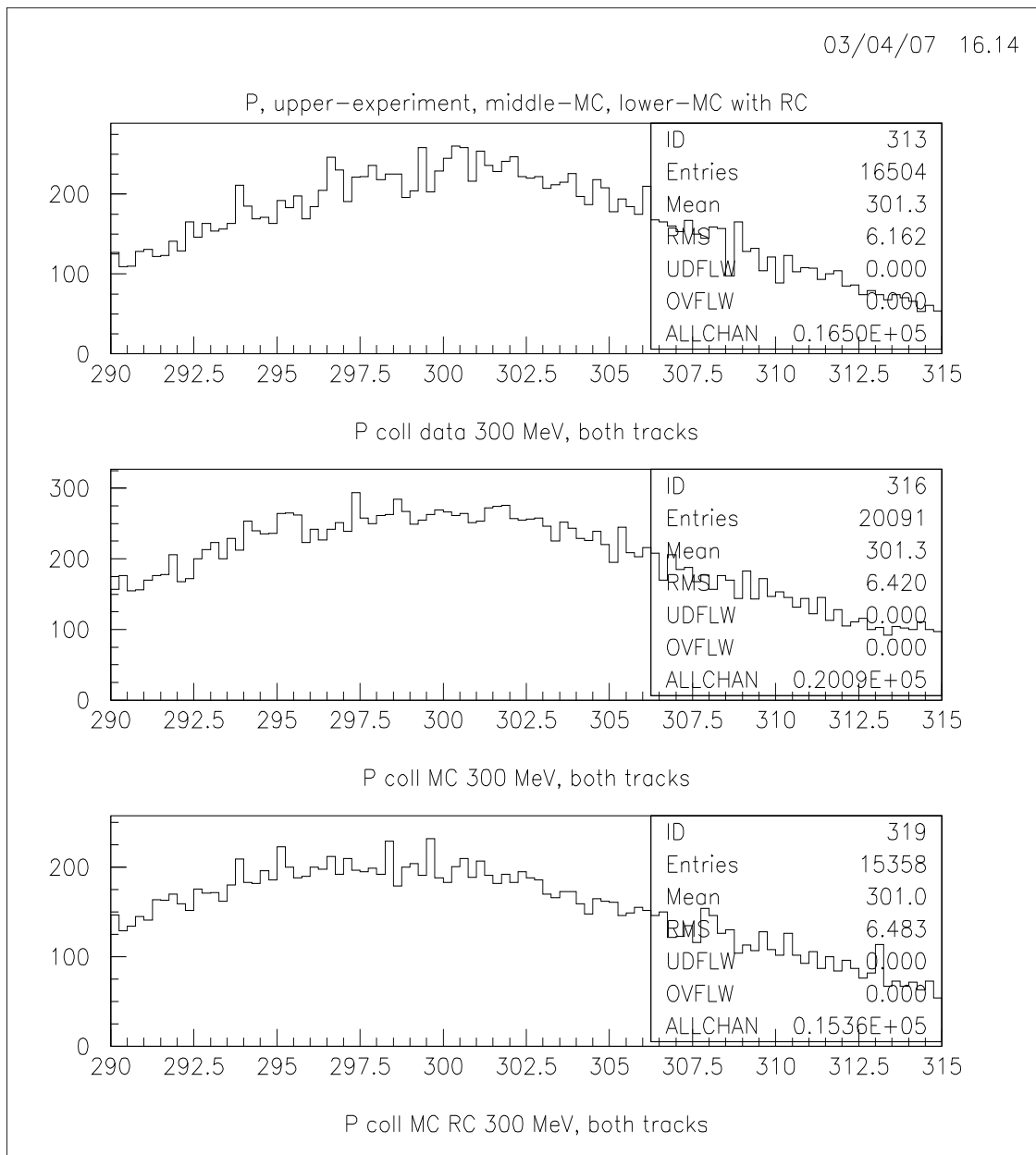


Figure 59: Momentum, upper plot – the data, middle–simulation without radiative corrections, lower–simulation with radiative corrections.

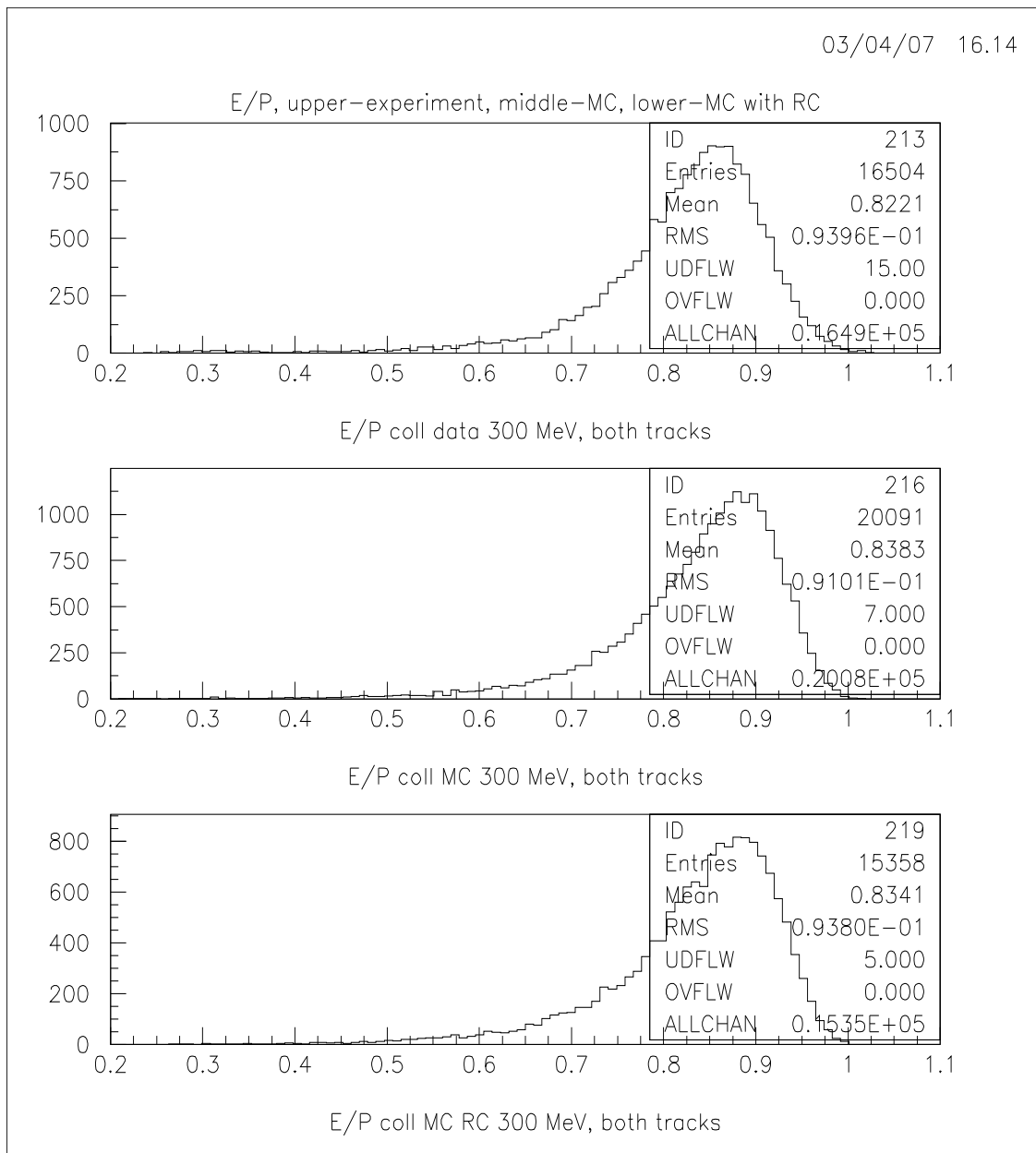


Figure 60: Ratio  $E_{clus}/P$ , upper plot — the data, middle — simulation without radiative corrections, lower — simulation with radiative corrections.

## 6.2.2 Muon DPE

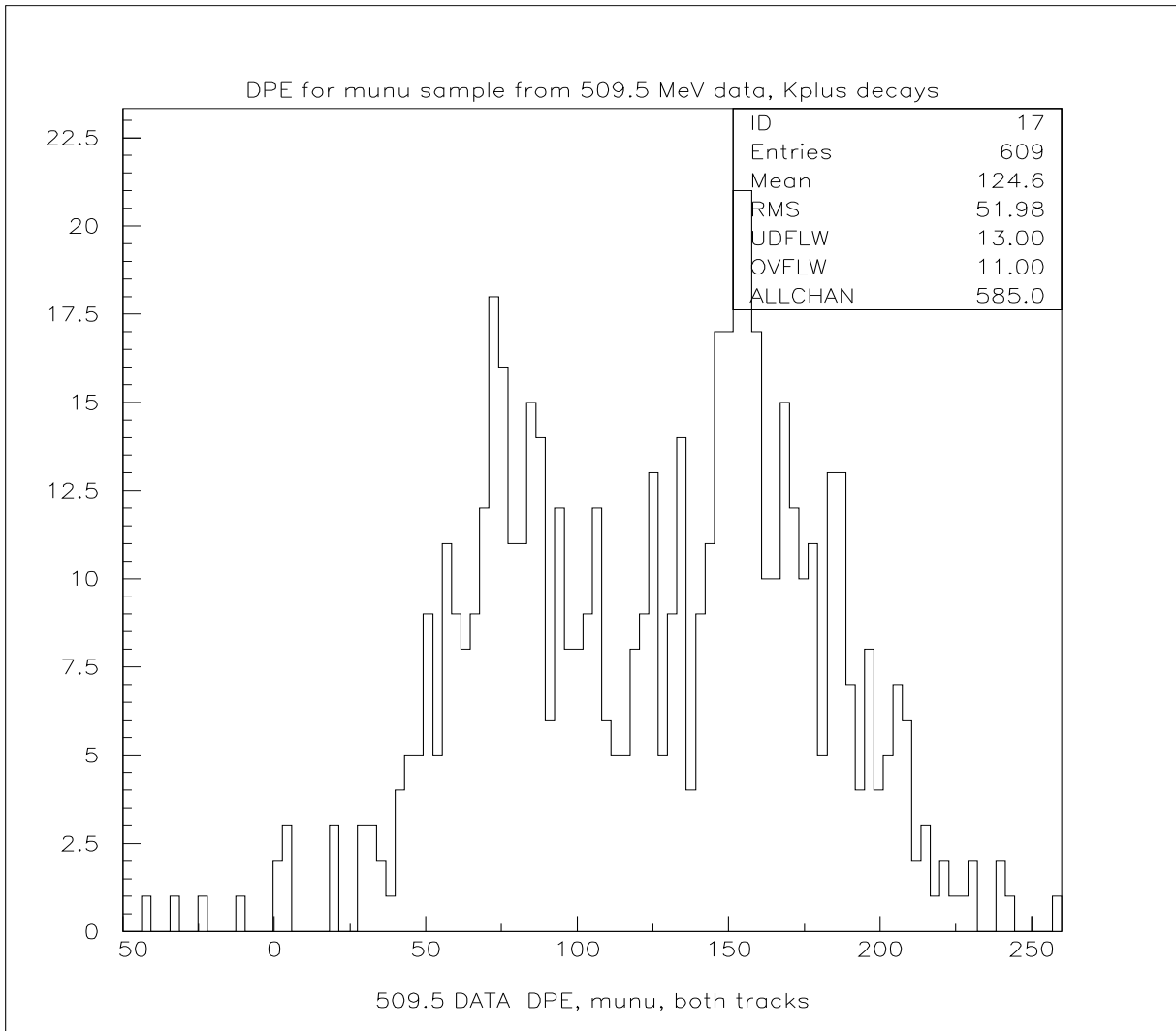


Figure 61: DPE for muons selected from 509.5 MeV data by requiring no photons in the event and  $MM2 < 35000$ ,  $K^+$  decays.

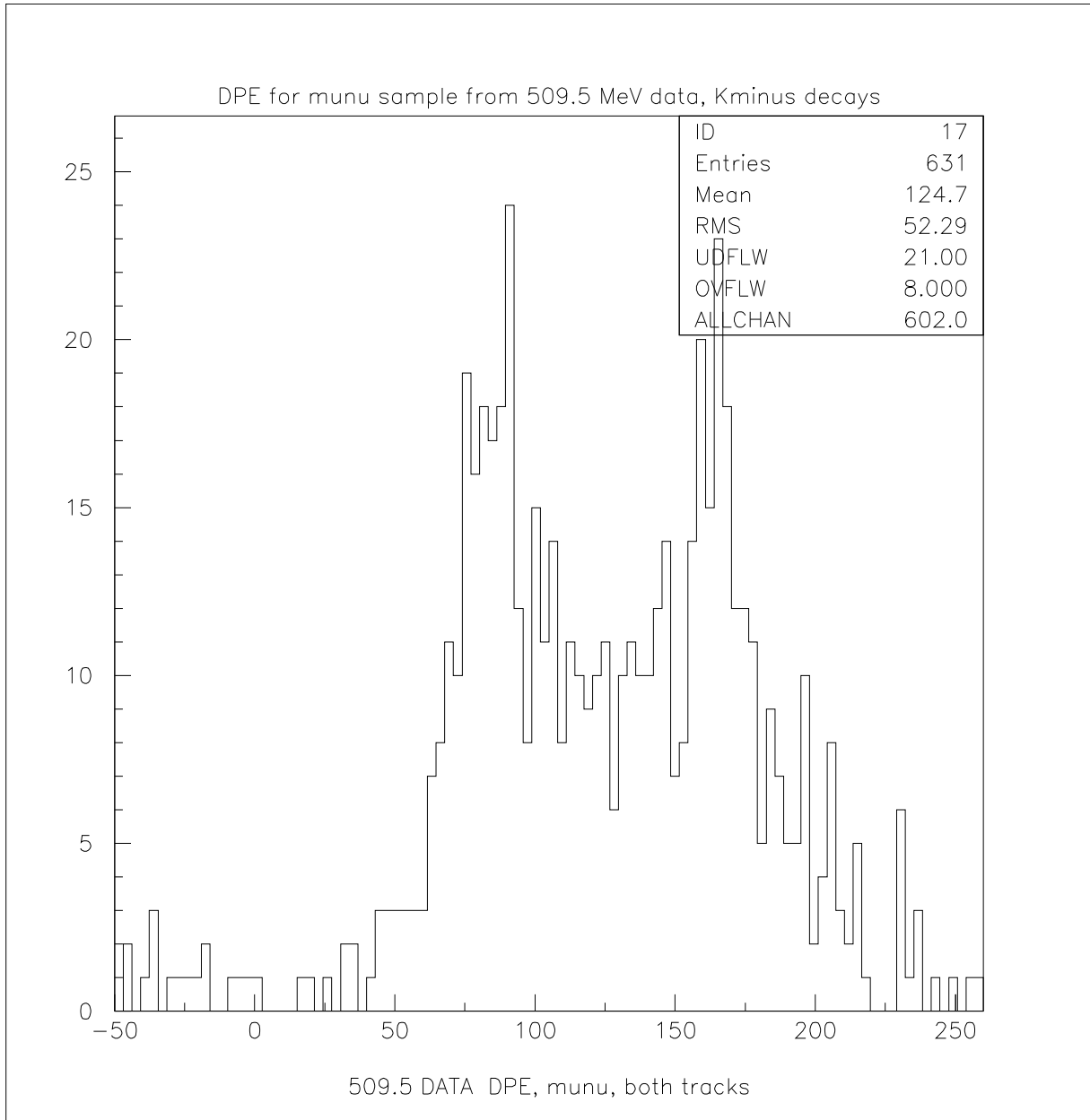


Figure 62: DPE for muons selected from 509.5 MeV data by requiring no photons in the event and  $MM2 < 35000$ ,  $K^-$  decays.

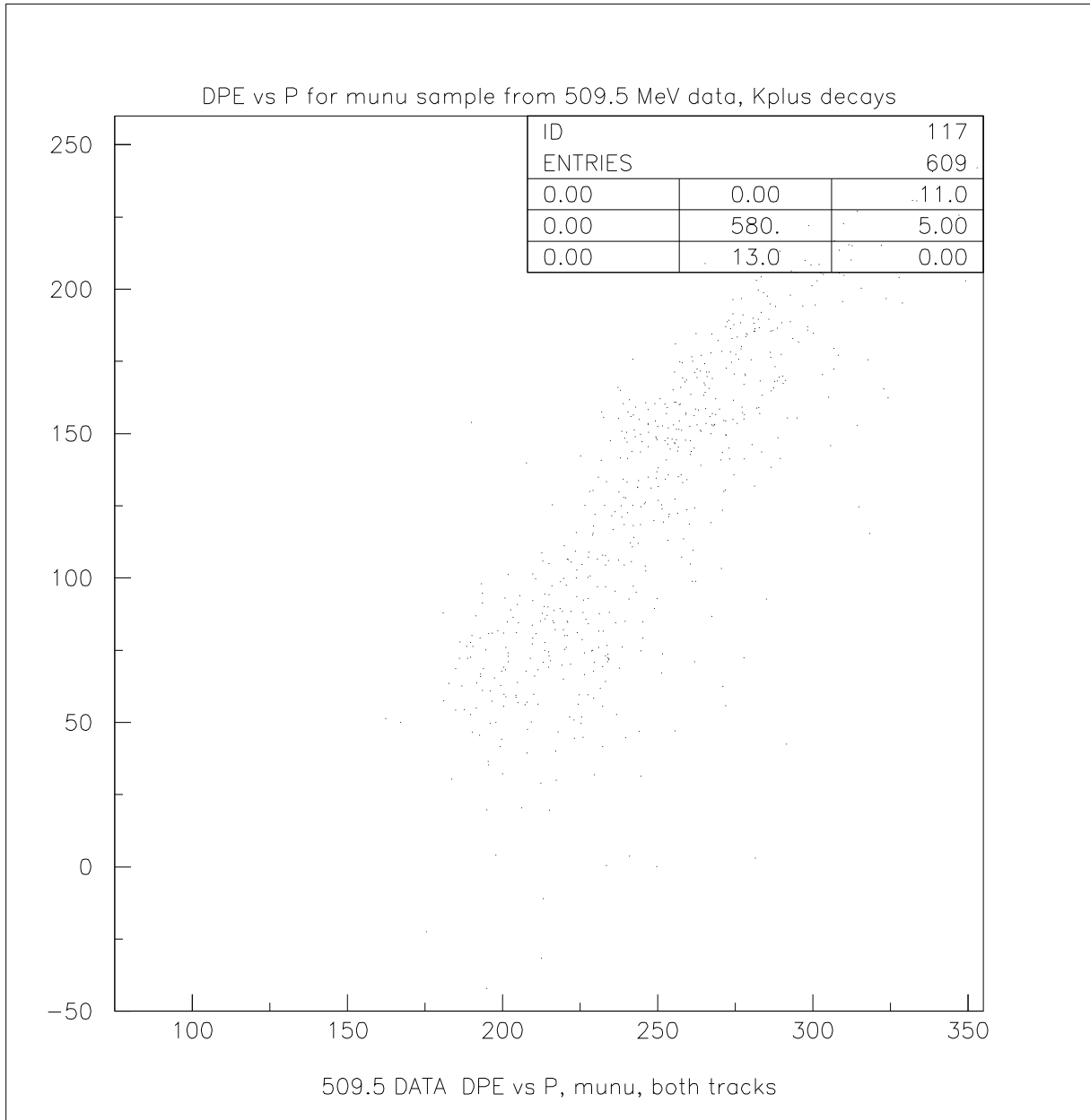


Figure 63: DPE versus momentum for muons selected from 509.5 MeV data by requiring no photons in the event and  $MM2 < 35000$ ,  $K^+$  decays.

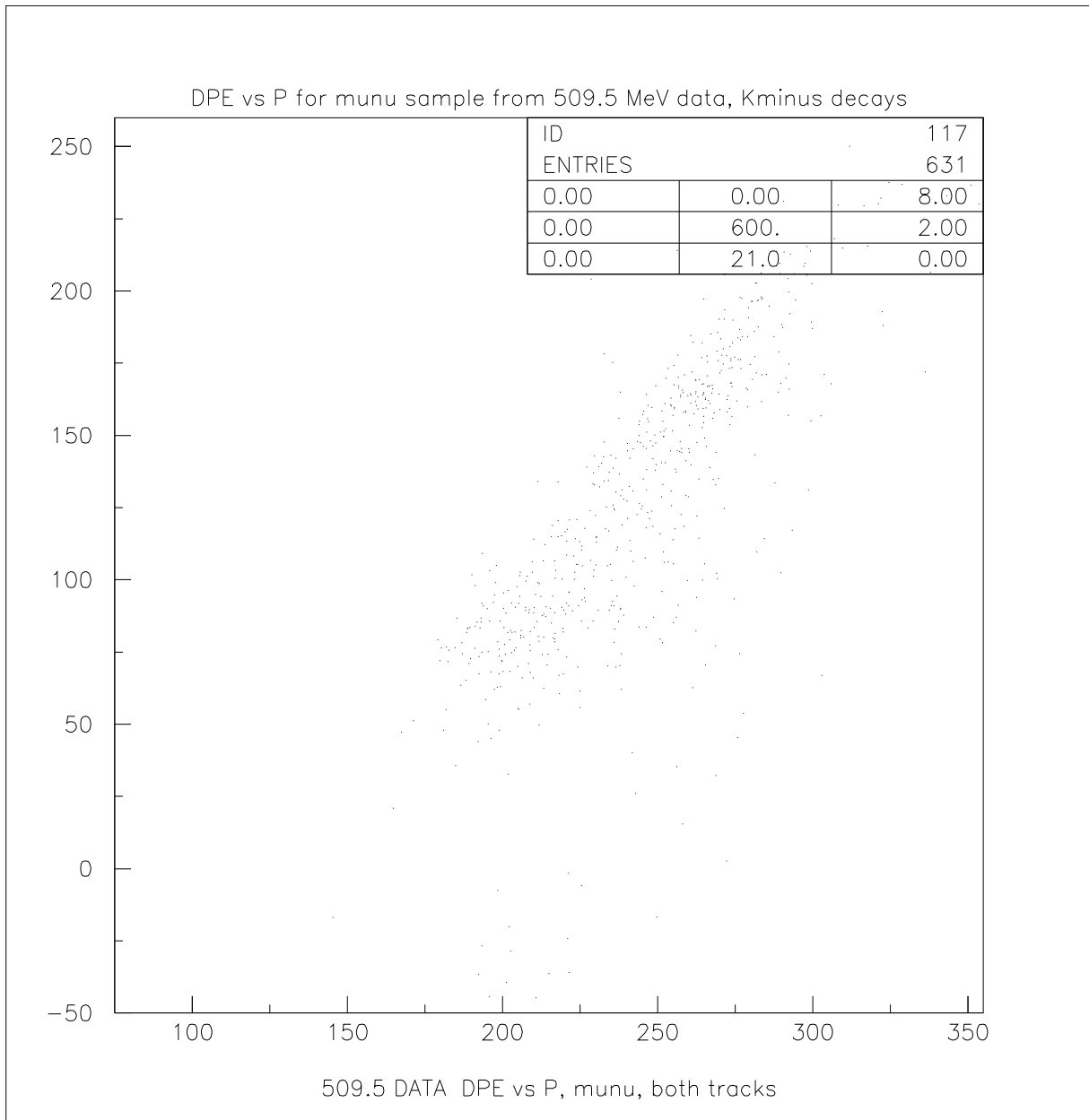


Figure 64: DPE versus momentum for muons selected from 509.5 MeV data by requiring no photons in the event and  $MM2 < 35000$ ,  $K^-$  decays.

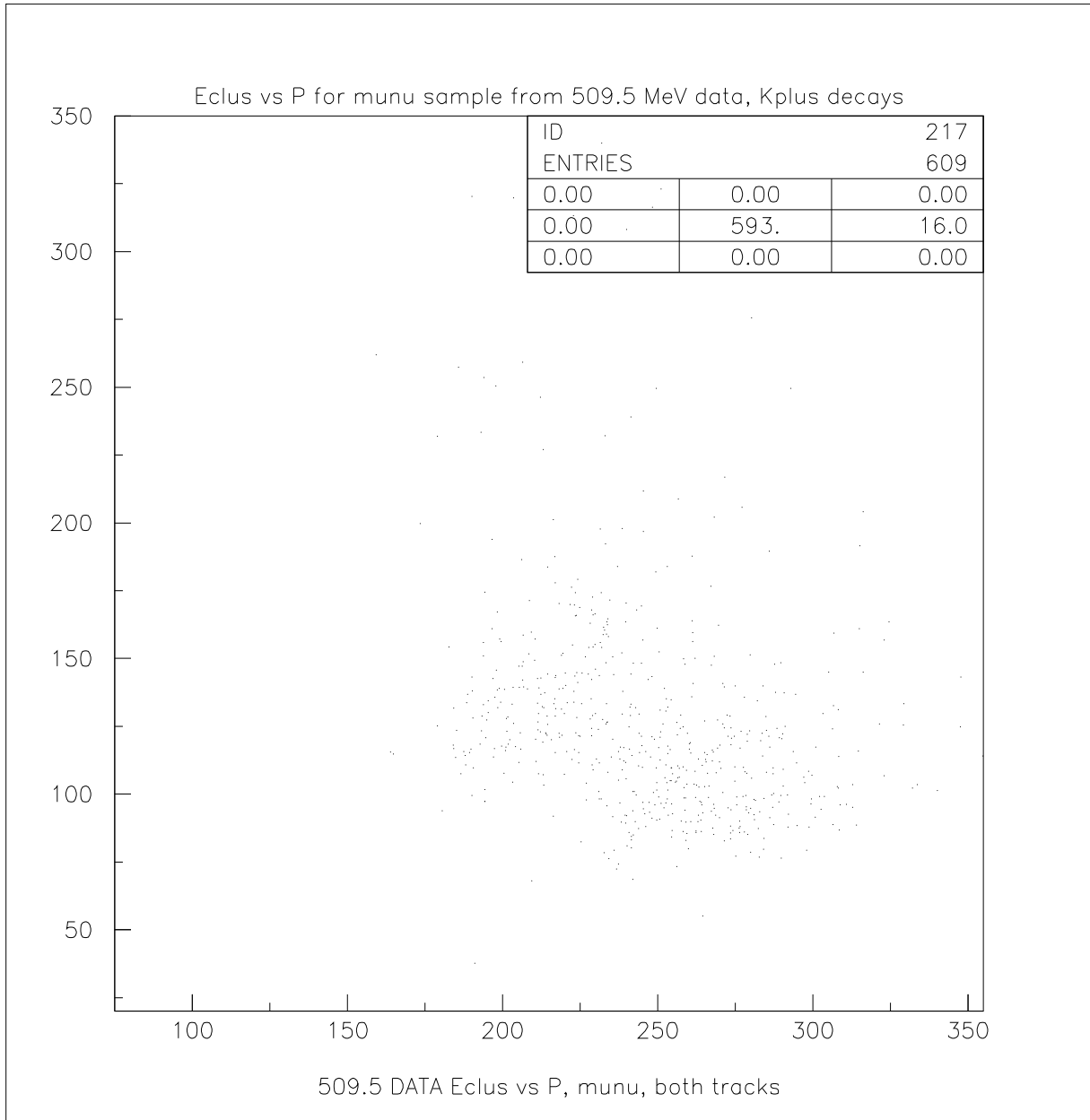


Figure 65:  $E_{clus}$  versus momentum for muons selected from 509.5 MeV data by requiring no photons in the event and  $MM2 < 35000$ ,  $K^+$  decays.

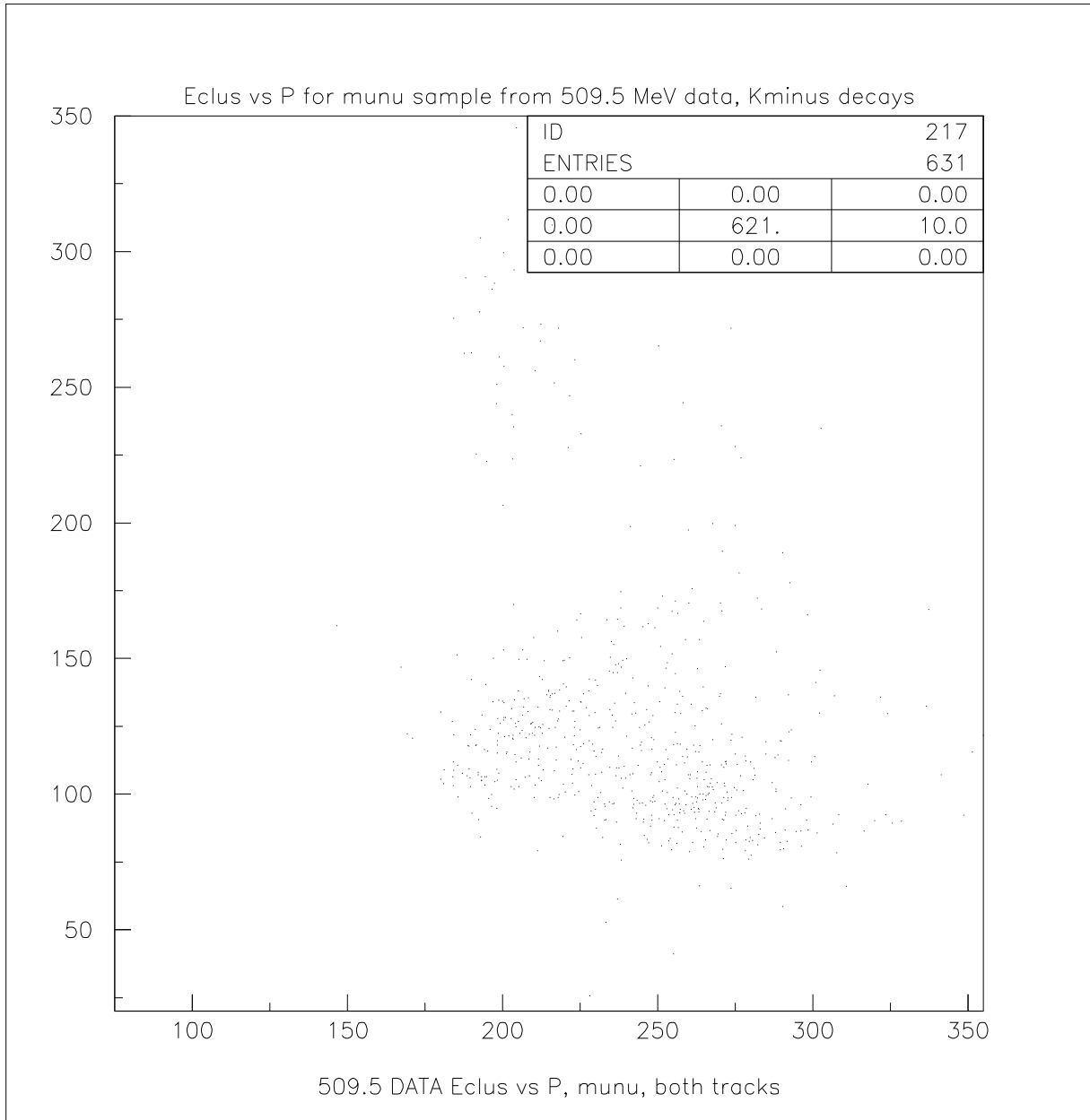


Figure 66:  $E_{clus}$  versus momentum for muons selected from 509.5 MeV data by requiring no photons in the event and  $MM2 < 35000$ ,  $K^-$  decays.

### 6.2.3 Pion DPE

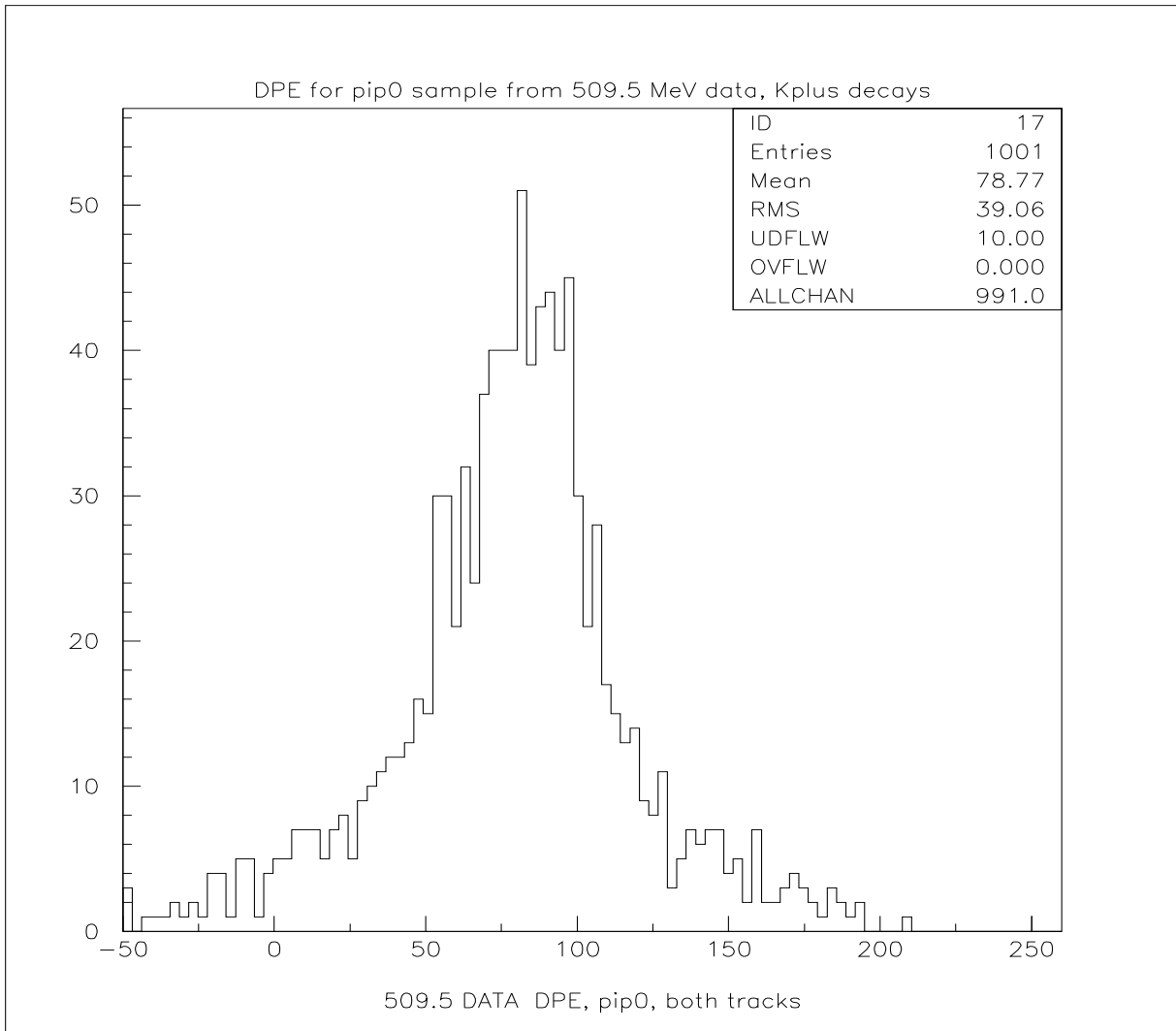


Figure 67: DPE for pions selected from 509.5 MeV data by requiring presence of  $\pi^0$  in the event and  $15000 < MM2 < 35000$ ,  $K^+$  decays.

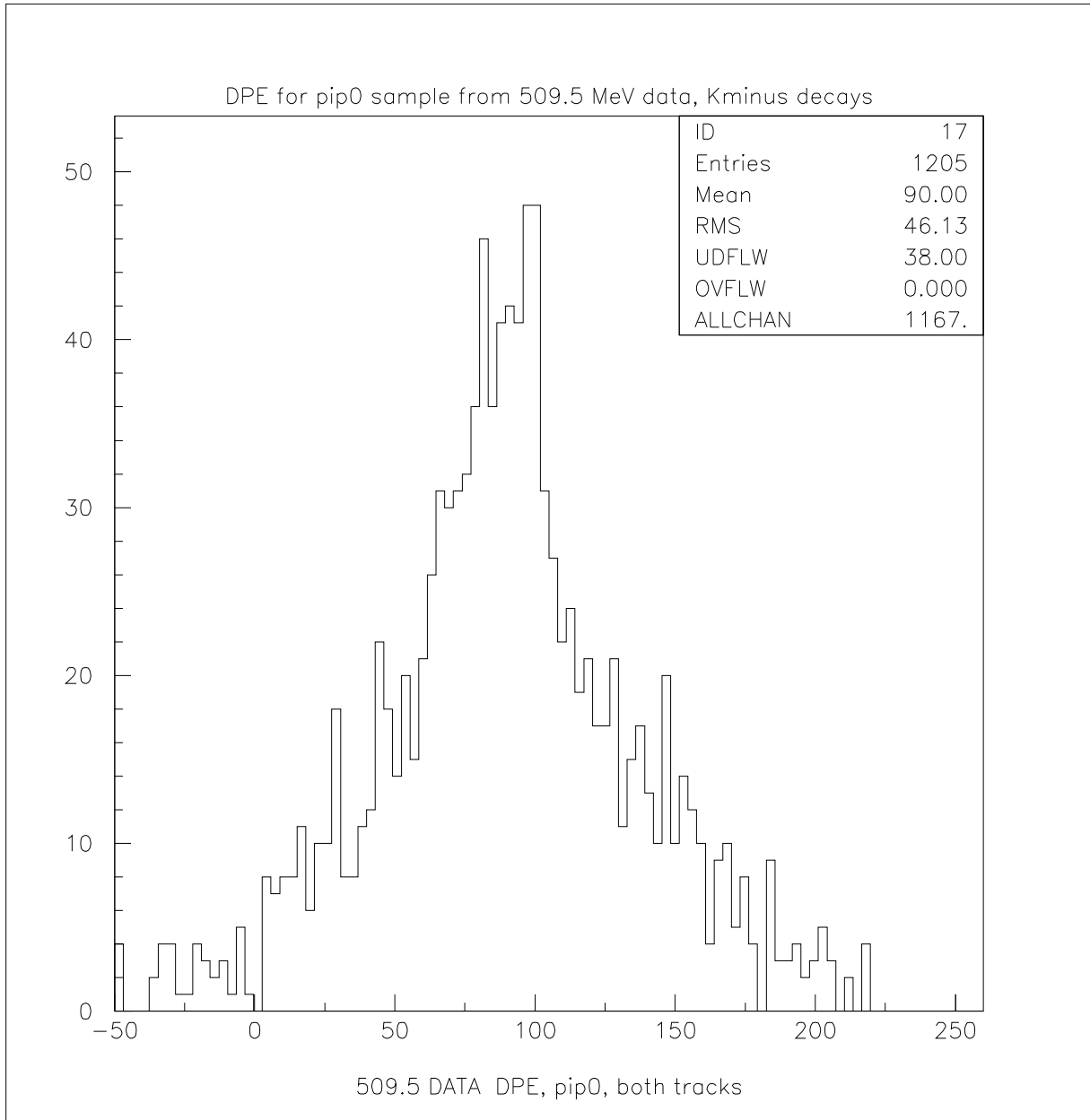


Figure 68: DPE for pions selected from 509.5 MeV data by requiring presence of  $\pi^0$  in the event and  $15000 < MM2 < 35000$ ,  $K^-$  decays.

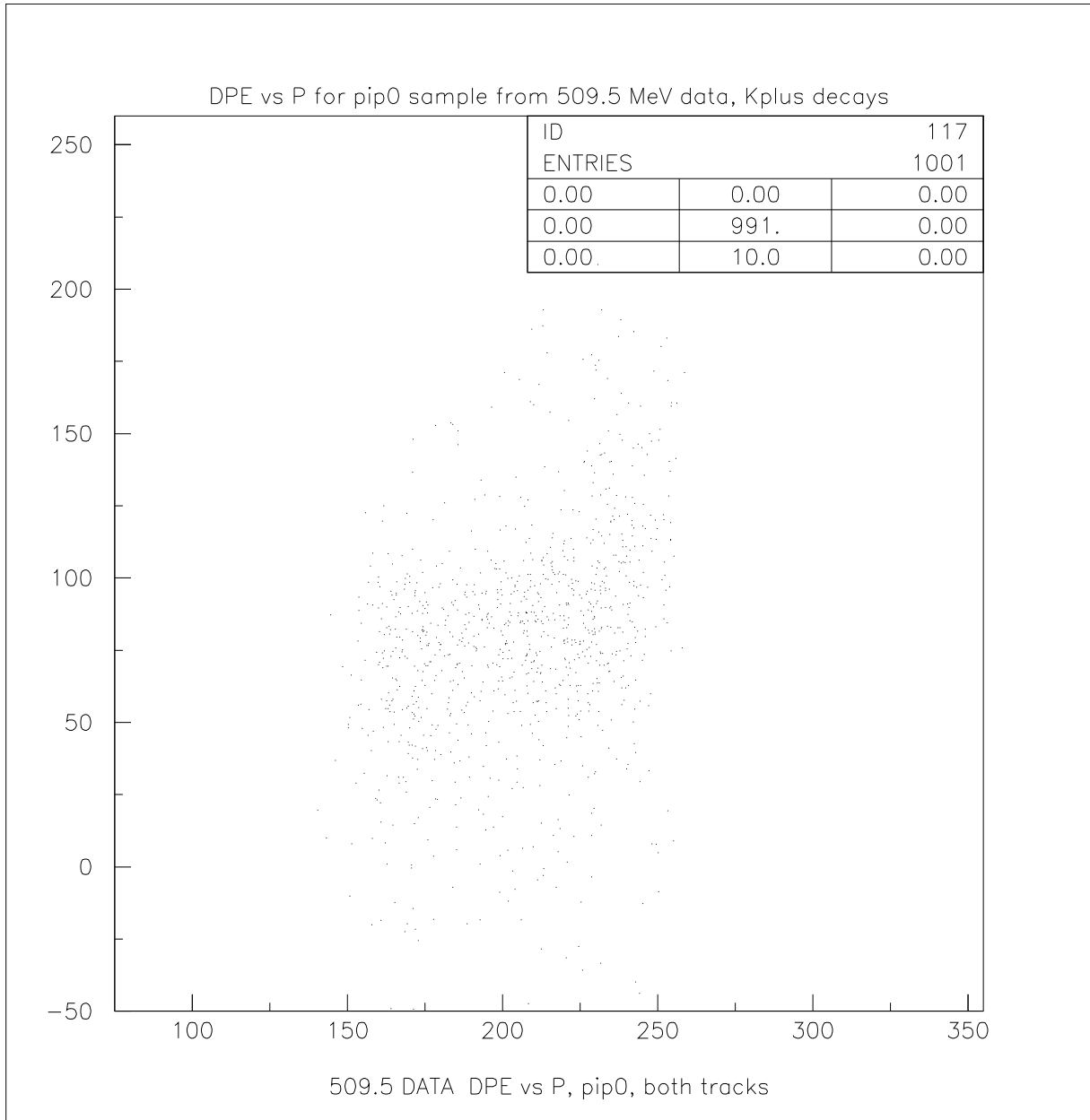


Figure 69: DPE versus momentum for pions selected from 509.5 MeV data by requiring presence of  $\pi^0$  in the event and  $15000 < MM2 < 35000$ ,  $K^+$  decays.

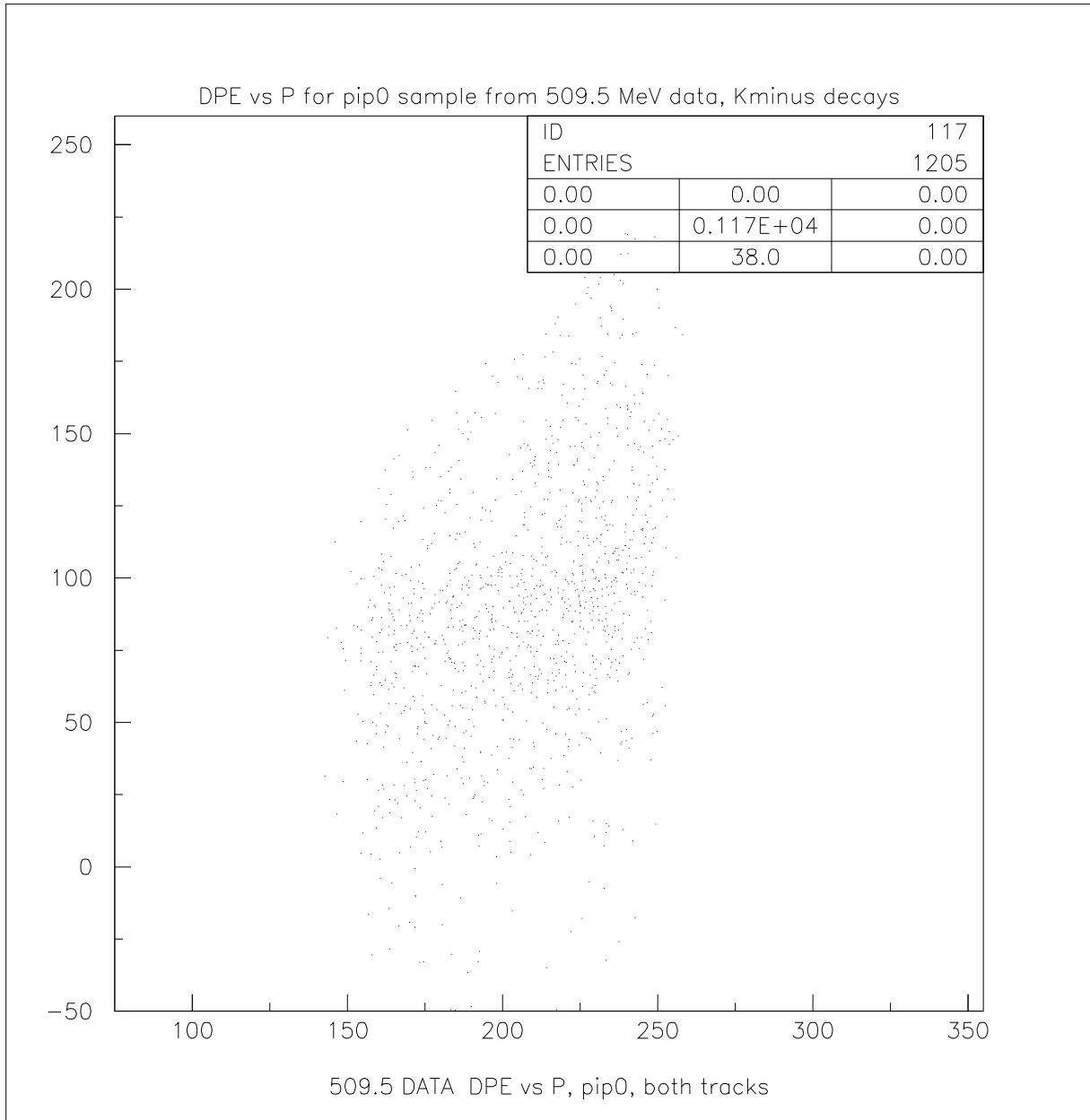


Figure 70: DPE versus momentum for pions selected from 509.5 MeV data by requiring presence of  $\pi^0$  in the event and  $15000 < MM2 < 35000$ ,  $K^-$  decays.

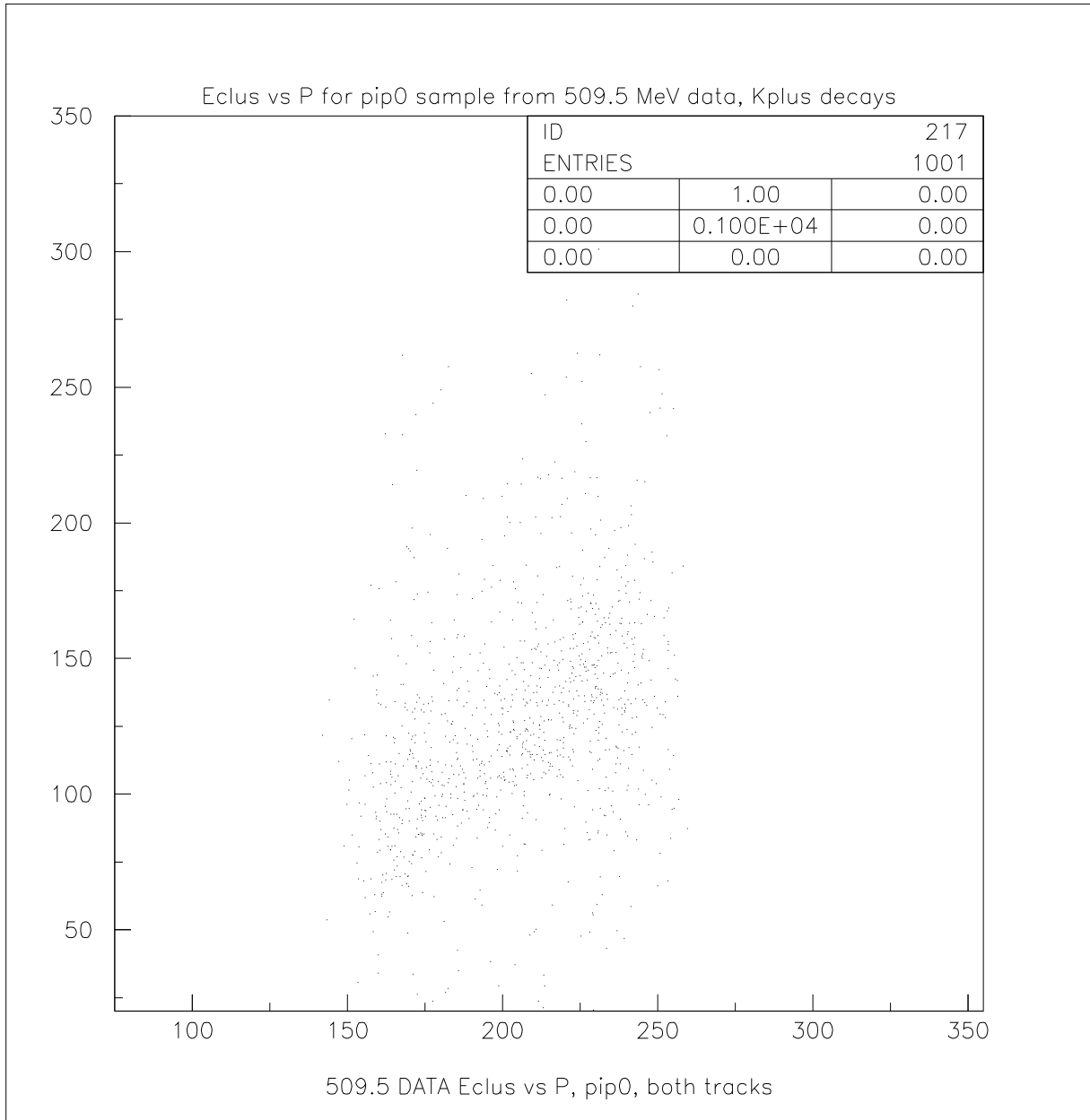


Figure 71:  $E_{clus}$  versus momentum for pions selected from 509.5 MeV data by requiring presence of  $\pi^0$  in the event and  $15000 < MM2 < 35000$ ,  $K^+$  decays.

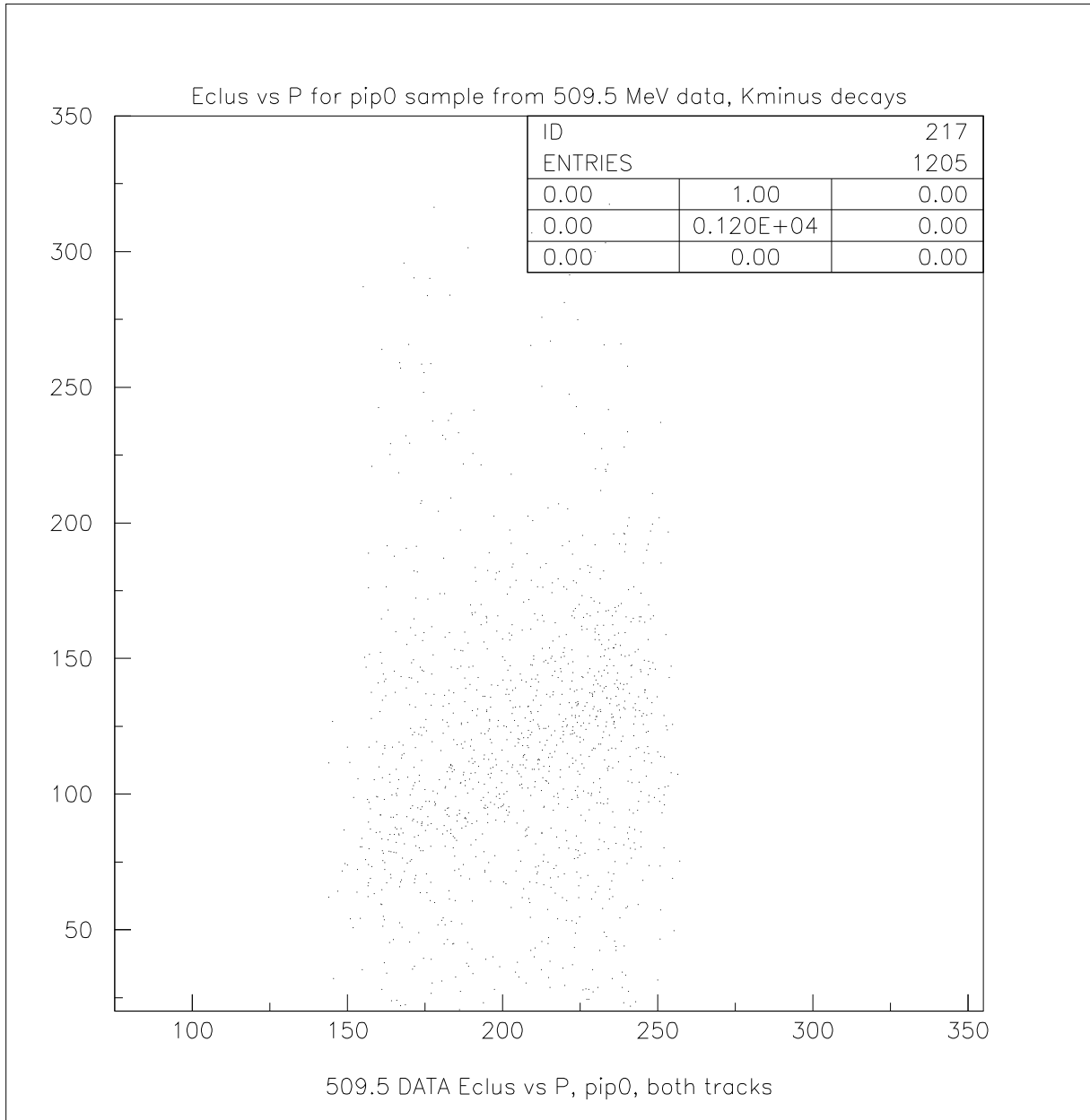


Figure 72:  $E_{clus}$  versus momentum for pions selected from 509.5 MeV data by requiring presence of  $\pi^0$  in the event and  $15000 < MM2 < 35000$ ,  $K^-$  decays.

#### 6.2.4 Comparison of Experimental and Simulated DPE distributions

DPE allows separation between the two semileptonic modes,  $K_{\mu 3}$  and  $K_{e 3}$ . The distribution in figure 73 is obtained from a sample consisting of mostly  $K_{\mu 3}$  and  $K_{e 3}$  decays; other modes are discriminated against by the requirement that missing mass squared is between 35000 and 70000  $\text{MeV}^2$ . The 510.0 MeV data sample was used. As will be explained in the analysis chapter, the peaks have been brought into agreement using certain transformations of the simulated DPE distributions, but the width disagreements indicate that further fine tuning of the dpe plots would have improved the final agreement of data and simulation. The relative insensitivity of our matrix method (described in the analysis section) to the exact shape of the DPE is one reason for its choice. Figure 74 shows DPE for a predominantly semileptonic sample of events which was selected by the MM2 parameter. As the figure illustrates, only negative decays can be used to separate between the two semileptonic modes,  $K_{\mu 3}$  and  $K_{e 3}$ . Since positive muons decay within the calorimeter and thus may in some cases fake electron energy losses, the DPE distributions of  $\mu^+$  and  $e^+$  coming from  $K_{\mu 3}$  and  $K_{e 3}$  overlap to the degree that does not allow the separation. Negative muons are captured and give mostly  $dE/dx$  energy losses, therefore the DPE distributions of  $\mu^-$  and  $e^-$  differ substantially.

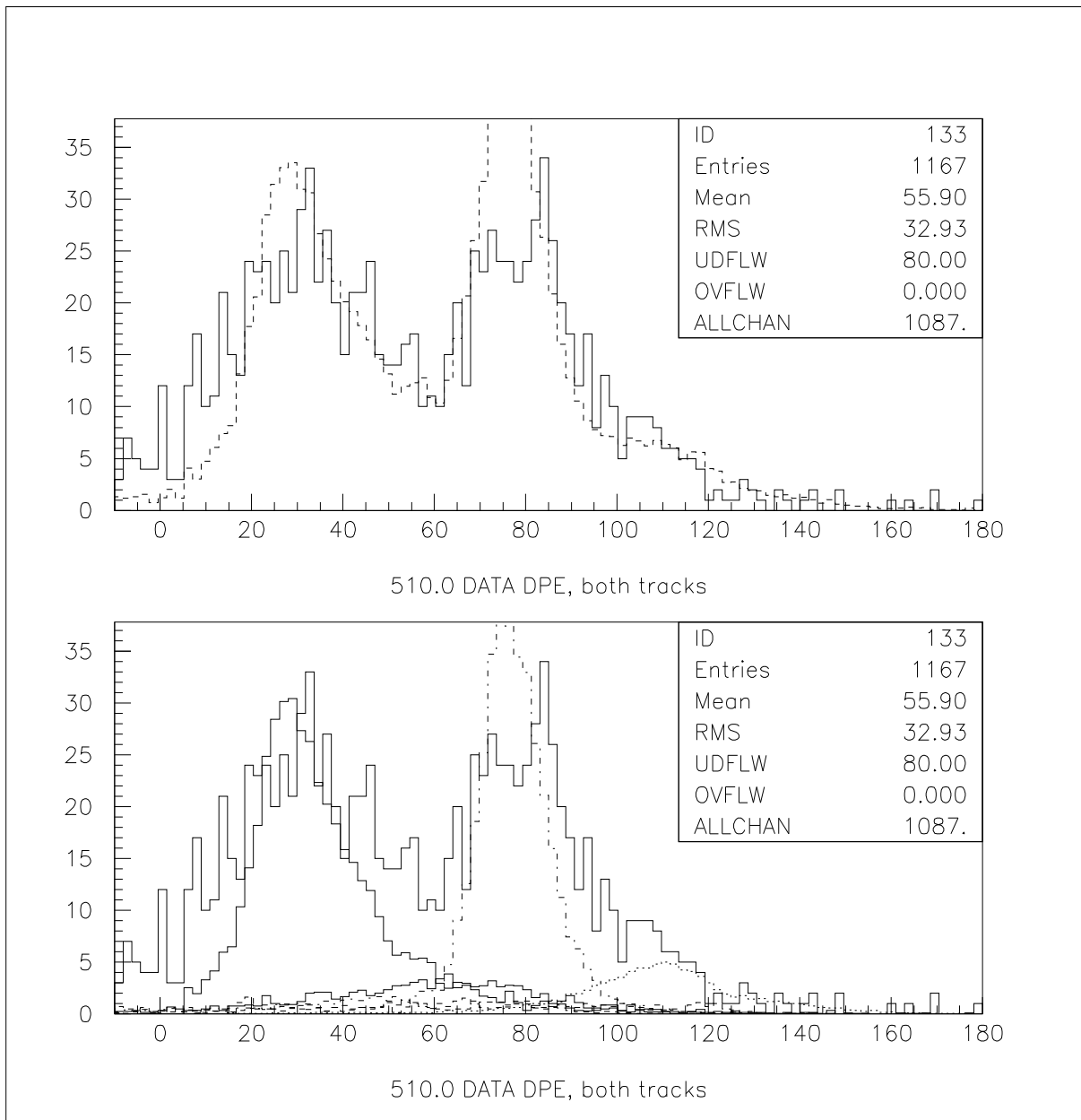


Figure 73: DPE distribution for the 510.0 MeV sample is represented by the solid line, dashed line shows the simulated distributions.  $K^-$  data is used.

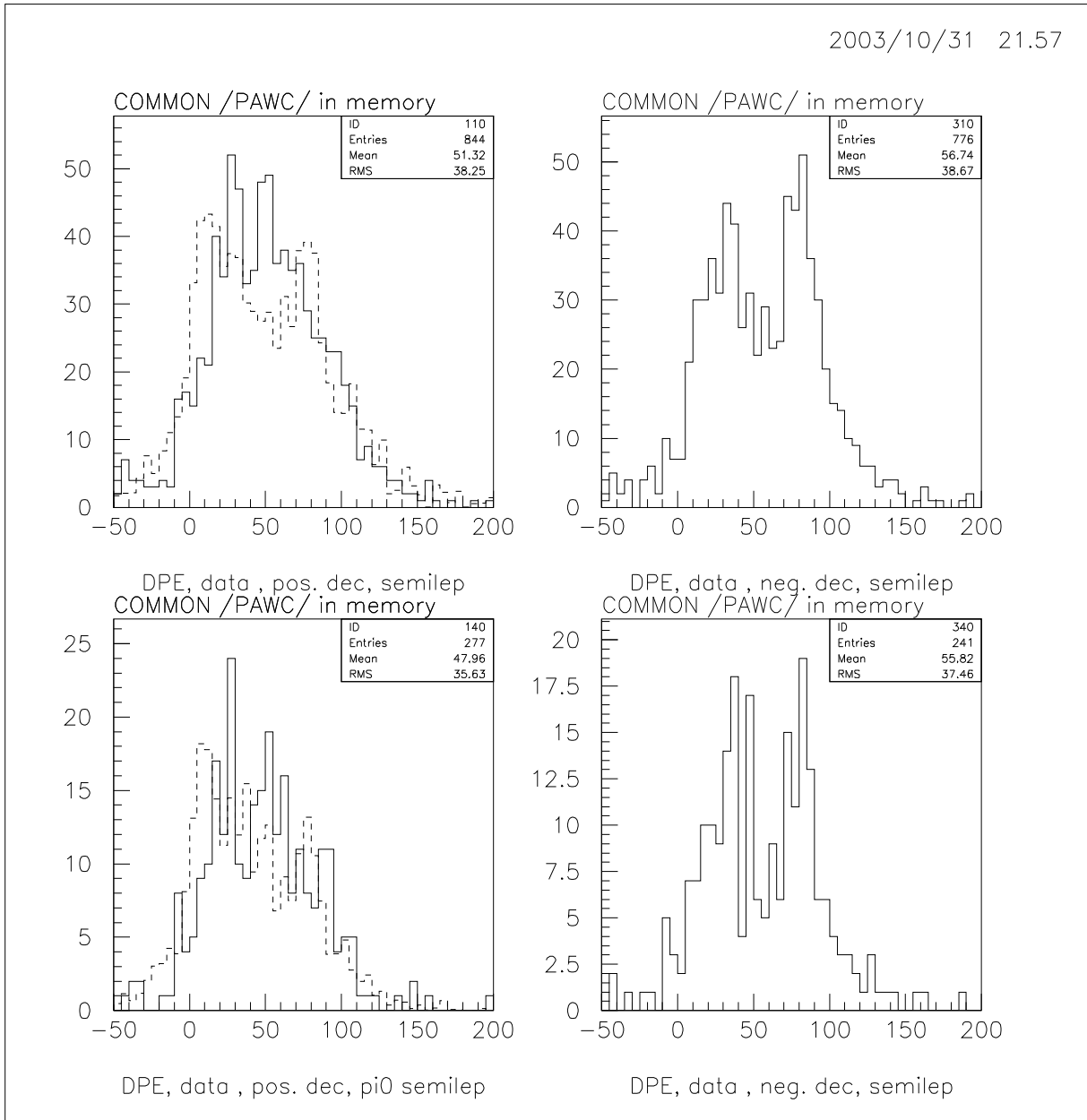


Figure 74: DPE for events in the semileptonic MM2 region. DPE separates  $e^-$  from  $\mu^-$  and  $\pi^-$  better than  $e^+$  from  $\mu^+$  and  $\pi^+$ . The plots come from a preliminary analysis before I introduced the DPE transformations that offset the differences in the calibrations.

## 7.0 ANALYSIS

In this chapter I describe the methods and algorithms used to perform the measurements.

### 7.1 RATIOS TO BE MEASURED

The following three ratios are determined from the missing mass distributions:

1.  $R_{2body} \equiv (Br(K^+ \rightarrow \pi^+\pi^0)/Br(K^+ \rightarrow \mu^+\nu))$
2.  $R_{semilep} \equiv (Br(K^+ \rightarrow \pi^0\mu^+\nu) + Br(K^+ \rightarrow \pi^0e^+\nu))/Br(K^+ \rightarrow \pi^+\pi^0)$
3.  $R_{3pion} \equiv (Br(K^+ \rightarrow \pi^+\pi^+\pi^-) + Br(K^+ \rightarrow \pi^+\pi^0\pi^0))/Br(K^+ \rightarrow \pi^+\pi^0)$

One more ratio is determined from the DPE distributions:

$$R_{e\mu} \equiv Br(K^+ \rightarrow \pi^0e^+\nu)/Br(K^+ \rightarrow \pi^0\mu^+\nu)$$

### 7.2 MM2 ANALYSIS

The MM2 analysis is done in two ways:  $K \rightarrow \mu\nu$  MM2 distribution taken from the simulation and from the data. The difference between the results reflects imperfections of the simulation and is used to estimate the systematic error of our measurements.

Once the MM2 distributions of all the modes are obtained I apply the following procedure:

1.  $K \rightarrow \mu\nu$  and  $K \rightarrow \pi\pi^0$  MM2 distributions are fit with a sum of 3 gaussians each
2. the MM2 distributions of  $K_{\mu 3}$  and  $K_{e3}$  are added together with the weights being equal to their known branchings and these two modes are effectively treated as one – semileptonic mode. The resulting distribution is fit with splines

3. the MM2 distributions of  $K^\pm \rightarrow \pi^\pm \pi^\pm \pi^\mp$  and  $K^\pm \rightarrow \pi^\pm \pi^0 \pi^0$  modes are added together as in the case of the semileptonic decays thereby making up the 3-pion mode. Again, the resulting distribution is fit with splines
4. once the four analytic curves are ready (sums of 3 gaussians for  $K \rightarrow \mu\nu$  and  $K \rightarrow \pi\pi^0$  distributions and splines functions for the semileptonic and 3-pion modes) the experimental MM2 distribution is fit with a weighted sum of these 4 analytic curves, each of them normalized to unity. The coefficients by which the normalized curves are multiplied are parameters of the fit and are once the fit is completed are interpreted as numbers of events of the corresponding modes.

### 7.2.1 Expected MM2 Distributions From Simulation

Missing mass distributions for each particular mode are taken from the simulation. Figure 44 shows the MM2 distributions for all 6 modes. Figure 75 shows the experimental MM2 distribution overlaid with the sum of appropriately normalized simulated MM2 distributions.

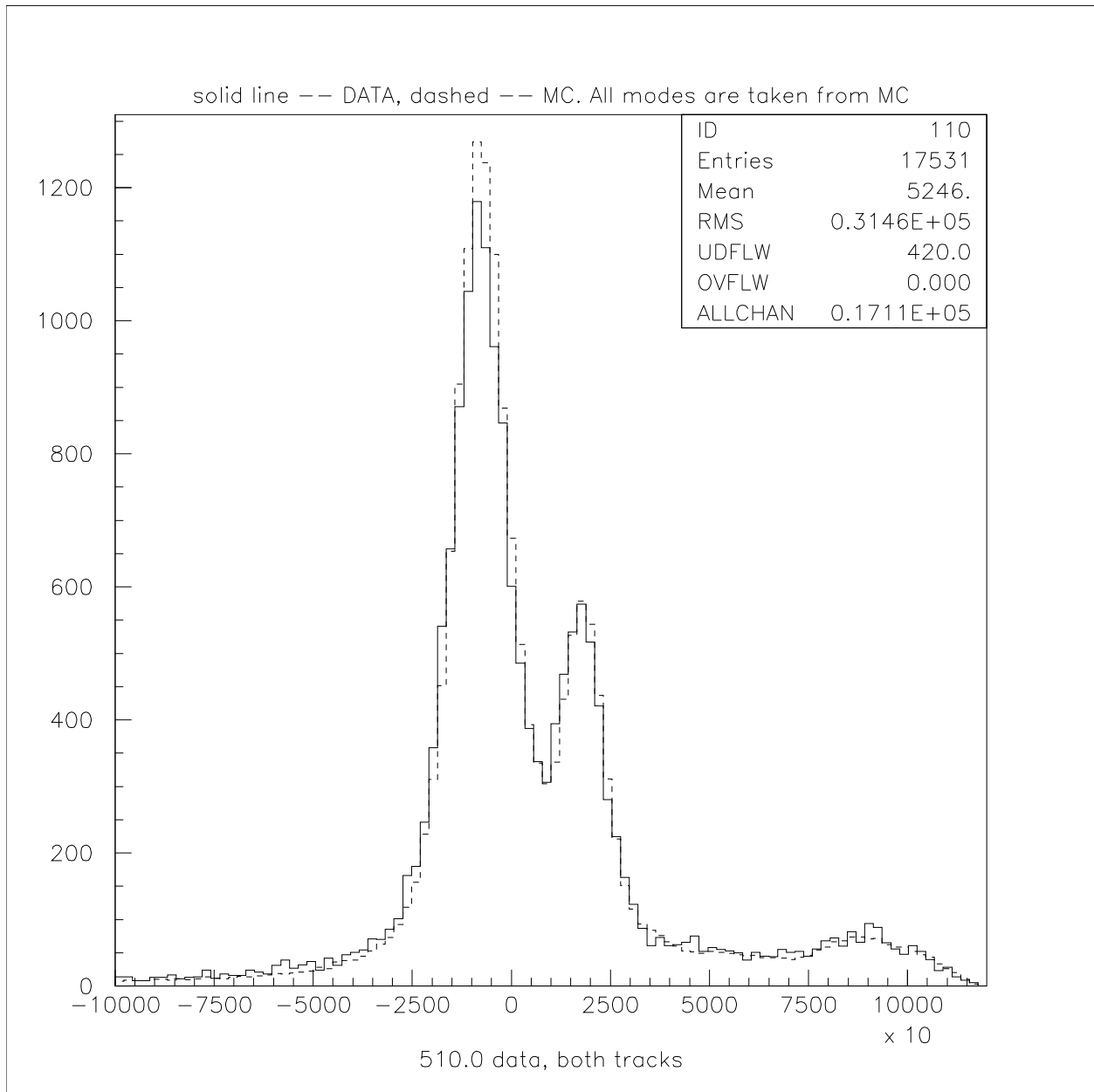


Figure 75: Experimental MM2 distribution overlaid with the sum of simulated MM2 distributions. The simulated MM2 modes were normalized to the numbers of events we would expect from the known efficiencies and branching ratios; 510.0 MeV samples are used.

### 7.2.2 $K \rightarrow \mu\nu$ Distribution: MM2 From Data

Missing mass distribution for the  $K \rightarrow \mu\nu$  mode can be also obtained from the data by application of requirement that no photons are present in the event. The contamination of this sample by events from other modes is estimated from the simulation and turns out to be less than 3%. To analyze the contamination I looked at the  $K^+$  decays and used the

Table 9: Percentages of the events that survive the no photons requirement. All 6 modes are taken from the 510.0 MeV MC simulation.

| mode                              | events, % |
|-----------------------------------|-----------|
| $K^+ \rightarrow \mu^+\nu$        | 97.38     |
| $K^+ \rightarrow \pi^+\pi^0$      | 0.46      |
| $K^+ \rightarrow \pi^0\mu^+\nu$   | 0.08      |
| $K^+ \rightarrow \pi^0e^+\nu$     | 0.11      |
| $K^+ \rightarrow \pi^+\pi^+\pi^-$ | 1.96      |
| $K^+ \rightarrow \pi^+\pi^0\pi^0$ | 0.00      |

data and the simulated samples of 510.0 MeV. The percentages of the  $K^+ \rightarrow \mu^+\nu$  events and of the contaminating events from other modes that are present in the sample obtained by the no photons requirement are shown in table 9. Figure 76 shows distributions of the contaminating modes overlaid on top of the  $K^+ \rightarrow \mu^+\nu$  MM2 distribution; all distributions were obtained from the 510.0 simulated samples with no photons requirement imposed. As one can see from the table and from the figure, the main contamination comes from the  $K^+ \rightarrow \pi^+\pi^+\pi^-$  mode. To account for this 3% contamination I use the following procedure:

1. I apply no photons requirement to all of the simulated modes and determine how many contaminating events of each mode we should expect in our experimental sample obtained by no photons requirement
2. I normalize the MM2 distributions of the contaminating modes by the expected numbers and construct a function which is the sum of these missing mass distributions and 3 gaussians

3. finally I fit the experimental sample obtained by the no photon requirement with the constructed function. The parameters of the contaminating modes are kept fixed while the parameters of the 3 gaussians vary. In this way I obtain an analytic function which is a sum of 3 gaussians and represents the  $K \rightarrow \mu\nu$  MM2 distribution

Figure 77 shows the experimental MM2 distribution with the no photon requirement imposed, overlaid with the sum of appropriately normalized MM2 distributions of 6 modes with the same requirement imposed. All but  $K \rightarrow \mu\nu$  MM2 distribution are taken from the simulation; the  $K \rightarrow \mu\nu$  MM2 distribution is obtained by procedure described above.

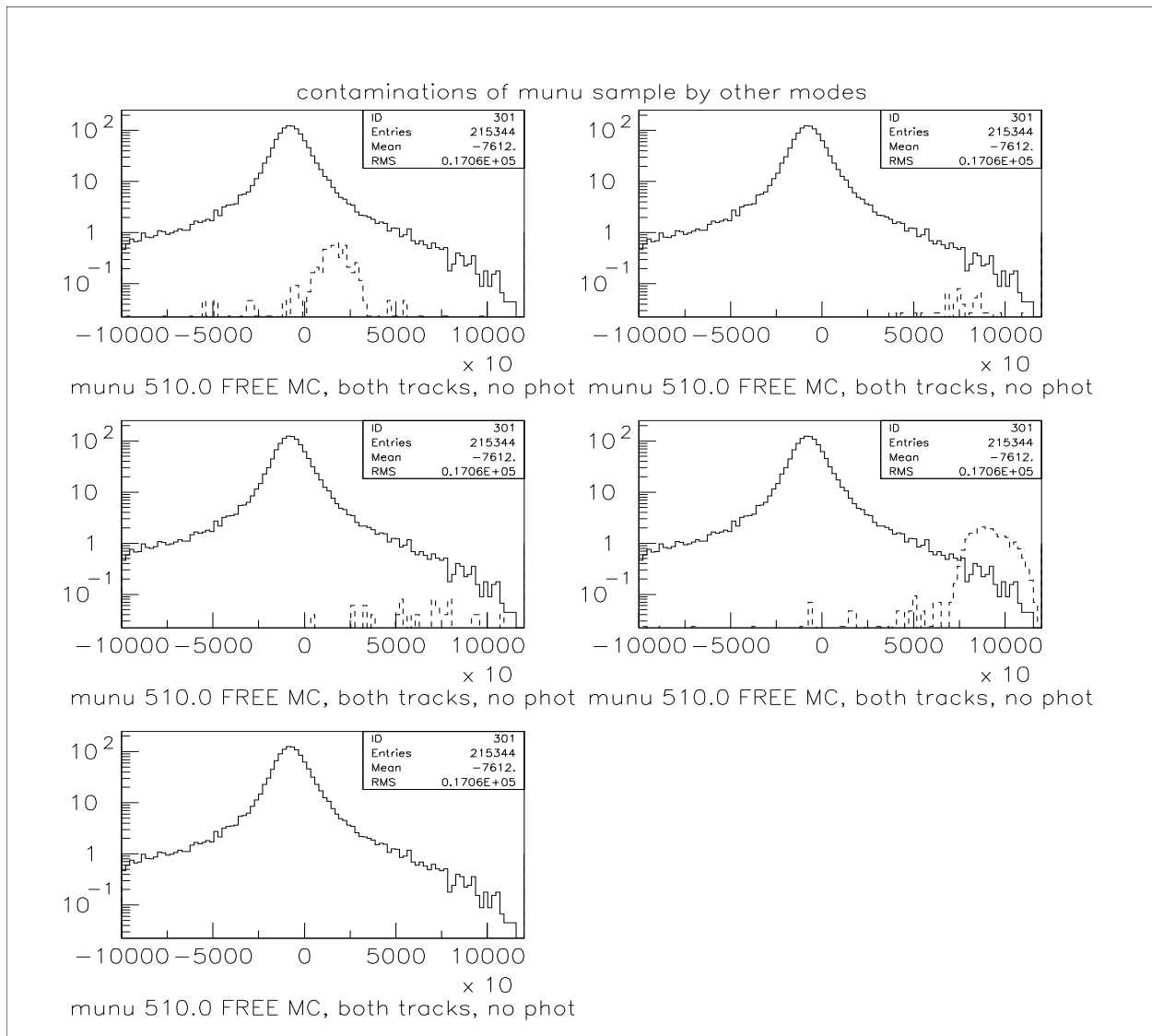


Figure 76: MM2 distributions from the sample of  $K^+ \rightarrow \mu^+ \nu$  events overlaid with contaminations from the other modes. All distributions are taken from the 510.0 MeV simulation with no photons requirement imposed. Upper left plot is  $K^+ \rightarrow \mu^+ \nu$  overlaid with  $K^+ \rightarrow \pi^+ \pi^0$ , upper right is  $K^+ \rightarrow \mu^+ \nu$  overlaid with  $K^+ \rightarrow \pi^0 \mu^+ \nu$ , middle left is  $K^+ \rightarrow \mu^+ \nu$  overlaid with  $K^+ \rightarrow \pi^0 e^+ \nu$ , middle right is  $K^+ \rightarrow \mu^+ \nu$  overlaid with  $K^+ \rightarrow \pi^+ \pi^+ \pi^-$ , lower left is  $K^+ \rightarrow \mu^+ \nu$  overlaid with  $K^+ \rightarrow \pi^+ \pi^0 \pi^0$ .

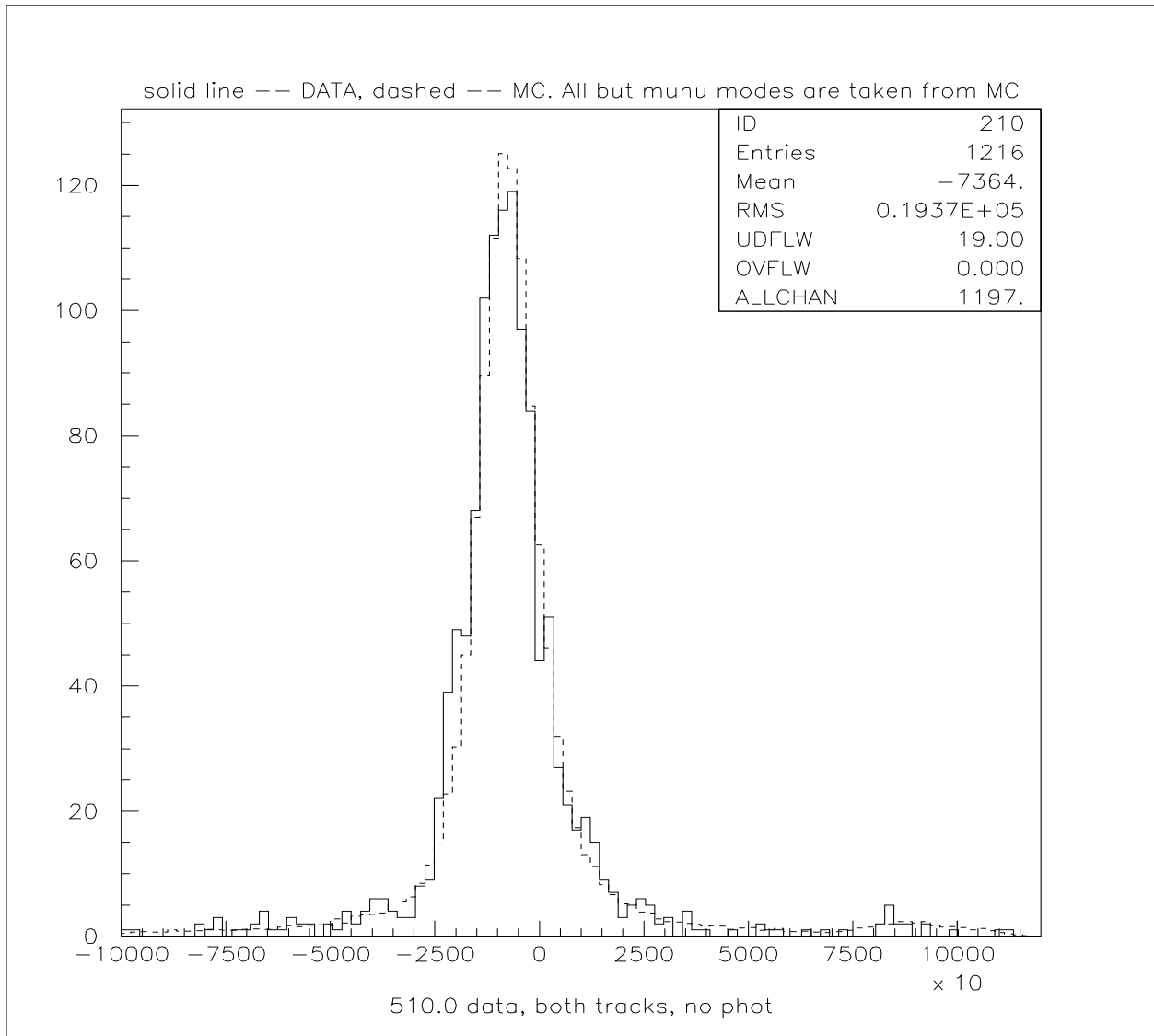


Figure 77: Experimental MM2 distribution overlaid with the sum of 6 MM2 distributions. No photon requirement is applied. MM2 distribution of  $K \rightarrow \mu\nu$  mode is obtained from the data, the rest of the distributions are taken from the simulation.

### 7.2.3 Analysis Variations

The data and simulation samples to be fit were chosen in different ways:

1.  $R_{3-8}$ : all cuts listed in the section 4.4.1 are applied, the cuts on  $\sigma_R$  and  $\sigma_Z$  of the kaon track are applied to the data only (no analogous cuts are applied to the decay track). Simulated MM2 distribution of  $K \rightarrow \mu\nu$  was used. The radius of the vertex varies from 3 to 8 cm.
2.  $R_{3-5}$ : the cuts are as in  $R_{3-8}$  except that the radius of the vertex varies from 3 to 5 cm.
3.  $R_{5-8}$ : the cuts are as in  $R_{3-8}$  except that the radius of the vertex varies from 5 to 8 cm.
4.  $R_{\pi^0}$ : same as  $R_{3-8}$  plus requirement of  $\pi^0$  presence
5.  $R_{\mu\nu \text{ data}}$ : same as  $R_{3-8}$  but the  $K \rightarrow \mu\nu$  distribution is taken from the data rather than the simulation.
6.  $R_{lik-K}$ : all but  $dE/dx$ ,  $\sigma_R$ , and  $\sigma_Z$  of kaon track cuts are applied directly:  $dE/dx$ ,  $\sigma_R$ ,  $\sigma_Z$  are applied in a likelihood manner. This means that both in the data and the simulation each event is assigned a probability associated with each of these three parameters. For example, probability 0.9 associated with  $\sigma_R$  means that this event belongs to 90% category of events with smaller  $\sigma_R$ . Then for each event the product of these probabilities is taken and a cut is chosen for this joint probability. In this way the information on  $dE/dx$ ,  $\sigma_R$ , and  $\sigma_Z$  of kaon track is used in both data and simulation in spite of the fact that these parameters are not simulated correctly. Lower likelihood values correspond to less likely events.
7.  $R_{lik-2tr}$ : same as  $R_{lik-K}$  above but  $dE/dx$ ,  $\sigma_R$ , and  $\sigma_Z$  of the decay track are also considered in the same likelihood manner.

The different approaches listed above yield different results for the  $R_{2body}$ ,  $R_{semilep}$ , and  $R_{3pion}$ ; the differences reflect the systematic flaws in this analysis and are taken into account in the evaluation of the systematic error.

### 7.3 DPE ANALYSIS

To calculate  $R_{e\mu} \equiv Br(K^+ \rightarrow \pi^0 e^+ \nu) / Br(K^+ \rightarrow \pi^0 \mu^+ \nu)$  I use the DPE range between -10 and 180 MeV. As the separation point between the  $K_{e3}$  and  $K_{\mu3}$  peaks I choose 60 MeV. Then the following algorithm is used:

1. DPE distributions for a data sample and all of the 6 modes are obtained:
  - a. DPE distribution of the  $K^- \rightarrow \mu^- \nu$  mode is taken from the simulation.
  - b. DPE distribution of the  $K^- \rightarrow \pi^- \pi^0$  mode is taken from the simulation and rescaled by the linear transformation  $X' = aX + b$  with  $a = 0.94$  and  $b = 26.0$ .
  - c. DPE distribution of the  $K^- \rightarrow \pi^0 \mu^- \nu$  mode is taken from the simulation.
  - d. DPE distribution of the  $K^- \rightarrow \pi^0 e^- \nu$  mode is taken from the simulation and shifted to the right by 15 MeV.
  - e. DPE distributions of the both 3-pion modes is taken from the simulation.

In addition to the usual cuts three more requirements were imposed:

- the energy deposition of the decay product is greater than 20 MeV – to discriminate against noise in the calorimeter.
  - the momentum of the decay product is lesser than 500 MeV – to discriminate against events with poorly measured momentum.
  - MM2 is between 35000 and 70000 MeV – to select a sample of mostly semileptonic decays.
2. DPE distributions of  $K^- \rightarrow \mu^- \nu$ ,  $K^- \rightarrow \pi^- \pi^0$ , and 3-pion modes are subtracted from the experimental DPE distribution – in this way a cleaner DPE semileptonic distribution is obtained.
  3. DPE range between -10 and 180 MeV is considered. As the separation point between the  $K_{e3}$  and  $K_{\mu3}$  peaks I chose 60 MeV. Then the so called matrix method is used.

Let A be the DPE range between 10 and 60 MeV, and

B the DPE range between 60 and 90 MeV,

$N_{K_{\mu3}}$  – number of  $K_{\mu3}$  events in the obtained sample,

$N_{K_{e3}}$  – number of  $K_{e3}$  events in the obtained sample,

$N_A^D$  – number of events in the sample that fall into range A,

$N_B^D$  – number of events in the sample that fall into range B,

$f_A^{K_{\mu 3}}$  – fraction of  $K_{\mu 3}$  events that fall into range A,

$f_A^{K_{e 3}}$  – fraction of  $K_{e 3}$  events that fall into range A,

$f_B^{K_{\mu 3}}$  – fraction of  $K_{\mu 3}$  events that fall into range B,

$f_B^{K_{e 3}}$  – fraction of  $K_{e 3}$  events that fall into range B.

Then the following equations should be satisfied:

$$N_A^D = f_A^{K_{\mu 3}} N_{K_{\mu 3}} + f_A^{K_{e 3}} N_{K_{e 3}} \quad (7.1)$$

$$N_B^D = f_B^{K_{\mu 3}} N_{K_{\mu 3}} + f_B^{K_{e 3}} N_{K_{e 3}} \quad (7.2)$$

$N_A^D$  and  $N_B^D$  are calculated from the experimental DPE distribution;  $f_A^{K_{\mu 3}}$ ,  $f_A^{K_{e 3}}$ ,  $f_B^{K_{\mu 3}}$ , and  $f_B^{K_{e 3}}$  are calculated from the simulated DPE distributions of  $K_{\mu 3}$  and  $K_{e 3}$  modes.

Then, from eqs 7.1 and 7.2

$$N_{K_{\mu 3}} = \frac{f_A^{K_{e 3}} N_B^D - f_B^{K_{e 3}} N_A^D}{f_A^{K_{e 3}} f_B^{K_{\mu 3}} - f_B^{K_{e 3}} f_A^{K_{\mu 3}}} \quad (7.3)$$

$$N_{K_{e 3}} = \frac{f_B^{K_{\mu 3}} N_A^D - f_A^{K_{\mu 3}} N_B^D}{f_A^{K_{e 3}} f_B^{K_{\mu 3}} - f_B^{K_{e 3}} f_A^{K_{\mu 3}}} \quad (7.4)$$

4. The registration efficiencies for the  $K_{\mu 3}$  and  $K_{e 3}$  modes are calculated from the simulation.

Finally,  $R_{e\mu} = Br(K^+ \rightarrow \pi^0 e^+ \nu) / Br(K^+ \rightarrow \pi^0 \mu^+ \nu)$  is given by

$$R_{e\mu} = \frac{N_{K_{e 3}} \epsilon_{\mu 3}}{N_{K_{\mu 3}} \epsilon_{e 3}} \quad (7.5)$$

where  $\epsilon_{\mu 3}$  and  $\epsilon_{e 3}$  are registration efficiencies of  $K_{\mu 3}$  and  $K_{e 3}$  modes correspondingly.

In table 10 I show numbers of events of all 6 modes and the data sample that fall into regions A and B, the beam energy is 509.5 MeV. From the numbers in the table I obtain  $f_A^{K_{\mu 3}} = 0.078$ ,  $f_A^{K_{e 3}} = 0.909$ ,  $f_B^{K_{\mu 3}} = 0.922$ ,  $f_B^{K_{e 3}} = 0.090$ , and then  $N_{K_{\mu 3}} = 231.2$ ,  $N_{K_{e 3}} = 318.1$ . The registration efficiencies are  $\epsilon_{\mu 3} = 0.0036$  and  $\epsilon_{e 3} = 0.0029$ , so the ratio of the branching ratios is 1.7.

Table 10: Numbers of events in regions A and B, standard set of cuts is applied,  $3 < R_{vertex} < 8$ , 509.5 MeV sample.

| mode                                | region A | region B | total |
|-------------------------------------|----------|----------|-------|
| $K^- \rightarrow \mu^- \nu$         | 16.0     | 31.3     | 47.3  |
| $K^- \rightarrow \pi^- \pi^0$       | 11.4     | 97.7     | 109.1 |
| $K^- \rightarrow \pi^0 e^- \nu$     | 288.0    | 34.8     | 322.8 |
| $K^- \rightarrow \pi^0 \mu^- \nu$   | 20.3     | 250.3    | 270.6 |
| $K^- \rightarrow \pi^- \pi^- \pi^+$ | 1.1      | 6.1      | 7.2   |
| $K^- \rightarrow \pi^- \pi^0 \pi^0$ | 0.4      | 1.7      | 2.1   |
| DATA before subtraction             | 360.0    | 401.0    | 761.0 |
| DATA after subtraction              | 331.1    | 264.2    | 595.3 |

Table 11: Numbers of events in the regions A and B.

|                                                                              | 509.0 MeV |     | 509.5 MeV |     | 510.0 MeV |     | 510.5 MeV |     |
|------------------------------------------------------------------------------|-----------|-----|-----------|-----|-----------|-----|-----------|-----|
|                                                                              | A         | B   | A         | B   | A         | B   | A         | B   |
| central values,<br>$3 < R_{vertex} < 8$                                      | 263       | 259 | 360       | 401 | 355       | 374 | 202       | 200 |
| central values,<br>$3 < R_{vertex} < 5$                                      | 128       | 101 | 158       | 174 | 168       | 132 | 91        | 91  |
| central values,<br>$5 < R_{vertex} < 8$                                      | 135       | 158 | 202       | 227 | 187       | 242 | 111       | 109 |
| central values,<br>$3 < R_{vertex} < 8$ ,<br>$\pi^0$ requirement             | 81        | 88  | 128       | 117 | 107       | 106 | 65        | 51  |
| central values,<br>$3 < R_{vertex} < 8$ ,<br>$\mu\nu$ MM2 taken<br>from DATA | 263       | 259 | 360       | 401 | 355       | 374 | 202       | 200 |

## 8.0 RESULTS

Tables 12–21 summarize the results of our measurements. Tables 12–19 relate to the measurements of  $Br(K \rightarrow \pi\pi^0)/Br(K \rightarrow \mu\nu)$ ,  $(Br(K \rightarrow \pi^0\mu\nu) + Br(K \rightarrow \pi^0e\nu))/Br(K \rightarrow \pi\pi^0)$ , and  $(Br(K \rightarrow \pi\pi\pi) + Br(K \rightarrow \pi\pi^0\pi^0))/Br(K \rightarrow \pi\pi^0)$ . These measurements were made for both  $K^+$  and  $K^-$  decays and used MM2 as the separation parameter. Tables 20 and 21 relate to the measurement of  $Br(K \rightarrow \pi^0e\nu)/Br(K \rightarrow \pi^0\mu\nu)$  which was made for  $K^-$  decays only and used DPE as the separation parameter.

Figure 78 shows the expected sum of simulated modes overlaid with the experimental MM2 distribution taken from 510.0 MeV data. The expected sum is normalized to the total number of events in the experimental sample. The expected numbers of events of each mode are calculated on the basis of the known registration efficiencies and branching ratios. Figure 79 shows the sum of simulated modes, each of them normalized to the corresponding number of events obtained from the fit.

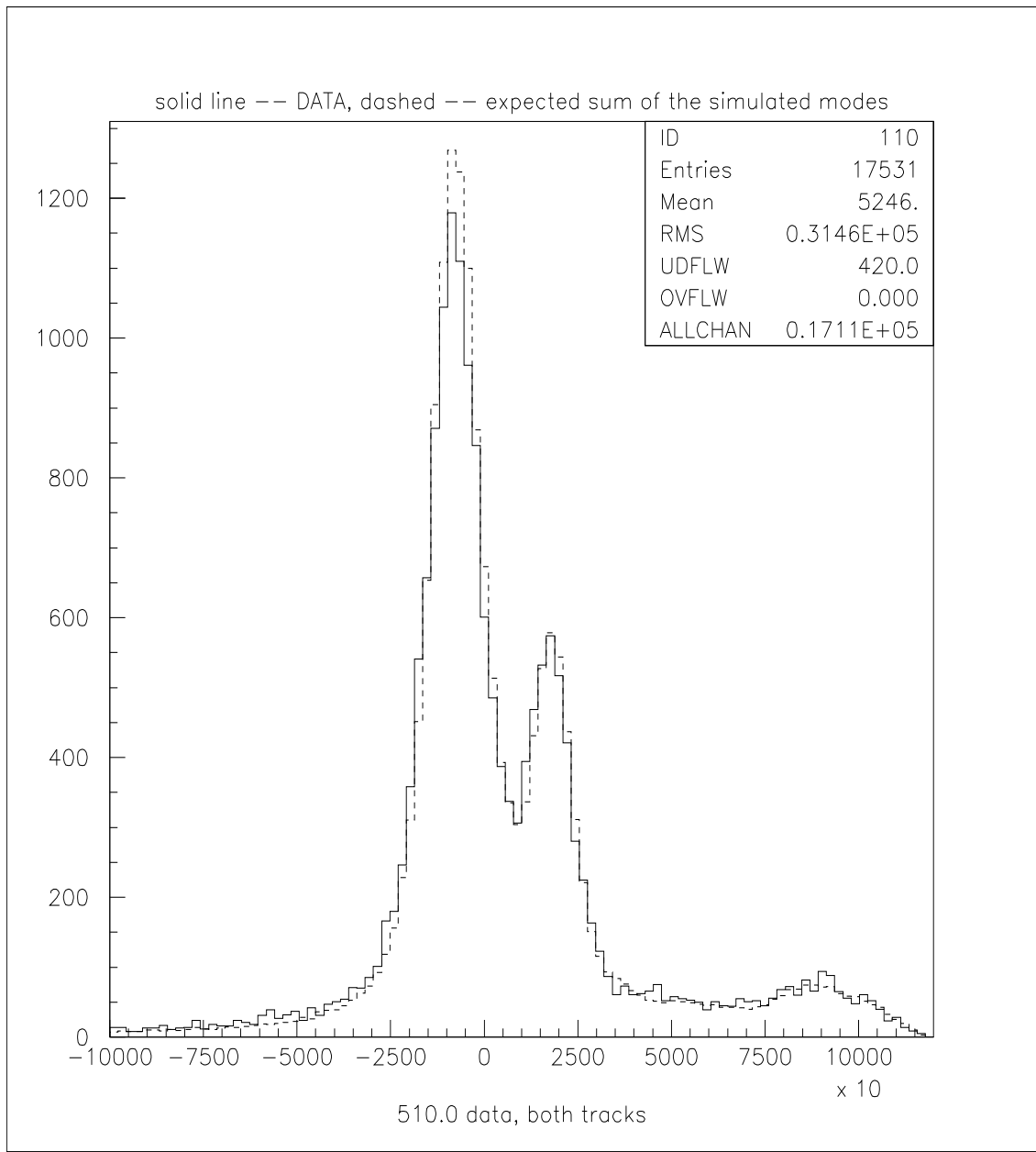


Figure 78: MM2 distribution of the expected sum of simulated modes overlaid with the experimental MM2 distribution of 510.0 MeV data. The expected sum is normalized to the total number of events in the experimental sample.

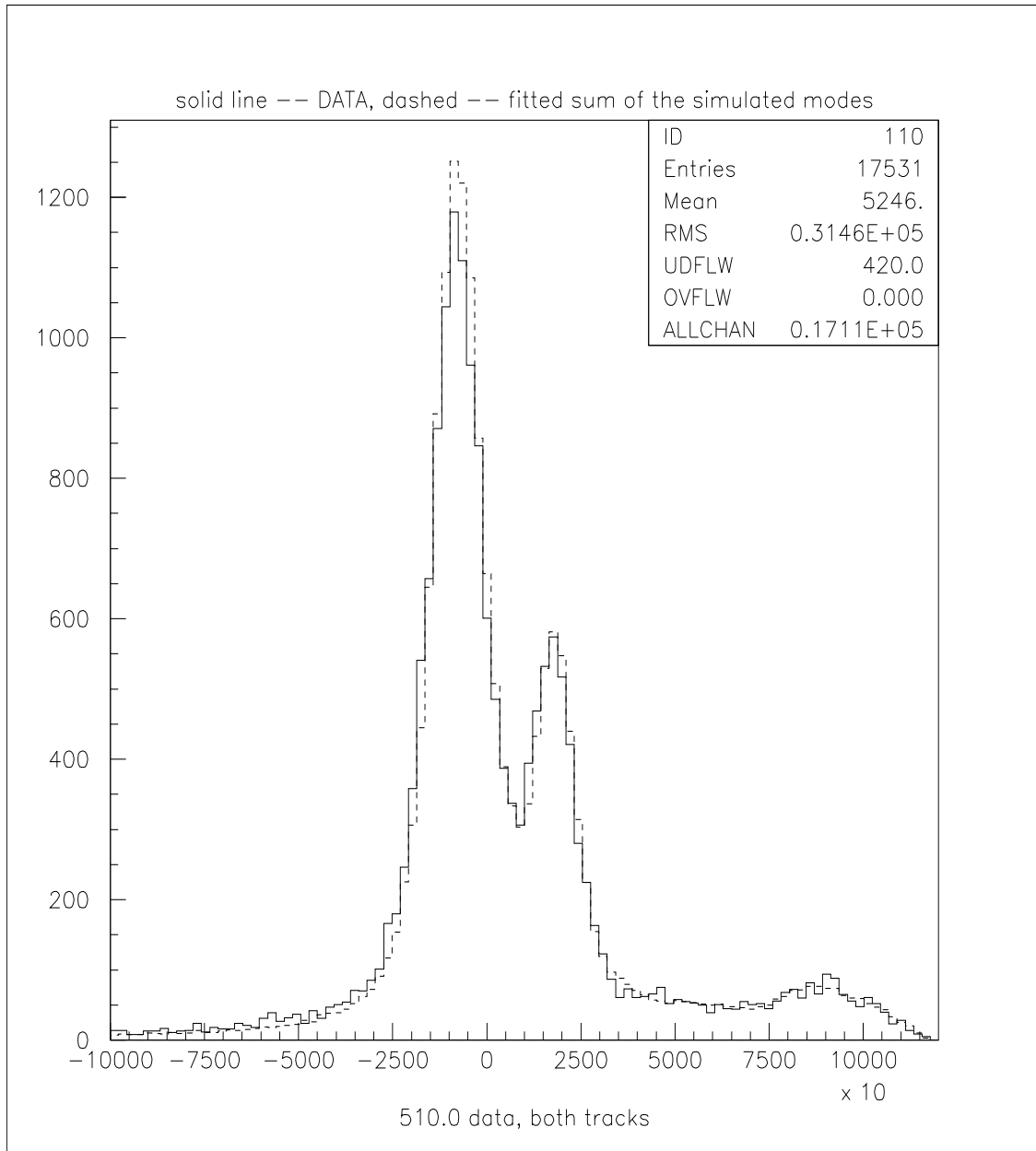


Figure 79: MM2 distribution of the fitted sum of simulated modes overlaid with experimental the MM2 distribution of 510.0 MeV data.

## 8.1 SUMMARY OF THE RESULTS

To check the stability of the results and estimate the systematic errors, the analysis was performed with the following variations of the selection criteria:

1.  $R_{3-8}$ : set of cuts with the central values is applied,  $3 < R_{vertex} < 8$
2.  $R_{3-5}$ : set of cuts with the central values is applied,  $3 < R_{vertex} < 5$
3.  $R_{5-8}$ : set of cuts with the central values is applied,  $5 < R_{vertex} < 8$
4.  $R_{\pi^0}$ : set of cuts with the central values is applied,  $3 < R_{vertex} < 8$ , presence of  $\pi^0$  is required
5.  $R_{\mu\nu \text{ data}}$ : set of cuts with the central values is applied,  $3 < R_{vertex} < 8$ , MM2 distribution for  $K \rightarrow \mu\nu$  decay is taken from the data; for the rest of the variations it is taken from the MC simulation
6.  $R_{lik-K}$ : all but qualities of track and  $dE/dx$  cuts are applied, the qualities of track and  $dE/dx$  parameters are combined in a likelihood function, this applies only to the kaon track;  $3 < R_{vertex} < 8$
7.  $R_{lik-2tr}$ : as above, but with the likelihood function constructed from qualities of track and  $dE/dx$  parameters of both tracks

The variations 6 and 7 were not applied to the  $Br(K \rightarrow \pi^0 e\nu)/Br(K \rightarrow \pi^0 \mu\nu)$  measurements.

Table 12: Results of the  $\frac{Br(K^+ \rightarrow \pi^+ \pi^0)}{Br(K^+ \rightarrow \mu^+ \nu)}$  measurements. The PDG averages yield  $0.3331 \pm 0.0024$ .

|                                                                              | 509.0 MeV           | 509.5 MeV           | 510.0 MeV           | 510.5 MeV           |
|------------------------------------------------------------------------------|---------------------|---------------------|---------------------|---------------------|
| central values,<br>$3 < R_{vertex} < 8$                                      | $0.3254 \pm 0.0103$ | $0.3313 \pm 0.0089$ | $0.3388 \pm 0.0087$ | $0.3148 \pm 0.0110$ |
| central values,<br>$3 < R_{vertex} < 5$                                      | $0.3170 \pm 0.0137$ | $0.3449 \pm 0.0125$ | $0.3417 \pm 0.0119$ | $0.3270 \pm 0.0153$ |
| central values,<br>$5 < R_{vertex} < 8$                                      | $0.3338 \pm 0.0154$ | $0.3179 \pm 0.0127$ | $0.3360 \pm 0.0127$ | $0.3023 \pm 0.0158$ |
| central values,<br>$3 < R_{vertex} < 8$ ,<br>$\pi^0$ requirement             | $0.2069 \pm 0.0150$ | $0.1949 \pm 0.0125$ | $0.1795 \pm 0.0106$ | $0.1758 \pm 0.0139$ |
| central values,<br>$3 < R_{vertex} < 8$ ,<br>$\mu\nu$ MM2 taken<br>from DATA | $0.3374 \pm 0.0103$ | $0.3093 \pm 0.0087$ | $0.3336 \pm 0.0088$ | $0.3258 \pm 0.0110$ |
| kaon track<br>likelihood,<br>$3 < R_{vertex} < 8$                            | $0.3285 \pm 0.0110$ | $0.3346 \pm 0.0095$ | $0.3396 \pm 0.0093$ | $0.3144 \pm 0.0116$ |
| both tracks<br>likelihood,<br>$3 < R_{vertex} < 8$                           | $0.3400 \pm 0.0115$ | $0.3325 \pm 0.0098$ | $0.3479 \pm 0.0097$ | $0.3217 \pm 0.0122$ |

Table 13: Results of the  $\frac{Br(K^- \rightarrow \pi^- \pi^0)}{Br(K^- \rightarrow \mu^- \nu)}$  measurements. The PDG averages yield  $0.3331 \pm 0.0024$ .

|                                                                              | 509.0 MeV           | 509.5 MeV           | 510.0 MeV           | 510.5 MeV           |
|------------------------------------------------------------------------------|---------------------|---------------------|---------------------|---------------------|
| central values,<br>$3 < R_{vertex} < 8$                                      | $0.4011 \pm 0.0113$ | $0.3913 \pm 0.0094$ | $0.4132 \pm 0.0096$ | $0.4111 \pm 0.0127$ |
| central values,<br>$3 < R_{vertex} < 5$                                      | $0.3790 \pm 0.0148$ | $0.3588 \pm 0.0119$ | $0.3946 \pm 0.0126$ | $0.3817 \pm 0.0161$ |
| central values,<br>$5 < R_{vertex} < 8$                                      | $0.4276 \pm 0.0172$ | $0.4316 \pm 0.0150$ | $0.4374 \pm 0.0146$ | $0.4478 \pm 0.0201$ |
| central values,<br>$3 < R_{vertex} < 8$ ,<br>$\pi^0$ requirement             | $0.3880 \pm 0.0350$ | $0.3202 \pm 0.0233$ | $0.3528 \pm 0.0256$ | $0.3087 \pm 0.0287$ |
| central values,<br>$3 < R_{vertex} < 8$ ,<br>$\mu\nu$ MM2 taken<br>from DATA | $0.3349 \pm 0.0103$ | $0.3315 \pm 0.0086$ | $0.3479 \pm 0.0087$ | $0.3710 \pm 0.0119$ |
| kaon track<br>likelihood,<br>$3 < R_{vertex} < 8$                            | $0.3972 \pm 0.0117$ | $0.3853 \pm 0.0098$ | $0.4139 \pm 0.0100$ | $0.4033 \pm 0.0131$ |
| both tracks<br>likelihood,<br>$3 < R_{vertex} < 8$                           | $0.3981 \pm 0.0122$ | $0.3852 \pm 0.0102$ | $0.4175 \pm 0.0105$ | $0.4131 \pm 0.0139$ |

Table 14: Results of the  $\frac{Br(K^+ \rightarrow \pi^0 \mu^+ \nu) + Br(K^+ \rightarrow \pi^0 e^+ \nu)}{Br(K^+ \rightarrow \pi^+ \pi^0)}$  measurements. The PDG averages yield  $0.3852 \pm 0.0048$ .

|                                                                              | 509.0 MeV           | 509.5 MeV           | 510.0 MeV           | 510.5 MeV           |
|------------------------------------------------------------------------------|---------------------|---------------------|---------------------|---------------------|
| central values,<br>$3 < R_{vertex} < 8$                                      | $0.5601 \pm 0.0372$ | $0.4698 \pm 0.0288$ | $0.4438 \pm 0.0275$ | $0.4657 \pm 0.0385$ |
| central values,<br>$3 < R_{vertex} < 5$                                      | $0.5033 \pm 0.0483$ | $0.4377 \pm 0.0368$ | $0.4252 \pm 0.0364$ | $0.4071 \pm 0.0486$ |
| central values,<br>$5 < R_{vertex} < 8$                                      | $0.6137 \pm 0.0566$ | $0.5061 \pm 0.0448$ | $0.4591 \pm 0.0408$ | $0.5345 \pm 0.0614$ |
| central values,<br>$3 < R_{vertex} < 8$ ,<br>$\pi^0$ requirement             | $0.5640 \pm 0.0542$ | $0.5620 \pm 0.0475$ | $0.5147 \pm 0.0449$ | $0.5286 \pm 0.0598$ |
| central values,<br>$3 < R_{vertex} < 8$ ,<br>$\mu\nu$ MM2 taken<br>from DATA | $0.5374 \pm 0.0356$ | $0.4764 \pm 0.0304$ | $0.5378 \pm 0.0296$ | $0.4260 \pm 0.0366$ |
| kaon track<br>likelihood,<br>$3 < R_{vertex} < 8$                            | $0.5406 \pm 0.0386$ | $0.4445 \pm 0.0299$ | $0.4356 \pm 0.0292$ | $0.4649 \pm 0.0412$ |
| both tracks<br>likelihood,<br>$3 < R_{vertex} < 8$                           | $0.5248 \pm 0.0366$ | $0.4843 \pm 0.0305$ | $0.4396 \pm 0.0283$ | $0.4973 \pm 0.0414$ |

Table 15: Results of the  $\frac{Br(K^- \rightarrow \pi^0 \mu^- \nu) + Br(K^- \rightarrow \pi^0 e^- \nu)}{Br(K^- \rightarrow \pi^- \pi^0)}$  measurements. The PDG averages yield  $0.3852 \pm 0.0048$ .

|                                                                              | 509.0 MeV           | 509.5 MeV           | 510.0 MeV           | 510.5 MeV           |
|------------------------------------------------------------------------------|---------------------|---------------------|---------------------|---------------------|
| central values,<br>$3 < R_{vertex} < 8$                                      | $0.5442 \pm 0.0301$ | $0.5828 \pm 0.0271$ | $0.5182 \pm 0.0240$ | $0.5419 \pm 0.0332$ |
| central values,<br>$3 < R_{vertex} < 5$                                      | $0.5603 \pm 0.0430$ | $0.5703 \pm 0.0370$ | $0.4823 \pm 0.0322$ | $0.5359 \pm 0.0450$ |
| central values,<br>$5 < R_{vertex} < 8$                                      | $0.5208 \pm 0.0416$ | $0.5941 \pm 0.0391$ | $0.5523 \pm 0.0352$ | $0.5542 \pm 0.0485$ |
| central values,<br>$3 < R_{vertex} < 8$ ,<br>$\pi^0$ requirement             | $0.5510 \pm 0.0495$ | $0.6208 \pm 0.0461$ | $0.5261 \pm 0.0403$ | $0.5476 \pm 0.0561$ |
| central values,<br>$3 < R_{vertex} < 8$ ,<br>$\mu\nu$ MM2 taken<br>from DATA | $0.5736 \pm 0.0341$ | $0.5783 \pm 0.0295$ | $0.5223 \pm 0.0263$ | $0.4853 \pm 0.0338$ |
| kaon track<br>likelihood,<br>$3 < R_{vertex} < 8$                            | $0.5326 \pm 0.0312$ | $0.6126 \pm 0.0295$ | $0.5125 \pm 0.0251$ | $0.5536 \pm 0.0356$ |
| both tracks<br>likelihood,<br>$3 < R_{vertex} < 8$                           | $0.5473 \pm 0.0326$ | $0.5875 \pm 0.0295$ | $0.5107 \pm 0.0255$ | $0.5468 \pm 0.0359$ |

Table 16: Results of the  $\frac{Br(K^+ \rightarrow \pi^+ \pi^+ \pi^-) + Br(K^+ \rightarrow \pi^+ \pi^0 \pi^0)}{Br(K^+ \rightarrow \pi^+ \pi^0)}$  measurements. The PDG averages yield  $0.3459 \pm 0.0033$ .

|                                                                              | 509.0 MeV           | 509.5 MeV           | 510.0 MeV           | 510.5 MeV           |
|------------------------------------------------------------------------------|---------------------|---------------------|---------------------|---------------------|
| central values,<br>$3 < R_{vertex} < 8$                                      | $0.3051 \pm 0.0305$ | $0.2898 \pm 0.0244$ | $0.3294 \pm 0.0243$ | $0.3490 \pm 0.0346$ |
| central values,<br>$3 < R_{vertex} < 5$                                      | $0.3211 \pm 0.0494$ | $0.2768 \pm 0.0379$ | $0.3404 \pm 0.0388$ | $0.3527 \pm 0.0542$ |
| central values,<br>$5 < R_{vertex} < 8$                                      | $0.2979 \pm 0.0390$ | $0.3047 \pm 0.0325$ | $0.3291 \pm 0.0314$ | $0.3522 \pm 0.0463$ |
| central values,<br>$3 < R_{vertex} < 8$ ,<br>$\pi^0$ requirement             | $0.3232 \pm 0.0756$ | $0.2235 \pm 0.0628$ | $0.3273 \pm 0.0634$ | $0.3074 \pm 0.0807$ |
| central values,<br>$3 < R_{vertex} < 8$ ,<br>$\mu\nu$ MM2 taken<br>from DATA | $0.3018 \pm 0.0296$ | $0.2874 \pm 0.0255$ | $0.3147 \pm 0.0248$ | $0.2994 \pm 0.0330$ |
| kaon track<br>likelihood,<br>$3 < R_{vertex} < 8$                            | $0.3075 \pm 0.0305$ | $0.3207 \pm 0.0250$ | $0.3475 \pm 0.0253$ | $0.3673 \pm 0.0357$ |
| both tracks<br>likelihood,<br>$3 < R_{vertex} < 8$                           | $0.2132 \pm 0.0273$ | $0.1734 \pm 0.0221$ | $0.2528 \pm 0.0231$ | $0.2326 \pm 0.0323$ |

Table 17: Results of the  $\frac{Br(K^- \rightarrow \pi^- \pi^- \pi^+) + Br(K^- \rightarrow \pi^- \pi^0 \pi^0)}{Br(K^- \rightarrow \pi^- \pi^0)}$  measurements. The PDG averages yield  $0.3459 \pm 0.0033$ .

|                                                                              | 509.0 MeV           | 509.5 MeV           | 510.0 MeV           | 510.5 MeV           |
|------------------------------------------------------------------------------|---------------------|---------------------|---------------------|---------------------|
| central values,<br>$3 < R_{vertex} < 8$                                      | $0.2535 \pm 0.0308$ | $0.2655 \pm 0.0271$ | $0.2844 \pm 0.0246$ | $0.2775 \pm 0.0354$ |
| central values,<br>$3 < R_{vertex} < 5$                                      | $0.2766 \pm 0.0522$ | $0.2798 \pm 0.0439$ | $0.3625 \pm 0.0425$ | $0.2890 \pm 0.0576$ |
| central values,<br>$5 < R_{vertex} < 8$                                      | $0.2379 \pm 0.0376$ | $0.2473 \pm 0.0339$ | $0.2274 \pm 0.0298$ | $0.2588 \pm 0.0448$ |
| central values,<br>$3 < R_{vertex} < 8$ ,<br>$\pi^0$ requirement             | $0.3133 \pm 0.0746$ | $0.3325 \pm 0.0682$ | $0.3694 \pm 0.0602$ | $0.2684 \pm 0.0803$ |
| central values,<br>$3 < R_{vertex} < 8$ ,<br>$\mu\nu$ MM2 taken<br>from DATA | $0.3021 \pm 0.0351$ | $0.3478 \pm 0.0307$ | $0.3653 \pm 0.0282$ | $0.3036 \pm 0.0376$ |
| kaon track<br>likelihood,<br>$3 < R_{vertex} < 8$                            | $0.2871 \pm 0.0317$ | $0.2556 \pm 0.0279$ | $0.2997 \pm 0.0253$ | $0.2802 \pm 0.0362$ |
| both tracks<br>likelihood,<br>$3 < R_{vertex} < 8$                           | $0.2010 \pm 0.0307$ | $0.1709 \pm 0.0266$ | $0.2107 \pm 0.0244$ | $0.1540 \pm 0.0336$ |

Table 18: Averages over the energies for  $K^+$  measurements

|                                                                              | $\frac{Br(K^+ \rightarrow \pi^+ \pi^0)}{Br(K^+ \rightarrow \mu^+ \nu)}$ | $\frac{Br(K^+ \rightarrow \pi^0 \mu^+ \nu) + Br(K^+ \rightarrow \pi^0 e^+ \nu)}{Br(K^+ \rightarrow \pi^+ \pi^0)}$ | $\frac{Br(K^+ \rightarrow \pi^+ \pi^+ \pi^-) + Br(K^+ \rightarrow \pi^+ \pi^0 \pi^0)}{Br(K^+ \rightarrow \pi^+ \pi^0)}$ |
|------------------------------------------------------------------------------|-------------------------------------------------------------------------|-------------------------------------------------------------------------------------------------------------------|-------------------------------------------------------------------------------------------------------------------------|
| central values,<br>$3 < R_{vertex} < 8$                                      | $0.3292 \pm 0.0048$                                                     | $0.4770 \pm 0.0159$                                                                                               | $0.3150 \pm 0.0137$                                                                                                     |
| central values,<br>$3 < R_{vertex} < 5$                                      | $0.3342 \pm 0.0066$                                                     | $0.4401 \pm 0.0206$                                                                                               | $0.3177 \pm 0.0218$                                                                                                     |
| central values,<br>$5 < R_{vertex} < 8$                                      | $0.3236 \pm 0.0070$                                                     | $0.5138 \pm 0.0244$                                                                                               | $0.3184 \pm 0.0180$                                                                                                     |
| central values,<br>$3 < R_{vertex} < 8$ ,<br>$\pi^0$ requirement             | $0.1876 \pm 0.0063$                                                     | $0.5414 \pm 0.0253$                                                                                               | $0.2911 \pm 0.0347$                                                                                                     |
| central values,<br>$3 < R_{vertex} < 8$ ,<br>$\mu\nu$ MM2 taken<br>from DATA | $0.3256 \pm 0.0048$                                                     | $0.4978 \pm 0.0163$                                                                                               | $0.3011 \pm 0.0138$                                                                                                     |
| kaon track<br>likelihood,<br>$3 < R_{vertex} < 8$                            | $0.3309 \pm 0.0051$                                                     | $0.4631 \pm 0.0167$                                                                                               | $0.3335 \pm 0.0141$                                                                                                     |
| both tracks<br>likelihood,<br>$3 < R_{vertex} < 8$                           | $0.3366 \pm 0.0053$                                                     | $0.4794 \pm 0.0165$                                                                                               | $0.2150 \pm 0.0127$                                                                                                     |
| PDG average                                                                  | $0.3331 \pm 0.0024$                                                     | $0.3852 \pm 0.0048$                                                                                               | $0.3459 \pm 0.0033$                                                                                                     |

Table 19: Averages over the energies for  $K^-$  measurements

|                                                                              | $\frac{Br(K^- \rightarrow \pi^- \pi^0)}{Br(K^- \rightarrow \mu^- \nu)}$ | $\frac{Br(K^- \rightarrow \pi^0 \mu^- \nu) + Br(K^- \rightarrow \pi^0 e^- \nu)}{Br(K^- \rightarrow \pi^- \pi^0)}$ | $\frac{Br(K^- \rightarrow \pi^- \pi^- \pi^-) + Br(K^- \rightarrow \pi^- \pi^0 \pi^0)}{Br(K^- \rightarrow \pi^- \pi^0)}$ |
|------------------------------------------------------------------------------|-------------------------------------------------------------------------|-------------------------------------------------------------------------------------------------------------------|-------------------------------------------------------------------------------------------------------------------------|
| central values,<br>$3 < R_{vertex} < 8$                                      | $0.4034 \pm 0.0053$                                                     | $0.5452 \pm 0.0140$                                                                                               | $0.2713 \pm 0.0143$                                                                                                     |
| central values,<br>$3 < R_{vertex} < 5$                                      | $0.3774 \pm 0.0068$                                                     | $0.5310 \pm 0.0191$                                                                                               | $0.3070 \pm 0.0240$                                                                                                     |
| central values,<br>$5 < R_{vertex} < 8$                                      | $0.4352 \pm 0.0082$                                                     | $0.5563 \pm 0.0201$                                                                                               | $0.2400 \pm 0.0177$                                                                                                     |
| central values,<br>$3 < R_{vertex} < 8$ ,<br>$\pi^0$ requirement             | $0.3371 \pm 0.0136$                                                     | $0.5601 \pm 0.0235$                                                                                               | $0.3286 \pm 0.0348$                                                                                                     |
| central values,<br>$3 < R_{vertex} < 8$ ,<br>$\mu\nu$ MM2 taken<br>from DATA | $0.3437 \pm 0.0048$                                                     | $0.5399 \pm 0.0152$                                                                                               | $0.3357 \pm 0.0161$                                                                                                     |
| kaon track<br>likelihood,<br>$3 < R_{vertex} < 8$                            | $0.3995 \pm 0.0055$                                                     | $0.5494 \pm 0.0148$                                                                                               | $0.2814 \pm 0.0147$                                                                                                     |
| both tracks<br>likelihood,<br>$3 < R_{vertex} < 8$                           | $0.4023 \pm 0.0057$                                                     | $0.5449 \pm 0.0151$                                                                                               | $0.1875 \pm 0.0141$                                                                                                     |
| PDG average                                                                  | $0.3331 \pm 0.0024$                                                     | $0.3852 \pm 0.0048$                                                                                               | $0.3459 \pm 0.0033$                                                                                                     |

Table 20: Results of the  $\frac{Br(K^- \rightarrow \pi^0 e^- \nu)}{Br(K^- \rightarrow \pi^0 \mu^- \nu)}$  measurements in each energy point.

|                                                                              | 509.0 MeV           | 509.5 MeV           | 510.0 MeV           | 510.5 MeV           |
|------------------------------------------------------------------------------|---------------------|---------------------|---------------------|---------------------|
| central values,<br>$3 < R_{vertex} < 8$                                      | $2.2492 \pm 0.2266$ | $1.7688 \pm 0.1473$ | $1.9272 \pm 0.1695$ | $2.3423 \pm 0.2681$ |
| central values,<br>$3 < R_{vertex} < 5$                                      | $2.5925 \pm 0.3842$ | $1.4351 \pm 0.1715$ | $2.3480 \pm 0.3139$ | $1.7779 \pm 0.2919$ |
| central values,<br>$5 < R_{vertex} < 8$                                      | $1.9670 \pm 0.2701$ | $2.1301 \pm 0.2500$ | $1.6512 \pm 0.1944$ | $3.0025 \pm 0.4865$ |
| central values,<br>$3 < R_{vertex} < 8$ ,<br>$\pi^0$ requirement             | $2.0178 \pm 0.3371$ | $2.6661 \pm 0.4051$ | $2.1536 \pm 0.3385$ | $3.5753 \pm 0.8164$ |
| central values,<br>$3 < R_{vertex} < 8$ ,<br>$\mu\nu$ MM2 taken<br>from DATA | $2.8968 \pm 0.3162$ | $2.4802 \pm 0.2294$ | $2.8069 \pm 0.2812$ | $2.6650 \pm 0.3163$ |

Table 21: Results of the  $\frac{Br(K^- \rightarrow \pi^0 e^- \nu)}{Br(K^- \rightarrow \pi^0 \mu^- \nu)}$  measurements, averages over the energies.

|                                                                              |                     |
|------------------------------------------------------------------------------|---------------------|
| central values,<br>$3 < R_{vertex} < 8$                                      | $1.9687 \pm 0.0935$ |
| central values,<br>$3 < R_{vertex} < 5$                                      | $1.7723 \pm 0.1263$ |
| central values,<br>$5 < R_{vertex} < 8$                                      | $1.9443 \pm 0.1287$ |
| central values,<br>$3 < R_{vertex} < 8$ ,<br>$\pi^0$ requirement             | $2.3152 \pm 0.1995$ |
| central values,<br>$3 < R_{vertex} < 8$ ,<br>$\mu\nu$ MM2 taken<br>from DATA | $2.6766 \pm 0.1391$ |
| PDG                                                                          | $1.48 \pm 0.03$     |

## 8.2 SYSTEMATIC ERRORS

We consider three sources of systematic error:

1. inconsistencies among different beam energies;
2. inconsistencies among analysis variations;
3. possible distortion due to an apparent excess in the semileptonic region.

### 8.2.1 MM2 Fits: Consistency Among Energies

Table 22 shows the  $\chi^2/d.f.$  of the consistency of the results; table 23 shows  $\chi^2/d.f.$ 's of the MM2 fits for each energy point.

Table 22: Consistency of the results obtained at different energies represented by the  $\chi^2/d.f.$ .

|                                                                                                    | K <sup>+</sup> decays | K <sup>-</sup> decays |
|----------------------------------------------------------------------------------------------------|-----------------------|-----------------------|
| $\frac{Br(K \rightarrow \pi\pi^0)}{Br(K \rightarrow \mu\nu)}$                                      | 1.04                  | 1.04                  |
| $\frac{Br(K \rightarrow \pi^0\mu\nu) + Br(K \rightarrow \pi^0e\nu)}{Br(K \rightarrow \pi\pi^0)}$   | 2.20                  | 1.07                  |
| $\frac{Br(K \rightarrow \pi\pi\pi) + Br(K \rightarrow \pi\pi^0\pi^0)}{Br(K \rightarrow \pi\pi^0)}$ | 0.83                  | 0.23                  |

Table 23:  $\chi^2/d.f.$  of the MM2 fits.

|                | 509.0 MeV | 509.5 MeV | 510.0 MeV | 510.5 MeV |
|----------------|-----------|-----------|-----------|-----------|
| K <sup>+</sup> | 1.8       | 2.9       | 2.4       | 2.2       |
| K <sup>-</sup> | 2.4       | 2.9       | 3.3       | 2.0       |

Although the  $\chi^2/d.f.$  for the individual energies are approximately 2.0 the branching ratios obtained, as a group, are consistent between energies. Therefore we choose not to rescale the statistical errors or otherwise adjust for the fact the individual energy  $\chi^2/d.f.$  are greater than 1. Including such a rescaling would not substantially affect the final quoted systematic errors.

### 8.2.2 MM2 Fits: Analysis Variations, $Br(K \rightarrow \pi\pi^0)/Br(K \rightarrow \mu\nu)$

To estimate the systematic error of the  $Br(K \rightarrow \pi\pi^0)/Br(K \rightarrow \mu\nu)$  ratio I use the following quantities:

1. difference between the results of the  $R_{3-5}$  and  $R_{5-8}$  fits;
2. difference between the results of the  $R_{3-8}$  and  $R_{\mu\nu \text{ data}}$  fits;
3. difference between the results of the  $R_{3-8}$  and  $R_{lik-2tr}$  fits;
4. error that comes from the excess in the semileptonic region, evaluated in the flat background model;
5. error that comes from the excess in the semileptonic region, evaluated in the model in which the background's shape follows the shape of the semileptonic distributions.

The  $R_{\pi^0}$  variation is not used since  $K \rightarrow \pi\pi^0$  mode has a real  $\pi^0$  and the  $K \rightarrow \mu\nu$  mode does not and 'noise' photons are not simulated. Thus, on the average, an experimental event has a few photons more than a simulated event. Therefore the experimental  $K \rightarrow \mu\nu$  event is more likely to have a  $\pi^0$  than a simulated event would, and the  $\pi^0$  requirement affects the real and simulated data differently.

The  $R_{lik-K}$  variation is not used because it is contained within the  $R_{lik-2tr}$  variation, which is used.

For the  $K^+$  data two approaches are possible to evaluate this systematic error. The first is the 'conservative' approach: to add all of the listed above contributions in quadrature, out of the two semileptonic excess models taking the one that yields larger error. The second is the 'optimistic' approach: the  $R_{3-5} - R_{5-8}$  contribution in this particular case is  $(3.2 \pm 2.9)\%$  and is consistent with zero; contributions 2 and 4 may be correlated and then one can take into account only the largest of them, and finally out of the two semileptonic excess models taking the average of the error that they yield. Adding all these in quadrature, yields 2.6%.

For the  $K^-$  data one cannot argue that the contribution  $R_{3-5} - R_{5-8}$  is consistent with zero. Adding all contributions in quadrature yields 21.0%.

### 8.2.3 MM2 Fits: Analysis Variations,

$$(Br(K \rightarrow \pi^0 \mu \nu) + Br(K \rightarrow \pi^0 e \nu))/Br(K \rightarrow \pi \pi^0)$$

To estimate the systematic error of the  $(Br(K \rightarrow \pi^0 \mu \nu) + Br(K \rightarrow \pi^0 e \nu))/Br(K \rightarrow \pi \pi^0)$  ratio I use the following quantities:

1. difference between the results of the  $R_{3-5}$  and  $R_{5-8}$  fits
2. difference between the results of the  $R_{3-8}$  and  $R_{\pi^0}$  fits
3. difference between the results of the  $R_{3-8}$  and  $R_{\mu \nu \text{ data}}$  fits
4. difference between the results of the  $R_{3-8}$  and  $R_{lik-2tr}$  fits.

Again,  $R_{lik-K}$  variation is not used because it is contained within the  $R_{lik-2tr}$  variation.

Adding all the contributions in quadrature yields 20.9% for  $K^+$  decays and 5.4% for  $K^-$  decays.

### 8.2.4 MM2 Fits: Analysis Variations,

$$(Br(K \rightarrow \pi \pi \pi) + Br(K \rightarrow \pi \pi^0 \pi^0))/Br(K \rightarrow \pi \pi^0)$$

To estimate the systematic error of the  $(Br(K \rightarrow \pi \pi \pi) + Br(K \rightarrow \pi \pi^0 \pi^0))/Br(K \rightarrow \pi \pi^0)$  ratio I use the following quantities:

1. difference between the results of the  $R_{3-5}$  and  $R_{5-8}$  fits
2. difference between the results of the  $R_{3-8}$  and  $R_{\pi^0}$  fits
3. difference between the results of the  $R_{3-8}$  and  $R_{\mu \nu \text{ data}}$  fits
4. difference between the results of the  $R_{3-8}$  and  $R_{lik-K}$  fits.
5. error that comes from the excess in the semileptonic region, evaluated in the flat background model
6. error that comes from the excess in the semileptonic region, evaluated in the model in which the background's shape follows the shape of the semileptonic distributions

Here the  $R_{lik-K}$  variation was used rather than the  $R_{lik-2tr}$  variation since in the case of the 3 charged pions decay the probability that the kaon and decay product tracks are confused is higher than in any other mode. This happens because this decay mode involves 3 soft pions whose  $dE/dx$  in some cases comes close to that of the kaon.

Adding all the contributions in quadrature yields 17.3% for  $K^+$  decays and 43.4% for  $K^-$  decays.

### 8.2.5 Semileptonic Region Excess

The error that comes from the excess in the semileptonic region is evaluated assuming two different models: the background that causes the excess is flat, and the model in which this background follows the shape of the semileptonic decays distribution.

The distortion of the branching ratio is estimated from the fraction of the excess that would fall in  $\mu\nu$ ,  $\pi\pi^0$ , and  $3\pi$  MM2 regions.

The results of these calculations are summarized in table 24.

Table 24: Errors due to the excess in the semileptonic region evaluated in two models: flat background, and 3-body decays shaped background.

|                   | flat background | 3-body shaped background |
|-------------------|-----------------|--------------------------|
| 509.0 $K^+$       | 3.0%            | 2.2%                     |
| 509.5 $K^+$       | 1.5%            | 1.2%                     |
| 510.0 $K^+$       | 1.1%            | 1.0%                     |
| 510.5 $K^+$       | 1.1%            | 1.0%                     |
| 509.0 $K^-$       | 3.5%            | 2.7%                     |
| 509.5 $K^-$       | 4.1%            | 3.0%                     |
| 510.0 $K^-$       | 3.1%            | 2.4%                     |
| 510.5 $K^-$       | 3.5%            | 2.8%                     |
| average for $K^+$ | 1.6%            | 1.3%                     |
| average for $K^-$ | 3.5%            | 2.7%                     |

### 8.2.6 Systematic Error for the MM2 measurements: $K^+$

Tables 25 and 26 summarize the systematic errors due to relevant variations for all three measurements discussed above.

Table 25: Systematic errors for  $K^+$  measurements

|                                              | $\frac{Br(K^+ \rightarrow \pi^+ \pi^0)}{Br(K^+ \rightarrow \mu^+ \nu)}$ | $\frac{Br(K^+ \rightarrow \pi^0 \mu^+ \nu) + Br(K^+ \rightarrow \pi^0 e^+ \nu)}{Br(K^+ \rightarrow \pi^+ \pi^0)}$ | $\frac{Br(K^+ \rightarrow \pi^+ \pi^+ \pi^-) + Br(K^+ \rightarrow \pi^+ \pi^0 \pi^0)}{Br(K^+ \rightarrow \pi^+ \pi^0)}$ |
|----------------------------------------------|-------------------------------------------------------------------------|-------------------------------------------------------------------------------------------------------------------|-------------------------------------------------------------------------------------------------------------------------|
| $3 < R < 5$ and<br>$5 < R < 8$               | $3.2\% \pm 2.9\%$                                                       | $15.4\% \pm 6.7\%$                                                                                                | $0.2\% \pm 9.0\%$                                                                                                       |
| $\pi^0$ requirement<br>and $3 < R < 8$       |                                                                         | $13.5\% \pm 6.3\%$                                                                                                | $7.6\% \pm 11.8\%$                                                                                                      |
| $\mu\nu$ from data<br>and $3 < R < 8$        | 1.1%                                                                    | 4.4%                                                                                                              | 3.2%                                                                                                                    |
| kaon track<br>likelihood and<br>$3 < R < 8$  |                                                                         |                                                                                                                   | 5.9%                                                                                                                    |
| both tracks<br>likelihood and<br>$3 < R < 8$ | 2.2%                                                                    | 0.5%                                                                                                              |                                                                                                                         |
| smlp excess<br>flat model                    | 1.6%                                                                    |                                                                                                                   | $\approx 14\%$                                                                                                          |
| smlp excess<br>shaped model                  | 1.3%                                                                    |                                                                                                                   | $\approx 14\%$                                                                                                          |
| Total                                        |                                                                         |                                                                                                                   |                                                                                                                         |
| conservative                                 | $(4.3 \pm 2.9)\%$                                                       | 20.9%                                                                                                             | 17.3%                                                                                                                   |
| optimistic                                   | 2.6%                                                                    |                                                                                                                   |                                                                                                                         |

### 8.2.7 Systematic Error for the MM2 measurements: $K^-$

Studies of the data have shown that the inherent backgrounds in the  $K^-$  sample are more substantial than in  $K^+$ . This is shown by the study of non-resonance beam energy points and by the independent estimate of  $e^- N$  interactions. While these cuts should have substantially removed these backgrounds the differences in MM2 results between  $K^+$  and  $K^-$  samples are worrisome. Therefore I take an additional source of uncertainty for the  $K^-$  measurements the difference between the  $K^+$  and  $K^-$  results. the belief that the  $K^+$  results are more reliable is reinforced by superior internal consistency of the  $Br(K \rightarrow \pi\pi^0)/Br(K \rightarrow \mu\nu)$  results. This ratio is the most straightforward and its internal consistency serves as a measure of our understanding of the sample.

Table 26: Systematic errors for  $K^-$  measurements

|                                              | $\frac{Br(K^+ \rightarrow \pi^+ \pi^0)}{Br(K^+ \rightarrow \mu^+ \nu)}$ | $\frac{Br(K^+ \rightarrow \pi^0 \mu^+ \nu) + Br(K^+ \rightarrow \pi^0 e^+ \nu)}{Br(K^+ \rightarrow \pi^+ \pi^0)}$ | $\frac{Br(K^+ \rightarrow \pi^+ \pi^+ \pi^-) + Br(K^+ \rightarrow \pi^+ \pi^0 \pi^0)}{Br(K^+ \rightarrow \pi^+ \pi^0)}$ |
|----------------------------------------------|-------------------------------------------------------------------------|-------------------------------------------------------------------------------------------------------------------|-------------------------------------------------------------------------------------------------------------------------|
| $3 < R < 5$ and<br>$5 < R < 8$               | $14.3\% \pm 2.6\%$                                                      | $4.6\% \pm 5.1\%$                                                                                                 | $24.7\% \pm 11.0\%$                                                                                                     |
| $\pi^0$ requirement<br>and $3 < R < 8$       |                                                                         | $2.7\% \pm 5.0\%$                                                                                                 | $21.1\% \pm 13.9\%$                                                                                                     |
| $\mu\nu$ from data<br>and $3 < R < 8$        | 14.8%                                                                   | 1.0%                                                                                                              | 23.7%                                                                                                                   |
| kaon track<br>likelihood and<br>$3 < R < 8$  |                                                                         |                                                                                                                   | 3.7%                                                                                                                    |
| both tracks<br>likelihood and<br>$3 < R < 8$ | 2.7%                                                                    | 0.1%                                                                                                              |                                                                                                                         |
| smlp excess<br>flat model                    | 3.5%                                                                    |                                                                                                                   | $\approx 16\%$                                                                                                          |
| smlp excess<br>shaped model                  | 2.7%                                                                    |                                                                                                                   | $\approx 16\%$                                                                                                          |
| Subtotal                                     |                                                                         |                                                                                                                   |                                                                                                                         |
| conservative                                 | $(21.0 \pm 2.6)\%$                                                      | $(5.4 \pm 7.0)\%$                                                                                                 | $(43.4 \pm 17.7)\%$                                                                                                     |
| Difference from<br>$K^+$                     | $(18.4 \pm 1.8)\%$                                                      | $(12.5 \pm 3.7)\%$                                                                                                | $(16.0 \pm 7.2)\%$                                                                                                      |
| Total                                        | $(27.9 \pm 3.2)\%$                                                      | $(13.6 \pm 7.9)\%$                                                                                                | $(46.2 \pm 19.1)\%$                                                                                                     |

### 8.2.8 Systematic Error of the Ratio Obtained from the DPE

To estimate the systematic error of the  $Br(K^- \rightarrow \pi^0 e^- \nu)/Br(K^- \rightarrow \pi^0 \mu^- \nu)$  ratio I use the following quantities:

1. difference between the results of the  $R_{3-5}$  and  $R_{5-8}$  fits:  $(8.7 \pm 9.1)\%$ ;
2. difference between the results of the  $R_{3-8}$  and  $R_{\pi^0}$  fits:  $(17.6 \pm 11.2)\%$ ;
3. difference between the results of the  $R_{3-8}$  and  $R_{\mu\nu \text{ data}}$  fits:  $(36.0 \pm 8.5)\%$ .

These errors, added in quadrature, give  $(41.0 \pm 16.7)\%$ .

### 8.2.9 Final Results

Table 27: Ratios obtained in this dissertation for the  $K^+$  and  $K^-$  samples compared to the current results from the Particle Data Group. The first error is statistical, the second is systematic.

|               | $K^+$                         | $K^-$                        | PDG                 |
|---------------|-------------------------------|------------------------------|---------------------|
| $R_{2body}$   | $0.3292 \pm 0.0048 \pm 0.011$ | $0.4034 \pm 0.0053 \pm 0.11$ | $0.3331 \pm 0.0024$ |
| $R_{semilep}$ | $0.477 \pm 0.016 \pm 0.10$    | $0.545 \pm 0.014 \pm 0.076$  | $0.3852 \pm 0.0048$ |
| $R_{3pion}$   | $0.315 \pm 0.014 \pm 0.054$   | $0.271 \pm 0.015 \pm 0.13$   | $0.3459 \pm 0.0033$ |
| $R_{e\mu}$    |                               | $1.97 \pm 0.09 \pm 0.81$     | $1.49 \pm 0.03$     |

Table 27 summarizes the ratios obtained in the course of work on this dissertation for the  $K^+$  and  $K^-$  samples.

All but  $R_{2body}$  have substantial systematic errors.  $R_{2body}$  for the  $K^-$  sample is consistent with that of  $K^+$  sample, but  $\sigma_{sys}$  for  $K^-$  is factor of 10 larger than that of  $K^+$ .  $K^-$  data shows internal inconsistencies, as seen in table 26. Within the systematic errors all the results are consistent with the PDG values.  $R_{semilep}$  is about 20% higher than the PDG value but with the 21% systematic uncertainty and therefore cannot discriminate between the PDG value and the recent E865 result which is 5% higher than that in PDG.

### 8.2.10 Conclusions

In the course of work on this dissertation several branching ratios of the charged kaons were extracted using the data from  $e^+e^-$  collisions at  $\phi$  energy. The data with  $K^+$  decaying is found to be more reliable than the data with  $K^-$  decaying. This conclusion is drawn by internal consistency checks. I believe the cause of the inconsistencies is the impact of the  $e^-N$  collision background.

We started this project hoping to measure all branching ratios of the charged kaons, in both signs. This plan proved to be unrealistic. The main problems encountered are:

1. imperfections of the Monte Carlo simulation, in particular the difficulties in simulating propagation of the charged kaons;
2. apparent backgrounds, most notably the  $e^-N$  collision background;
3. inconsistencies in the calorimeter calibrations used in the analysis of experimental data and in the Monte Carlo simulation.

In this dissertation I have described the methods we used for the analysis, and shown results that indicate remaining serious inconsistencies in  $K^-$  data and between  $K^-$  and  $K^+$  data. Because of the observed inconsistencies in  $K^-$  data, we trust the  $K^+$  data more. The  $K^+$  data has better internal consistency in  $Br(K \rightarrow \pi\pi^0)/Br(K \rightarrow \mu\nu)$ , the most straightforward and easiest to evaluate ratio. Final results are shown in table 27. All results obtained from the analysis of  $K^+$  data are consistent with the PDG values though the systematic errors for  $R_{semilep}$  and  $R_{3pion}$  are large.

In general,  $R_{semilep}$  is the most delicate since it is the most sensitive to all sorts of background, most notably the  $e^-N$  background which is present in the  $K^-$  data – the only data from which this ratio can be measured. This result is about two standard deviations higher than the PDG value but the errors of about 20% are too large to draw conclusions relevant to  $V_{us}$  discussion. The ratios obtained from the MM2 analysis, namely  $R_{2body}$  and  $R_{3pion}$ , from both  $K^+$  and  $K^-$  data, agree within assigned systematic errors with PDG values. Detailed values and discussion of systematic error assignments are in the previous chapter. Such an approach of looking at the consistency of all the branching ratios ( $K^+$  and  $K^-$  data separately) in one experiment is helpful in uncovering and testing for systematic

errors.

## 9.0 RADIATIVE CORRECTIONS TO THE $K_{E3}^{\pm}$ DECAY

### 9.1 INTRODUCTION AND MOTIVATION

The  $K_{e3}$  decay is important since it is the cleanest way to measure the  $V_{us}$  matrix element of the CKM matrix. If one uses the current values for  $V_{ud}$ ,  $V_{us}$ , and  $V_{ub}$  taken from the PDG [1] then  $|V_{ud}|^2 + |V_{us}|^2 + |V_{ub}|^2$  misses unity by 2.3 standard deviations:

$$|V_{ud}| = 0.9734 \pm 0.0008, \quad |V_{us}| = 0.2196 \pm 0.0026, \quad |V_{ub}| = 0.0036 \pm 0.0007 \quad (9.1)$$

$$|V_{ud}|^2 + |V_{us}|^2 + |V_{ub}|^2 = 0.9957 \pm 0.0019 . \quad (9.2)$$

This contradicts the unitarity of the CKM matrix and might indicate physics beyond the Standard Model. The uncertainty brought to the above expression by  $V_{us}$  is about the same as the uncertainty that comes from  $V_{ud}$ . Therefore reducing the error in the  $V_{us}$  matrix element would reduce substantially the error in the whole unitarity equation. Reliable radiative corrections, potentially of the order of a few percent are necessary to extract the  $V_{us}$  matrix element from the  $K_{e3}$  decay width with high precision.

The momentum transfer dependence of the form factor is customarily parameterized by

$$f_+(t) = f_+(0) \left( 1 + \frac{\lambda_+}{m_\pi^2} t \right) \quad (9.3)$$

The parameter  $\lambda_+$  is extracted from  $K_{e3}$  Dalitz plot distribution, and reliable calculation of the radiative corrections to the Dalitz plot density would help to determine  $\lambda_+$  with better precision.

Another application of the radiative corrections calculation is creation of the Monte Carlo simulation generator for  $K_{e3}$  that would include these radiative correction.

And finally, the methods developed in this study can be applied to calculations of radiative corrections to other decays,  $K_{\mu 3}$  being an immediate candidate. The existing calculations of the radiative corrections to the  $K_{e3}$  decay were performed independently by E.S. Ginsberg and T. Becherrawy in the late 60's [5, 6]. Their results for corrections to the decay rate, Dalitz plot, pion and electron spectra disagree, in some places quite sharply; for example Ginsberg's correction to the decay rate is  $-0.45\%$  while that of Becherrawy is  $-2\%$  (corresponding to corrections to the total width  $\Gamma_{K_{e3}}$  of  $0.45\%$  and  $2\%$  respectively). In addition, calculations by E.S. Ginsberg are ultraviolet cutoff sensitive. Recently the radiative corrections to the  $K_{e3}$  decay were calculated in the framework of Chiral Perturbation Theory (ChPT) [3]; however the authors did not present the Dalitz plot corrections and correction to the full width in their paper. We have decided to perform a new calculation since results of the experiments (including ours) will become available soon and to explore the causes of the discrepancies in the previous calculations. The results of our work are corrections to the Dalitz plot, corrections to the spectra of  $e^\pm$  and  $\pi^0$ , and correction to the total width. Comparing this work with the older calculations [5, 6], I made the following improvements:

1. used the short distance enhancement factor  $S_{EW}$ . It accounts for most of the differences between our results and those of E.S. Ginsberg;
2. the dependance of the results on the electron mass logarithm  $L_e$  is given in all orders of the perturbation theory
3. the strong interaction effects are treated by the means of the chiral perturbation theory (ChPT);
4. explicit formulas for the corrections to the Dalitz plot and corrections to the spectra of  $e^\pm$  and  $\pi^0$  are given; these may be used for experimental analysis.

This work was begun in collaboration with E. Kuraev and V. Bytev from the Joint Institute of Nuclear Research (JINR) in Dubna, Russia. The present discussion has three differences from our collaborative work [27]:

1. different estimate of the uncertainty of the result;
2. correction of the error in the pion mass used (in the original paper the mass of the charged pion was used instead of the mass of the neutral pion);

3. different treatment of the photons with energies above the mass of the  $\rho$ -meson.

The numerical effect of these differences is small; they will be pointed out at relevant junctures in this chapter. Discussions with A. Milstein, S. Eidelman and V. Cirigliano were instrumental in clarifying my understanding and deciding upon the final approach described here.

Figures [Introduction and Motivation](#) and [Introduction and Motivation](#) demonstrate all Feynman diagrams involved. Figure [Introduction and Motivation](#) shows the corrections due to virtual photons, figure [Introduction and Motivation](#) shows the corrections due to real photons.

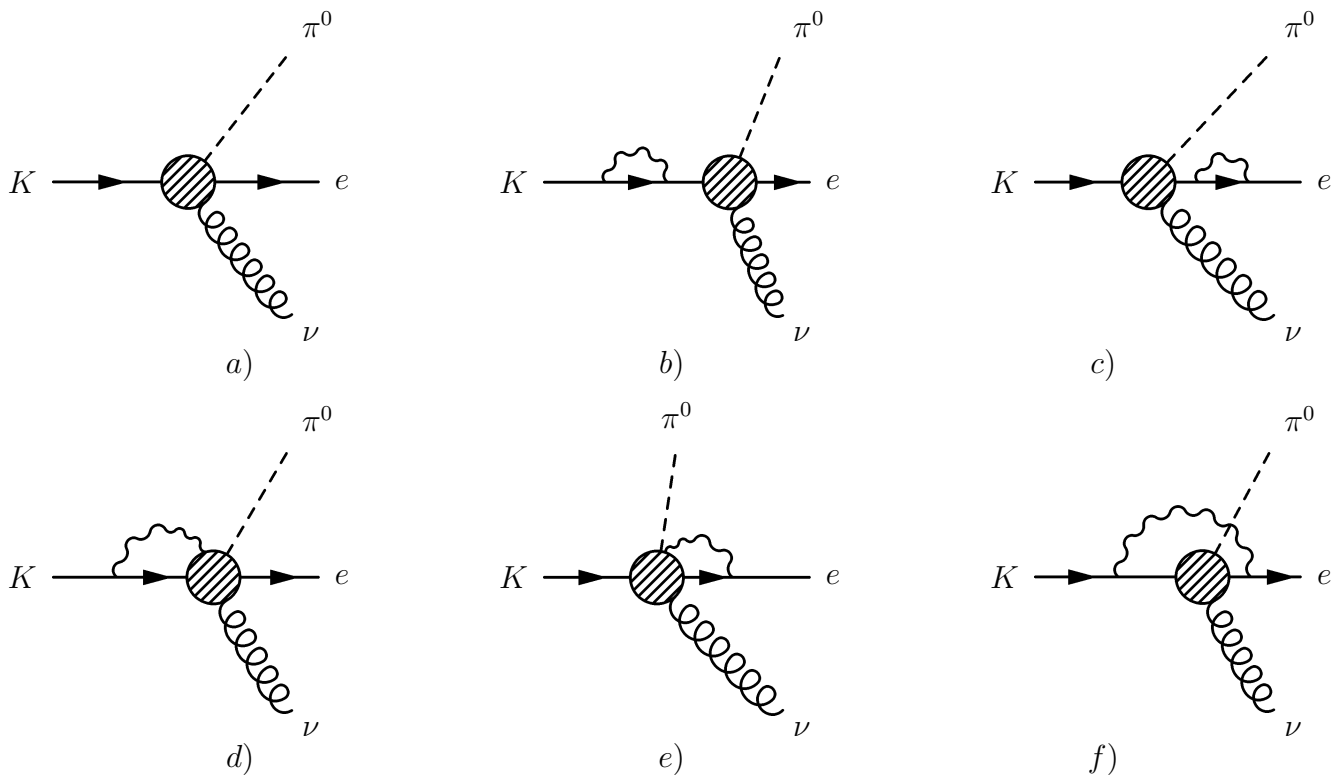


Figure 80: Virtual photons.

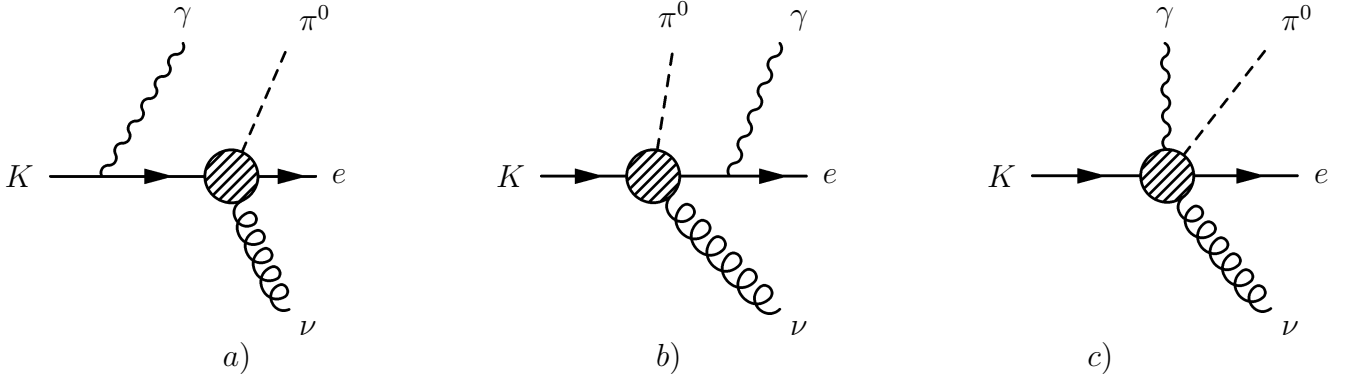


Figure 81: Real photons.

## 9.2 MATRIX ELEMENTS AND KINEMATICS

The matrix element for

$$K^+(p) \rightarrow \pi^0(p') + e^+(p_e) + \nu(p_\nu) \quad (9.4)$$

has the general structure

$$M = \frac{G_F}{\sqrt{2}} V_{us}^* F_\nu(t) \bar{u}(p_\nu) \gamma_\nu (1 + \gamma_5) v(p_e) \quad (9.5)$$

where

$$F_\nu(t) = \frac{1}{\sqrt{2}} [(p + p')_\nu f_+(t) + (p - p')_\nu f_-(t)]. \quad (9.6)$$

Here  $f_+$  and  $f_-$  are the form factors that depend on the square of the four momentum transfer to the leptons:

$$t = (p - p')^2 = (p_e + p_\nu)^2. \quad (9.7)$$

Using Dirac equation one can see that the second term in eq [Matrix Elements and Kinematics](#) becomes proportional to the electron mass and therefore is always neglected, so that  $f_-$  becomes irrelevant. As for  $f_+(t)$  in  $K_{e3}$  analysis it is customary to assume its linear dependence on the momentum transfer:

$$f_+(t) = f_+(0) \left( 1 + \lambda_+ \frac{t}{m_\pi^2} \right). \quad (9.8)$$

According to PDG [1]

$$\lambda_+ = 0.0276 \pm 0.0021 . \quad (9.9)$$

To simplify the notation I will use  $M^2$  for the mass of kaon.

Following the notation of [28]:

$$r_e \equiv m_e^2/M^2, \quad r_\pi \equiv m_\pi^2/M^2 ; \quad (9.10)$$

where  $m_e$ ,  $m_\pi$ , and  $M$  are the masses of electron, neutral pion, and kaon; two convenient kinematic variables are

$$y \equiv 2pp_e/M^2, \quad z \equiv 2pp'/M^2 . \quad (9.11)$$

In the kaon's rest frame, which I will use throughout this chapter,  $y$  and  $z$  become the energy fractions of electron and pion:

$$y = 2E_e/M, \quad z = 2E_\pi/M . \quad (9.12)$$

Later, when dealing with real photons we'll also use

$$x = 2\omega/M . \quad (9.13)$$

where  $\omega$  is the photon energy. Plotting the  $K_{e3}$  events on  $z$  vs  $y$  plane one obtains Dalitz plot density from which  $\lambda_+$  is measured.

The kinematically allowed region for  $y$  and  $z$  in the 3-body (non-radiative)  $K_{e3}$  decay is given by ([28])

$$\begin{aligned} 2\sqrt{r_e} &\leq y \leq 1 + r_e - r_\pi , \\ F_1(y) - F_2(y) &\leq z \leq F_1(y) + F_2(y) , \\ F_1(y) &= (2 - y)(1 + r_e + r_\pi - y)/[2(1 + r_e - y)] , \\ F_2(y) &= \sqrt{y^2 - 4r_e}(1 + r_e - r_\pi - y)/[2(1 + r_e - y)] ; \end{aligned} \quad (9.14)$$

or, equivalently,

$$\begin{aligned}
2\sqrt{r_\pi} &\leq z \leq 1 + r_\pi - r_e , \\
F_3(z) - F_4(z) &\leq y \leq F_3(z) + F_4(z) , \\
F_3(z) &= (2 - z)(1 + r_\pi + r_e - z)/[2(1 + r_\pi - z)] , \\
F_4(z) &= \sqrt{z^2 - 4r_\pi}(1 + r_\pi - r_e - z)/[2(1 + r_\pi - z)] .
\end{aligned} \tag{9.15}$$

For our aims I omit the terms of the order of  $r_e$  and use the simplified form of physical region:

$$2\sqrt{r_e} \leq y \leq 1 - r_\pi , \quad c(y) \leq z \leq 1 + r_\pi , \tag{9.16}$$

with

$$c(y) = 1 - y + \frac{r_\pi}{1 - y} . \tag{9.17}$$

Or, equivalently,

$$2\sqrt{r_\pi} \leq z \leq 1 + r_\pi , \quad b_-(z) \leq y \leq b(z) , \tag{9.18}$$

with

$$b_-(z) = 1 - \frac{1}{2} \left( z + \sqrt{z^2 - 4r_\pi} \right) , \tag{9.19}$$

and

$$b(z) = 1 - \frac{1}{2} \left( z - \sqrt{z^2 - 4r_\pi} \right) . \tag{9.20}$$

The Dalitz plot density is

$$\frac{d^2\Gamma}{dydz} = \frac{M^5 G_F^2 |V_{us}|^2}{64\pi^3} |f_+(t)|^2 a_0(y, z) , \tag{9.21}$$

where

$$a_0(y, z) = (z + y - 1)(1 - y) - r_\pi + O(r_e) . \tag{9.22}$$

Figure [Matrix Elements and Kinematics](#) shows the kinematically allowed regions for the non-radiative and radiative  $K_{e3}$  decay. On this plot the abscissa is  $y$  – the energy fraction of the electron, the ordinate is  $z$  – the energy fraction of the pion, both in the units of half of the mass of  $K^\pm$ . Kinematically allowed region for non-radiative, 3-body  $K_{e3}$  decay is marked by the letter  $D$ . If the decay is radiative (sometimes called  $K_{e3\gamma}$ ) and a 'hard enough' (high enough momentum) photon is emitted by the electron, then the event can move to the left of the boundary of  $D$  to the area marked by  $A$ . So the kinematically allowed region for  $K_{e3\gamma}$  is  $D+A$ . In this analysis I assume such experimental setup in which events from both of the areas  $D$  and  $A$  are included in  $K_{e3(\gamma)}$ , and the corrections to the spectra of electron and pion and the correction to the total width are obtained by integration over both  $D$  and  $A$ .

### 9.3 VIRTUAL AND SOFT REAL PHOTON EMISSION

Let  $\delta$  be the total radiative correction to the  $K_{e3}$  decay rate. I will distinguish 3 kinds of contributions to  $\delta$ : corrections that come from virtual photon exchanges, emission of real soft photons, and emission of real hard photons:

$$\delta = \delta_V + \delta_S + \delta_H . \quad (9.23)$$

All corrections are calculated in the rest frame of the kaon.

Standard calculations (see Appendix A for details) yield the following contributions:

- contribution from the real soft photons is

$$\delta_S = \frac{\alpha}{\pi} \left\{ (L_e - 2) \ln \frac{2\Delta\epsilon}{\lambda} + \frac{1}{2}L_e - \frac{1}{4}L_e^2 + 1 - \frac{\pi^2}{6} \right\} (1 + O(r_e)) , \quad (9.24)$$

where  $\Delta\epsilon$  is the maximal energy of a real soft photon in the rest frame of the kaon (I assume  $\Delta\epsilon \ll M/2$ ), and

$$L_e = 2 \ln y + \ln(1/r_e) ; \quad (9.25)$$

- contribution from the virtual photons make up charged fermion mass renormalization and is convenient to split into

$$\delta_V = \delta_C + \delta_{PLM} . \quad (9.26)$$

Using the Feynman gauge I obtain for  $\delta_C$  (Figs. 1b,c)

$$\delta_C = \frac{\alpha}{2\pi} \left\{ \left[ -\frac{1}{2}L_\Lambda + \frac{3}{2} \ln r_e + \ln \frac{M^2}{\lambda^2} - \frac{9}{4} \right] + \left[ L_\Lambda + \ln \frac{M^2}{\lambda^2} - \frac{3}{4} \right] \right\} , \quad (9.27)$$

where  $\lambda$  is fictitious "photon mass",  $L_\Lambda = \ln(\Lambda^2/M^2)$ , and  $\Lambda$  is the ultraviolet momentum cutoff. The first term in the curly braces comes from the electron, the second comes from the kaon;

- $\delta_{PLM}$  stands for the contribution from the diagram in Fig. 1f. I calculate it in the point like meson (PLM) approximation:

$$\delta_{PLM} = -\frac{\alpha}{2\pi} \left\{ -L_\Lambda - \frac{1}{2} \ln^2 r_e - 2L_e + \ln \frac{M^2}{\lambda^2} L_e - 1 + 2 \ln^2 y + 2 \ln y + 2Li_2(1-y) \right\} . \quad (9.28)$$

When these contributions are summed up the dependence on  $\lambda$  disappears.

I set the ultraviolet cutoff at the mass of the  $\rho$ -meson. This is physically correct because when one calculates loops with photons, pions and kaons as internal propagating particles, one uses the pion–pion–photon vertex dictated by scalar QED. However this is strictly valid only for point–like pions, which is not the case. In principle I should use a more general interaction vertex, namely ( $p, p'$  are pion momenta,  $q$  is photon momentum):

$$(p + p')_\mu \rightarrow F(q^2)(p + p')_\mu \quad (9.29)$$

I know from QCD that the form factor  $F(q^2)$  goes to zero for large photon virtuality  $q^2$ . Indeed I know that a very good approximate formula in the euclidean region ( $q^2 = -Q^2$ ) is

$$F(Q^2) = \frac{M_\rho^2}{M_\rho^2 + Q^2} . \quad (9.30)$$

So at  $Q^2 \rightarrow 0$  I recover  $F(Q^2) \rightarrow 1$ , but already at  $Q^2 = M_\rho^2$  the interaction is very much suppressed. If one inserts these modified vertices in loop diagrams, the integrals are UV

convergent, and one obtains a result very close to the one obtained with point-like vertices and the cutoff  $\Lambda = M_\rho$ . So the hadron form factors will 'effectively' cut off the loops around the mass of the  $\rho$ -meson.

Next I define

$$\Delta = \Delta\epsilon/E_e, \quad L_\rho = \ln(M_\rho^2/M^2), \quad S_\rho = 1 + \frac{3\alpha}{4\pi}L_\rho; \quad (9.31)$$

these quantities will be used below. <sup>1</sup>

Contribution from the structure-dependent part of soft photon emission (Figs. 1d,e), such as for example, interaction with resonances and intermediate  $W^\pm$ , is small, of the order

$$\frac{\alpha}{\pi} \frac{\Delta\epsilon}{M} \ll 1 \quad (9.32)$$

and thus I neglect it.

#### 9.4 HARD PHOTON EMISSION. STRUCTURE FUNCTIONS APPROACH

To calculate the hard photon contribution  $\delta_H$  it is convenient to split the total correction  $\delta(y, z)$  in the form

$$\delta(y, z) = \delta_L + \delta_{NL} \quad (9.33)$$

where  $\delta_L$  is the leading order contribution i.e. it contains the 'large logarithm'  $L_e$ ;  $\delta_{NL}$  is the non-leading contribution and contains the rest of the terms. First I calculate  $\delta_L$  using the evolution equation kernel and subtract from it the leading order terms that come from  $\delta_C$ ,  $\delta_S$ , and  $\delta_{PLM}$ . In this way I obtain the leading order contribution of  $\delta_H$ . Then I calculate the non-leading contribution of  $\delta_H$  directly from the matrix element of the radiative  $K_{e3}$  decay.

---

<sup>1</sup> In the original version of our paper [27] I have set the UV cutoff at the mass of  $W$  and defined  $S_W$  which depends on  $M_W$  the same way  $S_\rho$  depends on  $M_\rho$ . Then I argued that in order to account for the evolution of the coupling constant effects  $S_W$  should be replaced by the short distance enhancement factor  $S_{EW}$  (which will be discussed later). Now I believe that it is more appropriate to use  $S_\rho$  to account for the long distance effects, and  $S_{EW}$  should be used as overall multiplicative factor — the same way it was used in [3]. But since  $S_\rho = 1.0015$ , the result presented here differs very little from our previous result given in [27].

For the electron emitted by the kaon I use the point-like-meson approximation, i.e. neglect the kaon's form factor.

The leading order contribution from the virtual and soft photon emissions is associated with the so called  $\delta$ -part of the evolution equation kernel:

$$(\delta_C + \delta_S + \delta_{PLM})^{leading} = \frac{\alpha}{2\pi} (L_e - 1) \int \frac{a_0(t, z)}{a_0(y, z)} P_\delta^{(1)}\left(\frac{y}{t}\right) \frac{dt}{t} \quad (9.34)$$

where

$$P_\delta^{(1)}(t) = \delta(1-t) \left( 2 \ln \Delta + \frac{3}{2} \right) . \quad (9.35)$$

The contribution of the hard photon emission in the leading order can be found with the method of quasi-real electrons [29] as a convolution of the Born approximation with the  $\theta$ -part of the evolution equation kernel  $P_\theta(z)$ :

$$\delta_H^{leading} \sim \frac{\alpha}{2\pi} (L_e - 1) \int \frac{dt}{t} \frac{a_0(t, z)}{a_0(y, z)} P_\theta^{(1)}\left(\frac{y}{t}\right) \quad (9.36)$$

where

$$P_\theta^{(1)}(z) = \frac{1+z^2}{1-z} \theta(1-z-\Delta). \quad (9.37)$$

In this way the whole leading order contribution can be expressed in terms of convolution of the width in the Born approximation with the whole kernel of the evolution equation:

$$P^{(1)}(z) = \lim_{\Delta \rightarrow 0} \left( P_\delta^{(1)}(z) + P_\theta^{(1)}(z) \right) . \quad (9.38)$$

The total leading order contribution is proportional to

$$\Psi(y, z) = \int_{\max[y, b_-(z)]}^{b(z)} \frac{dt}{t} a_0(t, z) P^{(1)}\left(\frac{y}{t}\right) , \quad (9.39)$$

more precisely,

$$\delta_L = \frac{\alpha(L_e - 1)}{2\pi a_0(y, z)} \Psi(y, z) . \quad (9.40)$$

Using this approach I can check if our calculation is consistent with the Kinoshita–Lee–Nauenberg (KLN) theorem [30] as well as with the results of E. Ginsberg [5]. Since, as

one can check the leading logarithmic contribution to the total width as well as to the pion spectrum is zero due to:

$$\int_{2\sqrt{r\pi}}^{1+r\pi} dz \int_0^{b(z)} dy \Psi(y, z) = 0 . \quad (9.41)$$

terms that contain  $m_e$  do not contribute to the total width in correspondence with the KLN theorem and with Ginsberg's results. Explicit formulas for  $\Psi(y, z)$  are given in the Appendix B.

Now I need to find the non-leading contribution. The matrix element of the radiative  $K_{e3}$  decay

$$K^+(p) \rightarrow \pi^0(p') + e^+(p_e) + \nu(p_\nu) + \gamma(q) \quad (9.42)$$

with terms up to  $O(p^2)$  in CHPT [31, 28, 32, 33] has the form

$$M^{hard} = \frac{G}{2} f_+ V_{us}^* \sqrt{4\pi\alpha} \bar{u}(p_\nu) Q_\mu^{hard} (1 + \gamma_5) v(p_e) \epsilon^\mu(q) , \quad (9.43)$$

where

$$Q_\mu^{hard} = Q_\mu^e + Q_\mu^\pi + Q_\mu^{SD} = Q_\mu^{IB} + Q_\mu^{SD} , \quad (9.44)$$

$$Q_\mu^{IB} = (\hat{p} + \hat{p}') \left[ \frac{(-\hat{p}_e - \hat{q} + m_e)\gamma_\mu}{2p_e q} + \frac{p_\mu}{pq} \right] , \quad (9.45)$$

$$Q_\mu^{SD} = \gamma_\nu R_{\mu\nu} . \quad (9.46)$$

In eq (Hard Photon Emission. Structure Functions Approach) the tensor  $R_{\mu\nu}$  describes [28] structure-dependent emission (Fig. 2(c)) and is given by

$$R_{\mu\nu} = g_{\mu\nu} - \frac{q_\nu p_\mu}{pq} . \quad (9.47)$$

Terms singular at  $\chi = 2p_e q \rightarrow 0$  which provide contribution containing large logarithm  $L_e$  arise only from  $Q_\mu^e$ . To extract the corresponding terms I introduce four-vector  $v = (x/y)p_e - q$ , where  $x$  is the energy fraction of the photon (9). Note that  $v \rightarrow 0$  when  $\chi \rightarrow 0$ .

Separating leading and non-leading terms I obtain for the non-leading contribution:

$$\delta_H^{non-leading} = \frac{d\Gamma^{hard}}{d\Gamma_0} = \frac{\alpha}{2\pi a_0(y, z)} \int \frac{dx}{x} \int \frac{dO_\gamma}{2\pi} T, x > y\Delta. \quad (9.48)$$

where

$$T = \frac{x^2}{8} \sum_{spins} \left| \bar{u}(p_\nu) (Q_{IB}^{hard} + Q_{SD}^{hard}) (1 + \gamma_5) v(p_e) \right|^2 = \frac{y a_0(x+y, z)}{x+y} \left[ \frac{y^2 + (x+y)^2}{y^2(1-\beta_e C_e)} - 2 \frac{(1-\beta_e)(x+y)}{y(1-\beta_e C_e)^2} \right] - \frac{y a_0(x+y, z)}{x+y} + \mathcal{P}. \quad (9.49)$$

$\mathcal{P}$  is given by

$$\mathcal{P} = \left( \frac{p_e q}{M^2} \left( \frac{p_\nu q}{M^2} + z - \frac{2y}{x+y} (1-x-y) \right) + \frac{p' v}{M^2} \frac{y(2-x-y)}{x+y} \right) \left( \frac{x M^2}{4y p_e q} (y^2 + (x+y)^2) - 1 \right) - \frac{M^2 x^2}{8 p_e q} \left( T_v + \frac{2}{x} T_{1v} \right) - \frac{x^2}{8} (T_{RR} + 2T_R), \quad (9.50)$$

with

$$T_v = \frac{1}{4M^4} Sp (\hat{p} + \hat{p}') \hat{p}_\nu (\hat{p} + \hat{p}') \hat{v}; \quad (9.51)$$

$$T_{1v} = \frac{1}{4M^6} Sp (\hat{p} + \hat{p}') \hat{p}_\nu (\hat{p} + \hat{p}') \hat{v} \hat{p}_e; \quad (9.52)$$

$$T_{RR} = R_{\mu\lambda} R_{\mu\sigma} \frac{1}{4M^2} Sp \hat{p}_\nu \gamma_\lambda \hat{p}_e \gamma_\sigma; \quad (9.53)$$

$$T_R = R_{\mu\lambda} \frac{1}{4M^2} Sp \hat{p}_\nu (\hat{p} + \hat{p}') \left[ \frac{p_\mu}{pq} - \frac{(\hat{p}_e + \hat{q}) \gamma_\mu}{\chi} \right] \hat{p}_e \gamma_\lambda. \quad (9.54)$$

To calculate these traces I use the following scalar products of the 4-momenta (in units of  $M$ ):

$$p^2 = 1, \quad q^2 = 0, \quad p_\nu^2 = 0, \quad p'^2 = r_\pi, \quad p_e^2 = 0, \quad pp_e = \frac{y}{2},$$

$$pp' = \frac{z}{2}, \quad pq = \frac{x}{2}, \quad pp_\nu = \frac{1}{2} (2 - y - z - x),$$

$$p'p_\nu = \frac{1}{2} (1 - x - y - r_\pi + A_e), \quad p'q = \frac{1}{2} (x - A_e - A_\nu),$$

$$p'p_e = \frac{1}{2}(y - R(z) + A_\nu), \quad p_\nu q = \frac{1}{2}A_\nu, \quad p_e q = \frac{1}{2}A_e,$$

$$p_e p_\nu = \frac{1}{2}(R(z) - A_e - A_\nu), \quad p v = 0, \quad p_e v = -\frac{1}{2}A_e,$$

$$q v = \frac{1}{2} \frac{x}{y} A_e, \quad p' v = \frac{1}{2} \left( \frac{x+y}{y} \tilde{A}_\nu + A_e \right),$$

$$p_\nu v = -\frac{1}{2y} \left( x A_e + (x+y) \tilde{A}_\nu \right),$$

$$\tilde{A}_\nu = A_\nu - \frac{x}{x+y} R(z).$$

Three terms in the rhs of ([Hard Photon Emission. Structure Functions Approach](#)) behave differently. The first term corresponds to the kinematic region of the collinear emission, when photon is emitted along electron's momentum. The relevant phase space has essentially a 3-particle form:

$$\begin{aligned} (d\phi_4)^{coll} &= \left( \frac{d^3 p_e}{2\epsilon_e} \frac{d^3 q}{2\omega} \frac{d^3 p'}{2\epsilon'} d^4 p_\nu \delta(p_\nu^2) \delta^4(p - p_e - p_\nu - p' - q) \right)^{coll} = \\ &M^4 \frac{\pi^2}{64} \beta_\pi \, z dz \, y dy \, x dx \, dO_\gamma \, dC_{e\pi} \times \\ &\delta \left( 1 - x - y - z + r_\pi + \frac{x+y}{y} \frac{zy}{2} (1 - \beta_\pi C_{e\pi}) + \frac{2p_e q}{M^2} \right) = \\ &\frac{y}{x+y} M^4 \frac{\pi^2}{32} \, dO_\gamma \, x dx \, dy \, dz. \quad (9.55) \end{aligned}$$

The photon energy fraction varies in the interval  $y\Delta < x < b(z) - y$ ; the upper limit is imposed by the 3-body decay kinematics.

The second term corresponds to emission of a photon by the kaon. The relevant kinematics is isotropic. The kinematics of the radiative kaon decay and the comparison of our and E. Ginsberg's approaches is given in Appendix F. The third term corresponds to the rest

of the contributions which contain neither collinear nor infrared singularities. Performing the integration over photon's phase space I obtain:

$$\begin{aligned}
\int \frac{dx}{x} \int \frac{dO_\gamma}{2\pi} T = & \\
& \int_{y\Delta}^{b(z)-y} \frac{dx}{x} \frac{y^2}{(y+x)^2} a_0(y+x, z) \left[ \frac{y^2 + (y+x)^2}{y^2} (L_e - 1) + \frac{x^2}{y^2} \right] \\
& - 2 \int_{y\Delta}^{b(z)-y} \frac{dx}{x} \left[ a_0(y, z) + x \left( \frac{R(z)}{x+y} - y \right) \right] + \int_0^{\mathcal{N}} dx \mathcal{J}(x, y, z) . \quad (9.56)
\end{aligned}$$

where

$$\mathcal{J}(x, y, z) = \frac{1}{x} \int \frac{dO_\gamma}{2\pi} \mathcal{P} , \quad (9.57)$$

and

$$\mathcal{N} = \frac{b_-(z)(b(z) - y)}{b(z)} . \quad (9.58)$$

The non-leading contribution from the hard photon emission can be written in the form

$$\begin{aligned}
\delta_H^{non-leading} = & \frac{\alpha}{2\pi a_0(y, z)} \left\{ -2a_0(y, z) \ln \frac{b(z) - y}{y\Delta} - \right. \\
& 2 \left( R(z) \ln \frac{b(z)}{y} - y(b(z) - y) \right) - (R(z) + y(2 - z)) \ln \frac{b(z)}{y} \\
& \left. + (b(z) - y) \left( \frac{R(z)}{b(z)} + 2 - z - \frac{b(z) - y}{2} \right) + \int_0^{\mathcal{N}} dx \mathcal{J}(x, y, z) \right\} \quad (9.59)
\end{aligned}$$

The way to calculate the integral of  $\mathcal{J}(x, y, z)$  is shown in Appendix B. One can check that the sum of RC arising from hard, soft and virtual photons does not depend on the auxiliary parameter  $\Delta$ .

## 9.5 CORRECTIONS TO THE DALITZ PLOT AND THE ELECTRON AND PION SPECTRA

Now I have all components of  $\delta(y, z)$ . Fig. [Corrections to the Dalitz Plot and the Electron and Pion Spectra](#) shows the corrections to the Dalitz plot in percents of the unperturbed Dalitz density <sup>2</sup>. Qualitatively our Dalitz plot corrections picture agrees with those by Ginsberg and Becherrawy.

Let  $\phi(z)$  and  $f(y)$  be the pion and electron spectra in the Born approximation correspondingly. They are given by

$$\phi(z) = \frac{1}{\mathcal{C}} \frac{d\Gamma_0}{dz} = \left(1 + \frac{\lambda_+}{r_\pi} R(z)\right)^2 \int_{b_-(z)}^{b(z)} dy a_0(y, z) = \left(1 + \frac{\lambda_+}{r_\pi} R(z)\right)^2 \frac{1}{6} (z^2 - 4r_\pi)^{3/2}, \quad (9.60)$$

and

$$f(y) = \frac{1}{\mathcal{C}} \frac{d\Gamma_0}{dy} = \frac{y^2(1 - r_\pi - y)^2}{2(1 - y)} \left[ 1 + \frac{2}{3} \left(\frac{\lambda_+}{r_\pi}\right) \frac{y(1 - r_\pi - y)}{1 - y} + \frac{1}{6} \left(\frac{\lambda_+}{r_\pi}\right)^2 \frac{y^2(1 - r_\pi - y)^2}{(1 - y)^2} \right], \quad (9.61)$$

where

$$\mathcal{C} = \frac{M^5 G_F^2 |V_{us}|^2}{64\pi^3} |f_+(0)|^2 \quad (9.62)$$

and

$$R(z) = 1 + r_\pi - z \quad (9.63)$$

$R(z)$  comes from the momentum transfer dependence of the form factor; the momentum transfer squared can be written as

$$t = (p - p')^2 = M^2(1 + r_\pi - z) = M^2 R(z). \quad (9.64)$$

---

<sup>2</sup>The numbers on the plot are slightly different from the numbers given in the table in our original paper [27], the corrected numbers were submitted in the erratum.

In the above formulas I dropped terms  $O(r_e) \sim 10^{-6}$ .

The inclusive electron and pion spectra may be written as  $f(y) + (\alpha/\pi)f_1(y)$  and  $\phi(z) + (\alpha/\pi)\phi_1(z)$ ; the corrections to the spectra,  $\phi_1(z)$  and  $f_1(y)$  are obtained by integration of  $\delta(y, z)$ . The explicit formulas are cumbersome and given in Appendix E. Here I present the plots. Figures [Corrections to the Dalitz Plot and the Electron and Pion Spectra](#) and [Corrections to the Dalitz Plot and the Electron and Pion Spectra](#) show unperturbed pion and electron spectra, while figures [Corrections to the Dalitz Plot and the Electron and Pion Spectra](#) and [Corrections to the Dalitz Plot and the Electron and Pion Spectra](#) show the corrections. Units are arbitrary.

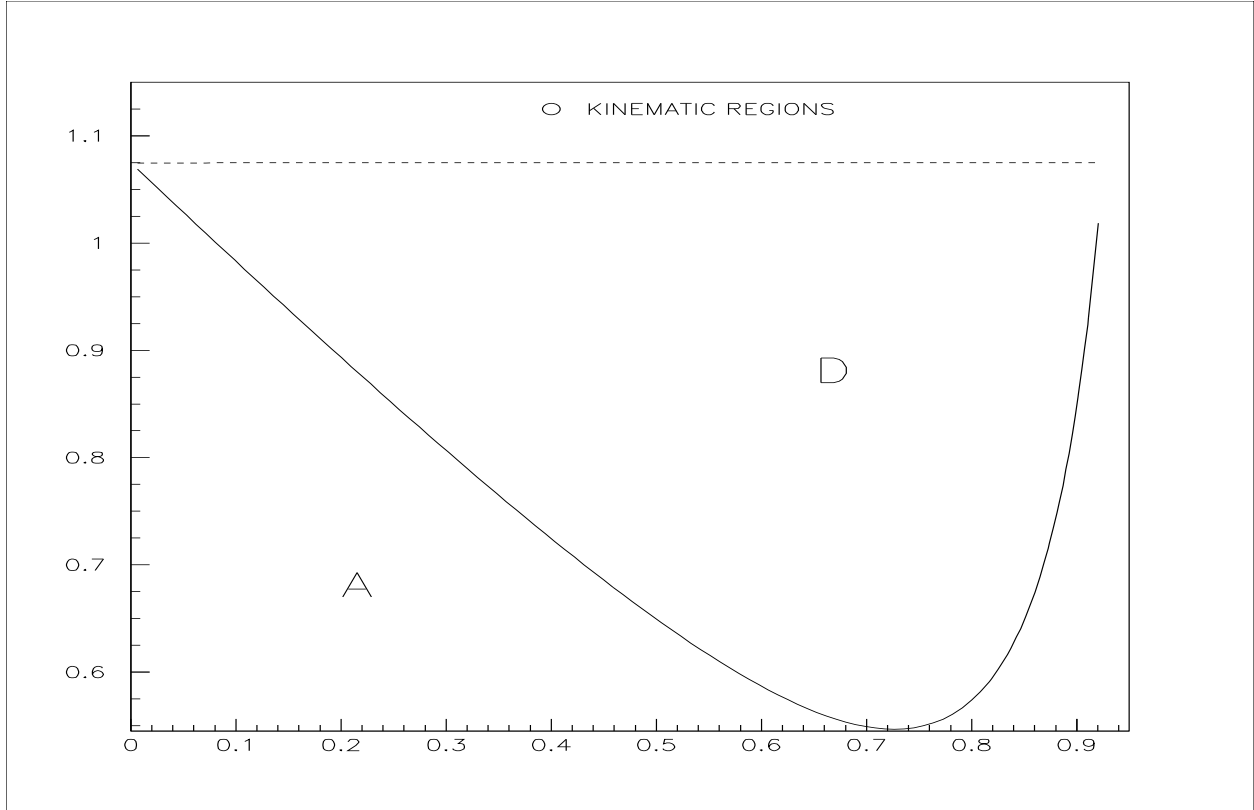


Figure 82:  $D$  – kinematically allowed region for non-radiative decay,  $A$  – region where some of the radiative events can land,  $D+A$  – region allowed for both non-radiative and radiative decays. The boundaries of the  $D$  – region are given by eqs ([Matrix Elements and Kinematics](#)) and ([Matrix Elements and Kinematics](#)).

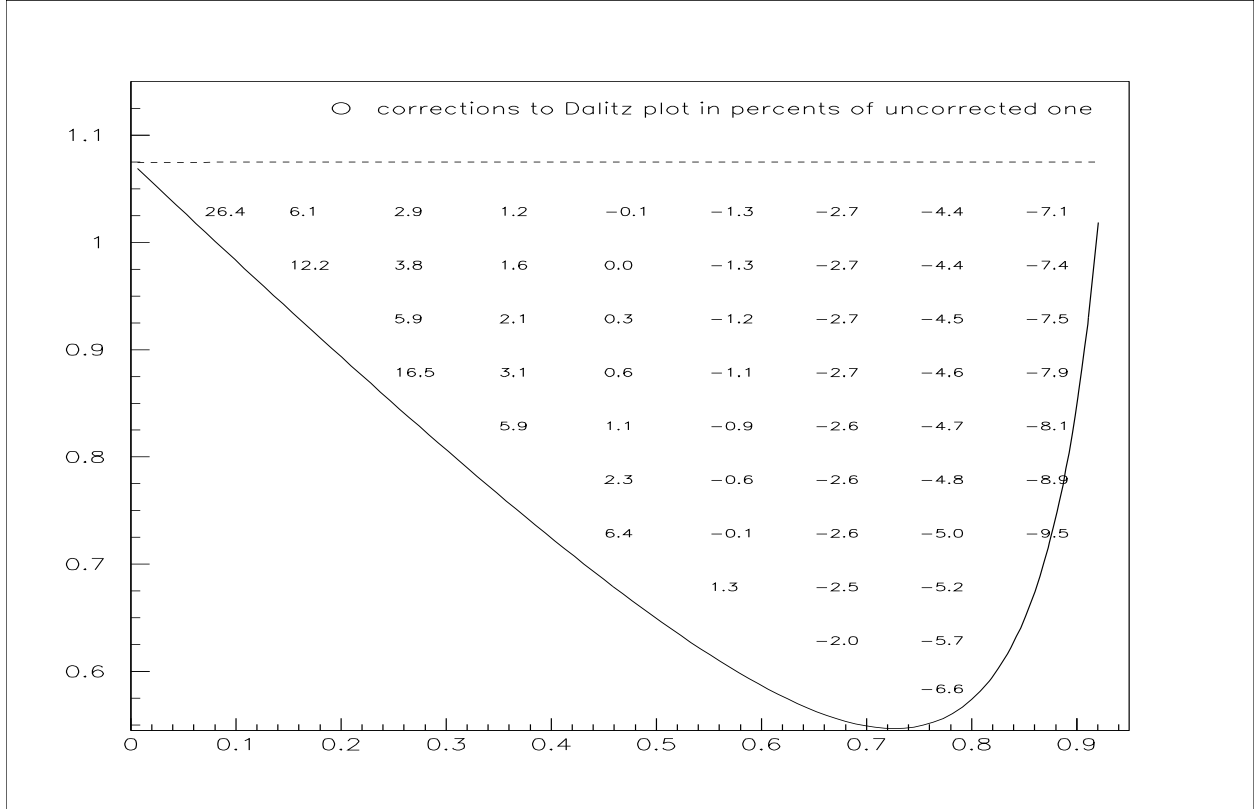


Figure 83: Corrections to the Dalitz plot in percents of unperturbed Dalitz density. The abscissa is the reduced energy of the electron, the ordinate is the reduced energy of the pion, both are defined in eq (Matrix Elements and Kinematics). In terms of the energies in the kaon's rest frame the abscissa covers the interval between 0 and 234.5 MeV with the spacing of 24.7 MeV, the ordinate covers the interval between 134.5 and 265.4 MeV with the spacing of 24.7 MeV. The boundaries of the Dalitz plot are given by eqs (Matrix Elements and Kinematics) and (Matrix Elements and Kinematics).

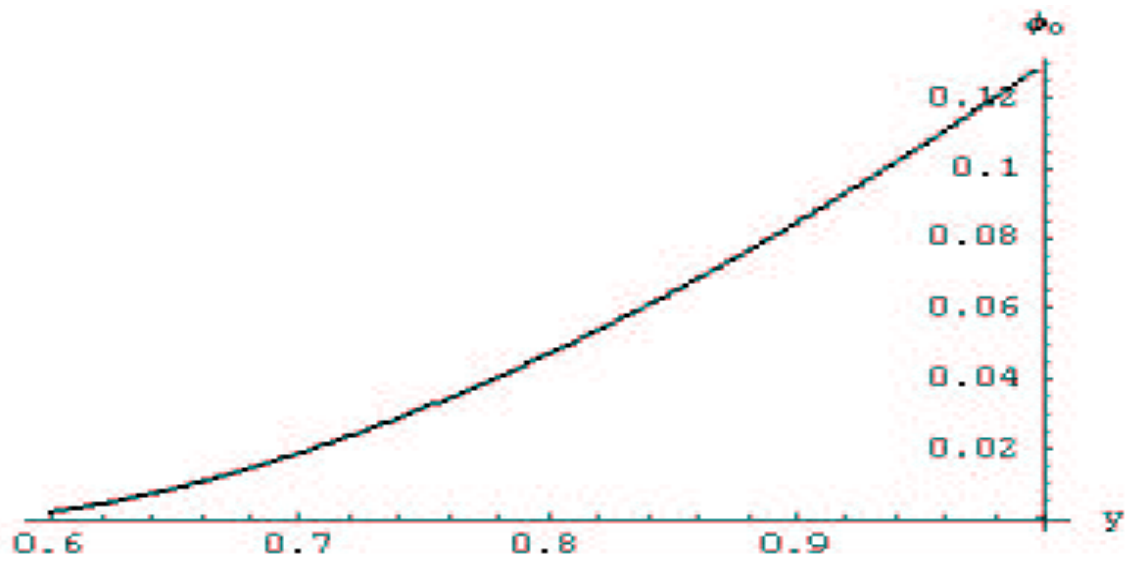


Figure 84: Pion spectrum in Born approximation

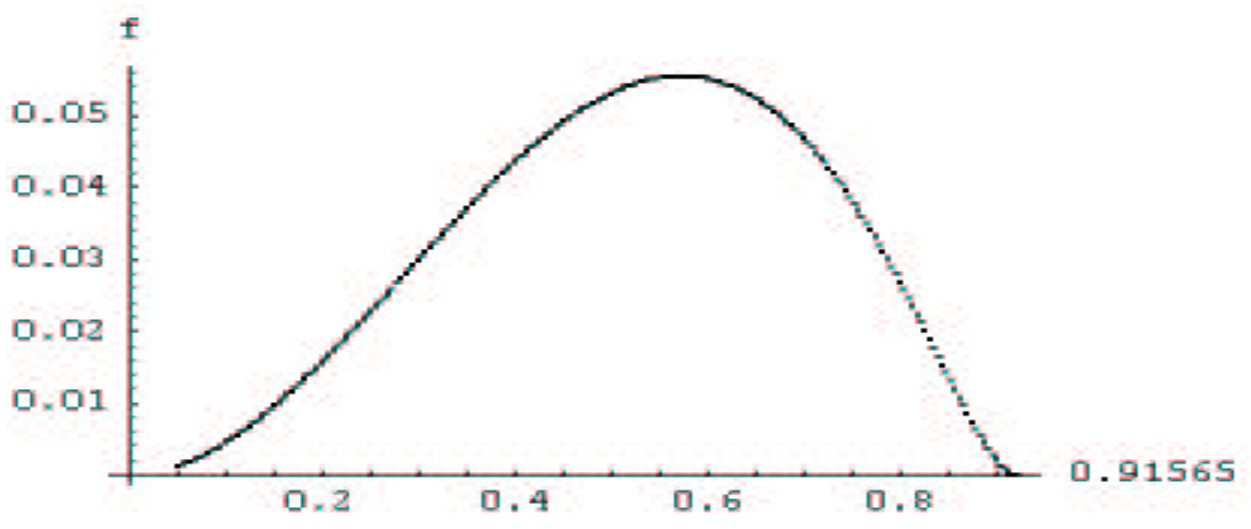


Figure 85: Electron spectrum in Born approximation

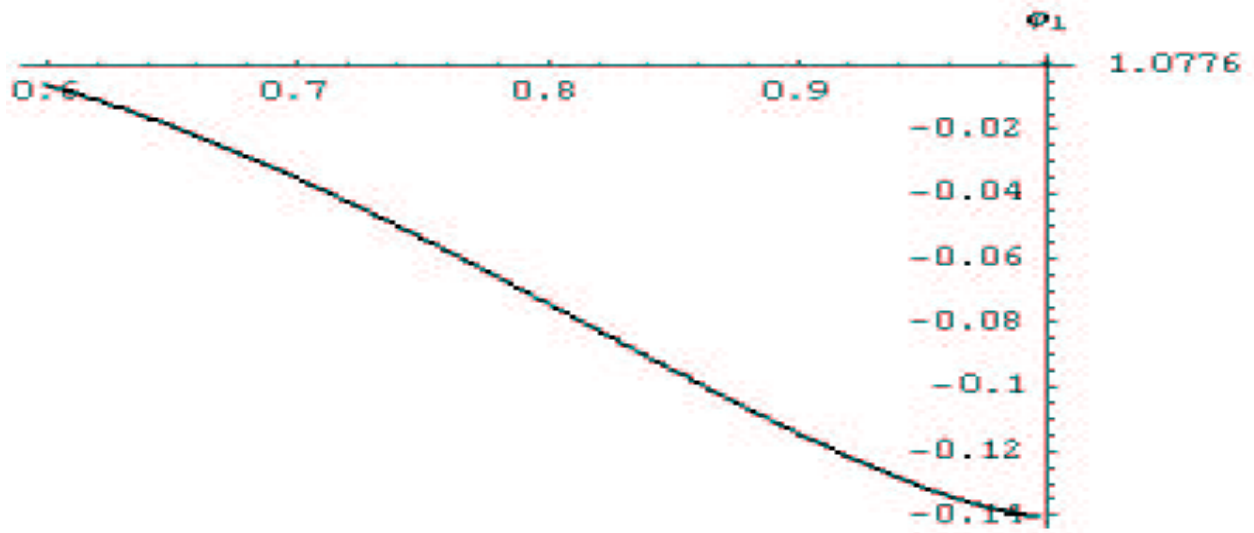


Figure 86: Correction to the pion spectrum

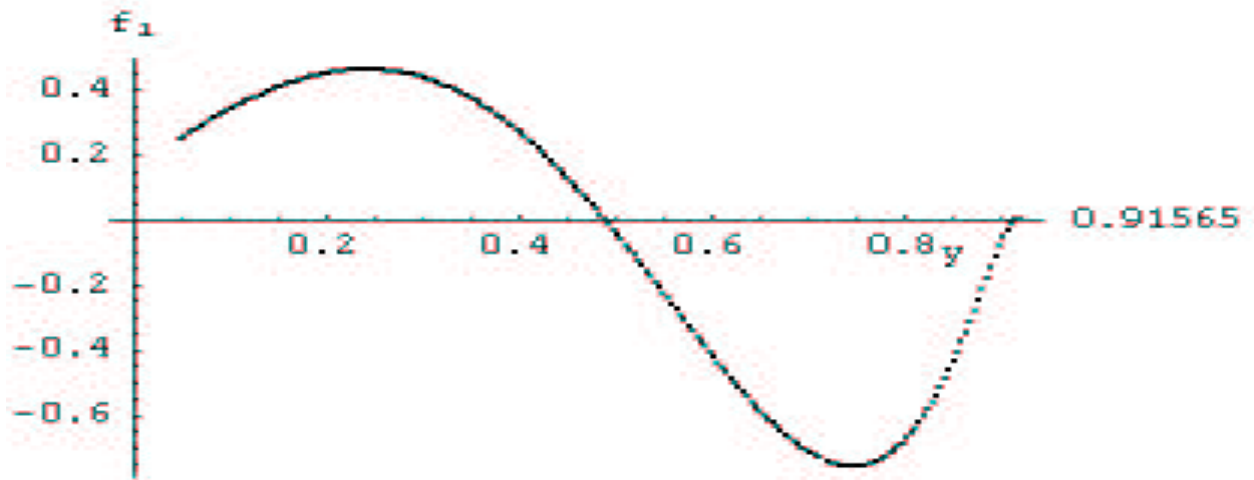


Figure 87: Correction to the electron spectrum

## 9.6 SPECTRAL DISTRIBUTION OF RADIATIVE $K_{E3}$

I present here the general expression for the differential width of the hard photon emission which might be useful for construction of the Monte Carlo simulation of real photon emission in  $K_{e3}$ :

$$d\Gamma_{\gamma}^{hard} = d\Gamma_0 \frac{\alpha}{2\pi} \frac{dx}{x} \frac{dO_{\gamma}}{2\pi a_0(y, z)} T, \quad (9.65)$$

with

$$x = \frac{2\omega}{M} > \frac{2\Delta\epsilon}{M} = y \frac{\Delta\epsilon}{E_e}, \quad \frac{\Delta\epsilon}{E_e} \ll 1; \quad (9.66)$$

and  $dO_{\gamma}$  is an element of the photon's solid angle. The quantity  $T$  was explained above.

For the soft photon emission I have

$$d\Gamma_{\gamma}^{soft} = d\Gamma_0 \frac{\alpha}{2\pi} \frac{dx}{x} \frac{dO_{\gamma}}{2\pi} \left[ -1 - \frac{r_e}{(1 - \beta_e C_e)^2} + \frac{y}{1 - \beta_e C_e} \right], \quad x < y \frac{\Delta\epsilon}{E_e}. \quad (9.67)$$

Integrating over angles within the phase space of the hard photon I obtain the spectral distribution of the radiative kaon decay:

$$\frac{d\Gamma}{d\Gamma_0 dx} = \frac{\alpha}{2\pi} \frac{1}{a_0(y, z)} \left[ \frac{a_0(x+y, z)}{x(x+y)^2} ((y^2 + (x+y)^2)(L_e - 1) + x^2) - \frac{2}{x} a_0(y, z) - 2 \left( \frac{R(z)}{x+y} - y \right) + \mathcal{J}(x, y, z) \right], \quad (9.68)$$

with

$$y\Delta < x < b(z) - y \quad \text{and} \quad \Delta = \frac{\Delta\epsilon}{E_e} \ll 1. \quad (9.69)$$

## 9.7 DISCUSSION OF THE RESULTS

I used the following assumptions:

- Structure-dependent contribution to the emission of virtual photons (see Fig. 1 d), e)) can be interpreted as a correction to the strong form-factor of the  $K\pi$  transition,  $f_+(t)$ . I assume that this form factor can be extracted from experiment and thus do not consider it;
- As in the paper [5] I assume a phenomenological form for the hadronic contribution to the  $K - \pi$  vertex, but here I use explicitly the dependence of the form factor in the form of eq (Matrix Elements and Kinematics).

Comparing with the previous calculations [6, 5] I made the following improvements:

- I use the short distance enhancement factor  $S_{EW}$  which comes from short distance renormalization of 4-Fermi operator and encodes the photon virtualities from  $M_\rho$  to the electroweak scale  $M_Z$ ;
- I describe the dependence on the lepton mass logarithm  $L_e$  in all orders of the perturbation theory and explain why the correction to the total width does not depend on  $m_e$ ;
- I treat the strong interaction effects by the means of ChPT in its lowest order  $O(P^2)$  and show that the next order contribution is small;
- I give an explicit formula for the total differential cross section and explicit results for corrections to the Dalitz plot and the particle spectra that may be used in experimental analysis.

The result for the correction to the total width is

$$\frac{\Gamma}{\Gamma_0} = 1 + \delta = 1.02 \quad (9.70)$$

i.e. 2.0%, while Ginsberg's result is 0.45% and Becherrawy's is 2%. Neither Ginsberg nor Becherrawy used the factor  $S_{EW} = 1.0232$ , and this factor accounts for most of the difference between Ginsberg's and our results. Electromagnetic corrections become negative and have

the order of  $10^{-3}$ . The effect of the SD part, which E.Ginsberg did not consider is small, of the order of 0.1%.

The accuracy of these formulas is determined by the following (the percentages are taken with respect to the Born approximation):

1. I don't account for higher order terms in PT, the ones of the order of  $(\alpha L_e/\pi)^n, n \geq 2$  which is smaller than 0.03%;
2. structure-dependent real hard photon emission contribution to RC I estimate to be at the level of 0.0005;
3. higher order ChPT contributions to the structure dependent part are of the order 0.05% [28, 32];
4. the accuracy of the correction to the total width is dominated by the accuracies of  $S_\rho$  (sum of all contributions to  $\delta$  can be rearranged in such a way that  $S_\rho$  is factorized) and of the short distance enhancement factor  $S_{EW}$  which with the help of renormalization group is calculated to be

$$S_{EW}(m_\rho, m_Z) = \left(\frac{\alpha(m_c)}{\alpha(m_\rho)}\right)^{3/4} \left(\frac{\alpha(m_\tau)}{\alpha(m_c)}\right)^{9/16} \left(\frac{\alpha(m_b)}{\alpha(m_\tau)}\right)^{9/19} \left(\frac{\alpha(m_W)}{\alpha(m_b)}\right)^{9/20} \left(\frac{\alpha(m_Z)}{\alpha(m_W)}\right)^{36/17} \approx 1 + 2 \left(\frac{\alpha}{\pi}\right) \ln\left(\frac{m_Z}{m_\rho}\right) . \quad (9.71)$$

In both cases  $M_\rho$  is chosen somewhat arbitrarily; in the case of  $S_{EW}$  it represents a typical hadronic mass scale used as a demarcation between the short- and long-distance loop corrections. To check the uncertainty in  $S_{EW}$  I estimated  $\alpha(300MeV)$  and  $\alpha(1000MeV)$  and calculated the ratio

$$\frac{S_{EW}(300MeV, m_Z)}{S_{EW}(1000MeV, m_Z)} = 0.999 . \quad (9.72)$$

Thus I may conclude that the short distance enhancement factor is known with precision of 0.1%. The uncertainty in  $S_\rho$  can be estimated by plugging  $2M_\rho$  instead of  $M_\rho$  into  $S_\rho$ , eq (Virtual and Soft Real Photon Emission). It turns out that

$$\frac{S_\rho}{S_{2\rho}} = 0.998 , \quad (9.73)$$

so the factor  $S_\rho$  introduces uncertainty at the level of 0.2%. Therefore, the correction to the total width is

$$\delta = (2.0 \pm 0.3)\% . \quad (9.74)$$

## 9.8 APPENDIX A

Here I explain how to calculate the terms  $\delta_S$ ,  $\delta_C$ , and  $\delta_{PLM}$ .

Contribution from emission of a soft real photon can be written in a standard form in terms of the classical currents:

$$\delta_S = -\frac{4\pi\alpha}{(2\pi)^3} \int \frac{d^3q}{2\omega} \left( \frac{p}{p \cdot q} - \frac{p_e}{p_e \cdot q} \right)^2 \Big|_{\omega=\sqrt{q^2+\lambda^2}<\Delta\epsilon} , \quad (9.75)$$

where  $\lambda$  is the fictitious mass of photon. I use the following formulas:

$$\frac{1}{2\pi} \int \frac{d^3q}{2\omega} \left( \frac{p}{p \cdot q} \right)^2 = \ln \left( \frac{2\Delta\epsilon}{\lambda} \right) - 1 ; \quad (9.76)$$

$$\frac{1}{2\pi} \int \frac{d^3q}{2\omega} \left( \frac{p_e}{p_e \cdot q} \right)^2 = \ln \left( \frac{2\Delta\epsilon}{\lambda} \right) - \frac{1}{2}L_e ; \quad (9.77)$$

$$\frac{1}{2\pi} \int \frac{d^3q}{2\omega} \frac{2(p \cdot p_e)}{(p \cdot q)(p_e \cdot q)} = L_e \ln \left( \frac{2\Delta\epsilon}{\lambda} \right) - \frac{\pi^2}{6} - \frac{1}{4}L_e^2 . \quad (9.78)$$

From them I obtain eq ([Virtual and Soft Real Photon Emission](#)).

Consider now the radiative corrections that arise from emission of virtual photons (excluding SD virtual photons).

Feynman graphs containing self-energy insertion to the electron and kaon Green functions (Fig. 1,b,c) can be taken into account by introducing the wave function renormalization constants  $Z_e$  and  $Z_K$ :  $M_0 \rightarrow M_0(Z_K Z_e)^{1/2}$ . I use the expression for  $Z_e$  given in the textbooks [34]; the expression for  $Z_K$  is given in the paper [35]. The result is eq ([Virtual and Soft Real Photon Emission](#)).

Now consider the Feynman graph in which a virtual photon is emitted by the kaon and absorbed by an electron or by a  $W$ -boson in the intermediate state (Fig. 1,d,e,f). This long

distance contribution is calculated using a phenomenological model with point-like mesons serving as the relevant degrees of freedom. To calculate the contribution from the region  $|k|^2 < \Lambda^2$  ( $\Lambda$  is the ultra violet cutoff) I use the following expressions for loop momenta scalar, vector, and tensor integrals:

$$Re \int \frac{d^4 k}{i\pi^2} \frac{1, k^\mu, k^2}{(k^2 - \lambda^2)((k-p)^2 - M^2)((k-p_e)^2 - m_e^2)} = I, I^\mu, J. \quad (9.79)$$

A standard calculation yields:

$$I = \frac{-1}{yM^2} \left\{ \frac{1}{2} \ln \frac{M^2}{\lambda^2} L_e + \ln^2 y + Li_2(1-y) - \frac{1}{4} \ln^2 r_e \right\}; \quad (9.80)$$

$$I^\mu = \frac{-1}{yM^2} \left\{ \frac{-y \ln y}{1-y} p^\mu + p_e^\mu \left( \frac{y \ln y}{1-y} + L_e \right) \right\}; \quad (9.81)$$

$$J = L_\Lambda + \frac{y \ln y}{1-y} + 1. \quad (9.82)$$

where  $L_\Lambda = \ln(\Lambda^2/M^2)$  and I omitted terms of the order of  $O(m_e^2/M^2)$ . As a result I obtain

$$\int \frac{d^4 k}{i\pi^2} \frac{(1/4) S p p_\nu (p+p') (-\hat{p}_e + \hat{k})(2\hat{p} - \hat{k}) p_e (p+p')}{(k^2 - \lambda^2)((k-p)^2 - M^2)((k-p_e)^2 - m_e^2)} = 2M^4 a_0(y, z) \times \left\{ -L_\Lambda - \frac{1}{2} \ln^2 r_e - 2L_e + \ln \frac{M^2}{\lambda^2} L_e - 1 + 2 \ln^2 y + 2 \ln y + 2Li_2(1-y) \right\}. \quad (9.83)$$

## 9.9 APPENDIX B

To perform the integration over the phase volume of final states it is convenient to use the following parameterization (see Appendix F):

$$d\phi_4 = \frac{d^3p' d^3p_e d^3p_\nu d^3q}{2\epsilon' 2E_e 2\epsilon_\nu 2\omega} \delta^4(p - p' - p_e - p_\nu - q) = \beta_\pi \frac{\pi^2}{16} M^4 dy dz x dx \frac{dC_e dC_\pi}{\sqrt{D}}, \quad (9.84)$$

with

$$D = \beta_\pi^2 (1 - C^2 - C_\pi^2 - C_e^2 + 2CC_\pi C_e), \quad \beta_\pi = \sqrt{1 - \frac{4r_\pi}{z^2}}, \quad (9.85)$$

$$C = \cos(\vec{p}_e, \vec{p}'), \quad C_e = \cos(\vec{q}, \vec{p}_e), \quad C_\pi = \cos(\vec{q}, \vec{p}').$$

The neutrino on-mass shell (NMS) condition provides the relation

$$1 - \beta_\pi C = \frac{2}{yz} \left[ x + y + z - 1 - r_\pi - \frac{xz}{2} (1 - \beta_\pi C_\pi) - \frac{xy}{2} (1 - C_e) \right]. \quad (9.86)$$

For the aim of further integration of  $\mathcal{P}$  over angular variables I put it in the form:

$$\mathcal{P} = xP_1 \frac{\tilde{A}_\nu}{A_e} + xP_2 + P_3 A_e + P_4 A_\nu + P_5 A_\nu A_e, \quad (9.87)$$

$$A_e = \frac{xy}{2} (1 - C_e), \quad (9.88)$$

$$A_\nu = x - A_e - \frac{xz}{2} (1 - \beta_\pi C_\pi). \quad (9.89)$$

and

$$P_1 = \frac{y}{2} (1 - x - y); \quad (9.90)$$

$$P_2 = \frac{R(z)}{x+y} + \frac{1}{2} (z(2x+3y+1) + 2x^2 + 4xy + 3y^2 - 2x - 3y - 2); \quad (9.91)$$

$$P_3 = 1 - z - y - \frac{1}{2} x(x+y+z); \quad (9.92)$$

$$P_4 = -1 + x + y + \frac{1}{2} xy; \quad (9.93)$$

$$P_5 = -1 . \quad (9.94)$$

The angular integration can be performed explicitly:

$$\int \frac{\beta_\pi dC_\pi}{\pi\sqrt{D}} = \frac{y}{\sqrt{A}} , \int \frac{\beta_\pi C_\pi dC_\pi}{\pi\sqrt{D}} = \frac{y(x+y-yt)}{z\beta_\pi A^{3/2}} [2R(z) - (x+y)(2-z) + xyt] , \quad (9.95)$$

with

$$A = (x+y)^2 - 2xyt, \quad t = 1 - C_e . \quad (9.96)$$

Performing the integration over  $C_\pi$  I have:

$$\begin{aligned} \frac{1}{x} \int \frac{dC_\pi \beta_\pi}{\pi\sqrt{D}} \mathcal{P} = & \frac{2y}{A^{3/2}} \left( (y-x) \left( 1 - \frac{z}{2} - \frac{R}{x+y} \right) - \frac{1}{2} y(x+y-xt) \right) P_1 + \\ & \frac{y}{A^{1/2}} \left( P_2 + \frac{y}{2} t P_3 \right) + \left( P_4 + \frac{xy}{2} t P_5 \right) \times \\ & \left\{ \frac{y}{A^{1/2}} \left( 1 - \frac{z}{2} - \frac{y}{2} t \right) + \frac{y}{A^{3/2}} (x+y-yt) \left( R - (x+y) \left( 1 - \frac{z}{2} \right) + \frac{xy}{2} t \right) \right\} . \quad (9.97) \end{aligned}$$

The following integrals are helpful in integrating the above expression. I define

$$I_n^m = \int_0^2 \frac{dt t^m}{\sqrt{A}^n}, \quad m = 0, 1, 2, 3; \quad n = 1, 3. \quad (9.98)$$

Then

$$\begin{aligned} I_1^0 &= \frac{4}{\sigma}, \quad I_1^1 = \frac{8(x+y+\sigma)}{3\sigma^2}, \\ I_1^2 &= \frac{16}{15\sigma^3} (3\sigma^2 + 3(x+y)\rho + 5(x+y)^2), \\ I_3^0 &= \frac{4}{\rho\sigma(x+y)}, \quad I_3^1 = \frac{8}{\rho\sigma^2}, \\ I_3^2 &= \frac{16}{3\rho\sigma^3} (2(x+y) + \sigma), \\ I_3^3 &= \frac{32}{5\rho\sigma^4} (\sigma^2 + 2(x+y)\rho + 4(x+y)^2), \quad (9.99) \end{aligned}$$

where  $\rho = |x-y|$  and  $\sigma = x+y+\rho$ .

The first term in  $d\Gamma^{\text{hard}}$  together with the leading contributions from virtual and soft real photons was given in the form required by RG approach eq([Hard Photon Emission. Structure Functions Approach](#)).

The non-leading contributions,  $\delta^{hard}$  from hard photon emission includes SD emission, IB of point-like mesons as well as the interference terms. It is free from the infrared and mass singularities and is given by

$$\delta^{hard} = \frac{\alpha}{2\pi a_0(y, z)} Z_2(y, z) , \quad (9.100)$$

where

$$Z_2(y, z) = -2Rphot_{1D}(y, z) + Rphot_{2D}(y, z) + \int_0^{b(z)-y} dx \mathcal{J}(x, y, z) , \quad (9.101)$$

$$Rphot_{1D} = \int_0^{b(z)-y} dx \left( \frac{R(z)}{x+y} - y \right) = R(z) \ln \frac{b(z)}{y} - y(b(z) - y) , \quad (9.102)$$

$$Rphot_{2D}(y, z) = \int_0^{b(z)-y} dx \frac{x a_0(y+x, z)}{(y+x)^2} = - (R(z) + y(2-z)) \ln \frac{b(z)}{y} + \frac{1}{2} (b(z) - y) \left( 2 \frac{R(z)}{b(z)} + 4 - 2z - b(z) + y \right) , \quad (9.103)$$

and

$$\mathcal{J}(x, y, z) = P_1 R_1 + P_2 y I_1^0 + P_3 \frac{y^2}{2} I_1^1 + \frac{y}{2} P_4 R_4 + \frac{xy^2}{4} P_5 R_5 , \quad (9.104)$$

with

$$\begin{aligned} R_1 &= \frac{y}{x+y} (y-x) ((2-z)(x+y) - 2R(z)) I_3^0 - y^2 ((x+y) I_3^0 - x I_3^1) , \\ R_4 &= (2-z) I_1^0 - y I_1^1 + (2R(z) - (x+y)(2-z)) ((x+y) I_3^0 - y I_3^1) + \\ &\quad xy ((x+y) I_3^1 - y I_3^2) , \\ R_5 &= (2-z) I_1^1 - y I_1^2 + (2R(z) - (x+y)(2-z)) ((x+y) I_3^1 - y I_3^2) + \\ &\quad xy ((x+y) I_3^2 - y I_3^3) . \end{aligned}$$

## 9.10 APPENDIX C

The contribution to  $\delta^{hard}$  from SD emission has the form:

$$\delta_{SD}^{hard} = \frac{\alpha}{2\pi a_0(y, z)} \int_0^{\mathcal{N}} dx J^{SD}(x, y, z) , \quad (9.105)$$

where

$$J^{SD}(x, y, z) = Q_1 R_1 + y Q_2 I_1^0 + \frac{y^2}{2} Q_3 I_1^1 + \frac{y}{2} Q_4 R_4 + \frac{xy^2}{4} Q_5 R_5 , \quad (9.106)$$

with  $R_i$  given in Appendix B and

$$\begin{aligned} Q_1 &= -\frac{1}{4} y (x + y) , \\ Q_2 &= \frac{1}{4} [2x(x + 2y + z - 2) + 3y(y + z - 2)] , \\ Q_3 &= -\frac{1}{8} [-8 + (z + y)(4 + 3x) - 2x + 3x^2] , \\ Q_4 &= \frac{1}{8} [4y + 4x + 3xy] , \quad Q_5 = -\frac{3}{4} . \end{aligned} \quad (9.107)$$

The contribution to the total width has the following form:

$$\delta^{SD} = \frac{\alpha}{2\pi} \frac{\int \int dydz (1 + \frac{\lambda_{\pm}}{r_{\pi}} R(z))^2 \int_0^{\mathcal{N}} dx J^{SD}(x, y, z)}{\int \int dydz a_0(y, z) (1 + \frac{\lambda_{\pm}}{r_{\pi}} R(z))^2} . \quad (9.108)$$

Numerical estimation gives:

$$\delta^{SD} = -0.00045. \quad (9.109)$$

## 9.11 APPENDIX D

The function  $\Psi$ , defined as

$$\Psi(y, z) = \int_{b_-(z)}^{b(z)} \frac{dt}{t} a_0(t, z) P^{(1)}\left(\frac{y}{t}\right), \quad (9.110)$$

contains a restriction on the domain of integration, namely  $t$  exceeds  $y$  or equal to it, which is implied by the kernel  $P^{(1)}(y/t)$ . Explicit calculation yields for area  $D$ :

$$\begin{aligned} \Psi_{<}(y, z) = \int_{b_-(z)}^{b(z)} \frac{dt}{t} a_0(t, z) \frac{y^2 + t^2}{t(t-y)} = (R(z) - y(2-z)) \ln \frac{b(z)}{b_-(z)} + \\ 2a_0(y, z) \ln \frac{b(z) - y}{b_-(z) - y} + \frac{1}{2}(b(z)^2 - b_-(z)^2), \end{aligned} \quad (9.111)$$

and for area  $A$ :

$$\begin{aligned} \Psi_{>}(y, z) = \int_y^{b(z)} \frac{dt}{t} a_0(t, z) P^{(1)}\left(\frac{y}{t}\right) = a_0(y, z) \left( 2 \ln \frac{b(z) - y}{y} + \frac{3}{2} \right) - \\ \frac{1}{2}(b(z)^2 - y^2) + (b(z) - y)(2 - y - z + b_-(z)) + (R(z) - y(2 - z)) \ln \frac{b(z)}{y}. \end{aligned} \quad (9.112)$$

One can convince oneself of the validity of the relations:

$$j_0(y) = \int_{2\sqrt{r_\pi}}^{c(y)} dz \Psi_{<}(y, z) + \int_{c(y)}^{1+r_\pi} dz \Psi_{>}(y, z); \quad (9.113)$$

and

$$\int_0^{b_-(z)} dy \Psi_{<}(y, z) + \int_{b_-(z)}^{b(z)} dy \Psi_{>}(y, z) = 0. \quad (9.114)$$

The last relation demonstrates the KLN cancellation for the pion spectrum obtained by integration of the corrections over  $y$  in the interval  $0 < y < b(z)$ .

The explicit expressions for  $j_1(y)$  and  $j_2(y)$  are:(for  $j_0(y)$  see ([Appendix E](#))).

$$\begin{aligned}
j_1(y) = & \frac{y^3(1-r_\pi-y)^3}{3(1-y)^2} \left( 2 \ln \frac{1-r_\pi-y}{y} + \frac{3}{2} \right) + \\
& \frac{r_\pi^2}{3(1-y)^2} [3(1-y)(1+y^2) + r_\pi(y^3 + 3y - 2)] \ln \frac{1-y}{r_\pi} - \\
& \frac{1-r_\pi-y}{36(1-y)^2} [(1-y)^2 (43y^3 - 15y^2 - 3y - 1 + r_\pi(83y^2 + 26y + 11) + 3r_\pi^3) + \\
& r_\pi^2(31y^3 - 15y^2 - 39y + 47)] , \quad (9.115)
\end{aligned}$$

$$\begin{aligned}
j_2(y) = & \frac{y^4(1-r_\pi-y)^4}{12(1-y)^3} \left( 2 \ln \frac{1-r_\pi-y}{y} + \frac{3}{2} \right) + \\
& \frac{r_\pi^2}{12(1-y)^3} \ln \frac{1-y}{r_\pi} \left[ 6(1+y^2)(1-y)^2 - 4r_\pi(1-y)(2y^3 - y^2 + 4y - 3) + \right. \\
& \left. r_\pi^2(y^4 + 6y^2 - 8y + 3) \right] + \frac{1-r_\pi-y}{720(1-y)^3} \left[ -(1-y)^3(247y^4 - 88y^3 - 28y^2 - 8y - 3) - \right. \\
& r_\pi(1-y)^3(733y^3 + 341y^2 + 129y + 57) - \\
& r_\pi^2(1-y)(707y^4 - 808y^3 + 212y^2 - 408y + 717) \\
& \left. + r_\pi^3(173y^4 - 72y^3 - 492y^2 + 1048y - 477) - 12r_\pi^4(1-y)^3 \right] . \quad (9.116)
\end{aligned}$$

## 9.12 APPENDIX E

Here I present a collection of the relevant formulas.

The Dalitz-plot distribution in the region  $D$ :

$$\begin{aligned}
\frac{1}{\mathcal{C}S_{EW}} \frac{d\Gamma}{dydz} = \\
\left( 1 + \lambda_+ \frac{t}{m_\pi^2} \right)^2 \left( a_0(y, z) + \frac{\alpha}{\pi} \left[ \frac{1}{2}(L_e - 1)\Psi_>(y, z) + a_0(y, z)Z_1 + \frac{1}{2}Z_2 \right] \right) , \quad (9.117)
\end{aligned}$$

where

$$Z_1(y, z) = \frac{3}{4} - \frac{\pi^2}{6} - \frac{3}{2} \ln y - \ln((b(z) - y)/y) - Li_2(1 - y) , \quad (9.118)$$

and

$$Z_2(y, z) = -2Rphot_{1D}(y, z) + Rphot_{2D}(y, z) + \int_0^{\mathcal{N}} dx \mathcal{J}(x, y, z) , \quad (9.119)$$

with

$$Rphot_{1D} = \int_0^{b(z)-y} dx \left( \frac{R(z)}{x+y} - y \right) = R(z) \ln \frac{b(z)}{y} - y(b(z) - y) , \quad (9.120)$$

$$Rphot_{2D}(y, z) = \int_0^{b(z)-y} dx \frac{x a_0(y+x, z)}{(y+x)^2} = -(R(z) + y(2-z)) \ln \frac{b(z)}{y} + \frac{1}{2} (b(z) - y) \left( 2 \frac{R(z)}{b(z)} + 4 - 2z - b(z) + y \right) , \quad (9.121)$$

and

$$\mathcal{J}(x, y, z) = \frac{1}{x} \int \frac{dO_\gamma}{2\pi} \mathcal{P} . \quad (9.122)$$

Correction to the total width (I include the contribution of the region outside of the region  $D$ ),  $\Gamma = \Gamma_0(1 + \delta)$ :

$$1 + \delta = S_{EW} + \frac{\alpha}{\pi} \frac{1}{\int \int dz dy a_0(y, z) \left( 1 + \frac{\lambda_\pm}{r_\pi} R(z) \right)^2} \left[ \int_0^{1-r_\pi} I(y) \ln y dy + \int_{\frac{1+r_\pi}{2\sqrt{r_\pi}}}^{1+r_\pi} dz \left( 1 + \frac{\lambda_\pm}{r_\pi} R(z) \right)^2 \left[ \int_0^{b_-(z)} dy \left[ -a_0(y, z) \ln \frac{b(z) - y}{b_-(z) - y} + (1/2) \tilde{Z}_2(y, z) \right] + \int_{b_-(z)}^{b(z)} dy \left[ a_0(y, z) Z_1 + (1/2) Z_2 \right] \right] , \quad (9.123)$$

with

$$\begin{aligned}
\tilde{Z}_2(y, z) &= Rphot_{2A}(y, z) - 2Rphot_{1A}(y, z) + \int_{b_-(z)-y}^{\mathcal{N}} dx \mathcal{J}(x, y, z); \\
Rphot_{1A}(y, z) &= R(z) \ln \frac{b(z)}{b_-(z)} - y(b(z) - b_-(z)) \\
Rphot_{2A}(y, z) &= \int_{b_-(z)-y}^{b(z)-y} \frac{dxx}{(x+y)^2} a_0(x+y, z) = \\
&= (b(z) - b_-(z)) \left(1 - \frac{z}{2} + 2y\right) - (y(2-z) + R(z)) \ln \frac{b(z)}{b_-(z)}. \quad (9.124)
\end{aligned}$$

The corrected pion spectrum in the inclusive set-up of the experiment when integrating over the whole region for  $y$  ( $0 < y < b(z)$ ) has the form  $\phi_0(z) + (\alpha/\pi)\phi_1(z)$  with

$$\begin{aligned}
\phi_1(z) &= \left(1 + \frac{\lambda_+}{r_\pi} R(z)\right)^2 \left[ \int_0^{b_-(z)} dy [\Psi_<(y, z) \ln y - a_0(y, z) \ln \frac{b(z)-y}{b_-(z)-y} + \right. \\
&\quad \left. \frac{1}{2} \tilde{Z}_2(y, z)] + \int_{b_-(z)}^{b(z)} dy [\Psi_>(y, z) \ln y + a_0(y, z) Z_1(y, z) + \frac{1}{2} Z_2(y, z)] \right], \quad (9.125)
\end{aligned}$$

The inclusive electron spectrum with the correction of the lowest order is  $f(y) + (\alpha/\pi)f_1(y)$  with  $f(y)$  given above and:

$$\begin{aligned}
f_1(y) &= \frac{1}{2} (L_e - 1) I(y) - \int_{c(y)}^{1+r_\pi} a_0(y, z) \left(1 + \frac{\lambda_+}{r_\pi} R(z)\right)^2 \ln((b(z)-y)/y) dz + \\
&\quad \left(\frac{3}{4} - \frac{\pi^2}{6} - \frac{3}{2} \ln y - Li_2(1-y)\right) f(y) + \frac{1}{2} \int_{c(y)}^{1+r_\pi} Z_2(y, z) \left(1 + \frac{\lambda_+}{r_\pi} R(z)\right)^2 dz + \\
&\quad \theta(1 - \sqrt{r_\pi} - y) \int_{2\sqrt{r_\pi}}^{c(y)} dz \left(1 + \frac{\lambda_+}{r_\pi} R(z)\right)^2 \left[\frac{1}{2} \tilde{Z}_2 - a_0(y, z) \ln \frac{b(z)-y}{b_-(z)-y}\right], \quad (9.126)
\end{aligned}$$

with

$$I(y) = j_0(y) + \left(\frac{\lambda_+}{r_\pi}\right) j_1(y) + \left(\frac{\lambda_+}{r_\pi}\right)^2 j_2(y), \quad (9.127)$$

$$\begin{aligned}
j_0(y) = & \int_y^{1-r_\pi} \frac{dt}{t} \int_{c(t)}^{1+r_\pi} dz a_0(t, z) P^{(1)}\left(\frac{y}{t}\right) = \\
& \left(2 \ln \frac{1-r_\pi-y}{y} + \frac{3}{2}\right) f_0(y) + \frac{r_\pi^2(1+y^2)}{2(1-y)} \ln \frac{1-y}{r_\pi} + \\
& \frac{1}{12}(1-r_\pi-y)[1-5r_\pi-2r_\pi^2+y(4-13r_\pi)-17y^2] ; \quad (9.128)
\end{aligned}$$

explicit expressions for  $j_1(y)$  and  $j_2(y)$  are given in Appendix D. As an additional check I made sure that integrals over  $\phi_1(z)$  and  $f_1(y)$  yield the same number:

$$\int_{2\sqrt{r_\pi}}^{1+r_\pi} \phi_1(z) dz = \int_{2\sqrt{r_e}}^{1-r_\pi} f_1(y) dy = -0.037 , \quad (9.129)$$

which when combined with the short-distance factor  $S_{EW}$  and with the factor  $S_\rho$  results in  $\delta = 0.025$ . For the inclusive set-up of the experiment (energy fraction of electron is not measured) I have for the pion energy spectrum given above, eq (Appendix E). When I restrict myself only by the region  $D$ , the spectrum becomes dependent on  $\ln(1/r_e)$ :

$$\begin{aligned}
\frac{1}{\mathcal{C}S_{EW}} \frac{d\Gamma}{dz} = & \left\{ \phi_0(z) + \frac{\alpha}{\pi} \left[ \frac{1}{2} P(z) \left( \ln \frac{1}{r_e} - 1 \right) + \right. \right. \\
& \left. \left. \int_{b_-(z)}^{b(z)} dy \left( \Psi_>(y, z) \ln y + a_0(y, z) Z_1 + \frac{1}{2} Z_2 \right) \right] \right\} \left( 1 + \frac{\lambda_+}{r_\pi} R(z) \right)^2 , \quad (9.130)
\end{aligned}$$

with

$$\begin{aligned}
P(z) = & \frac{1}{6} b_-(z)^2 (3b(z) + b_-(z)) \ln \frac{b(z)}{b_-(z)} + \frac{1}{3} (b(z) - b_-(z))^3 \ln \frac{b(z) - b_-(z)}{b(z)} - \\
& \frac{1}{6} b_-(z) (b(z) - b_-(z)) (3b_-(z) + b(z)). \quad (9.131)
\end{aligned}$$

### 9.13 APPENDIX F

My approach to study the radiative kaon decay has an advantage compared to the one used by E. Ginsberg – it has a simple interpretation of electron mass singularities based on Drell-Yan picture. However, in [5] the approach to study non-collinear kinematics is more transparent than mine. In [5] the following variable was introduced:

$$l = (p_\nu + k)^2/M^2 = A_\nu = (M - E_\pi - E_e)^2/M^2 - (\vec{p}_\pi + \vec{p}_e)^2/M^2 , \quad (9.132)$$

with the limits

$$0 < l < b_-(z)(b(z) - y) , \quad (9.133)$$

for  $y$  and  $z$  in the  $D$  region and

$$b(z)(b_-(z) - y) < l < b_-(z)(b(z) - y) , \quad (9.134)$$

for  $y$  and  $z$  in the  $A$  region, which is given by

$$0 < y < b_-(z), \quad 2\sqrt{r_\pi} < z < 1 + r_\pi . \quad (9.135)$$

In my approach which separates the cases of soft and hard photon emission I must modify the lower bound for  $l$  in the region  $D$ . It can be done using another representation of  $l$ :

$$l = x[1 - (y/2)(1 - C_e) - (z/2)(1 - \beta C_\pi)] , \quad (9.136)$$

where  $C_e$  is the cosine of the angle between 3-momenta of the photon and the electron,  $C_\pi$  is the cosine of the angle between 3-momenta of the photon and the pion, and  $\beta = \sqrt{1 - m^2/E_\pi^2}$  is the pion's velocity. Maximum of this quantity is  $b(z)$ . Taking this into account I obtain for the hard photon domain

$$x > 2\Delta\varepsilon/M = y\Delta, \quad \Delta = \Delta\varepsilon/E_e \ll 1 ; \quad (9.137)$$

for region  $D$ :

$$y\Delta < x < b(z) - y, \quad yb(z)\Delta < l < b_-(z)(b(z) - y) ; \quad (9.138)$$

and for region A:

$$b_-(z) - y < x < b(z) - y, \quad b(z)(b_-(z) - y) < l < b_-(z)(b(z) - y) . \quad (9.139)$$

In particular for the collinear case I must choose  $C_e = 1$  and  $C_\pi = -1$  which corresponds to  $x + y < b(z)$ . Same result can be derived from the neutrino mass shell condition:

$$(P_k - p_e - p_\pi - k)^2/M^2 = R(z) - x - y + (xy/2)(1 - C_e) + \\ (xz/2)(1 - \beta C_\pi) + (yz/2)(1 - \beta C_{e\pi}) = 0 . \quad (9.140)$$

In the collinear case I have  $C_e = 1$  and  $C_\pi = C_{e\pi}$ . From the same condition

$$1 - \beta C_\pi = (2/z(x + y))(x + y - R(z)) . \quad (9.141)$$

Then  $l_{coll} = R(z)x/(x + y)$ . Using further the relation  $R(z) = b(z)b_-(z)$  I obtain again  $x < b(z) - y$  in the case of collinear photon.

Comparing the phase volume calculated in my approach that uses neutrino mass shell condition with the phase space from [5] I obtain the relation:

$$\int x dx \int \frac{dO_\gamma}{4\pi} = \int dl \int d\gamma, \quad \int d\gamma = \int \frac{d^3 p_\nu}{E_\nu} \frac{d^3 k}{k_0} \frac{\delta^4(P - p_\nu - k)}{2\pi} . \quad (9.142)$$

The non-leading contribution arises from the hard photon emission considered above:

$$I_{IB} = \int \frac{dx}{x} \int \frac{dO_\gamma}{4\pi} \mathcal{P}_{IB} , \quad (9.143)$$

with

$$\mathcal{P}_{IB} = xG_1 \frac{\tilde{A}_\nu}{A_e} + xG_2 + G_3 A_e + G_4 A_\nu + G_5 A_e A_\nu , \quad (9.144)$$

where

$$G_1 = \frac{y}{4}(2 - y - x) ,$$

$$G_2 = \frac{R(z)}{2(x + y)} + \frac{x^2}{2} + \frac{1}{2}x(z + 2y) + \frac{1}{4}(2z + 3y(y + z)) - 1 ,$$

$$G_3 = -\frac{1}{8}x^2 - \frac{1}{8}x(2 + z + y) - \frac{1}{2}(y + z) ,$$

$$G_4 = \frac{1}{8}x(4+y) + \frac{1}{8}y - 1, \quad G_5 = -\frac{1}{4}, \quad (9.145)$$

(note that  $G_i + Q_i = P_i$ , see appendices B and C). Then

$$I_{IB} = \frac{1}{4} \int dl \left[ 4 - 2y - 4z - \frac{1}{4}R(z) + \frac{1}{4}l + y \ln \frac{(R(z) - l)^2}{l} - \right. \\ \left. 2 \ln \frac{y^2 R(z)^2}{l(l + y(2 - z))} + \left( z + \frac{3}{2}y(y + z) - 2 + \frac{1}{4}l(4 + y) \right) I_{10} - \right. \\ \left. (1/2)I_{1-1} - ((1/2)l + y + z)I_{2-1} + I_z \right]. \quad (9.146)$$

Here I use the list of integrals obtained in the paper of [5]:

$$I_{mn} = \int d\gamma \frac{1}{(kP_K/M^2)^m (kp_e/M^2)^n}; \quad (9.147) \\ I_{10} = \frac{2}{s} \ln \frac{2 - y - z + s}{2 - y - z - s}; \quad I_{20} = 4/l; \quad I_{00} = 1; \\ I_{-1,0} = (2 - y - z)/2; \quad I_{11} = \frac{4}{yl} \ln \frac{y^2}{l}; \\ I_{01} = \frac{2}{R(z) - l} \ln \frac{(R(z) - l)^2}{lr_e}; \\ I_{1-1} = \frac{R(z)(2 - y - z) - (2 + y - z)l}{s^2} + \\ \frac{2l(y(2 - y - z) - 2R(z) + 2l)}{s^3} \ln \frac{2 - y - z + s}{2 - y - z - s}; \\ I_{2-1} = \frac{2(y(2 - y - z) + 2l - 2R(z))}{s^2} + \\ \frac{R(z)(2 - y - z) - (2 + y - z)l}{s^3} \ln \frac{2 - y - z + s}{2 - y - z - s}, \\ s = \sqrt{(2 - y - z)^2 - 4l}.$$

Besides I need two additional ones:

$$I_e = \int d\gamma \frac{1}{(kp_e/M^2)(2(kP_K/M^2) + y)} = \frac{2}{yR(z)} \ln \frac{y^2 R(z)^2}{l(l + y(2 - z))r_e}; \quad (9.148) \\ I_z = \int d\gamma \frac{1}{(kP_K/M^2)(2(kP_K/M^2) + y)} = \frac{4}{ys} \ln \frac{2l + ys + y(2 - y - z)}{2l + ys - y(2 - y - z)}.$$

One can see the cancellation of mass singularities (terms containing  $\ln(1/r_e)$ ) in the expression for  $I_{IB}$ .

## 9.14 APPENDIX G. LISTS OF THE RUNS

In this Appendix I put the detailed information about the 1998 runs during which the data used for the described measurements was collected.

Table 28: List of the runs at 509.0 MeV. Total number of events is 44419244, the collected luminosity is 1618.918  $nb^{-1}$

| run  | date        | beam energy | events | luminosity integral |
|------|-------------|-------------|--------|---------------------|
| 7385 | 12-Dec-1997 | 508.986     | 318750 | 10.457              |
| 7386 | 12-Dec-1997 | 508.986     | 262118 | 7.835               |
| 7387 | 12-Dec-1997 | 508.986     | 401001 | 12.202              |
| 7388 | 12-Dec-1997 | 508.986     | 403690 | 12.635              |
| 7389 | 12-Dec-1997 | 508.986     | 403173 | 12.913              |
| 7390 | 13-Dec-1997 | 508.986     | 403756 | 12.391              |
| 7391 | 13-Dec-1997 | 508.986     | 61078  | 2.005               |
| 7392 | 13-Dec-1997 | 508.986     | 401750 | 12.726              |
| 7393 | 13-Dec-1997 | 508.986     | 312500 | 9.603               |
| 7394 | 13-Dec-1997 | 508.986     | 402611 | 12.435              |
| 7395 | 13-Dec-1997 | 508.986     | 405401 | 12.539              |
| 7396 | 13-Dec-1997 | 508.986     | 329000 | 9.748               |
| 7397 | 13-Dec-1997 | 508.986     | 402548 | 13.093              |
| 7398 | 13-Dec-1997 | 508.986     | 360250 | 9.812               |
| 7399 | 13-Dec-1997 | 508.986     | 348294 | 8.560               |
| 7400 | 14-Dec-1997 | 508.813     | 339000 | 9.263               |
| 7401 | 14-Dec-1997 | 509.074     | 315810 | 8.095               |
| 7402 | 14-Dec-1997 | 509.074     | 367644 | 8.876               |
| 7403 | 14-Dec-1997 | 509.074     | 117304 | 3.056               |

continued on the next page

| run                        | date        | beam energy | events | luminosity integral |
|----------------------------|-------------|-------------|--------|---------------------|
| 7404                       | 14-Dec-1997 | 509.074     | 240750 | 6.640               |
| 7405                       | 14-Dec-1997 | 508.889     | 147500 | 3.502               |
| 7406                       | 14-Dec-1997 | 508.889     | 301375 | 7.690               |
| 7407                       | 14-Dec-1997 | 508.889     | 302181 | 8.675               |
| 7408                       | 14-Dec-1997 | 508.889     | 308914 | 8.187               |
| 7409                       | 14-Dec-1997 | 508.889     | 305793 | 8.078               |
| 7410                       | 14-Dec-1997 | 508.889     | 120500 | 3.230               |
| 7411                       | 14-Dec-1997 | 508.889     | 402753 | 10.733              |
| 7412                       | 15-Dec-1997 | 508.889     | 405332 | 10.330              |
| 7413                       | 15-Dec-1997 | 509.004     | 592307 | 15.380              |
| 7414                       | 15-Dec-1997 | 509.004     | 873    | 0.019               |
| 7415                       | 15-Dec-1997 | 509.004     | 402405 | 12.201              |
| 7416                       | 15-Dec-1997 | 509.004     | 87734  | 2.779               |
| 7417                       | 15-Dec-1997 | 509.004     | 22524  | 0.688               |
| 7418                       | 15-Dec-1997 | 509.004     | 62500  | 1.682               |
| 7419                       | 15-Dec-1997 | 509.004     | 0      | 0.001               |
| 7420                       | 15-Dec-1997 | 509.004     | 0      | 0.000               |
| 7421                       | 15-Dec-1997 | 508.852     | 0      | 0.272               |
| 7422                       | 15-Dec-1997 | 508.852     | 401764 | 10.836              |
| 7423                       | 15-Dec-1997 | 508.852     | 401290 | 12.491              |
| 7424                       | 16-Dec-1997 | 508.852     | 402105 | 11.515              |
| 7425                       | 16-Dec-1997 | 508.852     | 405343 | 12.438              |
| 7426                       | 16-Dec-1997 | 508.852     | 282500 | 7.384               |
| 7427                       | 16-Dec-1997 | 508.852     | 140750 | 2.805               |
| 7428                       | 16-Dec-1997 | 508.852     | 346555 | 8.533               |
| 7429                       | 16-Dec-1997 | 508.852     | 391570 | 11.984              |
| 7430                       | 16-Dec-1997 | 508.852     | 402091 | 11.503              |
| continued on the next page |             |             |        |                     |

| run                        | date        | beam energy | events | luminosity integral |
|----------------------------|-------------|-------------|--------|---------------------|
| 7431                       | 16-Dec-1997 | 508.852     | 400625 | 11.740              |
| 7432                       | 16-Dec-1997 | 508.852     | 455340 | 13.500              |
| 7433                       | 16-Dec-1997 | 508.852     | 208910 | 6.605               |
| 7434                       | 17-Dec-1997 | 508.852     | 404591 | 12.874              |
| 7435                       | 17-Dec-1997 | 508.852     | 410793 | 13.051              |
| 7436                       | 17-Dec-1997 | 508.852     | 408366 | 13.305              |
| 7437                       | 17-Dec-1997 | 508.852     | 235959 | 7.350               |
| 7438                       | 17-Dec-1997 | 508.852     | 106006 | 3.513               |
| 7439                       | 17-Dec-1997 | 508.852     | 331696 | 10.701              |
| 7440                       | 17-Dec-1997 | 508.852     | 402132 | 13.455              |
| 7441                       | 17-Dec-1997 | 508.852     | 404250 | 12.707              |
| 7442                       | 17-Dec-1997 | 508.852     | 396467 | 12.534              |
| 7443                       | 17-Dec-1997 | 508.852     | 405164 | 12.431              |
| 7444                       | 17-Dec-1997 | 508.852     | 0      | 12.431              |
| 7445                       | 17-Dec-1997 | 508.852     | 403000 | 13.831              |
| 7446                       | 17-Dec-1997 | 508.852     | 368750 | 11.805              |
| 7447                       | 18-Dec-1997 | 508.852     | 43796  | 1.391               |
| 7448                       | 18-Dec-1997 | 508.852     | 401624 | 12.951              |
| 7449                       | 18-Dec-1997 | 508.852     | 394000 | 6.789               |
| 7450                       | 18-Dec-1997 | 508.852     | 396225 | 11.964              |
| 7451                       | 18-Dec-1997 | 508.852     | 60500  | 2.016               |
| 7904                       | 31-Jan-1998 | 509.032     | 330952 | 15.151              |
| 7905                       | 31-Jan-1998 | 509.032     | 354703 | 15.158              |
| 7906                       | 31-Jan-1998 | 509.032     | 386724 | 15.133              |
| 7907                       | 01-Feb-1998 | 509.032     | 382816 | 15.098              |
| 7908                       | 01-Feb-1998 | 509.032     | 378750 | 15.042              |
| 7909                       | 01-Feb-1998 | 509.032     | 400000 | 15.094              |
| continued on the next page |             |             |        |                     |

| run                        | date        | beam energy | events | luminosity integral |
|----------------------------|-------------|-------------|--------|---------------------|
| 7911                       | 01-Feb-1998 | 509.032     | 13352  | 0.379               |
| 7912                       | 01-Feb-1998 | 509.032     | 404127 | 14.862              |
| 7913                       | 01-Feb-1998 | 509.032     | 371587 | 15.160              |
| 7914                       | 01-Feb-1998 | 509.032     | 120750 | 4.959               |
| 7915                       | 01-Feb-1998 | 509.032     | 357007 | 15.130              |
| 7916                       | 01-Feb-1998 | 509.032     | 307500 | 15.114              |
| 7917                       | 01-Feb-1998 | 509.032     | 300250 | 14.449              |
| 7918                       | 01-Feb-1998 | 509.000     | 365762 | 16.326              |
| 7921                       | 02-Feb-1998 | 509.000     | 157328 | 6.896               |
| 7922                       | 02-Feb-1998 | 509.000     | 78844  | 3.417               |
| 7923                       | 02-Feb-1998 | 509.000     | 125250 | 3.549               |
| 7924                       | 02-Feb-1998 | 509.000     | 393005 | 15.757              |
| 7925                       | 02-Feb-1998 | 509.000     | 102250 | 3.859               |
| 7926                       | 02-Feb-1998 | 509.000     | 386125 | 15.187              |
| 7927                       | 02-Feb-1998 | 509.000     | 401325 | 15.103              |
| 7928                       | 03-Feb-1998 | 509.000     | 401908 | 13.939              |
| 7929                       | 03-Feb-1998 | 509.000     | 362500 | 13.452              |
| 7930                       | 03-Feb-1998 | 509.000     | 361396 | 14.513              |
| 7931                       | 03-Feb-1998 | 509.000     | 208500 | 8.303               |
| 7932                       | 03-Feb-1998 | 509.000     | 0      | 0.000               |
| 7933                       | 03-Feb-1998 | 509.001     | 384108 | 15.046              |
| 7934                       | 03-Feb-1998 | 509.001     | 250235 | 8.450               |
| 7935                       | 03-Feb-1998 | 509.001     | 292750 | 12.000              |
| 7936                       | 03-Feb-1998 | 509.001     | 342565 | 15.206              |
| 7937                       | 03-Feb-1998 | 509.001     | 400368 | 14.080              |
| 7938                       | 03-Feb-1998 | 509.001     | 432000 | 14.663              |
| 7939                       | 04-Feb-1998 | 509.001     | 435051 | 15.363              |
| continued on the next page |             |             |        |                     |

| run                        | date        | beam energy | events | luminosity integral |
|----------------------------|-------------|-------------|--------|---------------------|
| 7940                       | 04-Feb-1998 | 509.001     | 631254 | 18.342              |
| 7941                       | 04-Feb-1998 | 509.001     | 473250 | 14.463              |
| 7942                       | 04-Feb-1998 | 509.001     | 254500 | 3.638               |
| 7943                       | 04-Feb-1998 | 509.001     | 500360 | 19.360              |
| 7944                       | 04-Feb-1998 | 509.001     | 499253 | 20.572              |
| 7945                       | 04-Feb-1998 | 509.001     | 190750 | 7.673               |
| 7946                       | 04-Feb-1998 | 509.001     | 76769  | 3.171               |
| 8128                       | 20-Feb-1998 | 509.001     | 253181 | 10.951              |
| 8129                       | 20-Feb-1998 | 509.001     | 391450 | 17.655              |
| 8130                       | 20-Feb-1998 | 509.001     | 316704 | 15.147              |
| 8131                       | 20-Feb-1998 | 509.001     | 314884 | 15.058              |
| 8132                       | 20-Feb-1998 | 509.001     | 307620 | 15.174              |
| 8133                       | 20-Feb-1998 | 509.001     | 313564 | 15.226              |
| 8134                       | 20-Feb-1998 | 509.001     | 250704 | 12.342              |
| 8135                       | 20-Feb-1998 | 509.001     | 118858 | 5.762               |
| 8136                       | 20-Feb-1998 | 509.001     | 305441 | 15.718              |
| 8137                       | 21-Feb-1998 | 509.001     | 309945 | 15.406              |
| 8138                       | 21-Feb-1998 | 509.001     | 173575 | 7.982               |
| 8139                       | 21-Feb-1998 | 509.001     | 301715 | 15.024              |
| 8140                       | 21-Feb-1998 | 509.001     | 279620 | 14.126              |
| 8141                       | 21-Feb-1998 | 509.001     | 307518 | 15.217              |
| 8142                       | 21-Feb-1998 | 509.001     | 225626 | 11.495              |
| 8143                       | 21-Feb-1998 | 509.001     | 0      | 0.000               |
| 8144                       | 21-Feb-1998 | 509.001     | 0      | 0.000               |
| 8145                       | 21-Feb-1998 | 509.001     | 310209 | 15.301              |
| 8146                       | 21-Feb-1998 | 509.001     | 57343  | 2.950               |
| 8147                       | 21-Feb-1998 | 509.001     | 300502 | 15.105              |
| continued on the next page |             |             |        |                     |

| run  | date        | beam energy | events | luminosity integral |
|------|-------------|-------------|--------|---------------------|
| 8148 | 21-Feb-1998 | 509.001     | 330046 | 15.180              |
| 8149 | 21-Feb-1998 | 509.001     | 278630 | 12.837              |
| 8150 | 21-Feb-1998 | 509.001     | 368041 | 17.085              |
| 8151 | 21-Feb-1998 | 509.001     | 403890 | 18.169              |
| 8152 | 22-Feb-1998 | 509.001     | 369753 | 16.786              |
| 8153 | 22-Feb-1998 | 509.001     | 473610 | 20.381              |
| 8154 | 22-Feb-1998 | 509.001     | 413952 | 19.023              |
| 8155 | 22-Feb-1998 | 509.001     | 269250 | 12.939              |
| 8156 | 22-Feb-1998 | 509.001     | 375043 | 14.556              |
| 8157 | 22-Feb-1998 | 509.001     | 402063 | 17.921              |
| 8158 | 22-Feb-1998 | 509.001     | 375423 | 15.704              |
| 8159 | 22-Feb-1998 | 509.001     | 350792 | 15.171              |
| 8160 | 22-Feb-1998 | 509.001     | 340500 | 15.085              |
| 8161 | 22-Feb-1998 | 509.001     | 345500 | 15.119              |
| 8162 | 23-Feb-1998 | 509.001     | 341163 | 15.188              |
| 8163 | 23-Feb-1998 | 509.001     | 338200 | 15.196              |
| 8164 | 23-Feb-1998 | 509.001     | 380628 | 15.258              |
| 8165 | 23-Feb-1998 | 509.001     | 406000 | 13.814              |
| 8166 | 23-Feb-1998 | 509.001     | 324250 | 11.347              |
| 8167 | 23-Feb-1998 | 509.001     | 199438 | 8.370               |
| 8168 | 23-Feb-1998 | 509.001     | 7408   | 0.329               |
|      |             |             |        |                     |

Table 29: List of the runs at 509.5 MeV. Total number of events is 42143475, the collected luminosity is 1545.491  $nb^{-1}$

| run                        | date        | beam energy | events | luminosity integral |
|----------------------------|-------------|-------------|--------|---------------------|
| 7145                       | 27-Oct-1997 | 509.555     | 11754  | 0.135               |
| 7146                       | 27-Oct-1997 | 509.555     | 145250 | 1.834               |
| 7147                       | 28-Oct-1997 | 509.555     | 142266 | 1.407               |
| 7148                       | 28-Oct-1997 | 509.555     | 143000 | 1.059               |
| 7149                       | 28-Oct-1997 | 509.555     | 251250 | 3.153               |
| 7150                       | 28-Oct-1997 | 509.555     | 276750 | 3.353               |
| 7151                       | 28-Oct-1997 | 509.555     | 108000 | 1.143               |
| 7152                       | 28-Oct-1997 | 509.555     | 49047  | 0.552               |
| 7153                       | 28-Oct-1997 | 509.555     | 153500 | 1.377               |
| 7154                       | 28-Oct-1997 | 509.555     | 152057 | 1.511               |
| 7155                       | 29-Oct-1997 | 509.555     | 129500 | 0.710               |
| 7156                       | 29-Oct-1997 | 509.555     | 9500   | 0.000               |
| 7157                       | 29-Oct-1997 | 509.555     | 140931 | 1.355               |
| 7158                       | 29-Oct-1997 | 509.555     | 154322 | 1.266               |
| 7159                       | 29-Oct-1997 | 509.555     | 146750 | 1.161               |
| 7160                       | 29-Oct-1997 | 509.555     | 246500 | 2.213               |
| 7161                       | 29-Oct-1997 | 509.555     | 89500  | 0.794               |
| 7162                       | 29-Oct-1997 | 509.555     | 114066 | 1.221               |
| 7163                       | 29-Oct-1997 | 509.555     | 0      | 0.000               |
| 7164                       | 29-Oct-1997 | 509.555     | 0      | 0.000               |
| 7165                       | 29-Oct-1997 | 509.555     | 9250   | 0.078               |
| 7166                       | 29-Oct-1997 | 509.555     | 152435 | 1.539               |
| 7167                       | 29-Oct-1997 | 509.555     | 153607 | 1.963               |
| continued on the next page |             |             |        |                     |

| run                        | date        | beam energy | events | luminosity integral |
|----------------------------|-------------|-------------|--------|---------------------|
| 7168                       | 29-Oct-1997 | 509.555     | 152336 | 1.861               |
| 7169                       | 30-Oct-1997 | 509.555     | 144000 | 1.881               |
| 7170                       | 30-Oct-1997 | 509.555     | 150819 | 1.634               |
| 7172                       | 30-Oct-1997 | 509.555     | 151879 | 2.209               |
| 7173                       | 30-Oct-1997 | 509.555     | 152648 | 2.336               |
| 7174                       | 30-Oct-1997 | 509.555     | 151750 | 2.427               |
| 7175                       | 30-Oct-1997 | 509.555     | 63000  | 0.359               |
| 7176                       | 30-Oct-1997 | 509.555     | 152500 | 1.732               |
| 7177                       | 30-Oct-1997 | 509.555     | 85085  | 1.109               |
| 7452                       | 18-Dec-1997 | 509.471     | 406000 | 10.811              |
| 7453                       | 18-Dec-1997 | 509.471     | 379944 | 10.932              |
| 7454                       | 18-Dec-1997 | 509.471     | 8000   | 0.176               |
| 7455                       | 18-Dec-1997 | 509.471     | 97490  | 3.234               |
| 7456                       | 18-Dec-1997 | 509.471     | 272921 | 9.368               |
| 7457                       | 18-Dec-1997 | 509.471     | 404000 | 13.606              |
| 7458                       | 19-Dec-1997 | 509.471     | 404824 | 13.877              |
| 7459                       | 19-Dec-1997 | 509.471     | 402664 | 13.113              |
| 7460                       | 19-Dec-1997 | 509.471     | 402935 | 14.059              |
| 7461                       | 19-Dec-1997 | 509.471     | 404785 | 14.115              |
| 7462                       | 19-Dec-1997 | 509.471     | 73000  | 2.632               |
| 7464                       | 19-Dec-1997 | 509.471     | 402000 | 14.058              |
| 7465                       | 19-Dec-1997 | 509.471     | 1000   | 0.021               |
| 7466                       | 19-Dec-1997 | 509.471     | 410091 | 12.631              |
| 7467                       | 19-Dec-1997 | 509.471     | 468621 | 13.361              |
| 7468                       | 19-Dec-1997 | 509.471     | 403801 | 12.475              |
| 7469                       | 19-Dec-1997 | 509.471     | 404419 | 13.425              |
| 7470                       | 19-Dec-1997 | 509.471     | 402750 | 13.068              |
| continued on the next page |             |             |        |                     |

| run                        | date        | beam energy | events | luminosity integral |
|----------------------------|-------------|-------------|--------|---------------------|
| 7471                       | 20-Dec-1997 | 509.471     | 401797 | 12.740              |
| 7472                       | 20-Dec-1997 | 509.471     | 403124 | 10.859              |
| 7473                       | 20-Dec-1997 | 509.471     | 402535 | 12.422              |
| 7474                       | 20-Dec-1997 | 509.471     | 327827 | 10.434              |
| 7475                       | 20-Dec-1997 | 509.471     | 394502 | 12.863              |
| 7476                       | 20-Dec-1997 | 509.471     | 266676 | 8.334               |
| 7477                       | 20-Dec-1997 | 509.471     | 355070 | 12.150              |
| 7478                       | 20-Dec-1997 | 509.471     | 405396 | 13.527              |
| 7479                       | 20-Dec-1997 | 509.471     | 402336 | 13.950              |
| 7480                       | 20-Dec-1997 | 509.471     | 403196 | 14.088              |
| 7481                       | 21-Dec-1997 | 509.471     | 403924 | 13.933              |
| 7482                       | 21-Dec-1997 | 509.471     | 415250 | 14.029              |
| 7483                       | 21-Dec-1997 | 509.471     | 414875 | 14.320              |
| 7484                       | 21-Dec-1997 | 509.471     | 403624 | 14.493              |
| 7485                       | 21-Dec-1997 | 509.471     | 281801 | 9.925               |
| 7854                       | 27-Jan-1998 | 509.500     | 309615 | 13.370              |
| 7855                       | 27-Jan-1998 | 509.500     | 350750 | 15.063              |
| 7856                       | 27-Jan-1998 | 509.500     | 345809 | 15.190              |
| 7857                       | 27-Jan-1998 | 509.500     | 346693 | 15.145              |
| 7858                       | 28-Jan-1998 | 509.500     | 359367 | 15.124              |
| 7859                       | 28-Jan-1998 | 509.500     | 365286 | 15.133              |
| 7860                       | 28-Jan-1998 | 509.500     | 322777 | 14.166              |
| 7861                       | 28-Jan-1998 | 509.500     | 204653 | 9.130               |
| 7863                       | 28-Jan-1998 | 509.500     | 342339 | 15.134              |
| 7864                       | 28-Jan-1998 | 509.500     | 20558  | 0.900               |
| 7865                       | 28-Jan-1998 | 509.500     | 364315 | 15.363              |
| 7866                       | 28-Jan-1998 | 509.500     | 365026 | 15.206              |
| continued on the next page |             |             |        |                     |

| run                        | date        | beam energy | events | luminosity integral |
|----------------------------|-------------|-------------|--------|---------------------|
| 7867                       | 28-Jan-1998 | 509.500     | 107750 | 4.566               |
| 7868                       | 28-Jan-1998 | 509.500     | 0      | 4.566               |
| 7869                       | 28-Jan-1998 | 509.500     | 385864 | 15.161              |
| 7870                       | 28-Jan-1998 | 509.500     | 343816 | 15.254              |
| 7871                       | 28-Jan-1998 | 509.500     | 352394 | 15.016              |
| 7872                       | 28-Jan-1998 | 509.500     | 350775 | 15.015              |
| 7873                       | 29-Jan-1998 | 509.500     | 323250 | 14.013              |
| 7874                       | 29-Jan-1998 | 509.500     | 378217 | 16.263              |
| 7875                       | 29-Jan-1998 | 509.500     | 373161 | 16.293              |
| 7876                       | 29-Jan-1998 | 509.500     | 316189 | 14.129              |
| 7877                       | 29-Jan-1998 | 509.500     | 324250 | 14.500              |
| 7878                       | 29-Jan-1998 | 509.611     | 2000   | 0.014               |
| 7879                       | 29-Jan-1998 | 509.500     | 87561  | 3.561               |
| 7880                       | 29-Jan-1998 | 509.500     | 8500   | 0.390               |
| 7881                       | 29-Jan-1998 | 509.500     | 53342  | 2.064               |
| 7882                       | 29-Jan-1998 | 509.500     | 56627  | 2.359               |
| 7883                       | 29-Jan-1998 | 509.500     | 360105 | 15.234              |
| 7884                       | 29-Jan-1998 | 509.500     | 351426 | 15.108              |
| 7885                       | 30-Jan-1998 | 509.500     | 347713 | 14.693              |
| 7886                       | 30-Jan-1998 | 509.500     | 225951 | 14.054              |
| 7887                       | 30-Jan-1998 | 509.500     | 336310 | 14.054              |
| 7888                       | 30-Jan-1998 | 509.500     | 366458 | 15.599              |
| 7889                       | 30-Jan-1998 | 509.500     | 110250 | 4.490               |
| 7890                       | 30-Jan-1998 | 509.500     | 81000  | 2.916               |
| 7891                       | 30-Jan-1998 | 509.500     | 337000 | 14.824              |
| 7892                       | 30-Jan-1998 | 509.500     | 334684 | 15.179              |
| 7893                       | 30-Jan-1998 | 509.500     | 333948 | 15.168              |
| continued on the next page |             |             |        |                     |

| run                        | date        | beam energy | events | luminosity integral |
|----------------------------|-------------|-------------|--------|---------------------|
| 7894                       | 30-Jan-1998 | 509.500     | 322763 | 15.191              |
| 7895                       | 30-Jan-1998 | 509.500     | 367614 | 15.100              |
| 7896                       | 30-Jan-1998 | 509.500     | 341165 | 15.090              |
| 7897                       | 31-Jan-1998 | 509.500     | 338203 | 15.058              |
| 7898                       | 31-Jan-1998 | 509.500     | 363750 | 15.184              |
| 7899                       | 31-Jan-1998 | 509.500     | 354802 | 15.145              |
| 7900                       | 31-Jan-1998 | 509.500     | 356098 | 15.122              |
| 7901                       | 31-Jan-1998 | 509.500     | 207250 | 8.644               |
| 7902                       | 31-Jan-1998 | 509.500     | 346617 | 15.243              |
| 7903                       | 31-Jan-1998 | 509.500     | 312615 | 14.829              |
| 8169                       | 23-Feb-1998 | 509.500     | 189188 | 7.685               |
| 8170                       | 23-Feb-1998 | 509.500     | 197500 | 8.492               |
| 8171                       | 23-Feb-1998 | 509.500     | 347781 | 15.124              |
| 8172                       | 23-Feb-1998 | 509.500     | 404586 | 14.281              |
| 8173                       | 23-Feb-1998 | 509.500     | 150069 | 6.000               |
| 8176                       | 24-Feb-1998 | 509.500     | 356018 | 15.075              |
| 8177                       | 24-Feb-1998 | 509.500     | 350721 | 15.281              |
| 8178                       | 24-Feb-1998 | 509.500     | 357388 | 14.668              |
| 8179                       | 24-Feb-1998 | 509.500     | 300040 | 11.752              |
| 8182                       | 24-Feb-1998 | 509.500     | 374259 | 15.211              |
| 8183                       | 24-Feb-1998 | 509.500     | 401750 | 14.954              |
| 8184                       | 24-Feb-1998 | 509.500     | 407332 | 13.609              |
| 8185                       | 24-Feb-1998 | 509.500     | 227500 | 6.901               |
| 8186                       | 24-Feb-1998 | 509.500     | 406650 | 15.463              |
| 8187                       | 24-Feb-1998 | 509.500     | 404054 | 14.190              |
| 8188                       | 24-Feb-1998 | 509.500     | 388890 | 15.256              |
| 8189                       | 25-Feb-1998 | 509.500     | 386774 | 15.263              |
| continued on the next page |             |             |        |                     |

| run                        | date        | beam energy | events | luminosity integral |
|----------------------------|-------------|-------------|--------|---------------------|
| 8190                       | 25-Feb-1998 | 509.500     | 115929 | 3.095               |
| 8191                       | 25-Feb-1998 | 509.500     | 384862 | 15.083              |
| 8192                       | 25-Feb-1998 | 509.500     | 408906 | 15.311              |
| 8193                       | 25-Feb-1998 | 509.500     | 108309 | 4.600               |
| 8194                       | 25-Feb-1998 | 509.500     | 193715 | 7.480               |
| 8195                       | 25-Feb-1998 | 509.500     | 141726 | 4.577               |
| 8196                       | 25-Feb-1998 | 509.500     | 17012  | 0.507               |
| 8197                       | 25-Feb-1998 | 509.500     | 352346 | 15.188              |
| 8198                       | 25-Feb-1998 | 509.500     | 256752 | 10.884              |
| 8199                       | 25-Feb-1998 | 509.500     | 105113 | 4.986               |
| 8200                       | 25-Feb-1998 | 509.500     | 181940 | 8.349               |
| 8201                       | 25-Feb-1998 | 509.500     | 102750 | 3.582               |
| 8202                       | 25-Feb-1998 | 509.500     | 336790 | 15.229              |
| 8203                       | 25-Feb-1998 | 509.500     | 172250 | 7.335               |
| 8204                       | 26-Feb-1998 | 509.500     | 340776 | 15.052              |
| 8205                       | 26-Feb-1998 | 509.500     | 292864 | 11.691              |
| 8206                       | 26-Feb-1998 | 509.500     | 304500 | 13.000              |
| 8207                       | 26-Feb-1998 | 509.500     | 127250 | 5.634               |
| 8208                       | 26-Feb-1998 | 509.500     | 297093 | 11.641              |
| 8209                       | 26-Feb-1998 | 509.500     | 0      | 11.641              |
| 8210                       | 26-Feb-1998 | 509.500     | 58712  | 2.455               |
| 8211                       | 26-Feb-1998 | 509.500     | 356000 | 14.840              |
| 8212                       | 26-Feb-1998 | 509.500     | 392878 | 15.163              |
| 8213                       | 26-Feb-1998 | 509.500     | 389708 | 15.170              |
| 8214                       | 27-Feb-1998 | 509.500     | 375431 | 15.141              |
| 8215                       | 27-Feb-1998 | 509.500     | 389030 | 15.141              |
| 8216                       | 27-Feb-1998 | 509.500     | 261525 | 10.500              |
| continued on the next page |             |             |        |                     |

| run  | date        | beam energy | events | luminosity integral |
|------|-------------|-------------|--------|---------------------|
| 8217 | 27-Feb-1998 | 509.500     | 378046 | 15.077              |
| 8218 | 27-Feb-1998 | 509.500     | 171658 | 6.929               |
| 8219 | 27-Feb-1998 | 509.500     | 214318 | 8.869               |
| 8220 | 27-Feb-1998 | 509.500     | 193750 | 7.722               |
|      |             |             |        |                     |

Table 30: List of the runs at 510.0 MeV. Total number of events is 39721147, the collected luminosity is 1477.744  $nb^{-1}$

| run                        | date      | beam energy | events | luminosity integral |
|----------------------------|-----------|-------------|--------|---------------------|
| 7095                       | 21-Oct-97 | 510.000     | 35750  | 0.171               |
| 7096                       | 21-Oct-97 | 510.000     | 10500  | 0.121               |
| 7097                       | 21-Oct-97 | 510.000     | 221932 | 3.444               |
| 7098                       | 22-Oct-97 | 510.000     | 183793 | 3.369               |
| 7099                       | 22-Oct-97 | 510.000     | 335510 | 5.148               |
| 7100                       | 22-Oct-97 | 510.000     | 321808 | 3.285               |
| 7101                       | 22-Oct-97 | 510.000     | 13507  | 0.171               |
| 7102                       | 22-Oct-97 | 510.000     | 10259  | 0.382               |
| 7103                       | 22-Oct-97 | 510.000     | 10328  | 0.209               |
| 7104                       | 22-Oct-97 | 510.000     | 12750  | 0.155               |
| 7105                       | 22-Oct-97 | 510.000     | 11572  | 0.180               |
| 7106                       | 22-Oct-97 | 510.000     | 20411  | 0.422               |
| 7107                       | 22-Oct-97 | 510.000     | 34750  | 0.506               |
| 7108                       | 22-Oct-97 | 510.000     | 38250  | 0.762               |
| 7109                       | 22-Oct-97 | 510.000     | 19128  | 0.223               |
| 7110                       | 22-Oct-97 | 510.000     | 18750  | 0.275               |
| continued on the next page |           |             |        |                     |

| run                        | date      | beam energy | events | luminosity integral |
|----------------------------|-----------|-------------|--------|---------------------|
| 7111                       | 22-Oct-97 | 510.000     | 143750 | 1.728               |
| 7112                       | 22-Oct-97 | 510.000     | 9750   | 0.025               |
| 7113                       | 22-Oct-97 | 510.000     | 46750  | 0.479               |
| 7114                       | 22-Oct-97 | 510.000     | 34258  | 0.629               |
| 7115                       | 22-Oct-97 | 510.000     | 33121  | 0.467               |
| 7486                       | 21-Dec-97 | 509.985     | 427250 | 12.735              |
| 7487                       | 21-Dec-97 | 509.985     | 483524 | 16.373              |
| 7488                       | 21-Dec-97 | 509.985     | 513575 | 17.148              |
| 7489                       | 21-Dec-97 | 509.985     | 246505 | 8.644               |
| 7490                       | 21-Dec-97 | 509.985     | 0      | 8.644               |
| 7491                       | 21-Dec-97 | 509.985     | 401395 | 14.496              |
| 7492                       | 22-Dec-97 | 509.985     | 403712 | 13.424              |
| 7493                       | 22-Dec-97 | 509.985     | 403478 | 13.245              |
| 7494                       | 22-Dec-97 | 509.985     | 405750 | 13.114              |
| 7495                       | 22-Dec-97 | 509.985     | 121750 | 3.416               |
| 7496                       | 22-Dec-97 | 509.985     | 136750 | 4.369               |
| 7510                       | 23-Dec-97 | 509.985     | 1500   | 0.025               |
| 7511                       | 23-Dec-97 | 509.985     | 305500 | 10.113              |
| 7512                       | 23-Dec-97 | 509.985     | 428357 | 13.560              |
| 7513                       | 23-Dec-97 | 509.985     | 70750  | 2.263               |
| 7514                       | 23-Dec-97 | 509.985     | 411891 | 13.476              |
| 7515                       | 23-Dec-97 | 509.985     | 73000  | 2.34                |
| 7516                       | 23-Dec-97 | 509.985     | 471330 | 15.713              |
| 7517                       | 23-Dec-97 | 509.985     | 453267 | 15.893              |
| 7518                       | 24-Dec-97 | 509.985     | 429444 | 14.539              |
| 7519                       | 24-Dec-97 | 509.985     | 334904 | 11.591              |
| 7520                       | 24-Dec-97 | 509.985     | 108836 | 3.818               |
| continued on the next page |           |             |        |                     |

| run                        | date      | beam energy | events | luminosity integral |
|----------------------------|-----------|-------------|--------|---------------------|
| 7521                       | 24-Dec-97 | 509.985     | 45098  | 1.665               |
| 7522                       | 24-Dec-97 | 509.985     | 0      | 1.665               |
| 7523                       | 24-Dec-97 | 509.985     | 351204 | 12.286              |
| 7524                       | 24-Dec-97 | 509.985     | 65508  | 2.381               |
| 7525                       | 24-Dec-97 | 509.985     | 16109  | 0.547               |
| 7526                       | 24-Dec-97 | 509.985     | 157750 | 4.835               |
| 7527                       | 24-Dec-97 | 509.985     | 26400  | 1.38                |
| 7528                       | 24-Dec-97 | 509.985     | 132835 | 4.688               |
| 7529                       | 24-Dec-97 | 509.985     | 90593  | 2.975               |
| 7530                       | 24-Dec-97 | 509.985     | 402286 | 14.315              |
| 7531                       | 24-Dec-97 | 509.985     | 396879 | 14.165              |
| 7532                       | 25-Dec-97 | 509.985     | 404802 | 14.791              |
| 7533                       | 25-Dec-97 | 509.985     | 374514 | 14.569              |
| 7534                       | 25-Dec-97 | 509.985     | 404000 | 14.737              |
| 7535                       | 25-Dec-97 | 509.985     | 157755 | 5.717               |
| 7536                       | 25-Dec-97 | 509.985     | 404564 | 13.123              |
| 7537                       | 25-Dec-97 | 509.985     | 180327 | 5.071               |
| 7538                       | 25-Dec-97 | 509.985     | 81577  | 2.245               |
| 7808                       | 23-Jan-98 | 510.074     | 375671 | 13.91               |
| 7809                       | 23-Jan-98 | 510.030     | 403500 | 14.9                |
| 7810                       | 23-Jan-98 | 510.000     | 311606 | 12.129              |
| 7812                       | 24-Jan-98 | 510.000     | 400042 | 13.222              |
| 7813                       | 24-Jan-98 | 510.000     | 358273 | 13.523              |
| 7814                       | 24-Jan-98 | 510.000     | 379035 | 14.393              |
| 7815                       | 24-Jan-98 | 510.000     | 386950 | 14.055              |
| 7816                       | 24-Jan-98 | 510.000     | 390699 | 15.125              |
| 7817                       | 24-Jan-98 | 510.000     | 397250 | 15.109              |
| continued on the next page |           |             |        |                     |

| run                        | date      | beam energy | events | luminosity integral |
|----------------------------|-----------|-------------|--------|---------------------|
| 7818                       | 24-Jan-98 | 510.000     | 398864 | 14.545              |
| 7819                       | 24-Jan-98 | 510.000     | 378208 | 15.322              |
| 7820                       | 24-Jan-98 | 510.000     | 155000 | 6.345               |
| 7821                       | 24-Jan-98 | 510.000     | 363250 | 15.159              |
| 7822                       | 24-Jan-98 | 510.000     | 372434 | 15.449              |
| 7823                       | 24-Jan-98 | 510.000     | 390578 | 16.193              |
| 7824                       | 24-Jan-98 | 510.000     | 372750 | 15.116              |
| 7825                       | 25-Jan-98 | 510.000     | 362417 | 14.999              |
| 7826                       | 25-Jan-98 | 510.000     | 365111 | 15.209              |
| 7827                       | 25-Jan-98 | 510.000     | 366169 | 15.175              |
| 7828                       | 25-Jan-98 | 510.000     | 365320 | 15.053              |
| 7829                       | 25-Jan-98 | 510.000     | 474507 | 18.849              |
| 7830                       | 25-Jan-98 | 510.000     | 374350 | 15.196              |
| 7831                       | 25-Jan-98 | 510.000     | 357585 | 15.094              |
| 7832                       | 25-Jan-98 | 510.000     | 320500 | 13.836              |
| 7833                       | 25-Jan-98 | 510.000     | 355914 | 15.084              |
| 7834                       | 25-Jan-98 | 510.000     | 362475 | 15.092              |
| 7835                       | 25-Jan-98 | 510.000     | 352000 | 15.094              |
| 7836                       | 26-Jan-98 | 510.000     | 348259 | 15.11               |
| 7837                       | 26-Jan-98 | 510.000     | 352888 | 15.13               |
| 7838                       | 26-Jan-98 | 510.000     | 367678 | 15.16               |
| 7839                       | 26-Jan-98 | 510.000     | 351644 | 15.28               |
| 7840                       | 26-Jan-98 | 510.000     | 125750 | 5.169               |
| 7844                       | 26-Jan-98 | 510.000     | 317865 | 11.984              |
| 7845                       | 27-Jan-98 | 510.000     | 384899 | 15.101              |
| 7846                       | 27-Jan-98 | 510.000     | 369478 | 15.220              |
| 7847                       | 27-Jan-98 | 510.000     | 373674 | 15.089              |
| continued on the next page |           |             |        |                     |

| run                        | date      | beam energy | events | luminosity integral |
|----------------------------|-----------|-------------|--------|---------------------|
| 7848                       | 27-Jan-98 | 510.000     | 348630 | 15.293              |
| 7849                       | 27-Jan-98 | 510.000     | 303750 | 12.052              |
| 7850                       | 27-Jan-98 | 510.000     | 404358 | 15.237              |
| 7851                       | 27-Jan-98 | 510.000     | 342622 | 15.330              |
| 7853                       | 27-Jan-98 | 510.000     | 300285 | 13.498              |
| 8221                       | 27-Feb-98 | 509.994     | 369547 | 15.051              |
| 8222                       | 27-Feb-98 | 509.994     | 342172 | 15.092              |
| 8223                       | 27-Feb-98 | 509.994     | 350371 | 15.092              |
| 8224                       | 27-Feb-98 | 509.994     | 393775 | 14.258              |
| 8225                       | 27-Feb-98 | 509.994     | 109    | 0.003               |
| 8226                       | 27-Feb-98 | 509.994     | 412926 | 15.237              |
| 8227                       | 27-Feb-98 | 509.994     | 432565 | 15.096              |
| 8228                       | 28-Feb-98 | 509.994     | 416030 | 14.956              |
| 8229                       | 28-Feb-98 | 509.994     | 591101 | 21.346              |
| 8230                       | 28-Feb-98 | 509.994     | 334250 | 10.461              |
| 8231                       | 28-Feb-98 | 509.994     | 0      | 0.000               |
| 8232                       | 28-Feb-98 | 509.994     | 100214 | 3.942               |
| 8235                       | 28-Feb-98 | 509.994     | 0      | 0.000               |
| 8236                       | 28-Feb-98 | 509.994     | 312176 | 11.470              |
| 8237                       | 28-Feb-98 | 509.994     | 375634 | 13.163              |
| 8238                       | 28-Feb-98 | 509.994     | 402879 | 15.067              |
| 8239                       | 28-Feb-98 | 509.994     | 404852 | 14.611              |
| 8240                       | 28-Feb-98 | 509.994     | 399335 | 15.201              |
| 8241                       | 1-Mar-98  | 509.994     | 395122 | 15.158              |
| 8242                       | 1-Mar-98  | 509.994     | 445319 | 15.042              |
| 8243                       | 1-Mar-98  | 509.994     | 430074 | 15.230              |
| 8244                       | 1-Mar-98  | 509.994     | 418137 | 15.196              |
| continued on the next page |           |             |        |                     |

| run  | date      | beam energy | events | luminosity integral |
|------|-----------|-------------|--------|---------------------|
| 8245 | 1-Mar-98  | 509.994     | 385366 | 15.246              |
| 8246 | 1-Mar-98  | 509.994     | 366460 | 15.115              |
| 8247 | 1-Mar-98  | 509.994     | 357380 | 15.105              |
| 8248 | 1-Mar-98  | 509.994     | 198302 | 8.620               |
| 8249 | 1-Mar-98  | 509.994     | 349661 | 15.157              |
| 8250 | 1-Mar-98  | 509.994     | 373860 | 15.149              |
| 8251 | 1-Mar-98  | 509.994     | 12273  | 0.447               |
| 8252 | 1-Mar-98  | 509.994     | 381750 | 15.103              |
| 8253 | 2-Mar-98  | 509.994     | 389936 | 15.137              |
| 8254 | 2-Mar-98  | 509.994     | 97519  | 3.675               |
| 8255 | 2-Mar-98  | 509.994     | 351364 | 15.065              |
| 8256 | 2-Mar-98  | 509.994     | 310812 | 13.662              |
| 8257 | 2-Mar-98  | 509.994     | 307447 | 15.223              |
| 8258 | 3-Mar-98  | 509.994     | 282750 | 15.139              |
| 8259 | 3-Mar-98  | 509.994     | 279333 | 14.623              |
| 8260 | 3-Mar-98  | 509.994     | 83750  | 4.214               |
| 8261 | 3-Mar-98  | 509.994     | 298863 | 15.171              |
| 8262 | 3-Mar-98  | 509.994     | 179829 | 9.097               |
| 8424 | 22-Mar-98 | 510.017     | 154861 | 2.349               |
| 8425 | 22-Mar-98 | 510.000     | 301009 | 5.490               |
| 8426 | 23-Mar-98 | 510.000     | 317250 | 5.447               |
| 8427 | 23-Mar-98 | 510.000     | 141250 | 2.764               |
|      |           |             |        |                     |

Table 31: List of the runs at 510.5 MeV. Total number of events is 25045421, the collected luminosity is 946.823  $nb^{-1}$

| run                        | date        | beam energy | events | luminosity integral |
|----------------------------|-------------|-------------|--------|---------------------|
| 7539                       | 25-Dec-1997 | 510.443     | 402771 | 13.741              |
| 7540                       | 25-Dec-1997 | 510.443     | 403503 | 14.364              |
| 7541                       | 25-Dec-1997 | 510.443     | 403500 | 14.445              |
| 7542                       | 25-Dec-1997 | 510.443     | 402913 | 13.301              |
| 7543                       | 25-Dec-1997 | 510.443     | 401648 | 12.532              |
| 7544                       | 26-Dec-1997 | 510.443     | 405250 | 13.461              |
| 7545                       | 26-Dec-1997 | 510.443     | 398175 | 12.801              |
| 7546                       | 26-Dec-1997 | 510.443     | 402493 | 12.491              |
| 7547                       | 26-Dec-1997 | 510.443     | 403604 | 12.243              |
| 7548                       | 26-Dec-1997 | 510.443     | 232215 | 7.504               |
| 7549                       | 26-Dec-1997 | 510.480     | 408357 | 13.229              |
| 7550                       | 26-Dec-1997 | 510.480     | 306000 | 9.427               |
| 7551                       | 26-Dec-1997 | 510.480     | 403015 | 12.754              |
| 7552                       | 26-Dec-1997 | 510.480     | 218578 | 7.582               |
| 7553                       | 26-Dec-1997 | 510.480     | 401892 | 13.984              |
| 7554                       | 26-Dec-1997 | 510.480     | 404357 | 13.952              |
| 7555                       | 27-Dec-1997 | 510.480     | 404350 | 13.907              |
| 7556                       | 27-Dec-1997 | 510.480     | 19500  | 0.643               |
| 7557                       | 27-Dec-1997 | 510.480     | 404650 | 13.441              |
| 7558                       | 27-Dec-1997 | 510.480     | 405251 | 13.638              |
| 7559                       | 27-Dec-1997 | 510.480     | 404094 | 13.597              |
| 7560                       | 27-Dec-1997 | 510.480     | 404694 | 13.719              |
| 7778                       | 21-Jan-1998 | 510.611     | 96759  | 3.969               |
| continued on the next page |             |             |        |                     |

| run                        | date        | beam energy | events | luminosity integral |
|----------------------------|-------------|-------------|--------|---------------------|
| 7779                       | 21-Jan-1998 | 510.500     | 1162   | 0.055               |
| 7780                       | 21-Jan-1998 | 510.500     | 165222 | 6.659               |
| 7781                       | 21-Jan-1998 | 510.500     | 210000 | 8.456               |
| 7782                       | 21-Jan-1998 | 510.534     | 370058 | 15.190              |
| 7783                       | 21-Jan-1998 | 510.534     | 400687 | 15.192              |
| 7784                       | 21-Jan-1998 | 510.534     | 395936 | 15.121              |
| 7785                       | 21-Jan-1998 | 510.534     | 383000 | 15.100              |
| 7786                       | 22-Jan-1998 | 510.534     | 369895 | 14.812              |
| 7787                       | 22-Jan-1998 | 510.534     | 383000 | 15.097              |
| 7788                       | 22-Jan-1998 | 510.534     | 389005 | 15.242              |
| 7789                       | 22-Jan-1998 | 510.534     | 386346 | 15.124              |
| 7790                       | 22-Jan-1998 | 510.534     | 370000 | 15.178              |
| 7791                       | 22-Jan-1998 | 510.531     | 382500 | 15.185              |
| 7792                       | 22-Jan-1998 | 510.531     | 271326 | 10.860              |
| 7793                       | 22-Jan-1998 | 510.531     | 96750  | 3.337               |
| 7794                       | 22-Jan-1998 | 510.530     | 400755 | 15.127              |
| 7795                       | 22-Jan-1998 | 510.530     | 348500 | 14.112              |
| 7796                       | 22-Jan-1998 | 510.463     | 396750 | 15.206              |
| 7797                       | 22-Jan-1998 | 510.463     | 389000 | 15.122              |
| 7798                       | 23-Jan-1998 | 510.463     | 175000 | 7.126               |
| 7799                       | 23-Jan-1998 | 510.463     | 402057 | 15.166              |
| 7800                       | 23-Jan-1998 | 510.463     | 403000 | 13.702              |
| 7801                       | 23-Jan-1998 | 510.463     | 376666 | 15.098              |
| 7802                       | 23-Jan-1998 | 510.463     | 347000 | 13.345              |
| 7803                       | 23-Jan-1998 | 510.574     | 404189 | 14.985              |
| 7804                       | 23-Jan-1998 | 510.574     | 120345 | 4.824               |
| 7805                       | 23-Jan-1998 | 510.574     | 105000 | 4.256               |
| continued on the next page |             |             |        |                     |

| run                        | date        | beam energy | events | luminosity integral |
|----------------------------|-------------|-------------|--------|---------------------|
| 7806                       | 23-Jan-1998 | 510.574     | 39753  | 1.510               |
| 7807                       | 23-Jan-1998 | 510.426     | 315877 | 12.978              |
| 8263                       | 03-Mar-1998 | 510.500     | 179750 | 7.532               |
| 8264                       | 03-Mar-1998 | 510.505     | 237000 | 7.028               |
| 8265                       | 03-Mar-1998 | 510.505     | 365017 | 15.155              |
| 8266                       | 03-Mar-1998 | 510.505     | 343429 | 14.270              |
| 8267                       | 03-Mar-1998 | 510.505     | 413000 | 16.005              |
| 8268                       | 03-Mar-1998 | 510.505     | 369034 | 14.633              |
| 8269                       | 03-Mar-1998 | 510.505     | 348318 | 14.511              |
| 8270                       | 04-Mar-1998 | 510.505     | 373162 | 15.185              |
| 8271                       | 04-Mar-1998 | 510.505     | 334385 | 14.696              |
| 8272                       | 04-Mar-1998 | 510.505     | 370129 | 16.381              |
| 8273                       | 04-Mar-1998 | 510.505     | 2671   | 0.111               |
| 8274                       | 04-Mar-1998 | 510.505     | 65783  | 2.800               |
| 8275                       | 04-Mar-1998 | 510.505     | 345000 | 15.241              |
| 8276                       | 04-Mar-1998 | 510.505     | 345185 | 15.079              |
| 8277                       | 04-Mar-1998 | 510.505     | 248993 | 10.575              |
| 8278                       | 04-Mar-1998 | 510.505     | 354281 | 14.739              |
| 8279                       | 04-Mar-1998 | 510.505     | 375408 | 15.092              |
| 8280                       | 04-Mar-1998 | 510.505     | 373169 | 15.085              |
| 8281                       | 05-Mar-1998 | 510.505     | 395677 | 16.028              |
| 8283                       | 05-Mar-1998 | 510.505     | 374867 | 15.183              |
| 8284                       | 05-Mar-1998 | 510.505     | 368000 | 15.035              |
| 8285                       | 05-Mar-1998 | 510.505     | 306500 | 12.673              |
| 8286                       | 05-Mar-1998 | 510.505     | 66750  | 2.888               |
| 8287                       | 05-Mar-1998 | 510.516     | 404508 | 15.374              |
| 8288                       | 05-Mar-1998 | 510.516     | 309319 | 13.005              |
| continued on the next page |             |             |        |                     |

| run  | date        | beam energy | events | luminosity integral |
|------|-------------|-------------|--------|---------------------|
| 8289 | 05-Mar-1998 | 510.516     | 353060 | 15.387              |
| 8290 | 05-Mar-1998 | 510.516     | 86678  | 3.242               |
|      |             |             |        |                     |

Table 32: List of the runs at 492.0 MeV, used for background investigation. Total number of events is 5847585, the collected luminosity is 279.161  $nb^{-1}$ .

| run  | date      | beam energy | events | luminosity integral |
|------|-----------|-------------|--------|---------------------|
| 8020 | 10-Feb-98 | 492         | 324568 | 15.143              |
| 8021 | 10-Feb-98 | 492         | 322918 | 15.113              |
| 8022 | 10-Feb-98 | 492         | 69000  | 3.147               |
| 8023 | 10-Feb-98 | 492         | 323712 | 15.123              |
| 8024 | 10-Feb-98 | 492         | 327914 | 15.133              |
| 8025 | 10-Feb-98 | 492         | 927    | 0.031               |
| 8026 | 10-Feb-98 | 492         | 321329 | 15.168              |
| 8027 | 10-Feb-98 | 492         | 326853 | 15.167              |
| 8028 | 10-Feb-98 | 492         | 313135 | 14.837              |
| 8029 | 11-Feb-98 | 492         | 316510 | 15.105              |
| 8030 | 11-Feb-98 | 492         | 295158 | 15.635              |
| 8031 | 11-Feb-98 | 492         | 359256 | 15.157              |
| 8032 | 11-Feb-98 | 492         | 220825 | 11.310              |
| 8033 | 11-Feb-98 | 492         | 311198 | 15.765              |
| 8037 | 12-Feb-98 | 492         | 304689 | 15.138              |
| 8038 | 12-Feb-98 | 492         | 318866 | 15.220              |
| 8039 | 12-Feb-98 | 492         | 310061 | 15.273              |
| 8040 | 12-Feb-98 | 492         | 288309 | 14.029              |
| 8041 | 12-Feb-98 | 492         | 19661  | 0.901               |
| 8042 | 12-Feb-98 | 492         | 231750 | 11.086              |
| 8043 | 12-Feb-98 | 492         | 321502 | 15.167              |
| 8044 | 12-Feb-98 | 492         | 214303 | 10.200              |
| 8045 | 12-Feb-98 | 492         | 5144   | 0.313               |

Table 33: List of the runs at 502.0 MeV, used for background investigation. Total number of events is 4459995, the collected luminosity is  $206.609 \text{ nb}^{-1}$

| run  | date      | beam energy | events | luminosity integral |
|------|-----------|-------------|--------|---------------------|
| 7999 | 8-Feb-98  | 502.106     | 9373   | 0.291               |
| 8000 | 8-Feb-98  | 502.106     | 532250 | 21.234              |
| 8001 | 8-Feb-98  | 502.000     | 314753 | 15.149              |
| 8002 | 8-Feb-98  | 502.000     | 66500  | 3.176               |
| 8003 | 8-Feb-98  | 502.000     | 302250 | 15.016              |
| 8004 | 9-Feb-98  | 502.000     | 302549 | 15.042              |
| 8005 | 9-Feb-98  | 502.000     | 329843 | 15.398              |
| 8006 | 9-Feb-98  | 502.000     | 310410 | 15.377              |
| 8007 | 9-Feb-98  | 502.000     | 277250 | 13.749              |
| 8008 | 9-Feb-98  | 502.000     | 33806  | 1.550               |
| 8009 | 9-Feb-98  | 502.000     | 0      | 0                   |
| 8011 | 9-Feb-98  | 502.000     | 343975 | 15.209              |
| 8012 | 9-Feb-98  | 502.000     | 354159 | 15.143              |
| 8013 | 10-Feb-98 | 502.000     | 202553 | 8.948               |
| 8014 | 10-Feb-98 | 502.000     | 264000 | 12.627              |
| 8015 | 10-Feb-98 | 502.000     | 51609  | 2.134               |
| 8016 | 10-Feb-98 | 502.000     | 108750 | 5.230               |
| 8017 | 10-Feb-98 | 502.000     | 311543 | 15.151              |
| 8018 | 10-Feb-98 | 502.000     | 326108 | 15.320              |
| 8019 | 10-Feb-98 | 502.000     | 18314  | 0.865               |

## BIBLIOGRAPHY

- [1] K. Hagiwara et al, Phys. Rev. D66(2002), 113-114.
- [2] M. Herrero, Lectures presented at the NATO ASI 98 School, Techniques and Concepts of High Energy Physics; St. Croix, Virgin Islands, USA, June 18–29 1998.
- [3] V. Cirigliano, M. Knecht, H. Neufeld, H. Rupertsbergen, P. Talavera, Eur. Phys. J. C23 (2002), 121-133.
- [4] E.S. Ginsberg, Phys. Rev. D 1, 229 (1970).
- [5] E. Ginsberg, Phys. Rev. 162(1967), 1570; Phys. Rev. 142(1966), 1035; Phys. Rev. 171(1968), 1675; Phys. Rev. 187(1968), 2280.
- [6] T. Becherrawy, Phys. Rev. D1 (1970), 1452.
- [7] V. Anashin et al., Preprint 84-14, Budker Institute of Nuclear Physics, Novosibirsk, Russia.
- [8] V. Anashin et al., Preprint 83-98, Budker Institute of Nuclear Physics, Novosibirsk, Russia.
- [9] V. Anashin et al., Preprint 84-123, Budker Institute of Nuclear Physics, Novosibirsk, Russia.
- [10] E.P. Solodov, Rare processes in  $\phi$  meson decays, Doctor of physics and mathematic sciences degree dissertation, 1999.
- [11] E. Popkov, CMD-2 Memo, Oct 1994, Budker Institute of Nuclear Physics, Novosibirsk, Russia, (unpublished), translation by D.H. Brown available at <http://hep.bu.edu/~brown/ps/popkov.ps>.
- [12] Y. Derbenev et al., Preprint 76-64, Budker Institute of Nuclear Physics, Novosibirsk, Russia.
- [13] V. Baier et al., Physics Reports 78, 293 (1981).
- [14] E.V. Anashkin et al., ICFA Instr. Bulletin, 5 (1988) 18.

- [15] R.R. Akhmetshin et al (CMD-2 Collaboration ), Nucl.Phys. A675 (2000) 424, and references therein.
- [16] V.M. Aulchenko et al., A Drift Chamber for the CMD–2 detector at VEPP-2M. Nucl. Instr. and Meth., A252 (1986) 299–303.
- [17] V.M. Aulchenko et al., CMD–2 barrel calorimeter. Nucl. Instr. and Meth., A336 (1993) 53-58.
- [18] D.N. Grigoriev et al., IEEE Trans. Nucl. Sci. NS-42(4) (1995) 505.
- [19] V.M. Aulchenko et al., Nucl. Instr. and Meth., A265 (1988) 137.
- [20] E. Anashkin et al., Nuclear Instruments and Methods in Physics Research A 323, 178 (1992).
- [21] PDP–11 ONLINE DATA ACQUISITION MANUAL.
- [22] R.R. Akhmetshin et al., Phys. Lett. B466 (1999) 385; Erratum - ibid, B508 (2001) 217; updated in R.R. Akhmetshin et al., Phys. Lett. B578 (2004) 285.
- [23] M.N. Achasov, JETP Lett 67, 777-780, 1998.
- [24] R. Brun et al., GEANT3 User’s Guide, CERN Computer Centre Program Library Long Write-up; Y250, Geneve, 1987.
- [25] H.C. Fesefeldt, Simulation of hadronic showers, physics and applications. Technical Report PITHA 85-02, Physikalisches Institut, RWTH Aachen Physikzentrum, 5100 Aachen, Germany, September 1985.
- [26] P.A. Aarnio et al., FLUKA user’s guide. Technical Report TIS-RP-190, CERN, 1990.
- [27] V. Bytev, E. Kuraev, A. Baratt, J. Thompson, Eur. Phys. J. C27 57-71, 2003.
- [28] J. Bijnens, G. Colangelo, G. Ecker, and J. Gasser, The Second DAΦNE Physics Handbook, vol.1, 313.
- [29] V.N. Baier, V.S. Fadin, V.A. Khoze, Nucl. Phys. B65(1973), 381.
- [30] T. Kinoshita, J. Math. Phys. 3(1972), 650; T.D. Lee and M. Nauenberg, Phys. Rev. B133(1964), 1549.
- [31] J. Gasser and H. Leutwyler, Nucl. Phys. B250(1985), 464, 517.
- [32] J. Bijnens, G. Ecker, and J. Gasser, Nucl. Phys. B396(1993), 81.
- [33] B. Holstein Phys. Rev. D41(1990), 2829.

- [34] A.I. Akhiezer, V.B. Berestetski, 'Quantum Electrodynamics', Moscow, 1981; V.B. Berestetski, E. Lifshitz, L. Pitaevski, 'Quantum Electrodynamics', Moscow, 1989.
- [35] N-P. Chang, Phys. Rev. 131(1963),1272.
- [36] W. Marciano and A. Sirlin, Phys. Rev. Lett. 71(1993), 3629.
- [37] M.V. Terent'ev, Yad. Fiz. 18(1973), 870; Sov. J. Nucl. Phys. 18(1974), 449.
- [38] E.A. Kuraev, V.S. Fadin, Yad. Fiz. 41(1985), 466.
- [39] R. Decker and M. Finkemeier, Nucl. Phys. B438(1995), 17.
- [40] A. Sirlin, Phys. Rev. D5(1972), 436; Rev. Mod. Phys. 50(1978), 573; Nucl. Phys. B196(1982), 83.